Water Mass Circulation and Variability in the Subpolar North Atlantic

Dagmar Kieke

Universität Bremen 2005

Water Mass Circulation and Variability in the Subpolar North Atlantic

Vom Fachbereich für Physik und Elektrotechnik
der Universität Bremen

zur Erlangung des akademischen Grades eines

Doktor der Naturwissenschaften (Dr. rer. nat)

genehmigte Dissertation

von

Dipl. Oz. Dagmar Kieke

aus Hannover

1. Gutachterin:	Prof. Dr. rer. nat. Monika Rhein
2. Gutachter:	Prof. Dr. rer. nat. Claus Böning
Eingereicht am:	12.01.2005
Tag des Promotionskolloquiums:	15.03.2005

Zusammenfassung

Die vorliegende Arbeit befasst sich mit der Bildung von oberem und klassischem Labradorseewasser (ULSW und LSW), die im westlichen Teil des subpolaren Nordatlantiks (Labradorsee) durch ozeanische Tiefenkonvektion erfolgt. Beide Wassermassen bilden das obere Nordatlantische Tiefenwasser, das im kalten Zweig der thermohalinen Zirkulation den Weltozean durchströmt. Diverse Veröffentlichungen haben gezeigt, dass die Wassermasseneigenschaften des klassisches LSW auf jahreszeitlichen bis interdekadischen Zeitskalen Veränderungen ausgesetzt sind. Eine signifikante Abschwächung der Tiefenkonvektion in der Labradorsee nach 1996 führte zur lokalen Bildung einer leichteren Wassermasse, die als ULSW identifiziert wurde. Abschätzungen zur Veränderung in der Bildung von ULSW im Vergleich zur Bildung von klassischem LSW stehen im Vordergrund dieser Arbeit.

Die Analyse basiert auf einem umfangreichen Hydrographie- und Tracer-Datensatz der Jahre 1997, 1999 und 2001. Aus einzelnen Messprofilen wurden horizontale Verteilungen der Wassermassenschichtdicke und der Konzentration anthropogener Fluorchlorkohlenwasserstoffe (CFC, Komponenten CFC-11 und CFC-12) erzeugt. Die Eintragsfunktion dieser Gase in den Ozean ist gut bekannt. Verschiedene Methoden zur Behandlung auftretender Datenlücken (1999 und 2001) wurden verglichen. Innerhalb der Fehlergrenzen liefern sie konsistente Ergebnisse. Für die ULSW-Schicht ergab sich ein signifikanter Anstieg des CFC-11-Inventars im Zeitraum 1997-2001. Zeitgleich nahm das CFC-11-Inventar im darunterliegenden klassischen LSW ab. Die CFC-Inventare der jeweiligen Wassermassen wurden zur Bestimmung von Wassermassenbildungsraten benutzt. Es zeigte sich eine verstärkte Bildung von ULSW im Zeitraum 1997-1999 (6.9-9.2 Sv). In den folgenden zwei Jahren nahm die ULSW-Bildungsrate auf 3.7-4.0 Sv ab. Im genannten Zeitraum wurde kein klassisches LSW gebildet.

Die Wassermasseneigenschaften von ULSW und LSW wurden in der zentralen Labradorsee anhand von Daten der Jahre 1990-2001 verglichen. Einhergehend mit sich abschwächender Tiefenkonvektion zeigte sich eine beträchtliche Verlagerung der Isopykne σ_Θ = 27.74 kg/m^3 hin zu größeren Tiefen. Diese Dichte stellt per Definition die Trennung zwischen beiden Wassermassen dar. LSW war zunehmend von der Oberfläche entfernt. Die darüberliegende Schicht zeigte eine erhöhte Dichteschichtung, die vermutlich durch Einspeisung warmen und salzreichen Wassers aus dem Westgrönlandstrom in die zentrale Labradorsee unterstützt wurde. Zeitreihen von Meeresoberflächenflüssen (Impulsfluß, Wärme, Auftrieb) weisen auf eine Veränderung der atmosphärischen Bedingungen hin, die nach 1995/96 erfolgte. Die Konvektionsaktivität der späten 1990er Jahre war jedoch ausreichend, um verstärkt leichteres ULSW zu bilden.

Bisher wurde ULSW-Bildung nur im Randstromsystem der Labradorsee beobachtet. Der Zeitraum abgeschwächter Konvektion begünstigt jedoch eindeutig eine Bildung in der zentralen Labradorsee. Die Rekonstruktion dekadischer Zeitreihen zeigt starke Schwankungen in der ULSW- und LSW-Bildung mit einer signifikanten Anti-Korrelation (r = -0.85).

Desweiteren wurde die Ausbreitung von Tiefenwasser im Neufundlandbecken untersucht. Im Mittelpunkt stand die Frage, ob Tiefenwasserexportpfade ausserhalb des Randstromsystems existieren. Die Untersuchung der Eigenschaften von Tiefen- und Bodenwassermassen weist darauf hin, dass dem so ist. Die Abschätzung von Zeitskalen des LSW ergab eine schnelle Ausbreitung von LSW im Randstrom (1-2 Jahre von der Labradorsee bis $\sim$43°N) und eine langsame Ausbreitung im inneren Neufundlandbecken (3-6 Jahre, abhängig vom Ort). Die Untersuchung von horizontalen Gradienten der Meeresobeflächentemperatur zeigt ähnliche räumliche Muster, wie sie in der Tiefenzirkulation von Modellstudien gefunden wurden. Ein Zusammenhang zwischen Tiefenzirkulation und Variabilität in der Lage des Nordatlantikstroms wird als mögliche Ursache für küstenferne Tiefenwasserausbreitung betrachtet. Die Rekonstruktion von ULSW/LSW-Zeitreihen im Randstromsystem des Neufundlandbeckens zeigte eine starke Korrelation mit Änderungen im Bildungsgebiet.

Abstract

The present study deals with the formation of Upper and classical Labrador Sea Water (ULSW and LSW) which occurs in the western part of the subpolar North Atlantic (Labrador Sea). Both water masses represent the upper part of North Atlantic Deep Water. As part of the cold limb of the thermohaline circulation they spread into the world ocean. Various publications revealed that water mass properties of classical LSW are subject to variability on intraseasonal to interdecadal time scales. A significant weakening of the Labrador Sea convection intensity throughout the 1990s resulted in the formation of a lighter water mass, termed ULSW. The focus of the present study is on estimating the variability in the formation of ULSW. This is compared to formation of the denser classical LSW.

The analysis is based on a comprehensive hydrography/tracer data set from the years 1997, 1999, and 2001. Horizontal distributions of water mass layer thickness and mean concentrations of anthropogenic chlorofluorcarbon (CFC, component CFC-11) have been constructed from single profiles. The function describing the input of these gases into the oceans is well known. Different methods have been compared to handle data gaps which occurred in the fields of 1999 and 2001. Within the error margins these gave consistent results. For the ULSW layer a significant increase in the CFC-11 inventory was found in the period 1997-2001. At the same time the CFC-11 inventory of classical LSW reduced. The CFC inventories have been used to infer water mass formation rates. A significant formation of ULSW was found during 1997-1999 (6.9-9.2 Sv). In the subsequent two years the ULSW formation rate reduced to 3.7-4.0 Sv. LSW formation was absent during these four years.

Water mass properties of ULSW and LSW have been compared in the central Labrador Sea based on data from 1990-2001. Coinciding with weakening convection the isopycnal σ_Θ =27.74 kg/m^3 shifted to greater depths. Per definition this density surface separates ULSW from classical LSW. The water layer lying on top of LSW revealed an increasing stratification which is presumably strengthened by warm and saline water intruding from the West Greenland Current into the interior Labrador Sea. Time series of surface fluxes (momentum, heat, buoyancy) indicate a change in the atmopsheric conditions after 1995/96. The convection activity was, however, sufficient to ventilate the lighter ULSW layer.

So far ULSW formation was only observed in the boundary current of the Labrador Sea. The period of weakened convection, however, favoured considerable ULSW formation in the central Labrador Sea. A reconstruction of decadal time series indicated strong variability and a significant anti-correlation of ULSW and LSW formation (r = -0.85).

Furthermore, deep water spreading pathways have been analysed in the Newfoundland Basin. The question is addressed whether deep water export pathways additional to the boundary current exist. The analysis of deep and bottom water properties indeed provided evidence for the existence. The estimation of LSW spreading time scales point to a fast spreading in the boundary current (1-2 years from the Labrador Sea to 43°N) and a slow spreading in the interior Newfoundland Basin (3-6 years, depending on location). The analysis of horizontal gradients of sea surface temperatures revealed similar spatial patterns as was found in the deep water circulation of model studies. A relation between deep water circulation and variability in the pathway of the North Atlantic Current is considered as a likely cause for offshore deep water spreading. The reconstruction of ULSW/LSW time series in the boundary current system of the Newfoundland Basin revealed a strong correlation with changes in the formation region.

Contents

1. Introduction

"Concerning the ocean currents, we have to deal with a very complicated phenomenon, and various causes and forces are at work."
Otto Krümmel, geo- and oceanographer, 1909

The global large-scale circulation is a conglomerate of minor and major currents, driven by different forces. Beside the wind stress affecting directly the upper few hundred meters of the water column, the oceanic mass flow is driven by tidal forces (e.g. Munk, 1966) and fluxes of heat and fresh water across the sea surface. According to Wunsch (2002) the latter should not be considered as a real driving mechanism. Instead, he suggests to think of the ocean as a "mechanically driven fluid engine, capable of importing, exporting and transporting vast quantities of heat and freshwater". The term *thermohaline circulation* (THC) is often used with respect to temporal and spatial differences in both the salinity and temperature of the water, properties that affect the ocean's density[I]. Differences in temperature arise from heating and cooling at the sea surface. Evaporation and sea ice formation increase salinity, while precipitation, river runoff, and sea ice melting reduce it.

The classical simplified picture of THC consists of a light, warm, upper limb and a dense and cold lower limb. The upper limb is mainly wind-driven. There is an excess of energy in the equatorial regions and a deficit near the poles due to the uneven heating by the sun. Warm and saline water is transported to high latitudes, thereby losing buoyancy due to intense atmospheric cooling. As a result the cooled water becomes unstable, sinks, and recirculates as newly formed deep water towards the equator. Then it slowly diffuses upward throughout the world ocean and returns as a northward flow of warm water (Stommel and Arons, 1960a, 1960b; Wyrtki, 1961). These processes are part of a complex global circulation system with the North Atlantic having a key role. A very simplified circulation schematic is shown in Figure 1.1.

In the present climatic state, the warm poleward branch of the THC in the Atlantic Ocean is responsible for the moderate climate in the northern North Atlantic and northwestern Europe. Both are exceptionally warm for their latitude (Rahmstorf and Ganopolski, 1999). The corresponding northward heat transport across particular latitudes has been calculated by several authors (see Fig. 1.2 and references therein). At 24°N it is in the order of $1.3 \cdot 10^{15}$W (e.g., Hall and Bryden, 1982; Rintoul and Wunsch, 1991; Ganachaud and Wunsch, 2003), in contrast to about $0.8 \cdot 10^{15}$W crossing the same latitude in the Pacific Ocean. Further to the north, the Atlantic Ocean heat transport drops to about $0.6 \cdot 10^{15}$W at 47°N (Macdonald, 1998; Ganachaud and

[I] Wunsch (2002) notes at least seven different 'definitions' for the THC.

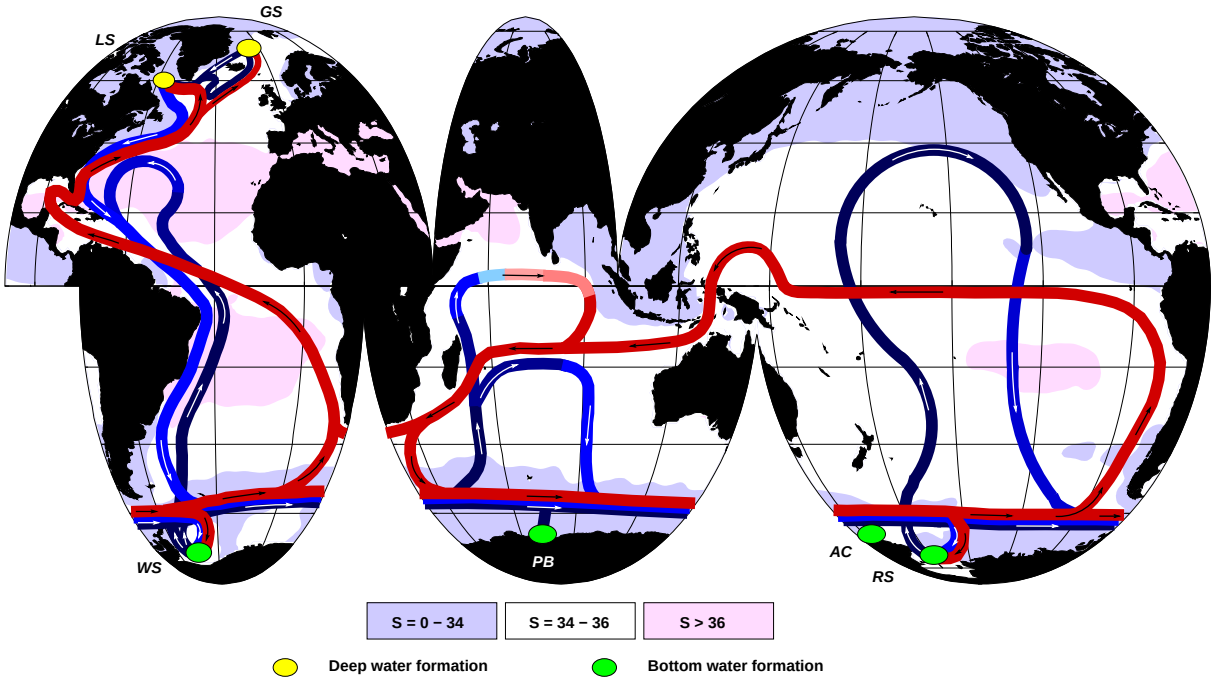

Fig. 1.1.: *Flow scheme of the global thermohaline circulation (the 'oceanic conveyor belt'), modified following* Schmitz *(1996) and* Rahmstorf *(2002). Warm surface currents are given in red colours, while cold deep currents are plotted blue. Ellipses indicate the major sites of deep and bottom water formation (Labrador and Greenland Seas (LS/GS) in the northern hemisphere, Weddell and Ross Seas (WS/RS), Adélie Coast (AC) and Prydz Bay (PB) in the southern hemisphere). Shaded areas denote annual sea surface salinities derived from World Ocean Atlas 1994 climatology (*Levitus *and* Boyer*, 1994).*

Wunsch, 2003) which indicates a major release of heat to the atmosphere (Béranger et al., 2000). To compensate the continuous heat loss at high latitudes, the North Atlantic Ocean imports about $0.7{\cdot}10^{15}$W of heat from both the Pacific and Indian Oceans (e.g., Ganachaud and Wunsch, 2000, 2003).

The lower limb of the THC is closely connected to the formation of deep and bottom water, a process that comprises the transformation of imported surface waters into deep layers located at about 2000 m and deeper. The world ocean is asymmetric concerning possible formation regions. Particularly important for the global deep circulation is the formation of Antarctic Bottom Water (AABW) which occurs at several locations close to the Antarctic continental shelves (cf. Fig. 1.1). Processes involved in the formation include sinking of saline water from the shelf breaks and different scenarios of mixing with adjacent water masses.

The northern hemisphere is the source region for the second important contributor to the global deep circulation. Since there isn't any high latitude part in the Indian Ocean of the northern hemisphere, the only other regions to think of are the North Atlantic and North Pacific. Both oceans differ markedly in salinity, the North Pacific being fresher by

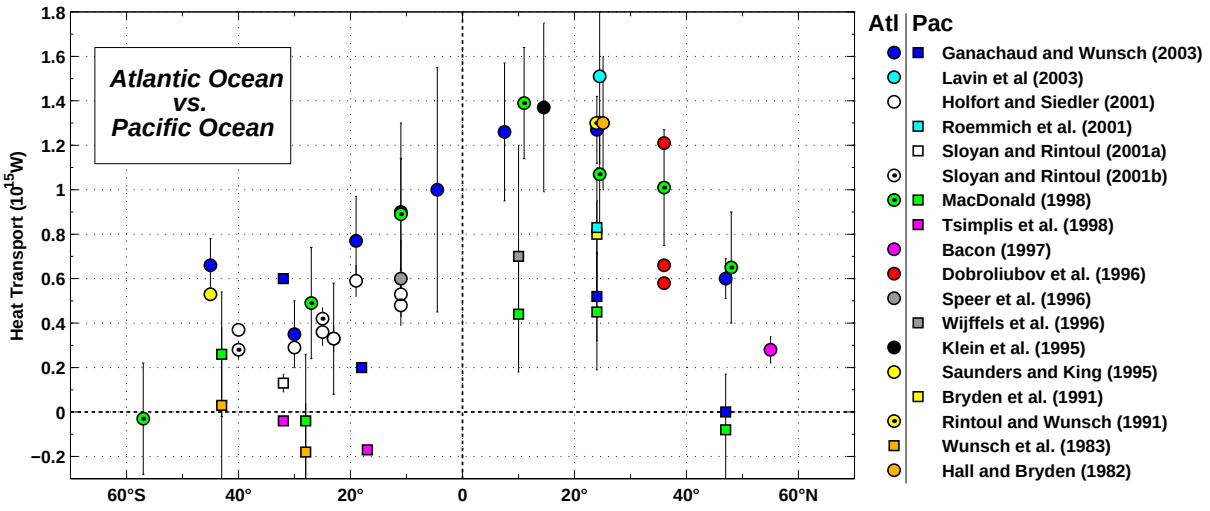

Fig. 1.2.: *Meridional heat transports (10^{15} W) of the Atlantic Ocean (circles) compared to the Pacific Ocean (squares). Calculation was done either directly across particular hydrographic sections or via inverse box models. Positive values denote northward transports. References for the particular estimates are given to the right.*

about 2 psu[II] (Warren, 1983). This difference is not only exhibited at the sea surface, also the salinity contrast between the upper and deep layers of the Pacific Ocean is of the same order (Emile-Geay et al., 2003). Warren (1983) stated, even a reduction of surface temperatures down to the freezing point is not enough to exceed the existing density contrast and initiate deep convection in the North Pacific. Deep convection, however, is one of the key processes involved in deep water formation. Weaver et al. (1999) summarised several reasons for the maintenance of the Pacific salinity contrast: The Mediterranean Sea provides a salty outflow at intermediate depth that contributes to the higher salinities of the high-latitude Atlantic Ocean. The evaporation is almost twice as much over the North Atlantic as over the North Pacific. Water vapour is transported from the Atlantic to the Pacific via the trade wind system which provides a significant freshwater import into the Pacific. Recently, Emile-Geay et al. (2003) suggested that the salinity contrast is sustained by the strength of the Asian monsoons and the associated transport of moisture. As a consequence, prevalent oceanic and atmospheric conditions are responsible for the absence of deep convection and the resulting lack of North Pacific Deep Water formation. Thus, the remaining site allowing the renewal of deep water is the North Atlantic Ocean which is important and unique in terms of oceanic circulation.

The formation of North Atlantic Deep Water (NADW) is subject to a chain of small-scale physical processes that are prominent in only a few regions of the subpolar and northern North Atlantic. The lower and older part of NADW consists of different source water masses. Some of them have their origin in the Nordic Seas (Greenland-Iceland-Norwegian Seas, hence GIN-Seas). These cross the ridge system located between Greenland and

[II]psu: practical salinity units

Scotland as dense slope currents. While overflowing the submarine sills, entrainment of surrounding water leads to an increase in volume transport in conjunction with intense mixing of water masses (Dickson and Brown, 1994; Krauss, 1995). Entrained water masses comprise modified Antarctic Bottom Water, Mediterranean Water, Labrador Sea Water, and Subpolar Mode Water. The overflow water follows the topography due to its high density and forms the bottom water of the subpolar North Atlantic (SPNA).

The upper part of NADW is the result of open-ocean convection which is an important process for the ventilation of the deep ocean. Through this mechanism several atmospheric constituents like oxygen, carbon dioxide, anthropogenic chlorofluorocarbon or bomb tritium are introduced into the deep layers (e.g., Fine, 1995; Gruber, 1998). Open-ocean convection occurs primarily in the Labrador Sea during late winter. Recent investigations by Pickart et al. (2003a, 2003b) re-discovered the southern Irminger Sea as an additional region favouring convective processes. During winter, these two regions are subject to extremes of coldness and wind. The cyclonic atmospheric circulation advects cold and dry air masses of Artic origin over the warmer surface waters. Intense air-sea interaction induces a strong upward heat flux at the sea surface. As a consequence, the water loses buoyancy, the weak density stratification breaks down, and water starts to sink. This process is intermittent and involves horizontal scales ranging from hundreds of kilometers (the size of the preconditioned region) to less than 1 km which is the actual convective plume scale (Marshall and Schott, 1999). The result of this transformation is a thick and homogeneous water mass called Labrador Sea Water (LSW, e.g. Lazier, 1973; Clarke and Gascard, 1983; The Lab Sea Group, 1998).

There are two different varieties of LSW: Classical LSW is the product of intense deep convection acting in the western part of the central Labrador Sea. During the early 1990s mixed layer depths increasing to a depth of 2300 m were observed (Lilly et al., 1999; Lazier et al., 2002). Typical features of classical LSW are minima in potential vorticity and salinity (Talley and McCartney, 1982). It further carries high concentrations of anthropogenic tracers such as chlorofluorocarbon (Smethie et al., 2000; Rhein et al., 2002) making it traceable throughout the SPNA. The lighter variety is called Upper Labrador Sea Water (ULSW). According to Pickart et al. (1996, 1997), its source region is located in the southern Labrador Sea (Fig. 1.3). ULSW is formed here as a result of shallower convection that is affected by the dynamics of the boundary current system. Both water masses, ULSW and the denser classical LSW, are located in the subpolar North Atlantic at intermediate depths (about 500-2000 m). Together with the overflow water masses they leave the SPNA as part of the Deep Western Boundary Current (DWBC) which provides an export route out of the subpolar gyre. NADW participates in the world ocean circulation (Fig. 1.1) and as such is identifiable in the southern Atlantic as well as in the Indian and Pacific Oceans (e.g. Tomczak and Godfrey, 1994).

Today, it appears natural to think that disturbances exerted on physical processes related to NADW formation will have impact on the THC beyond the subpolar gyre. But it is only about sixty years ago that oceanographers were thinking of the oceanic circulation as being steady. Differences between hydrographic casts were attributed to spatial changes rather than to temporal variability (Munk, 2000). In the meantime

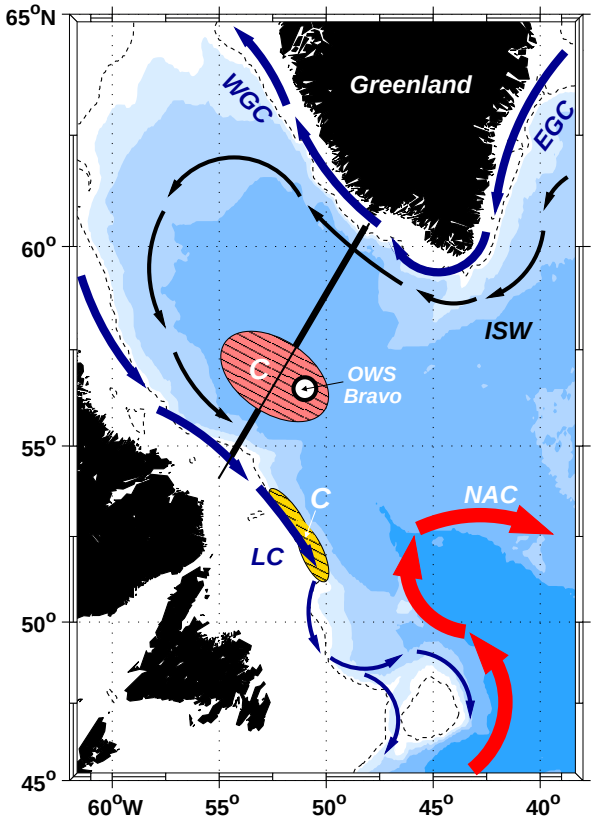

Fig. 1.3.: *Schematic surface circulation of the Labrador Sea with possible convection sites included. Warm and salty circulation branches are indicated by the North Atlantic Current (NAC) and the spreading of Irminger Sea Water (ISW), whereas East/West Greenland (EGC/WGC) and Labrador Currents (LC) are cold and fresh. Convection sites (C) are shown as red and yellow patches (classical Labrador Sea Water and Upper Labrador Sea Water formation, respectively). Bathymetry is shown every 1000 m, dashed lines denote the 500 m-isobath. The figure is adapted from* Marshall *and* Schott *(1999).*

a large number of scientific programmes has been carried out in the SPNA (Fig. 1.4). Among these, the *Ocean Weather Station* (OWS) programme was maintained for a period of about sixty years at isolated locations. The data set from *OWS Bravo*, located in the central Labrador Sea (Fig. 1.3), has been extended by subsequent programmes such as the *World Ocean Circulation Experiment* (WOCE), *Climate Variability and Predictability* (CLIVAR), and *Sonderforschungsbereich 460* (SFB 460). It provides the longest hydrographic time series of this region. One of the findings from the original *OWS Bravo* data set (years 1964-1974) was the occurrence of substantial interannual variability in the wintertime convective activity (Lazier, 1980). For example, during 1969-1971 convection ceased and winter mixed layers only penetrated the upper 200 m. In 1976, however, Clarke and Gascard (1983) observed convection depths reaching 2000 m. The early 1990s showed a four-year period of the most intense convection ever observed (mixed layer depths greater 2300 m, Lilly et al., 1999; Lazier et al., 2002). This was followed by a period of ongoing water mass restratification, leading again to a cessation of deep

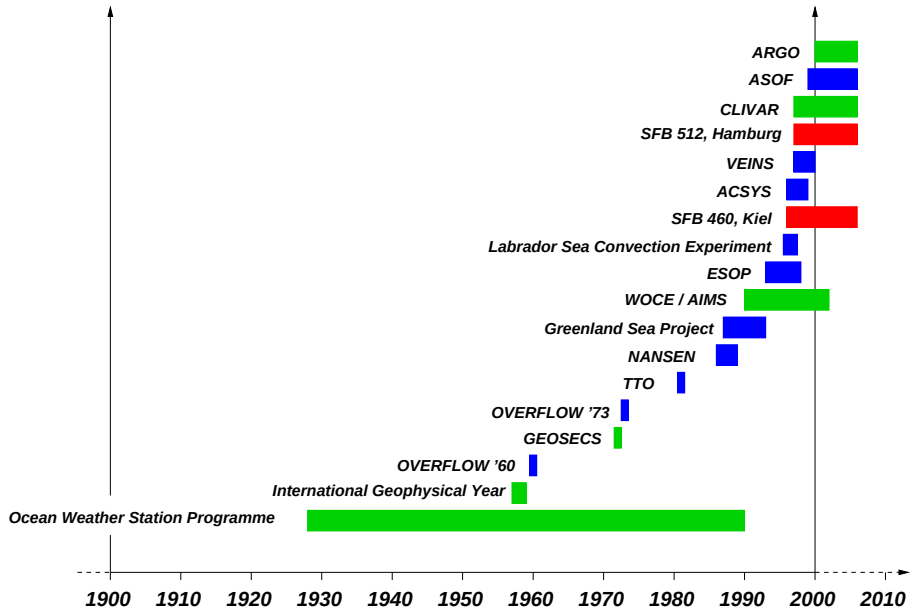

Fig. 1.4.: *A selection of observational field projects that are relevant for subpolar and northern North Atlantic related studies considering its role in and importance for the earth's climate system. Red: national efforts, blue: international efforts, and green: global campaigns having a SPNA component.*

convection (Lazier et al., 2002; Azetsu-Scott et al., 2003; Stramma et al., 2004). Decadal time series of LSW properties such as layer thickness and temperature revealed a clear correlation to variability of convection which in turn is related to large-scale atmospheric circulation variability (Curry et al., 1998). Intense cooling of LSW is a result of increased westerly winds, their strength being represented by the North Atlantic Oscillation (NAO) index (Hurrell, 1995). During years of positive NAO heat is increasingly released to the atmosphere. As the overturning of the water column progresses, this heat loss is distributed downward. Cooling of LSW coincides with a thickening of the layer as a result of LSW renewal. In contrast, a declining trend of the NAO is related to a warming of LSW. This is accompanied by a reduction of LSW thickness.

Beside the variability in heat loss, changes in the freshwater budget do affect the evolution of deep convection. The cessation of deep convection in the Labrador Sea during the early 1970s, for example, has been attributed to the presence of the so-called 'Great Salinity Anomaly' (GSA; Dickson et al., 1988). This GSA refers to an anomalous large import of Arctic freshwater and sea ice via Fram Strait that freshened the Labrador Sea. Belkin et al. (1998) noticed the occurrence of two further GSAs that occupied the Labrador Sea during the 1980s and early 1990s. In contrast to the remotely formed GSA of the 1970s, the two latter resulted locally from severe winter conditions exerted on the Labrador Sea/Baffin Bay, supplemented with a possible contribution of the Arctic freshwater outflow via the Canadian Archipelago.

The acquisition of data on water mass formation and associated variability by conventional oceanographic observation methods is not an easy task. Additional information is

provided by a hierarchy of numerical general circulation models. Among coarse to high resolution models there is, however, a strong discrepancy concerning likely implications of convection variability on the THC. Several coupled ocean-atmosphere models with a medium to coarse resolution show a strong link between convection activity in the subpolar North Atlantic resulting from heat and freshwater anomalies and the strength of the thermohaline overturning (e.g. Delworth et al., 1993; Weisse et al., 1994; Wood et al., 1999; Cheng and Rhines, 2004). Model studies carried out e.g. by Manabe and Stouffer (1995), Schiller et al. (1997), and Vellinga and Wood (2002) demonstrated that the THC can be considerably weakened if an increased freshwater flux is added to the upper layers of the SPNA. Cheng and Rhines (2004) noticed a further decrease of 3 to 5 Sv[III] in the modeled meridional overturning circulation (MOC) when the freshwater flux is shifted from the Fram Strait to the southern Baffin Bay area. Sensitivity studies with high-resolution simulations indicated that the subpolar circulation in these models is essentially dependent on the representation of outflows from the Nordic Seas (Böning et al., 1996; Döscher and Redler, 1997; Redler and Böning, 1997; Roberts and Wood, 1997; Beismann and Barnier, 2004). Especially a proper implementation of the Denmark Strait Overflow Water (DSOW) is necessary, whereas convective mixing has only a minor influence on net-sinking of upper layer waters in this region.

While variability in the formation of LSW is mainly subjected to local processes, this does not necessarily hold for the lower part of NADW that comprises the system of entrainment and overflow water masses. By analysing longterm hydrographic records Dickson et al. (2002) noticed a substantial freshening of the deep and abyssal SPNA over the past four decades. Time series from various regions of the SPNA indicated that this freshening spread along known deep water pathways and occurred basin-wide. The authors identified a large-scale and persistent salinity decrease in the upper 1000-1500 m of the Nordic Seas as the likely source for the observed trend in the SPNA. Curry et al. (2003) presented further evidence that is suggestive of a systematic freshening at both poleward ends of the Atlantic Ocean. This is contrasted to a salinity increase in the upper ocean layers located at low latitudes. Hansen et al. (2001) found considerable variability in the strength of the overflow crossing the Greenland-Scotland ridge. Using direct measurements and historical hydrographic data the authors presented evidence that the volume flux of the Faroe Bank channel overflow decreased by 20 % during 1950 to 1999. In contrast, the Denmark Strait overflow was found apparently stable on interannual time scales (Dickson and Brown, 1994). Recent analysis of further overflow time series, however, revealed interannual fluctuations in terms of volume transport, plume thickness, and temperature (A. Macrander, IFM-GEOMAR Kiel, pers. comm., 2004). Hansen et al. (2001) and Dickson et al. (2002) rose the question whether the observed changes already indicate the onset of global change.

Recently, Wu et al. (2004) succeeded in reproducing a similar freshening trend as observed by Dickson et al. (2002) and Curry et al. (2003). They used an ensemble of four simulations with a coupled atmosphere-ocean-sea ice model, run at medium ocean

[III] 1 Sv = 1 Sverdrup = 10^6 m^3/s.

resolution (1.25°×1.25°). Wu and co-authors were able to trace the origin of the freshening trend to the Arctic Ocean where sea surface salinity was reduced due to increased melting of sea ice and river runoff. However, the THC accompanying the freshening trend unexpectedly showed an upward trend rather than a decrease. In the model ensemble Labrador Sea convection intensified without being associated to any change in the NAO.

Against this background, measuring, modeling and understanding variability exerted on currents and water masses of the SPNA remains an important task for the oceanographic community. Having started in 1996, a comprehensive multi-parameter data set has been compiled as part of the German scientific project *Sonderforschungsbereich 460* (SFB 460), entitled "Dynamics of thermohaline circulation variability". SFB 460 is affiliated to the "Leibniz-Institut für Meereswissenschaften IFM-GEOMAR"[IV] located in Kiel, Germany. The data set comprises profiles of conventional hydrographic parameters (salinity, temperature, pressure, oxygen), anthropogenic tracers such as chlorofluorocarbon (CFC), as well as velocity profiles directly measured by means of Acoustic Doppler Current Profilers (ADCP). These have been taken almost annually during 1996 to 2001.

The present study is part of the SFB 460 sub-projects *A4* and *A7*. *A4* aims at investigating the variability of water masses and the associated circulation in the western subpolar North Atlantic. *A7* deals with the large-scale communication of water mass signals between the western and eastern basins. Based on the SFB 460 data set Stramma et al. (2004) traced signals of water mass variability from the Labrador Sea to the Newfoundland Basin, thereby concentrating on the boundary current region. One of the results was the detection of a considerable increase in ULSW formation that originated in the interior Labrador Sea during the late 1990s. ULSW formation, previously, was not observed in this region (Pickart, 1992; Pickart et al., 1996, 1997). Using data from 1997, Rhein et al. (2002) calculated the large-scale inventory of chlorofluorocarbon (CFC, component CFC-11) in the classical LSW and calculated corresponding LSW formation rates. CFCs belong to the group of anthropogenic tracers that have been released to the atmosphere since the early 1930s (Bullister, 1989). They enter the oceans via gas exchange and are helpful for the identification of water masses, their respective spreading pathways and their age. Since their atmospheric history is known, they are considered as transient tracers.

The CFC data set available to Rhein et al. (2002) has been extended by two additional large-scale field campaigns carried out in 1999 and 2001. Data from these three years provide the basis for many analyses introduced in the present study. Here, the focus is on estimating the variability in the formation of ULSW and reveal corresponding spreading pathways in the western SPNA. Similar calculations have been made for the denser classical LSW.

At first, a review concerning general circulation features and water masses of the SPNA is given (Chapter 2). The method to derive CFC inventories and formation rates for ULSW and classical LSW is introduced in Chapter 3. Horizontal distributions of layer thickness and CFC-11 are used highlight the spreading pathways within the SPNA. Changes

[IV] Since January 2004 IFM-GEOMAR is the successor of the former *Institut für Meereskunde Kiel*.

in the ULSW evolution are discussed and compared to changes in the denser classical LSW. Chapter 4 presents analyses of water mass variability on interannual to decadal scales. Changes in the water mass properties of ULSW and LSW are investigated by means of decadal time series. These are derived from historical stations located in the source region, i.e. , the central Labrador Sea. Changes in the water mass properties are compared and related to changes occurring in the surface forcing. Chapter 5 provides results on tracing the spreading of deep water components into the Newfoundland Basin. Observations are presented that point to the existence of deep water export routes that are additional to the DWBC. Decadal time series for ULSW and classical LSW in the DWBC region of the Newfoundland Basin are presented and correlated to time series of the central Labrador Sea. Finally, conclusions are drawn on likely impacts of the results and remaining questions.

Note

In the following, all given temperatures refer to the potential temperature Θ (°C), if not otherwise stated. The potential temperature is the effective temperature of a water parcel after subtracting a warming which is attributed solely to compression. A water parcel, lifted from the deep to the sea surface, will expand and cool due to the compressibility of water, which is very small, but nevertheless present. This effect is corrected through the introduction of Θ. It allows to compare temperatures of water masses at different depth levels (Pond and Pickard, 1983). The in situ density ρ (kg/m^3) is calculated as a function of salinity, in situ temperature, and pressure. The potential density σ_Θ is given as $\sigma_\Theta = \rho(S, \Theta, p) - 1000$ kg/m^3.

2. Circulation and Hydrography of the Subpolar North Atlantic

The present chapter introduces the main topographic and hydrographic characteristics of the subpolar North Atlantic. The major water masses in conjunction with their circulation pathways and likely driving mechanisms of the oceanic circulation are summarised. This provides the background for the analyses of deep water formation, associated variability and spreading pathways, discussed in the present study.

2.1. The importance of bottom topography

Framed by the European and North American continents, the subpolar North Atlantic (SPNA) covers the region from ∼40°N to ∼66°N. The sea floor exhibits a large variety of different topographic characteristics which have strong impact on the circulation of water masses. The dominant feature is the Mid-Atlantic Ridge (MAR), a huge submarine mountain range with the crest located more than 1700 m below the sea surface. It divides the SPNA into a series of deep eastern and western basins (Fig. 2.1). Its northward extension, the Reykjanes Ridge, runs from about 52°N in northeastern direction to Iceland. The continuity of the MAR is disturbed by several fracture zones. Having a sill depth of 3600 m, the Charlie-Gibbs Fracture Zone (CGFZ), located at the southern tip of the Reykjanes Ridge (∼32°W/52°N), is the deepest fracture zone of the SPNA. It provides a significant connection between the deep basins on both sides of the ridge system, thus allowing an inter-basin exchange of surface to deep water masses. For water masses located deeper than the sill depth the MAR system marks a natural barrier. As the MAR continues southward to the Azores, a series of shallower fracture zones exists (e.g. Faraday-, Maxwell-, and Kurchatov Fracture Zone with sill depths of about 3000 m, 2600 m, and 2200 m).

On both sides of the MAR, abyssal plains with water depths greater than 4800 m span to the western and eastern continental slopes (Newfoundland Basin and the West European Basin). The slopes, in turn, ascend towards the broad continental shelves. To the north, the deep SPNA flattens and finally is locked up by narrow and shallow sills that provide the only connection to the Arctic Ocean. West of Greenland, the Davis Strait (sill depth ∼ 650 m) connects the Labrador Sea to the seas of the Canadian Archipelago. Its pendant to the east of Greenland is the Denmark Strait (sill depth ∼ 600 m) which

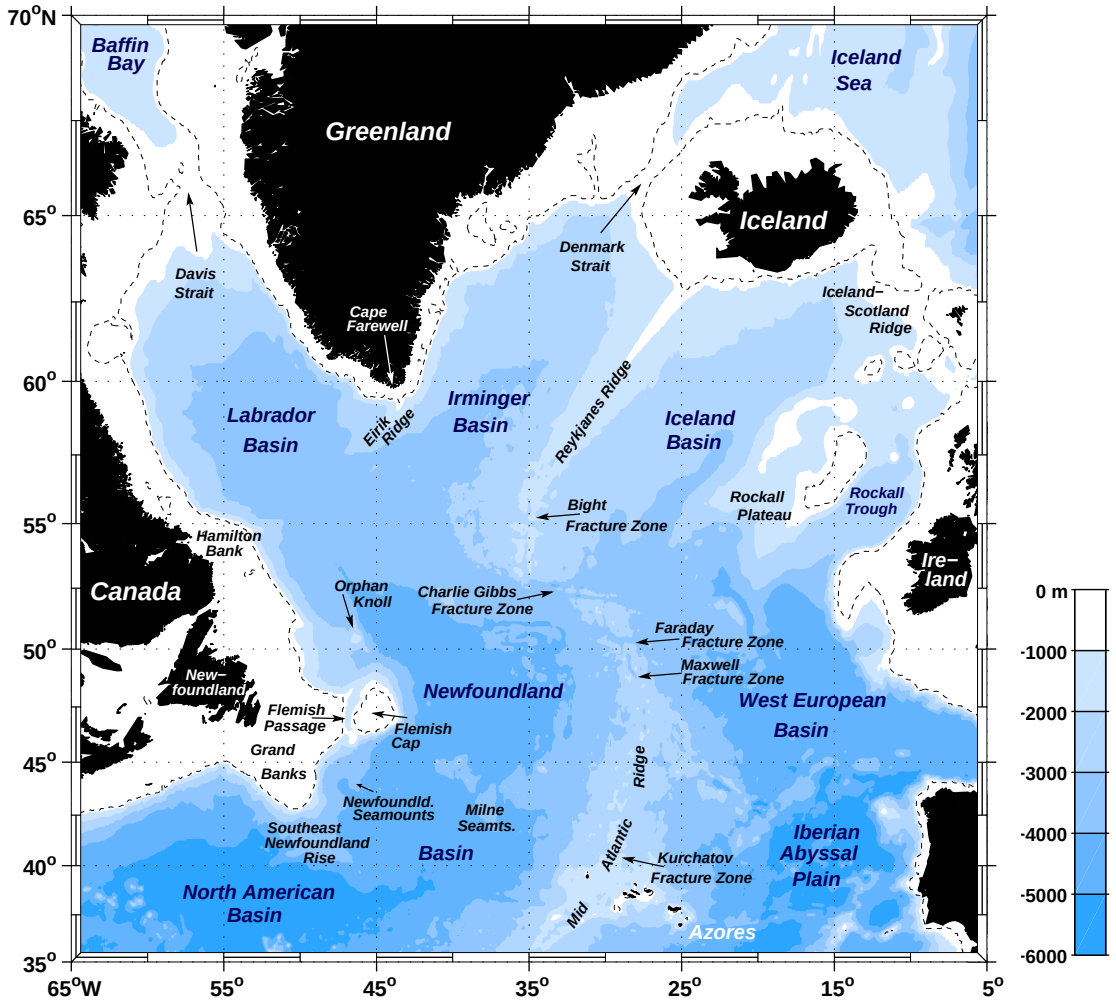

Fig. 2.1.: *Bottom topography of the subpolar North Atlantic derived from the TerrainBase Global Digital Terrain Model, gridded at 5-minute intervals. Dashed lines indicate the 500 m-isobath.*

links the Irminger Basin and the Iceland Sea. Southeast of Iceland, Denmark Strait sill continues as Iceland-Scotland Ridge (sill depth about 400-800 m). It marks the natural barrier between the Iceland Basin/Rockall Trough and the Norwegian Sea. The intermediate to bottom waters of the SPNA are captured in a series of deep basins which inhibit their export to the Arctic Ocean. To the south, however, the exchange of the SPNA with the subtropical North Atlantic is not prevented by any larger submarine sills. Nevertheless, several isolated seamounts, outliers of the MAR, exist. The topography has thus an important impact on restricting and steering the flow and spreading of North Atlantic water masses.

2.2. Circulation Pathways in the Subpolar North Atlantic

The subpolar gyre of the North Atlantic is formed by a complex system of currents that distribute different water masses. The top-to-bottom circulation can be split into two distinct systems: a surface and an intermediate to deep water circulation. Circulating upper and deep waters are connected via physical processes dealing with e.g. water mass transformation, deep convection, entrainment, vertical mixing. The upper flow is subject to intensive atmosphere-ocean interaction (e.g. influence of the atmospheric wind field, oceanic heat loss to the atmosphere, uptake of anthropogenic tracers like chlorofluorocarbon). The deep flow in general redistributes the water mass products of high latitude origin.

While there is a large amount of direct information about the upper layer circulation, movements in the deep ocean have largely been deduced from the distribution of water masses and their respective properties (Pickard and Emery, 1990). Throughout the past century, the pathways of the major currents have been identified quite well. The strength and variability of both current systems is, however, still insufficiently known.

2.2.1. Surface Circulation

The surface circulation of the SPNA is strongly influenced by the Gulf Stream that enters the SPNA at about 50°W (cf. Fig. 2.2). After having reached the southeastern tip of the Grand Banks south of Newfoundland, the Gulf Stream continues offshore of the Grand Banks towards the northeast, now termed North Atlantic Current (NAC). It meanders along the course of the continental shelf edge and is now an active player in the large-scale circulation of the SPNA. A further branch, the Azores Current, splits south of the Southeast Newfoundland Rise (SENR), flows to the southeast and extends into the Gulf of Cadíz near Spain (Sena Martins et al., 2002). This current, however, is not part of the subpolar gyre. Meinen et al. (2000), Meinen (2001), and recently Schott et al. (2004) investigated the absolute strength of the NAC to the north of the SENR using different sets of methods (moorings, repeated hydrography, inverted echo-sounders equipped with pressure sensors, floats, ADCPs). The associated northward transport from top to bottom was in the order of 120-140 Sv. The overall impression is that of a swift current with velocities exceeding 70 cm s^{-1} at the sea surface. The NAC is, however, not restricted to the surface but rather reaches from top to bottom, still featuring up to 10 cm s^{-1} close to the bottom (e.g., Meinen, 2001).

Kearns and Rossby (1998) quantified the path of the NAC within the Newfoundland Basin. Based on historical hydrographic data, they calculated two-dimensional distributions that describe the probability of finding dynamical and property fronts offshore of a given 0.5° box. The fronts were observed to have a stationary meander pattern of 300 km wavelength that is topographically controlled. Several troughs, previously suggested by Rossby (1996), emerged that are locked in space over the Flemish Cap, the

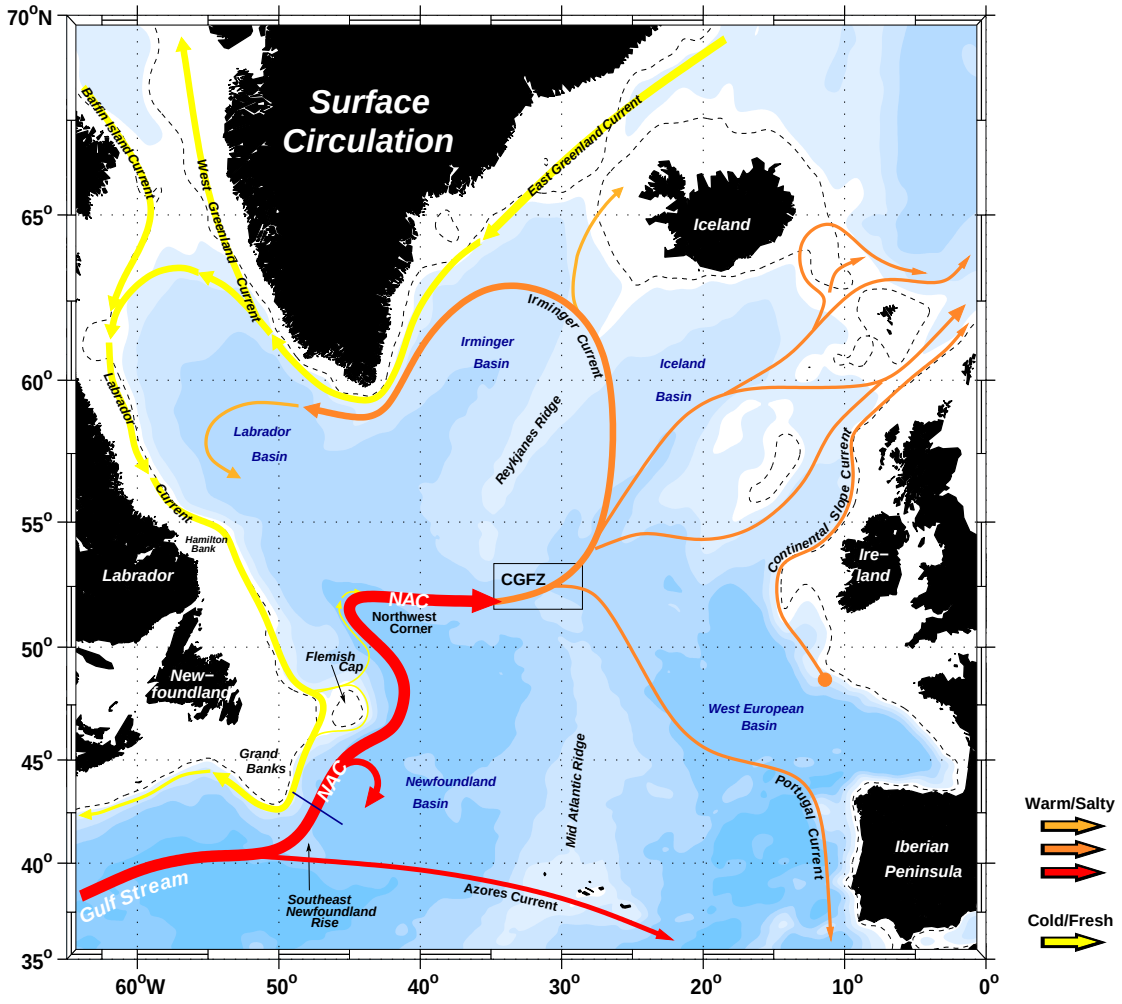

Fig. 2.2.: *Sketch of the near-surface circulation in the SPNA. The underlaid bottom topography is smoothed and contoured every 1000 m, the dashed line indicates the 500 m isobath. CGFZ: Charlie Gibbs Fracture Zone, NAC: North Atlantic Current.*

SENR, and the Newfoundland Seamounts. Recirculation cells are located adjacent to the NAC (Fratantoni, 2001; Pérez-Brunius et al., 2004). The *Mann Eddy* (Mann, 1967; Worthington, 1976) is centered at 42°N, 44°W (Fig. 2.2). The *Northwest Corner* steers recirculation at 52°N (Fratantoni, 2001; Bower et al., 2002). Based on surface drifters and CTD casts Lazier (1994) found this retroflection of the NAC to be highly variable in its intensity as well as in its path. White and Heywood (1995) and Fratantoni (2001) identified the Newfoundland Basin including the Northwest Corner as a region of high eddy kinetic energy (EKE) exceeding 500 cm^2/s^2.

Heading to the east the NAC flows in a zonal band towards the eastern basins of the SPNA. Its pathway is associated with the location of the Subpolar Front (SPF) which exhibits strong temperature gradients at 200 m (Rossby, 1996). As the NAC approximates the MAR, it converges to cross above the Charlie Gibbs and Faraday Fracture Zones (e.g., Arhan, 1990, Sy et al., 1992; Bower et al., 2002; Pérez-Brunius et al., 2004). Based

on geostrophic calculations referenced to 2000 m Sy et al. (1992) found 26 Sv crossing the MAR between the SPF and the Azores. Occasionally, the NAC is locked further to the north above CGFZ (Belkin and Levitus, 1996). The NAC modulates the deep water flow below, since eastern deep water masses are detained from entering the western basin through CGFZ during blocking events (Saunders, 1994; Schott et al., 1999).

Having reached the eastern basins, the NAC divides into several branches (Dietrich et al., 1975). By means of satellite-tracked drifters Sena Martins et al. (2002) identified the southward Portugal Current as a slow and variable circulation feature located between continental Portugal and the Azores. Two branches of the NAC cross the Iceland-Scotland Ridge by taking the route via the Iceland Basin and Rockall Trough (Fratantoni, 2001). Another branch returns in a big cyclonic loop to the Irminger Sea, hence called Irminger Current. According to Reverdin et al. (2003) the latter is associated with low EKE. Based on referenced geostrophy, Käse and Krauss (1996) give transports of 6 Sv for each of the northward branches.

The Continental Slope Current is directly located at the European Shelf. It carries the warmest and most saline water across the Greenland-Scotland Ridge and, thus, contributes to the salt budget of the Nordic Seas. According to Hansen and Østerhus (2000), it is not directly linked to the NAC. Its origin is supposed to be located off the Armorican Slope west of France. Here, the water gains its high salinity probably by winter cooling at constant temperature (Pollard et al., 1996).

Besides the supply of warm and salty surface waters, currents of Artic origin transport cold and and fresh waters into the SPNA. The East Greenland Current (EGC) enters the SPNA at Denmark Strait, follows the course of Greenland, and exits the Labrador Sea as the West Greenland Current (WGC). In the velocity field derived from surface drifters Fratantoni (2001) could not distinguish between the warm and salty Irminger Current and the cold and fresh EGC located onshore. Drifter analysis by Reverdin et al. (2003), however, indicated a sharp front located offshore of the East Greenland shelf break which is associated with a velocity maximum.

The topographical steering of the EGC/WGC is interrupted by the Eirik Ridge, located south of Greenland. West of Cape Farewell (Greenland's southern tip) the slope regions considerably steepens. While heading along the Greenland Shelf, the WGC accelerates, is partially detached from the slope, and becomes barotropically unstable (Eden and Böning, 2002). Centered at about 62°N, 52°W, it features a prominent patch of enhanced eddy intensity (e.g., Fratantoni, 2001; Cuny et al., 2002; Lilly et al., 2003). This patch extends into the interior Labrador Sea. Eddies shed from the WGC carry warm and salty Irminger Sea Water (ISW) into the interior basin (Prater, 2002; Lilly et al., 2003). Katsman et al. (2004) demonstrated that these eddies are important for the water mass transformation located in the Labrador Sea. They are efficient in altering the heat budget of the Labrador Sea and restratify the water column after deep convection.

On the opposite site of the Labrador Sea, the Baffin Island Current enters the SPNA, passes into the Labrador Current, which in turn exits the SPNA at about 43°N. The Labrador Current is concentrated over the break and upper slope of the Labrador Shelf (Lazier and Wright, 1993). It carries a mixture of cold and fresh water masses that

originate in the Canadian Archipelago and in the Hudson Bay. Additionally, ISW is imported from the WGC (Loder et al., 1998) which causes an intermediate salinity maximum located at 100-500 m underneath the freshwater cap (Fig. 1.3). Brandt et al. (2004) noticed an EKE maximum present in the Labrador Current north of 56°W. They attributed the observed annual harmonic of the EKE to local processes and suggested the instability of the Labrador Current as a likely cause. Recently, Lavender et al. (2000) revealed the existence of cyclonic recirculation cells located offshore of the rim current system at mid-depths (700 m). These constitute a flow that is opposite to the boundary currents and lead to an anticyclonic flow in the interior Labrador Sea. The interior counterflows have been revealed by surface drifters as well (Cuny et al., 2002). Studies by Straneo et al. (2003) indicated the importance of the recirculation cells for determining the pathways and timing the spreading of Labrador Sea Water.

The surface current system of the SPNA is, thus, dominated by a large-scale cyclonic gyre with warm and saline subtropical waters entering the northeastern Atlantic and subsequently recirculating to the north and west where they interact with cold and fresh waters of Arctic origin.

2.2.2. Deep Water Circulation

The deep circulation of the North Atlantic is fed by cold and dense water masses which cross the Denmark Strait sill and the Iceland-Scotland Ridge, hence called overflow water masses. They follow the western sides of the Iceland, Irminger, Labrador and Newfoundland Basins as pronounced deep northern and deep western boundary currents (DNBC/DWBC) and feed the cold limb of the global thermohaline circulation (Gordon, 1986; Broecker, 1991). A circulation schematic is shown in Figure 2.3.

The Denmark Strait Overflow Water (DSOW) is the deepest and densest layer of the DWBC. It enters the subpolar gyre by overflowing the sill of the Denmark Strait. Based on mooring data (month-long deployment during summer 1973), Ross (1984) reported about 2.9 Sv of water colder than 2°C crossing the Denmark Strait sill. Entrainment of surrounding waters near the sill and farther south results in a strengthening of transport (Dickson and Brown, 1994). One of the few available transport estimates for the deep boundary current passing the southern tip of Greenland gave 13.3 Sv (Dickson and Brown, 1994, herein R. A. Clarke, BIO, Dartmouth). This estimate was based on a currentmeter array (three moorings with a total of six instruments), deployed from February to April 1978 (Clarke, 1984). Calculation was done for water masses denser than $\sigma_\Theta = 27.80$ kg/m^3, thus including layers which lie on top of DSOW and originate in the eastern North Atlantic. More recent estimates from 1991 on the basis of inverse techniques combined with shipboard-Acoustic Doppler Current Profiler (ADCP) measurements gave only 5.5 Sv at nearly the same location (Bacon, 1997).

The DWBC layer which overlays the DSOW is fed by waters that originate in the Norwegian Sea and cross the Iceland-Scotland Ridge (about 2.7 Sv, Dickson and

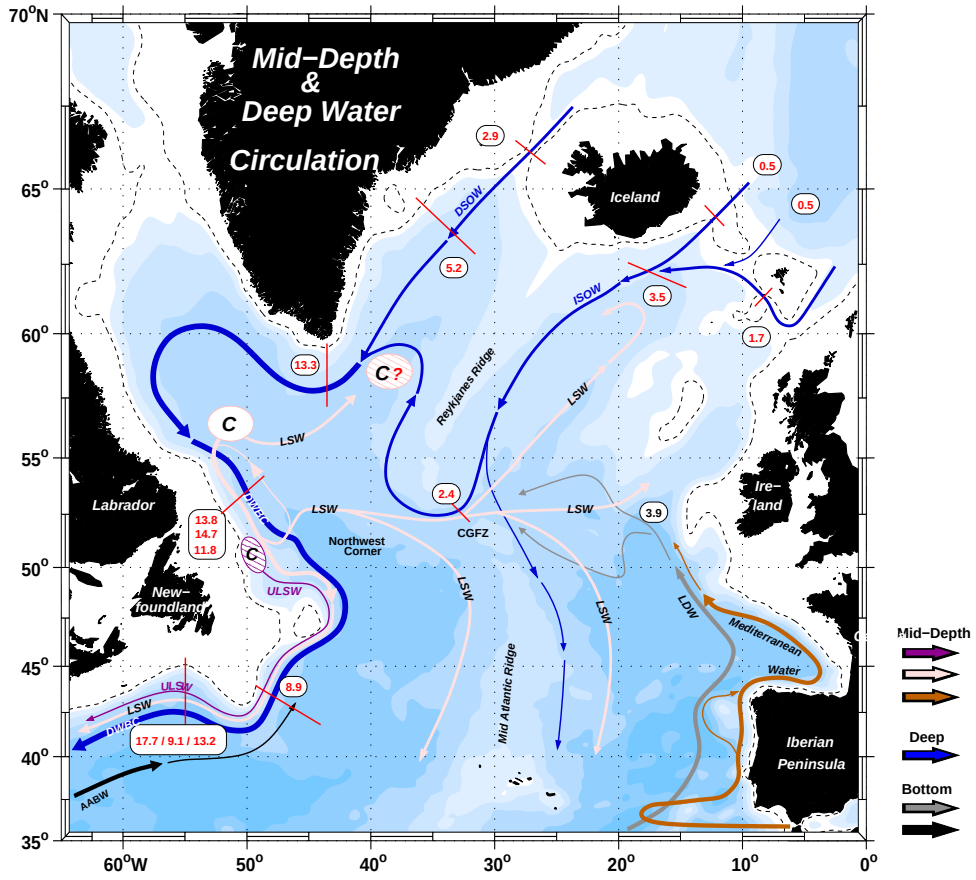

Fig. 2.3.: *Sketch of the intermediate to deep circulation in the SPNA. Given numbers denote deep water transport estimates (in Sv) for water masses denser than* $\sigma_\Theta = 27.80$ *kg/m*^{3}*, indicated by the blue arrows. Estimates are from various sources and based on combined hydrographic and mooring data or mooring data alone. See text for details. AABW: modified Antarctic Bottom Water, C: Convection region, CGFZ: Charlie Gibbs Fracture Zone, DSOW: Denmark Strait Overflow Water, DWBC: Deep Western Boundary Current, ISOW: Iceland Scotland Overflow Water, LDW: Lower Deep Water, LSW: Labrador Sea Water, ULSW: Upper Labrador Sea Water. Dashed lines indicate the 500 m isobath.*

Brown, 1994). Entrainment of salty and warm water of the Northeast Atlantic leads to a transport increase also in this region. The overflow water follows the slope of the Reykjanes Ridge in southward direction (see Fig. 2.3), and about 2.4 Sv enter the western Atlantic basins through the Charlie Gibbs Fracture Zone (CGFZ) (Saunders, 1994, estimated by moored instruments deployed during 1988/89). Tracer observations, however, show that parts of the overflow water (2.4-3.5 Sv) remain in the eastern Atlantic (Fleischmann et al., 2001). Following Worthington (1970, 1976) and McCartney and Talley (1984), the so-called Gibbs Fracture Zone Water (GFZW) flows along the Reykjanes Ridge into the Irminger Sea where it encounters and overlays the dense DSOW. As pointed out by Clarke (1984), part of the GFZW might also flow more directly from the CGFZ into the Labrador Sea.

Recent measurements of the absolute combined flow of GFZW and DSOW in the DWBC region of the western Labrador Sea (∼53°N) yielded 13.8 Sv, 14.7 Sv and 11.8 Sv (Fischer et al., 2004). While the first estimate is based on a comprehensive mooring array deployed during 1997-1999, the second estimate comes from six combined LADCP-surveys undertaken during summers 1996 to 1999 and summer 2001. The third estimate is from combined geostrophic calculations of the same years, referenced to moorings and floats drifting at 1500 m. Schott et al. (2004) traced the overflow water masses at the southwestern exit of the subpolar North Atlantic (DWBC region at ∼43°N) by means of combined mooring data of the periods 1993-1995 and 1997-1999, yielding a mean of 8.9 Sv of water denser than $\sigma_\Theta = 27.80$ kg/m^3 that is exported to the south.

The longest continuous current meter records lasting two years and more and allowing transport calculations are located south of the Denmark Strait (Dickson et al., 1990; Dickson and Brown 1994), in the western Labrador Sea (∼53°N, Fischer et al., 2004), and in the southern Newfoundland Basin at about 43°N (Clarke et al., 1998; Schott et al., 2004). Most of the records from other sources (e.g. Lazier and Wright 1993, western Labrador Sea) and from other regions (e.g., CGFZ) lasted only one year (Saunders, 1994) or were even shorter. From a mooring arrays deployed during September 1986 to August 1991 to the east of Greenland, Dickson and Brown (1994) concluded that the overflow in the Irminger Sea had been apparently stable. Variability rather happened on short time scales (1-12 days). Signals of seasonal variability were missing, and interannual variability, depicted from comparable 30-days averages at different Irminger Sea locations in the period 1987-1991, had been weak. Transport time series, however, have not been given by the authors. Saunders (2001) carried out a revision of these particular mooring time series and found several persistent events during late 1988 and early 1989, when the overflow transport decreased to almost zero. These events have not been reported before by Dickson and Brown (1994). Repeated investigations at the Denmark Strait sill 25 years after the "OVERFLOW '73" experiment showed again 2.9 Sv (Girton et al., 2001), as was previously estimated by Ross (1984). This led to their conclusion that the Denmark Strait Overflow is unchanging and hydraulically controlled on time scales longer than a few days. Recent findings by Macrander and Käse (2004), however, indicated a significant decrease in the overflow transport in the period September 1999 to July 2003. Time series derived from moored ADCPs and inverted echo sounders revealed a volume transport that decreased from 3.9 to 3.0 Sv.

In contrast to the Denmark Strait overflow, Hansen et al. (2001) found a significant reduction of the overflow branch flowing through the Faroe Bank Channel between Iceland and Scotland. From 1950 to 1999 it decreased by 0.5 Sv which is 20% of its assumed overflow transport. The transports were indirectly inferred from an observed longterm change in overflow layer heights above sill depth which is assumed to be proportional to the overflow flux.

Bacon (1997) concluded that there might be changes in the deep water flow on decadal scales which have not been revealed yet due to the lack of long-term measurements. By investigating historical baroclinic transports from the Irminger Sea as an index of the strength of the DWBC, Bacon (1998) showed that the baroclinic component of

the deep boundary current system revealed large variability in the period 1955-1996. Transports were low in the 1950s-60s, high in the late 1970s and early 1980s and then low again. Taking changes in the winter mean air temperature from the central Greenland-Iceland-Norwegian Sea during the same period into account, the author suggested that the transport changes might be linked to processes happening in the Arctic. By applying inverse methods to hydrographic sections from the years 1957, 1982, and 1993, Koltermann et al. (1999) found transport variability in the DWBC southeast of Newfoundland (Grand Banks), which seemed to coincide with the results from Bacon (1998).
Similar to Bacon (1998), Kieke and Rhein (2004) reconstructed baroclinic time series of the deep water transport in the western Labrador Sea. A comparison to reconstructed time series from the Irminger Sea did not reveal consistent signals of transport variability. Also a correlation to the NAO remained ambiguous. The exhibited variabiality in both time series was rather difficult to interpret since several sources of uncertainty are included in the estimates. Among these is the occasional presence of eddies that vertically shift the isopycnal $\sigma_\Theta = 27.80$ kg/m^3. This was defined as the upper boundary of the deep water flow. Entrainment variability and/or blocking events in the CGFZ could further obscure a correlation.

Analyses by Pickart and Smethie (1998) focused on repeated hydrographic/velocity sections across the DWBC further downstream (55°W, south of Grand Banks). During the years 1991, 1994, and 1995 the DWBC transport succumbed to significant variability (17.6 Sv, 9.1 Sv, and 13.2 Sv respectively, for water denser than σ_Θ =27.80 kg/m^3). Taking the mean of these three snapshots, as Pickart and Smethie (1998) have done, results in a value of 13.3 Sv, comparable to the transport calculated by Clarke (1984) during 1978 south of Greenland.

The dense NADW components dominate the near-bottom layers of the western SPNA north of 40°N, whereas modified Antarctic Bottom Water (AABW) and Lower Deep Water (LDW) enter the subpolar gyre at its southern limits and replaces the NADW. These are introduced in the next Section.

Circulation at intermediate depths

Figure 2.3 summarises the major surface currents and spreading pathways of various intermediate, deep and bottom water masses. The circulation at intermediate depths (about 500-2000 m) is dominated by the spreading of Upper and classical Labrador Sea Water as well as Mediterranean Water (MW). These are reviewed in detail in the following sections. The flow of Mediterranean Water, illustrated in Figure 2.3 is adopted from Iorga and Lozier (1999), the flow of the Lower Deep Water (LDW), sometimes called Easter Basin Bottom Water (EBBW), is taken from Fleischmann et al. (2001). The formation region and spreading pathways of Upper Labrador Sea Water (ULSW) are described by Pickart (1992) and Pickart et al. (1996, 1997). The presumption of a deep convection area located in the Irminger Sea was recently discussed by Pickart et al. (2003a, 2003b).

2.3. Water Masses of the Subpolar North Atlantic

"The deep and bottom waters are of a remarkably uniform character all over the Atlantic Ocean, as is evident from the excellent agreement between values of temperature and salinity which have been determined in different regions by different expeditions." (Sverdrup et al., 1942).

Throughout the last 60 years, knowledge about the water mass structure has become more detailed. On the one hand, both measurement technology and its precision have improved. On the other hand, the availability of spatially and temporally well-resolved observational data has increased. During the first half of the 20th century, oceanographers already knew about different deep to bottom water masses of Arctic or Antarctic origin present in the SPNA. Only about 50 years before, analyses of hydrographic data from the world-wide "HMS Challenger Oceanographic Expedition" (1872-1876) ended so far existing speculations on a continuous decrease of temperature with depth (Buchan, 1886; Buchanan, 1895). Instead alternating layers of different salinities and temperatures were revealed (see historic review in Krauss, 1996). A century later, a large variety of surface to bottom waters, located and formed in the SPNA are known, pointing to a variety of processes involved in their formation. An overview of the major water masses relevant for this study is given in Figure 2.4, followed by a review of their origin and properties.

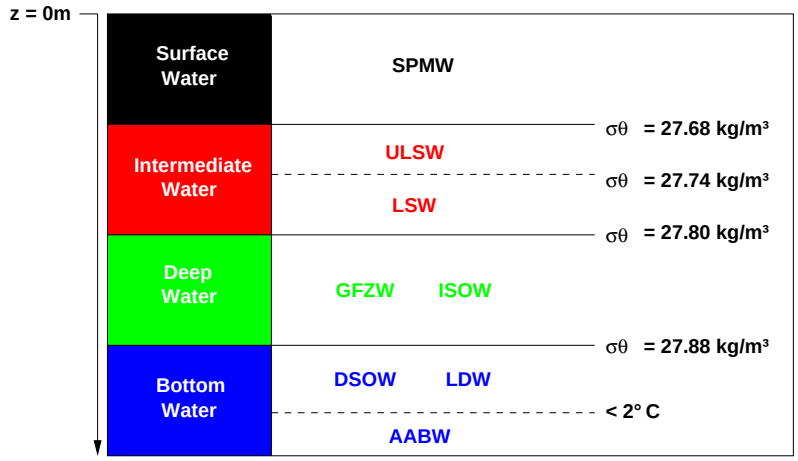

Fig. 2.4.: *Schematic overview of major water masses present in the western subpolar North Atlantic.*

2.3.1. Surface Water: SPMW

The SPNA is one of the regions of the world where the ocean exhibits a very thick wintertime mixed layer. This is one of the features characteristical for mode water formation (Hanawa and Talley, 2001). Mode Water is a layer of water distributed over a large

geographical area that has very low static stability and hence low potential vorticity[I]. Among the different mode waters, Subpolar Mode Water (SPMW) has the highest densities (σ_Θ = 26.9-27.75 kg/m^3). After its formation during late winter it is capped by the seasonal thermocline due to incident solar radiation and advected away from its source regions. According to McCartney and Talley (1982), SPMW originates as a warm (14-15°C) and thick layer in the NAC loop. It is advected south of the NAC to the eastern Atlantic, hence becoming colder and denser. SPMW with a temperature of 11-12°C then splits into a southward and a northward flow. The latter is the inflow of warm surface water into the subpolar gyre. On its further way, cooling as well as increase in density continue. SPMW is thought to split once more into a branch that exits into the Nordic Seas. Another branch circulates into the Irminger Sea and then into the Labrador Sea where it provides the source waters for LSW production (Talley and McCartney, 1982).

Talley (1999) suggested a major refinement to this picture of SPMW transformation and circulation. By comparing data from the 1950s to 1960s with observations from the recent WOCE period she found that the SPMW portion located to the south of the NAC is part of the subtropical gyre and not the subpolar gyre. The particular SPMW portion that turns northwards and is continuously transformed to higher densities has yet not been quantified well (Hanawa and Talley, 2001). Talley (1999) suggested NAC waters being the source water for this branch. The author, furthermore, indicated that the Subpolar Front separates SPMW into two distinct types, an eastern and a western SPMW that do not have any clear connection. SPMW that feeds the Labrador Sea originates from the north/western side of the NAC. In the present study, waters with densities below σ_Θ = 27.68 kg/m^3 are termed SPMW.

2.3.2. Intermediate Water: ULSW and LSW

The term *intermediate water* refers to water masses located in the depth range 500-1500 m (Emery and Meincke, 1986). Concerning the SPNA, these water masses often exhibit local extrema in their respective properties (Van Aken, 2000b). Both features hold for Upper Labrador Sea Water (ULSW) and the denser Labrador Sea Water (LSW) which together occupy a depth range of 200-2000 m in the western SPNA and e.g. have minima in salinity and potential vorticity. The formation and spreading of LSW are known for a longer time and in more detail, compared to ULSW. Therefore, the overview of the intermediate layers begins with LSW.

[I] Potential vorticity is defined as pv = $\frac{f}{\rho}\frac{\partial \rho}{\partial z}$ with units given in $m^{-1}s^{-1}$. f is the Coriolis parameter; ρ is the density of the water, and $\frac{\partial \rho}{\partial z}$ is the vertical density gradient.

LSW

Some important facts on Labrador Sea Water (LSW) formation were already provided in Chapter 1. LSW is considered the end member of SPMW transformation. It is formed by convection happening in the western part of the central Labrador Sea. In the SPNA it is characterised as a pycnostad[II] and a salinity minimum. Newly formed LSW is high in tracer and oxygen concentrations and carries low nutrients (e.g., Fine, 1995). Several studies revealed highly-variable water mass properties. Lazier (1980) found annual to interannual changes of the LSW temperature and salinity in the OWS Bravo data set. He attributed these changes to variability in the intensity of deep convection. Talley and McCartney (1982) and later Sy et al. (1997) and Curry et al. (1998) generated long-term time series of LSW properties and found considerable variability on interannual to decadal time scales. Curry et al. (1998) could link these changes to changes in the North Atlantic Oscillation (NAO), an atmospheric circulation pattern that is considered as a measure for the strength of winterly westerly winds (e.g., Hurrell, 1995; Jones et al., 1997; Greatbatch, 2000).

Due to the changing convection activity during the last decades the LSW was and still is subject to variable temperatures (2.70-3.57°C) and salinities (34.83-34.90) (Sy et al., 1997). The tendency to cooler and fresher values of both properties has been observed since the beginning of the 1990s because of the increased deep convection in this period.

LSW spreads along different pathways in the SPNA. One part of the LSW moves equatorwards within the DWBC, another follows the path of the NAC into the eastern basins, and a third branch spreads into the Irminger Sea which was independently found by analysis of hydrographic data (Talley and McCartney, 1982; Sy et al., 1997), anthropogenic tracers (Rhein et al., 2002) and float trajectories (Fischer and Schott, 2002).

ULSW

The water mass known as ULSW has originally been detected by means of dominant tritium and chlorofluorocarbon signals (components CFC-11, CFC-12). These were measured in the tropical to mid-latitude western North Atlantic during the 1970s to 1980s (Jenkins and Rhines, 1980; Weiss et al., 1985; Fine and Molinari, 1988; Pickart, 1992; Smethie,1993). At first, ULSW was identified as advected 'classical' LSW (Weiss et al., 1985) which is that particular water mass formed in the interior Labrador Sea during strong winter time convection (e.g., Lazier, 1973; Clarke and Gascard, 1983; The Lab Sea Group, 1998; Marshall and Schott, 1999). Fine and Molinari (1988), however, suggested ULSW is a lighter version of classical LSW or Subpolar Mode Water due to its warmer temperatures in comparison to LSW. Pickart (1992)

[II]The pycnostad describes a layer where the vertical change of density is very small and displays a local minimum.

analysed salinity-poor and CFC-rich water in the upper part of the Deep Western Boundary Current (DWBC) in the region between 70°W and 55°W south of the Grand Banks. He termed this water mass 'shallow DWBC water' and presented the first evidence for its formation in the boundary current region of the southern Labrador Sea. In a subsequent study, Pickart et al. (1996) renamed this water mass upper LSW. The authors found ULSW in the southern Labrador Sea in newly generated submesoscale eddies which were embedded in the DWBC. These eddies moved equatorward but decayed within several months. Despite the eddy erosion downstream of the Grand Banks region, their influence on the DWBC was nevertheless clearly visible due to the deposition of high CFC concentrations into the upper DWBC. Pickart et al. (1996) noticed that differences between ULSW and classical LSW were chiefly determined by salinity, ULSW being the less saline and hence less dense water mass. The authors chose σ_Θ = 27.68-27.72 kg/m^3 as an appropriate density. In a later study, Pickart et al. (1997) found coherence between ULSW being formed by winter-time overturning and the dynamics of the Labrador Current which gives support to ULSW having its origin in the western boundary current system in the southern Labrador Sea. Southward advection out of the central Labrador Sea and mixing did not seem to explain the resulting property distributions.

Several recent studies highlighted the switch from deep to shallow convection and the associated change in the water mass formation of the central Labrador Sea during the 1990s (e.g., Lazier et al., 2002; Azetsu-Scott et al., 2003; Stramma et al., 2004). These will be introduced in Chapter 3 since corresponding results are directly relevant for the analyses presented there.

2.3.3. Deep Water: ISOW/GFZW

The formation of Iceland-Scotland Overflow Water (ISOW) is related to water masses that have their origin in the Norwegian Sea. According to Van Aken and De Boer (1995) these comprise different water types of Artic Intermediate Water (AIW) as well as Norwegian Sea Deep Water (NSDW). While passing the Faroe Bank Channel as well as overflowing the Iceland-Scotland Ridge water properties homogenise because of diapycnal mixing. During the decent into the Iceland Basin adjacent water masses are entrained, e.g. warm and salty SPMW, LSW, portions of MW. As a result, a quite homogeneous water mass, ISOW, is formed. It passes the CGFZ into the western basins of the SPNA, identifyable by a salinity maximum located between 2500-3000 m (Harvey, 1980). Harvey and Theodorou (1986) found the contribution of overflow waters to the westward flow in the CGFZ to be greater than 40%. Fleischmann et al. (2001) noticed that 2.4-3.5 Sv of ISOW do not escape into the western basins but remain in the eastern basin. Van Aken (2000a) traced ISOW in the eastern basin southwards as far as the Madeira abyssal Plain.

Having arrived on the western side of the MAR ISOW is referred to as Gibbs Fracture

Zone Water (GFZW). Swift (1984) found GFZW penetrating into the Irminger Sea. Oxygen and CFC concentrations of GFZW are lower in the western basins compared to the eastern side of the MAR (Swift, 1984, Doney and Bullister, 1992). Smethie and Swift (1989) estimated that GFZW needs about 7.5+4/-6.5 years to propagate from the source region just south of the Iceland-Scotland Ridge to the region south of Denmark Strait.
Here, it overrides the denser Denmark Strait Overflow Water (DSOW) and continues as part of the boundary current system into the Labrador Sea and later on into the Newfoundland Basin. According to Swift (1984) GFZW/ISOW contributes 37% to the overflow-related deep water that is exported south of the Grand Banks into the subtropical Atlantic Ocean.

2.3.4. Bottom Water: DSOW and LDW/AABW

Also the DSOW is comprised of water masses that originate in the Nordic Seas. The predominant ingredient is upper AIW which is formed by winter time convection in the Greenland and Iceland Seas. Strass et al. (1993) stressed the importance of the EGC, where isopycnic mixing of upper AIW and recirculated Atlantic Water contribute to DSOW formation. The intensity of mixing was found to be correlated to variability in the EGC due to mesocale eddies. Mauritzen (1996a), however, provided evidence that the sources of DSOW are found rather in the Arctic Ocean. Water masses of Artic origin follow a direct advective pathway within the EGC, with mean streamlines of the total velocity field being parallel to the isobaths. Thus, EGC waters are isolated from waters of the Iceland Sea. A companion paper (Mauritzen, 1996b) showed that this revised circulation scheme is consistent with results from an inverse model approach.

By overflowing the Denmark Strait sill, the DSOW sinks to the bottom, entraining water on the southern side of the sill. Finally, it follows the topography in the Irminger Sea and Labrador Sea as part of the DWBC and can be traced into the southern hemisphere (Speer and McCartney, 1992; Rhein, 1994). Following Swift (1984), the DSOW contributes 31 % to the overflow-generated deep current that flows around the Grand Banks in the western North Atlantic.

McCartney (1992, 1993) and McCartney and Curry (1993) traced the flow of AABW from the equatorial regions into the SPNA. For the AABW version prominent in the eastern basins McCartney (1992) introduced the term Lower Deep Water (LDW). This represents a mixture of AABW entering the eastern Atlantic Ocean via the Vema Fracture Zone (located at 11°N) with warmer waters as it continues northwards. McCartney further postulated that the deep water flow through CGFZ should contain at least 40% of LDW and 60% of overflow water. A differentiation in the hydrographic and mooring data sampled directly in the CGFZ and analysed by Saunders could, however, not be made. AABW and its derivatives carry high concentrations of silica and low concenrations of oxygen due to the high age of this water mass. Analysing nutrients

Clarke et al. (1980) identified the northward spreading of modified AABW as it enters the Newfoundland Basin.

3. Spreading and Formation of ULSW and LSW, 1997-2001

Quantifying the formation of water masses having their origin in the subpolar North Atlantic is of major interest in oceanographic science. They contribute to NADW which is transported away from its source region throughout the world ocean. The use of chlorofluorocarbon (CFC) inventories has proven to be a valuable tool for estimating water mass formation rates (e.g. Orsi *et al., 1999;* Smethie *and* Fine*, 2001;* Rhein *et al., 2002,* Böning *et al., 2003). In applying these methods the present chapter is focused on estimating the formation rates and the associated variability of Upper Labrador Sea Water (ULSW) and the so-called 'classical' Labrador Sea Water (LSW) in the period 1997-2001.*

3.1. Introduction

Labrador Sea Water (LSW) and the shallower Upper Labrador Sea Water (ULSW) have increasingly attracted interest over the past decades. Both form the upper part of North Atlantic Deep Water (NADW) and contribute to the meridional overturning circulation, which in turn is considered the driving mechanism for northward heat transport in the Atlantic Ocean.

Water mass ventilation rates can be determined from anthropogenic tracers such as chlorofluorocarbon (CFC). The major advantage is a time-varying but well-known atmospheric history of CFCs. For the components CFC-11 and CFC-12 there is no biological consumption in the ocean, instead they have a long chemical lifetime (see review of Fine, 1995). The distribution of CFCs in the ocean can be considered as an integrated effect of any kind of transport pathways, e.g., advection and/or diffusion (Haine et al., 2003). Furthermore, there is a large oceanic data base available since the 1980s.

Smethie et al. (2000) traced the spreading of ULSW based on a large-scale CFC data set normalised to the year 1990. They put focus on that particular portion of ULSW that exits into the subtropical western Atlantic. In extending these analyses, Smethie and Fine (2001, SF01 hereafter) presented first estimates of the CFC-11 inventories of ULSW and corresponding formation rates. An inventory of 4.2 million moles and a corresponding mean formation rate of 2.2 Sv was given for the Atlantic Ocean south of about 46°N to 20°S. The source region of ULSW (the northwestern SPNA) was not taken into account. Similar estimates were given for the deeper and denser classical LSW but with the SPNA

included. For this water mass SF01 calculated a CFC-11 inventory of 14.7 million moles which led to a mean formation rate of 7.4 Sv. The formation rates for both water masses are representative for the period 1970-1990.

Hitherto existing analyses of ULSW in the subpolar North Atlantic were based on observational data from the late 1980s or early 1990s. This particular period is associated with the occurrence of strong and deep reaching winter-time convection in the Labrador Sea (Lazier et al., 2002). The strength of convective activity is supposed to be correlated to atmospheric variability (Dickson, 1999). It can be expressed in terms of the NAO-index (Hurrell 1995). The first half of the 1990s showed very strong winters with the highest NAO-indices ever recorded during the last 50 years. The conditions favouring deep convection, however, have changed throughout the 1990s (Lazier et al. 2002).

From hydrographic and CFC-12 data sampled in the central Labrador Sea during summers 1991-2000, Azetsu-Scott et al. (2003) generated property times series for various surface to deep water masses. The authors report on growing CFC-12 concentrations in the classical LSW layer during 1991 to 1994. This increase was due to the effect of the strong convective activity in this period. In the subsequent years the strongest increase of CFC-12 was confined to the upper 1000 m. For this newly ventilated layer, Azetsu-Scott et al. (2003) introduced the term 'shallow LSW'. It is defined as water in the density range σ_Θ = 27.72-27.75 kg/m^3. According to Azetsu-Scott et al. (2003), formation of this 'shallow LSW' started in 1995. The mean CFC-12 concentrations of the 'shallow LSW' increased from 1994 to 1995. The data of the subsequent years, however, are inconclusive. This could be caused by data gaps, which are present especially in 1996 and 1999. The authors did not discuss changes in layer thickness of either 'shallow LSW' or classical LSW.

In another study, Stramma et al. (2004) investigated the spreading and variability of deep water masses with focus on the years 1996-2001. The authors as well noticed the increased formation of a water mass lighter than classical LSW and used the term ULSW for water in the density range $\sigma_\Theta = 27.68 - 27.74$ kg/m^3. This layer partially comprises the 'shallow LSW' of Azetsu-Scott et al. (2003) and the density range of the ULSW introduced by Pickart et al. (1996, 1997). The second half of the 1990s was a period of fairly weak and shallow convection (depths < 1500 m) (Lazier et al., 2002). Renewal of classical LSW ceased, leading to increased salinities and temperatures and decreased layer thickness. At the same time, the formation of the lighter ULSW intensified. ULSW appeared as a thickened layer with a pronounced minimum of potential vorticity (Stramma et al., 2004). Potential vorticity and CFC distributions suggest that the central to northern Labrador Sea is the formation region of this newly formed ULSW (Stramma et al., 2004). For the second half of the 1990s, 'shallow LSW' and ULSW respectively as analysed by Azetsu-Scott et al. (2003) and Stramma et al. (2004) consequently appeared to be one mode lying within a broad band of densities associated with the formation of LSW.

Rhein et al. (2002) (referred to as R02, hereafter) highlighted the formation and large-scale spreading of classical LSW in the subpolar North Atlantic during 1997. Similar to SF01, the authors calculated the CFC-11 inventory as a function of layer thickness and

CFC-11 mean concentration. They found 16.6 million moles of CFC-11 located between 40°-65°N. The corresponding mean annual formation rate of LSW, representative for the period 1970–1997, resulted in 4.4–5.6 Sv. High-NAO-index and low-NAO-index LSW formation rates were estimated in the order of 8.1–10.8 Sv and 1.8–2.4 Sv, respectively (see R02 for details). While R02 studied formation and spreading of LSW, corresponding changes in this layer and in the lighter ULSW have, however, not been investigated.

Böning et al. (2003) analysed LSW formation rates by applying the CFC inventory method of R02 to an eddy-permitting ocean model. The horizontal grid resolution was $\frac{1}{3}^\circ \times \frac{1}{3}^\circ cos(\phi)$, ϕ being latitude. The model was forced with monthly mean atmospheric fluxes based on a 3-year climatology of ECMWF[I] analyses (Willebrand et al., 2001). Heat flux anomalies were derived from the NCEP/NCAR[II] reanalysis data set (Kalnay et al., 1996) with respect to the period 1959-1997. They were superimposed on the climatological forcing fields. In this manner a realistic forcing was implemented. The model was able to reproduce the observed CFC distribution quite well. The modeled LSW formation rates calculated by the CFC inventory method (3.4–4.4 Sv) agreed with the model's volumetric formation rate (4.3 Sv).

Gray and Haine (2001) applied inverse methods to constrain a coarse-resolution (4/3°) numerical ocean model with observed CFC data. These were taken from the years 1982-1994. The CFC inventory was diagnosed from the model Green's function. The corresponding equation contained terms that represent the internal source or sink of a tracer and the initial tracer concentration at a time $t = 0$. A third term described the tracer as it entered a considered domain across a given boundary. The Green's function was determined from the flow field, boundary conditions on the tracer concentration, and the diffusion coefficient. The inversion procedure found that particular air-sea flux of CFC which showed the best agreement between observations and the prediction from the numerical ocean model. Gray and Haine (2001) particularly studied Subtropical and Subpolar Mode Water. The latter was defined at densities $\sigma_\Theta \sim 27.75$ kg/m^3. The resulting mean formation rate, averaged over a period of 20-30 years prior to 1995, gave 6 Sv.

Haine et al. (2003) applied the same method on the same general circulation model but used an extended CFC data set (data from the years 1982-1998). They further analysed different model experiments with changing model key parameters. Especially the thickness diffusion was varied which sets the strength of unresolved eddy thickness fluxes. Haine et al. calculated a formation rate of 7 Sv for the density layer $\sigma_\Theta \geq 27.69$-27.78 kg/m^3. This is in reasonable agreement with formation rates derived from the observed CFC-11 inventory of SF01 and R02 (SF01: 7.0-11.2 Sv for $\sigma_\Theta = 27.68$-27.78 kg/m^3, R02: 4.4-5.6 Sv for $\sigma_\Theta = 27.74$-27.80 kg/m^3) but almost twice as high as the model result presented by Böning et al. (2003).

Further and very different approaches go back to the early work of Walin (1982). He suggested to understand the ocean circulation in terms of movement across isotherms,

[I]European Centre for Medium Range Weather Forecasts, Reading, UK
[II]National Center for Environmental Prediction/National Center for Atmospheric Research, USA

driven by heating and cooling. Later studies picked up this idea, but analysed flow across isopycnals. Speer and Tziperman (1992) investigated climatological air-sea fluxes (freshwater and heat) and surface density. Corresponding data were from years prior to the mid 1980s. The air-sea fluxes affect water mass properties at the sea surface and contribute to a conversion of water from one density into another. The authors diagnosed surface water mass formation rates throughout the range of sea surface density. Marsh (2000) calculated the buoyancy-forced contribution to the overturning rate in the North Atlantic (period 1980-1997). He assumed that the atmosphere dominantly drives the THC on interannual to decadal time scales and neglected ocean mixing. The analysis was based on observed heat and freshwater fluxes, provided by the Southampton Oceanography Centre (SOC; Josey et al., 1999), and the hydrographic climatology of Levitus (1982). Marsh derived time series for the production of various water masses including LSW (defined as σ_Θ = 27.65-27.775 kg/m^3). For the given period LSW formation rates exhibited trends on decadal time scales. While the mean value was 3.4 Sv, the time series revealed an increase from near-zero in 1980 to a peak of ∼10 Sv in 1990. Subsequent years showed again a decreasing trend. In 1997, the LSW production had returned to near-zero again.

The question now arises to what extent ULSW has been ventilated during the late 1990s. The methodology to analyse this issue follows R02. In the following, formation rates of ULSW are derived. This is based on hydrographic and mainly CFC-11 data. They originate from three large-scale field campaigns carried out in 1997, 1999, and 2001. The results are compared with formation rates of classical LSW, estimated for the same period. While R02 concentrated on the year 1997, the focus in the present study is on the variability of water mass formation between the years 1997, 1999, and 2001.

3.2. Data and applied methods

3.2.1. Chlorofluorocarbon and hydrographic data

A multitude of national and international observational field programs has dealt with North Atlantic related oceanic phenomena and physical processes. Among these, the most extensive projects persisting for almost a decade are WOCE, CLIVAR, and SFB 460 (cf. Fig. 1.4). Due to joined efforts, a large-scale quasi-synoptic chlorofluorocarbon (CFC) data set for the SPNA has become available for the years 1997, 1999, and 2001. Contributing cruises that yielded hydrographic and CFC measurements are summarised in Table 3.1 and displayed in Figure 3.1. The bulk of the CFC-11 data shown has been compiled within the framework of SFB 460, affiliated to the Leibniz-Institut für Meereswissenschaften IFM-GEOMAR in Kiel, Germany. The remaining data have been obtained from W. M. Smethie at Lamont-Doherty Earth Observatory (LDEO) and the WOCE Hydrographic Program Office (WHPO). The main focus of the present study is on CFC-11 analysis, though the methods illustrated in the following also hold for CFC-12

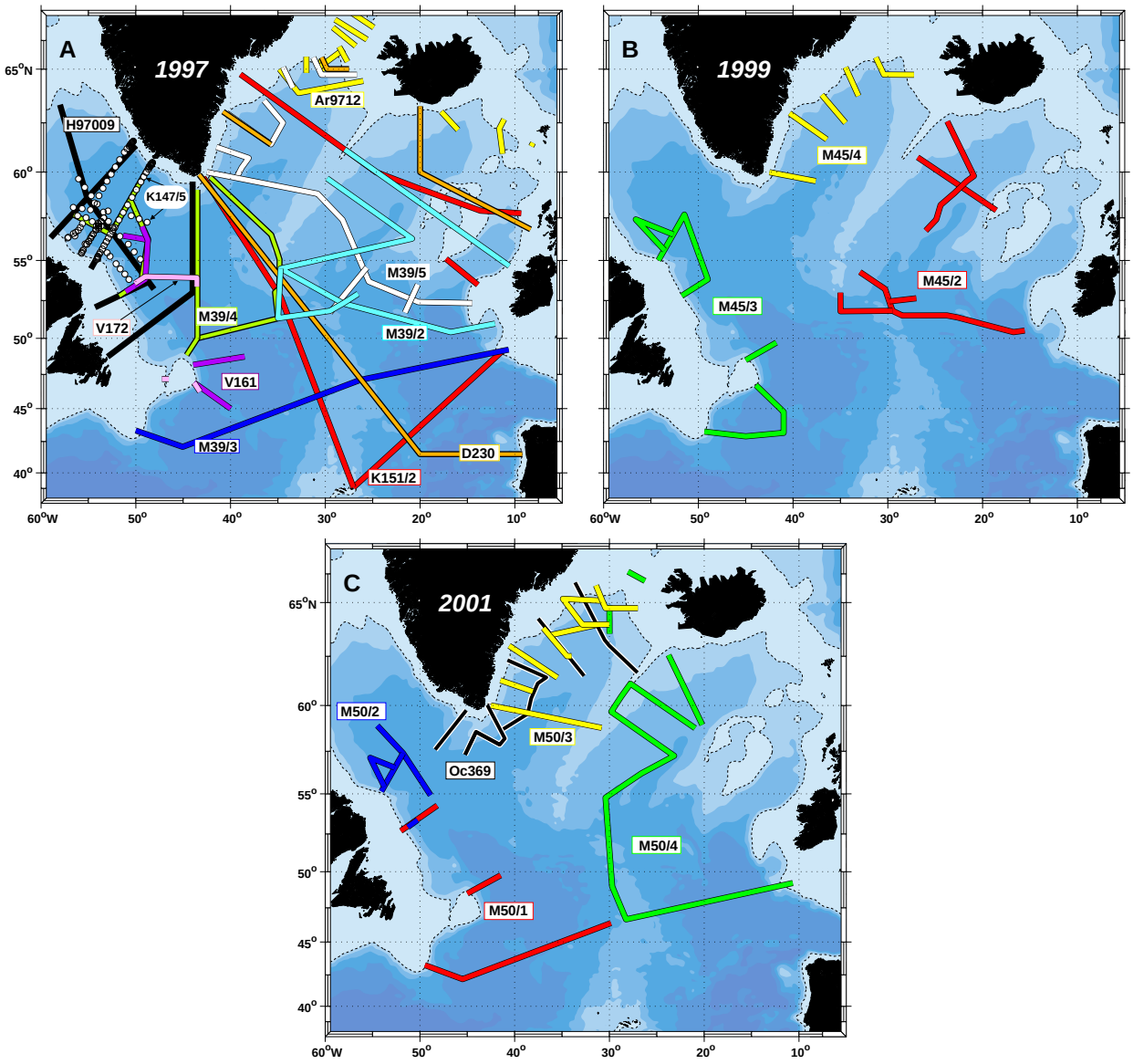

Fig. 3.1.: *Location of CFC-11 and CTD sections sampled during a) 1997, b) 1999, and c) 2001. Text labels and colours mark the individual cruises which are listed in Tab. 3.1. Bathymetric contours are given every 1000 m, with 1000 m indicated by dashed lines.*

data. Respective results derived from CFC-12 analysis are presented later on. Details on the CFC measurement technique are given in the appendix A.2.

The CFC-11 data of 1997 (Fig. 3.1a) have already been analysed by R02 with respect to LSW. CFC-11/CTD data from two cruises have been added in the present study (cruise AR9712 close to the Greenland-Scotland-Ridge as well as cruise H97009 in the central Labrador Sea). R02 quality-controlled the CFC-11 data set of 1997 for regions west of 32.5°W. For the density range 27.77 kg/m^3 $< \sigma_\Theta <$ 27.79 kg/m^3 they considered all samples that fell into a narrow temperature and salinity range ($\Theta \pm 0.003$°C, S $\pm$ 0.003). After 1995, this density range is regarded as not being affected by deep convection. Changes in

	Cruise	Date	PI CFCs	Institution
1997	K147/5	07 Feb-12 Mar 1997	W. M. Smethie	LDEO
	M39/2	15 May-08 Jun 1997	M. Rhein	IFMK
	H97009	09 May-11 Jun 1997	P. Jones	BIO
	K151/2	30 May-02 Jul 1997	R. Weiss	SIO
	M39/3	13 Jun-30 Jun 1997	W. Roether	IUP
	M39/4	07 Jul-08 Aug 1997	M. Rhein	IfMK
	Ar9712	05 Aug-25 Sep 1997	T. Tanhua	UGot
	D230	07 Aug-17 Sep 1997	D. Smythe-Wright	SOC
	M39/5	14 Aug-14 Sep 1997	M. Rhein	IfMK
	V161	19 Jul-16 Aug 1996	M. Rhein	IfMK
	V172	04 Jul-08 Aug 1998	M. Rhein	IfMK
1999	M45/2	11 Jun-08 Jul 1999	M. Rhein	IfMK
	M45/3	11 Jul-10 Aug 1999	M. Rhein	IfMK
	M45/4	14 Aug-26 Aug 1999	M. Rhein	IfMK
2001	M50/1	08 May-31 May 2001	M. Rhein	IUP
	M50/2	02 Jun-18 Jun 2001	M. Rhein	IUP
	M50/3	21 Jun-15 Jul 2001	M. Rhein	IUP
	M50/4	17 Jul-12 Aug 2001	M. Rhein	IUP
	Oc369	02 Aug-27 Aug 2001	W. M. Smethie	LDEO

Tab. 3.1.: *CFC measurements carried out during 1997, 1999 and 2001. For reasons of consistency with R02, sections from 1996 and 1998 have been added to the data set of 1997. This is to improve the resolution in the boundary current region in the western North Atlantic. The locations of all particular cruises are presented in Fig. 3.1. PI: Principal Investigator; BIO: Bedford Institute of Oceanography, Canada; IfMK: Institut für Meereskunde Kiel, Germany; IUP: Institut für Umweltphysik Bremen, Germany; LDEO: Lamont-Doherty Earth Observatory, USA; SIO: Scripps Institution of Oceanography, USA; SOC: Southampton Oceanography Centre, United Kingdom; UGot: University of Gothenburg, Sweden.*

the CFC-11 concentration should therefore remain small. The mean rms error of CFC-11 concentrations in the considered density range varied from 2.5 % to 3 % for individual cruises (see R02 for details). With the same method, the mean *rms* error for the data set of 1997 used here resulted in 5.1 %. This means, CFC-11 data from the different cruises are comparable within this percentage. For the 1999 data (Fig. 3.1b, Tab. 3.1), the mean CFC-11 *rms* varied from 0.5 % to 2.1 % for the individual cruises and gave 3.3 % for the complete data set. In 2001, the cruises M50/1-2 (Fig. 3.1c, Tab. 3.1) revealed anomalous high CFC-11/CFC-12 ratios. A comparison of all CFC-11 and CFC-12 data available in 2001 showed that the CFC-11 concentrations measured during M50/2 and to a lesser extent during M50/1 were too high. Despite this shortcoming, the combined data set of 2001 showed conformity within 5.2 % for all five cruises, while the mean standard deviation of CFC-11 for single cruises ranged from 1.8 % to 3.4 %. Nevertheless, the data set of 2001 has been corrected by reducing the CFC-11 data of M50/1 by 1 % and M50/2 by 5 %. All CFC concentrations are reported on SIO-93 scale (Cunnold et al. 1994).

Most of the CTD data are from SFB 460 and WHPO. Data from the Irminger Sea were to some part provided by the European Union-funded programs VEINS (*Variability of Exchanges in the Northern Seas*) and ASOF (*Arctic-Subarctic Ocean Fluxes*), carried out by the Institut für Meereskunde Hamburg, Germany (courtesy of J. Meincke). Cruise data from winter 1997 (K147/5) were obtained from the Labrador Sea Convection Experiment data repository (see Krahmann et al., 2003). The CTD equipment used during SFB 460 cruises was either a *Neil Brown MK III* or a *Seabird Electronics 9plus* instrument. For salinity calibration water samples were taken from sample bottles and analysed using an *Autosal* salinometer. Temperatures and pressures of the CTD system were compared to reversing electronic barometers and thermometers attached to some of the sample bottles. The resulting accuracies of the SFB 460 CTD data are 0.002-0.004 psu for salinity and 0.002°C-0.003°C for temperature (Schott et al., 1999, 2000, 2001). Accuracies of the remaining cruises are similar.

The data set retrieved in 1997 is probably one the best ever resolved. The Irminger Sea has the best horizontal and vertical data coverage in 1997-2001, followed by the Labrador Sea (Fig. 3.1). Unfortunately, large areas in the central and eastern SPNA were not sampled during 1999 and 2001. For example, there aren't any CTD/CFC profiles east of 40°W and south of 50°N in 1999. While the data coverage in 2001 was better compared to 1999, considerable gaps remain. This problem is particularly discussed in this study.

3.2.2. Gridded fields

Following Stramma et al. (2004) and R02, ULSW formed during the late 1990s is defined as water in the density range σ_Θ = 27.68-27.74 kg/m^3, whereas the classical LSW is defined as σ_Θ = 27.74-27.80 kg/m^3 (cf. Fig. 2.4). The vertical distance between the corresponding two isopycnals represents the layer thickness of either ULSW or LSW. These

estimates have been derived from all available hydrographic profiles of all particular years.

Most of the profiles have more than two CFC observations in the ULSW and classical LSW layers. In 1997, ULSW was represented by only one CFC-11 sample in 280 out of 606 profiles (LSW: 69 of 605 profiles). The positions of these profiles are spread throughout the subpolar North Atlantic. In 1999, the number of profiles having one sample in the ULSW was 70 out of 164 profiles (LSW: 4 out of 175). Most of them are located on the continental slope in the Irminger Sea as well as in the Newfoundland Basin. In 2001, 87 out of 285 profiles have less than two samples in the ULSW (LSW: 19 out of 285). The majority of these profiles is found above ridges like the Mid-Atlantic Ridge (MAR) and its northward extension, the Reykjanes Ridge. To estimate an average CFC-11 concentration for the ULSW and LSW layers, samples taken within the particular layer have been weighted according to the vertical depth range they represent in the water column. This is termed depth-weighting.

In a second step, data referring to the particular years were mapped on a common regular grid. This was done by applying a topography-following covariance function similar to that being introduced and described in detail by Davis (1998). This technique has been utilised widely to map float data (e.g., Davis, 1998; Lavender et al., 2000, 2002; Fischer and Schott, 2002). R02 compared the large-scale spreading of classical LSW in the subpolar North Atlantic by means of floats and CFC-11. The authors presented evidence that such a mapping scheme is suitable to be applied to CFC data as well. The CFC distribution of the classical LSW is controlled by topography and mainly follows contours of barotropic potential vorticity $\frac{\mathbf{f}}{\mathbf{H}}$ ($\mathbf{f}$: Coriolis parameter, $\mathbf{H}$: water depth). In the present study the topography-following mapping algorithm has been used as described by R02 to be consistent with their analysis.
The main features are summarised as follows:

- The spatial grid resolution is 0.5° longitude × 0.25° latitude.
- Water depths are derived from the ETOPO5 bathymetry data set (5'x5' grid resolution) to calculate for every grid point the potential vorticity $\frac{\mathbf{f}}{\mathbf{H}}$. The bathymetry data set is smoothed to reduce the impact of small-scale topographic features that are especially prominent close to the MAR (compare Fig. 2.1).
- A generalised distance $\mathbf{r}$ between observation locations and grid points is introduced that depends on horizontal separation as well as differences in potential vorticity, both being divided by a scaling factor.
- The exact formulation is

$$\mathbf{r}^2 = \frac{|\mathbf{a}-\mathbf{b}|^2}{\mathbf{\Lambda}} + \frac{\mathbf{1}}{\mathbf{\Phi}} \frac{|\frac{\mathbf{f}}{\mathbf{H}}(\mathbf{a}) - \frac{\mathbf{f}}{\mathbf{H}}(\mathbf{b})|^2}{(\frac{\mathbf{f}}{\mathbf{H}})^2(\mathbf{a}) + (\frac{\mathbf{f}}{\mathbf{H}})^2(\mathbf{b})} \tag{3.1}$$

  with $\mathbf{a}$ and $\mathbf{b}$ being the position of grid points and those of the measurements. $\mathbf{\Lambda}$ and $\mathbf{\Phi}$ are the scaling parameters.

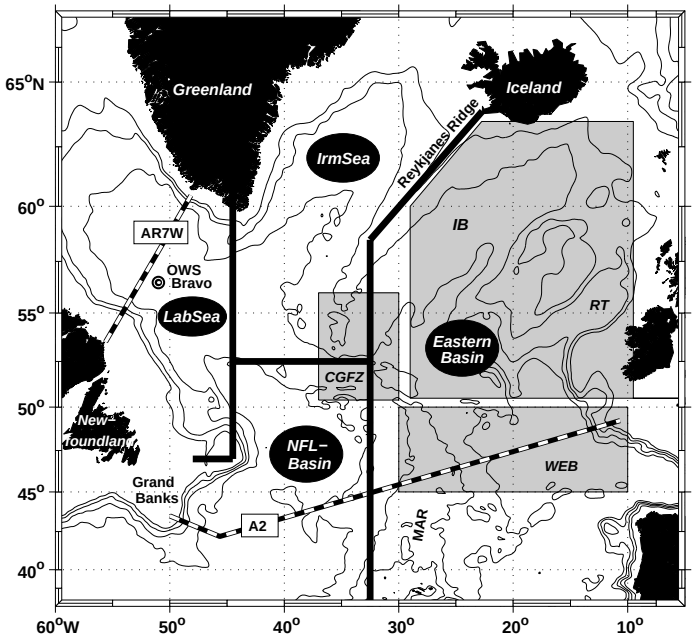

Fig. 3.2.: *Location of different basins of the subpolar North Atlantic. CGFZ: Charlie-Gibbs Fracture Zone region, IB: Iceland Basin, IrmSea: Irminger Sea, LabSea: Labrador Sea, MAR: Mid Atlantic Ridge, NFL-Basin: Newfoundland Basin, OWS: Ocean Weather Station, RT: Rockall Trough, WEB: West European Basin. Bold lines mark limits used to estimate regional contributions to the CFC-11 inventory. Shaded areas denote regions (IB/RT, CGFZ, WEB) discussed in detail in Section 3.3. Dashed lines indicate the course of WOCE-lines AR7W and A2.*

- The Gaussian covariance function $\mathbf{F}$ to weight the data is

$$\mathbf{F}(\mathbf{r}) = exp(-\mathbf{r}^2). \tag{3.2}$$

R02 have listed values for $\mathbf{\Lambda}$ and $\mathbf{\Phi}$, but these have to be rectified. The correct values which have actually been used by R02 must be: $\frac{\mathbf{1}}{\mathbf{\Lambda}} = 0.5{\times}10^{-4}$ (with units of km^{-2}) and $\frac{\mathbf{1}}{\mathbf{\Phi}}$ = 100 (dimensionless). These scaling parameters are also applied here. Their magnitudes result from the following reasoning: In the original notation given by Davis (1998), $\mathbf{\Lambda}$ is related to a typical horizontal correlation length scale ($\boldsymbol{\lambda}$) via the expression $\mathbf{\Lambda} = 2\boldsymbol{\lambda}^2$. $\mathbf{\Phi}$ refers to the scale of decorrelation ($\boldsymbol{\phi}$) produced by the change in potential vorticity via $\mathbf{\Phi} = \boldsymbol{\phi}^2$. R02 set $\boldsymbol{\lambda}$ = 100 km, which is a typical length scale in the boundary current regime. In comparison, Lavender et al. (2000) chose 185 km as a horizontal correlation length scale. The choice of $\mathbf{\Phi} = 100$ (i.e., $\boldsymbol{\phi} = 10$) matches a depth difference of 150 m in the second term of Equation 3.1.

The subpolar North Atlantic is subdivided into different regions. This allows to better investigate regional changes of water mass properties and estimate regional contributions to the CFC-11 inventory. Considered regions are the Labrador Sea, Irminger Sea, Newfoundland Basin, and the residual region east of the MAR, here collectively named Eastern Basin. The latter comprises the Iceland Basin, the Rockall Trough and West

European Basin. Corresponding limits are displayed in Figure 3.2.

3.2.3. Salinity/CFC-11 Correlation

During 1964-1974 oceanographic measurements carried out at OWS *Bravo* in the central Labrador Sea. Lazier (1980) noted that surface layers were fresher than the underlying water masses. The annual cycle of salinity found in the upper 100 m of the water column showed the strongest decrease of salinity during summer. This is related to an advection of low salinity waters from the Labrador Current, a region that is influenced by sea ice melting and freshwater run-off. The years with the strongest decrease in salinity (1967-1971) coincided with a period of shallow winter-time convection (100-200 m). Lazier (1980) attributed this to anomalous fresh and cold waters of Arctic origin. They were increasingly advected into the Labrador Sea via the West Greenland and Labrador Currents, thus further diluting the surface layer. In another study, Häkkinen (2002) analysed 50 years of summer surface salinity in the region 55°-50°W/45°-55°N. From these observations she found indications of a large freshening in the mid to late 1990s. Salinity time series from the years 1991-2000 (Azetsu-Scott et al., 2003) also pointed to surface layers that are in general fresher than the underlying water mass layers. Due to the solubility of CFC favouring fresh and cold conditions (Warner and Weiss 1985), ULSW carries high CFC concentrations. These are higher and salinities lower than in the underlying classical LSW. ULSW was more recently at the surface, and hence its salinity is more diluted. Lazier et al. (2002) noted that during 1990-1993 deep convection had penetrated into the saline deep water masses lying below LSW. The salinity of LSW was thus increased from below.

The CFC-11 versus salinity correlation for different regions of the subpolar North Atlantic is shown in Figure 3.3. In most regions both properties are correlated almost linearly. This is most obvious in the western North Atlantic (Labrador Sea, Irminger Sea and Newfoundland Basin). Here, the freshest water carries the highest CFC concentrations. Maximum CFC-11 concentrations are found in the Labrador Sea followed by the Irminger Sea. The salinities in the LSW layer fall into a smaller range, compared to ULSW. This is due to the huge and homogeneous body of water that characterises the LSW. It is located in a greater distance to the fresher surface layers than ULSW. Throughout the years, the CFC-11/salinity correlations in the ULSW layer showed a shift to higher salinities, which was more pronounced in the western basin.

There are fewer data available in the eastern than in the western basin. CFC-11 concentrations and salinities close to the CGFZ, for example, depend on the location of profiles to the east and west of the fracture zone. This subject is discussed in more detail in the subsequent Section 3.3. Some deviations from the linear CFC-11/salinity correlation are found, located in regions where different water masses are present. For example, most profiles presented in Figure 3.3c/d are from the Iceland Basin. Here, both ULSW and classical LSW mix with ISOW that carries high salinities (cf. Sect. 2.3) and

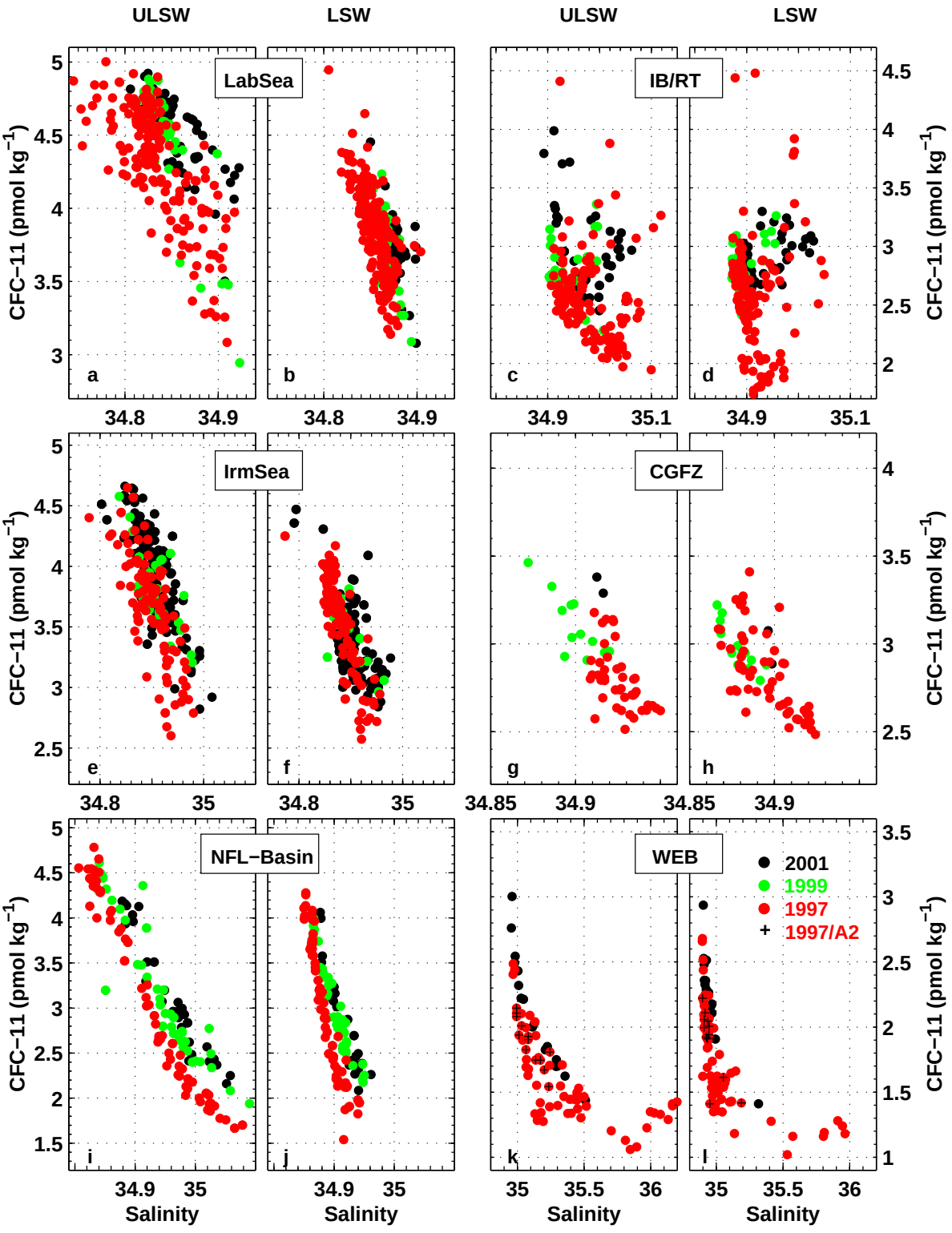

Fig. 3.3.: *Salinity/CFC-11 correlation of ULSW and LSW for the years 1997, 1999, and 2001, displayed for different geographical regions. (a/b) LabSea: Labrador Sea; (c/d) IB/RT: Iceland Basin/Rockall Trough; (e/f) IrmSea: Irminger Sea; (g/h) CGFZ: Charlie-Gibbs Fracture Zone; (i/j) NFL-Basin: Newfoundland Basin; (k/l) WEB: West European Basin. A2: along WOCE-A2 section. Axis scales differ due to the water masses regionally occupying a different S/CFC-11 space. The location of the mentioned regions is indicated in Fig. 3.2.*

enters the eastern North Atlantic by crossing the Iceland-Scotland-Ridge. Mixing of these water masses appears to be responsible for elevated CFC-11 values coinciding with high salinities. The high salinities present in the West European Basin (WEB) result from an inflow of saline Mediterranean Water.

3.3. Spreading pathways of ULSW and LSW

Horizontal property maps have been plotted to better address regional differences and changes throughout the years 1997 to 2001. Figure 3.4 presents the layer-averaged CFC-11 concentration and layer thickness distribution of ULSW for the years 1997, 1999, and 2001, while Figure 3.5 shows the corresponding properties of LSW. All property distributions were calculated as described in Section 3.2.2.

Gridded fields related to the CFC-11 and layer thickness distribution of classical LSW in 1997 were already presented by R02. Here, they are re-calculated and re-drawn for the purpose of comparing them to the gridded fields of 1999 and 2001. The additional data previously mentioned that was not available to R02 are included. Since the data resolution of the years 1999 and 2001 was coarser than in 1997, tracing relevant hydrographic features is in fact regionally confined.

Labrador Sea

The CFC-11 distributions shown in Figures 3.4/3.5 (left columns) reveal conspicuous maxima that are located in the western to central Labrador Sea (ULSW: > 4.7 pmol/kg in 1997, classical LSW: > 4.2 pmol/kg in 1997). In 1997, the respective maximum in the LSW layer is located in the region of the greatest layer thickness. Some of the 1997 profiles included in the analysis are from the winter cruise K147/5 (Tab. 3.1). If these are not considered, the horizontal CFC-11 distribution slightly changes qualitatively but not quantitatively. The large-scale maximum in the interior Labrador Sea is maintained which points to a slow leakage out of the interior Labrador Sea. Also the distribution of layer thickness in the central Labrador Sea is dominated by the summer data. A re-calculation of the 1997 layer thickness field without including the winter data did not show any significant difference.

The gradual CFC-11 increase in the ULSW layer was about 0.1 pmol/kg between the years. At the same time, CFC-11 in the LSW reduced. The 1997 maximum concentrations were eroded. In 2001, concentrations > 4.0 pmol/kg were only found in the boundary current regions of the eastern and western Labrador Sea.

From the central Labrador Sea, the CFC-11 maximum of both layers spread southwards within the western boundary current system. This was evident during all years. In 2001, Stramma et al. (2004) could not trace the spreading of the 2000 ULSW vintage out of the Labrador Sea farther than 53°N, indicating a rather slow spreading time.

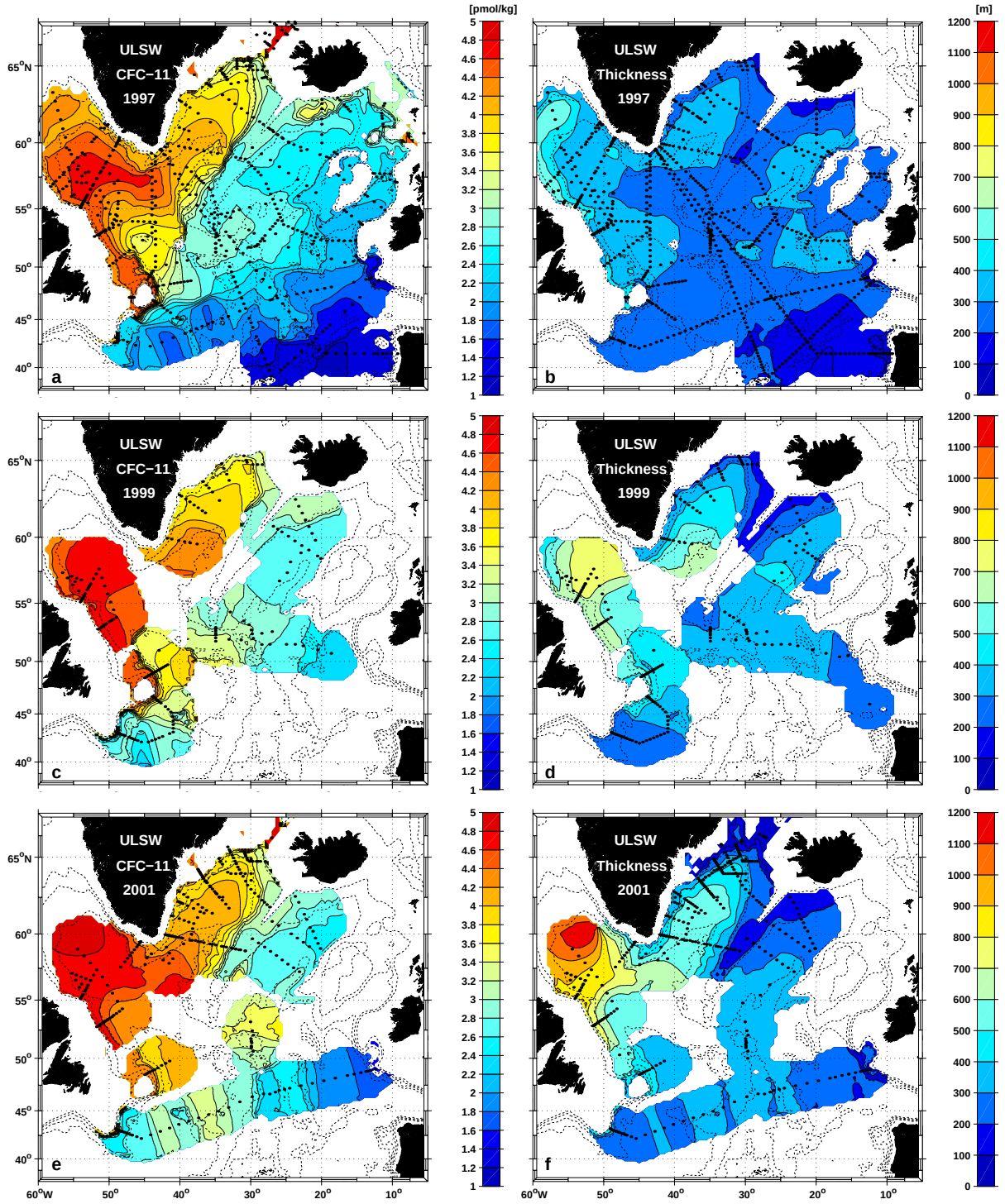

Fig. 3.4.: *Layer-averaged CFC-11 (pmol/kg) distribution (left column) and layer thickness (m) (right column) of ULSW during 1997 (top), 1999 (middle), and 2001 (bottom). Bathymetric contours are given every 1000 m.*

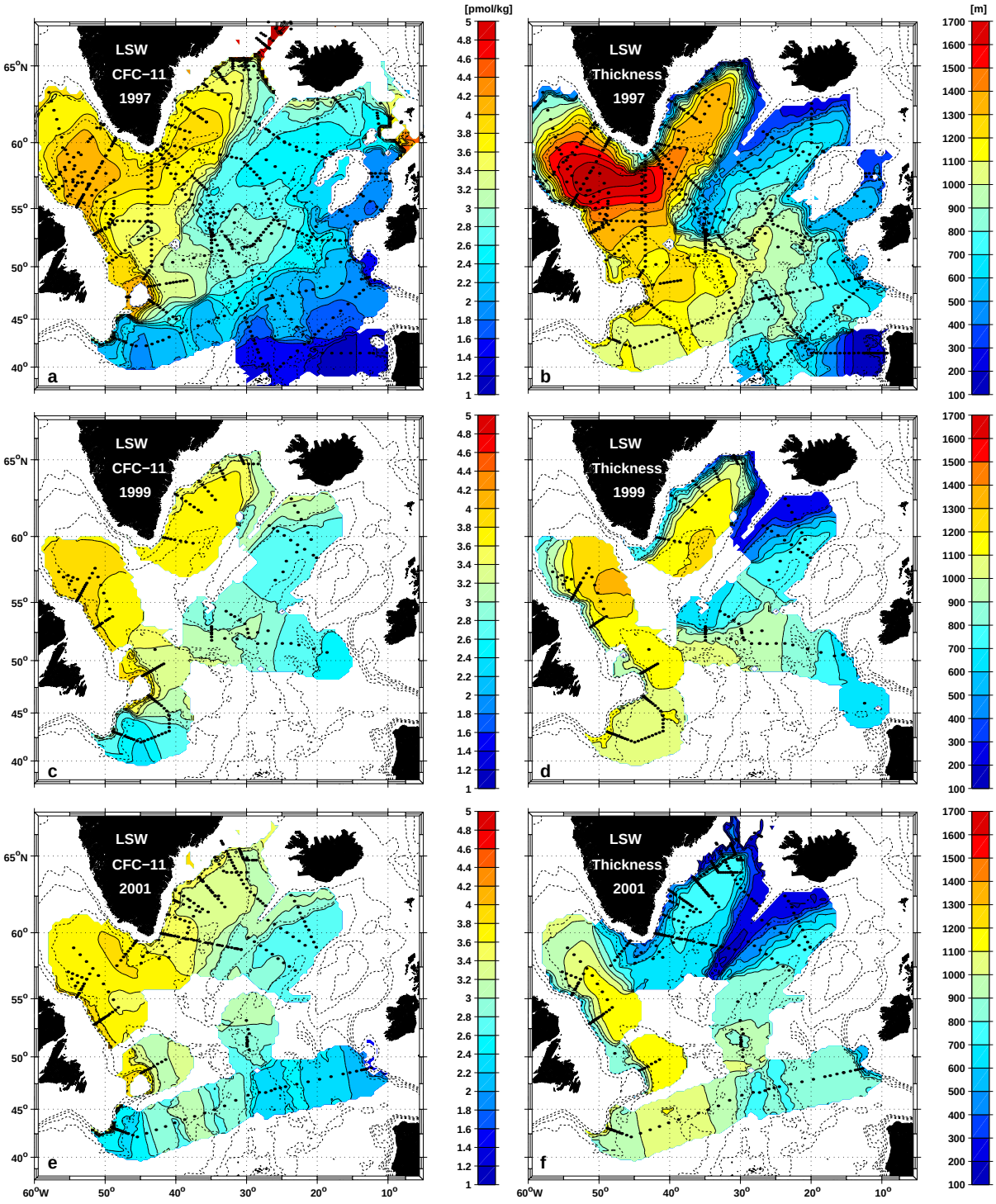

Fig. 3.5.: *Layer-averaged CFC-11 (pmol/kg) distribution (left column) and layer thickness (m) (right column) of classical LSW during 1997 (top), 1999 (middle), and 2001 (bottom). Bathymetric contours are given every 1000 m.*

This is indeed visible in the large-scale distribution of 2001 (Fig. 3.4) which shows CFC-11 > 4.6 pmol/kg confined to about 53°N.

The far greater change is in the thickness of both layers (Figs. 3.4/3.5, right columns). Whether the layer thickness maximum of ULSW observed in 1997 in the northern boundary current region of the Labrador Sea was also present in 1999 and/or 2001 is unknown due to the lack of data in the boundary current region north of about 58°N. The ULSW layer thickness considerably increased throughout the observed period. While in 1997 the maximum (500–600 m) was confined to the western and northern boundary of the Labrador Sea, it was shifted in the subsequent years to the central Labrador Sea, having almost doubled in 2001. The 2001 section along the axis of the central Labrador Sea exhibited the greatest ULSW layer thickness at its northern end, as was presented by Stramma et al. (2004). This signal is distributed over a greater area according to the constraints and weights applied in the gridding method (cf. Section 3.2.2).

The layer thickness of classical LSW layer decreased continuously from 1700 m in 1997 to less than 1200 m in 2001. At that time, the largest thickness was found away from the boundary current region in the interior Labrador Sea. This marks the remnant of the LSW formed during the deep convection phase of the early 1990s (Lazier et al., 2002). Since LSW ventilation had ceased by the mid 1990s, there has not been added any new classical LSW to the already present layer. In fact, the remaining LSW rather has started to drain out of the Labrador Sea.

Newfoundland Basin

At the southern exit of the Newfoundland Basin (WOCE-A2 section, ∼43°N) the highest signals of CFC-11 were confined to the shelf break (Fig. 3.6). The layer thickness was about 200-300 m for ULSW and 900-1200 m for LSW. Due to the small-scale nature of these features, they are hardly visible in the large-scale distribution of layer thickness (Figs. 3.4/3.5) but clearly appear in the particular vertical sections. In 2001, the LSW layer thickness was lower by 100-200 m compared to 1997 and 1999. The ULSW thickness increased since 1997 and was greatest in the boundary current region during 2001 (Stramma et al., 2004).

The offshore part next to the boundary current is dominated by the strong and deep-reaching NAC, transporting different water masses compared to the DWBC (Schott et al., 2004). From the analysis of LSW extremes determined from historical data, Koltermann et al. (1999) suggested a southward export path for LSW close to the western side of the MAR. This was also identified by floats deployed during 2001 within the LSW (Schott et al., 2004). However, due to their profiling nature, these floats had to spend some time at the surface to transmit their data to the satellite system. These estimates, therefore, do not indicate a true Lagrangian spreading. Nevertheless, in their analysis of LSW properties during 1997, R02 noticed increased CFC-11 concentrations off the boundary current region. In 1999, there was a lack of data east of 40°W. In 2001, however, increased CFC-11 in the ULSW emerged outside the western boundary

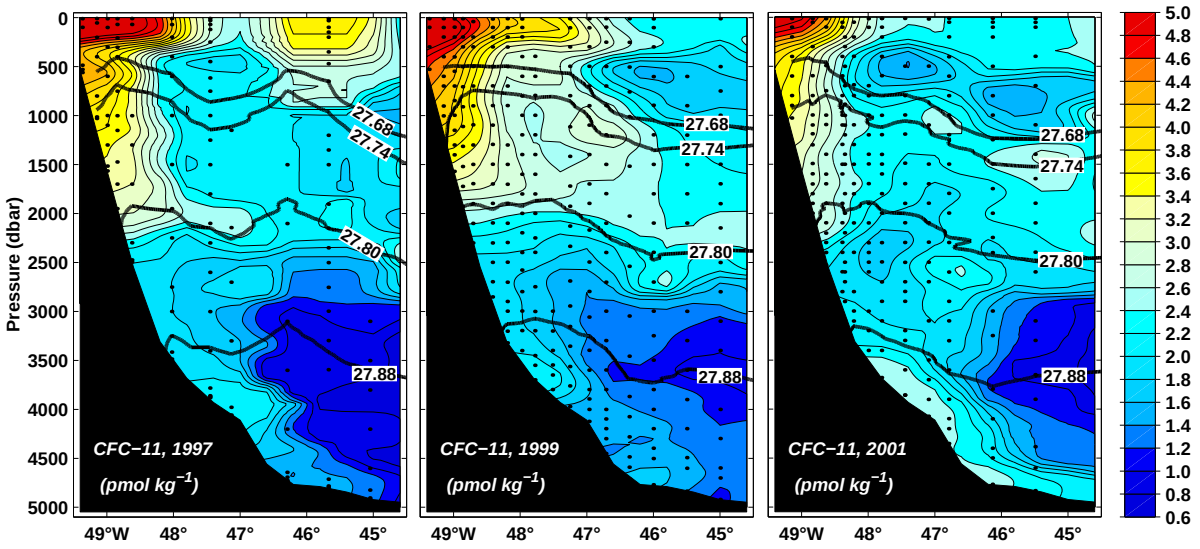

Fig. 3.6.: *CFC-11 (pmol/kg) distribution during 1997, 1999, and 2001 along the western part of WOCE-A2 section at about 43°N. Bold lines indicate the isopycnals σ_Θ = [27.68, 27.74, 27.80, 27.88] kg/m^3.*

(∼37°W-35°W, Figs. 3.4 and 3.5). They coincided with an increased layer thickness of values greater than 300 m. The offshore spreading of water masses in the Newfoundland Basin is discussed in detail in Chapter 5.

Irminger Sea

Freshly ventilated CFC-rich ULSW seems to intrude into the Irminger Sea (Fig. 3.4). While there is only a small ribbon of CFC-11 concentrations greater than 4.2 pmol/kg south of Greenland in 1997, increased concentrations of 4.3 pmol/kg and 4.5 pmol/kg were found during the following years at the southern exit of the Irminger Sea. The CFC-11 concentration of the LSW layer slightly decreased from maximum concentrations of $>$ 4.0 pmol/kg in 1997 to 3.6-3.8 pmol/kg.

As was found in the Labrador Sea, the greater change again affected the layer thickness. The LSW layer thinned from 1400-1700 m in 1997 to less than 800 m in 2001. This points to a significant drainage of LSW out of the Irminger Sea within these four years.

Profiles in the Denmark Strait indicate that CFC-11 concentrations and salinity of ULSW are of similar magnitude compared to the Labrador Sea but with reduced layer thickness (values are about 100-200 m). By analysing data from an extensive Denmark Strait survey Girton et al. (2001) found that DSOW descends from 500 m at sill depth to 1500 m at 200 km farther downstream. In 1997, the ULSW layer south of the Denmark Strait was located at about 800-1000 m. Mixing of water masses cannot be neglected due to entrainment and eddies present in the Irminger Sea (Krauss, 1995). The gradients of the CFC-11 and layer thickness distributions, however, point to the western SPNA as the far more important source for the high CFC-11 signals in the ULSW layer.

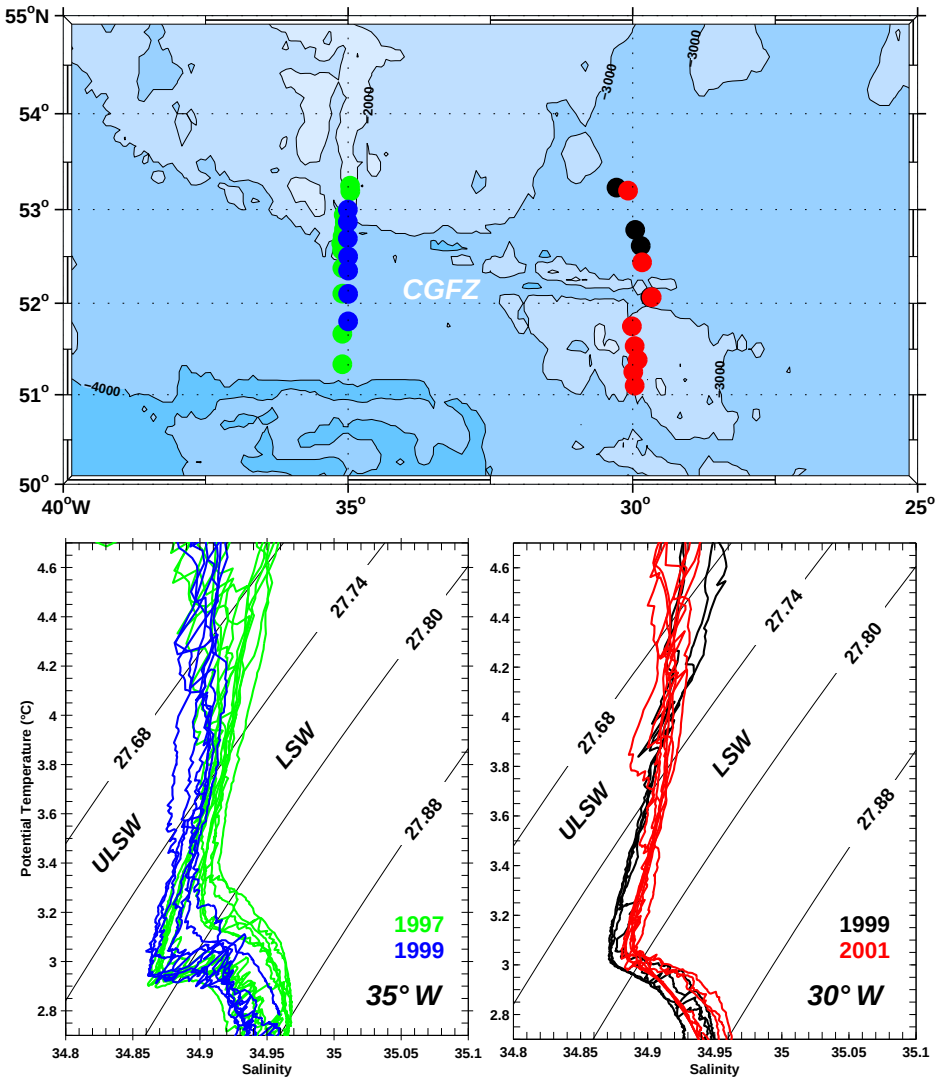

Fig. 3.7.: *Θ/S-diagram of profiles located to the west (along 35° W during 1997 and 1999) and east (along 30° W during 1999 and 2001) of CGFZ. Data are from cruises M39/4 (1997), M45/2 (1999), and M50/4 (2001) (see Tab. 3.1 and Fig. 3.1).*

Eastern Basin

Classical LSW is known as a prominent water mass of the eastern North Atlantic (see Sect. 2.3). However, there has not yet been carried out any analyses concerning the spreading of ULSW into the eastern basin. Smethie et al. (2000) and SF01 focused on ULSW spreading to subtropical and tropical latitudes rather than spreading within the subpolar gyre. The data from 1997 to 2001 reveal that lenses of the recently formed ULSW have crossed the MAR, presumably through the CGFZ (32°W/52°N30'). A CTD profile from 2001, located in the northern channel of the CGFZ at 30°W, exhibits a pronounced Θ/S minimum in the ULSW (Fig. 3.7) not being present there in 1999. It is accompanied

by the highest CFC-11 concentrations in the ULSW layer in this region. In contrast, the Θ/S minimum in the LSW is shifted to increased salinities at the same location. Though small-scale features at single stations cannot properly be resolved in the horizontal distribution maps, Figure 3.4 nevertheless exhibits increased CFC-11 concentrations east of the MAR at 30°W in 2001. This points to ULSW having entered the eastern basin through CGFZ. If it is assumed that this signal found in summer 2001 has been generated in the Labrador Sea in late winter of 2000, ULSW would have taken about 1.5 years to reach the eastern CGFZ, flowing at an estimated spreading rate of 5 cm s^{-1}.

Velocity measurements by Schott et al. (1999) and float results from Lavender et al. (2000) as well as Bower et al. (2002) indicated that the CGFZ is an important gateway for mid-depth water masses from the Labrador Sea entering the eastern North Atlantic basin. The floats analysed by Lavender et al. (2000) were ballasted to drift at 700 m depth. On average, they needed 1.6–2.6 years to reach the Iceland Basin, drifting at an average subsurface speed of 8.7 cm s^{-1}. As mentioned before, also this estimate does not indicate a true Lagrangian spreading, but it is comparable to the spreading rate of 5 cm/s given above.

West European Basin

The salinity/CFC-11 correlation in Figure 3.3k/l has indicated the presence of saline, CFC-poor Mediterranean Water in the WEB. The lowest CFC-11 concentrations were found close to the European Shelf associated to the lowest layer thickness (Figs. 3.4 and 3.5). However, an increase of CFC concentrations and layer thickness was found close to the MAR. Circulation maps provided by Bower et al. (2002) and Lavender et al. (2000) (cf. Fig. 3.8) indicate that the major flow enters the Eastern Basin via the fracture zones within the MAR and after a cyclonic loop turns southwards. The observed increase in CFC-11 and layer thickness close to the MAR obviously is related to an intrusion of southbound ULSW after having entered the Eastern Basin rather than an increase of water mass properties in the Mediterranean Water.

Obviously, ULSW of the late 1990s tends to follow similar pathways in the subpolar North Atlantic as have been revealed for the denser classical LSW by various authors (e.g., Talley and McCartney, 1982; Sy et al., 1997; Lavender et al., 2000; Rhein et al., 2002). Prior to this study, any significant spreading of ULSW close to the MAR and into the eastern basins so far was not investigated in detail or not even observed.

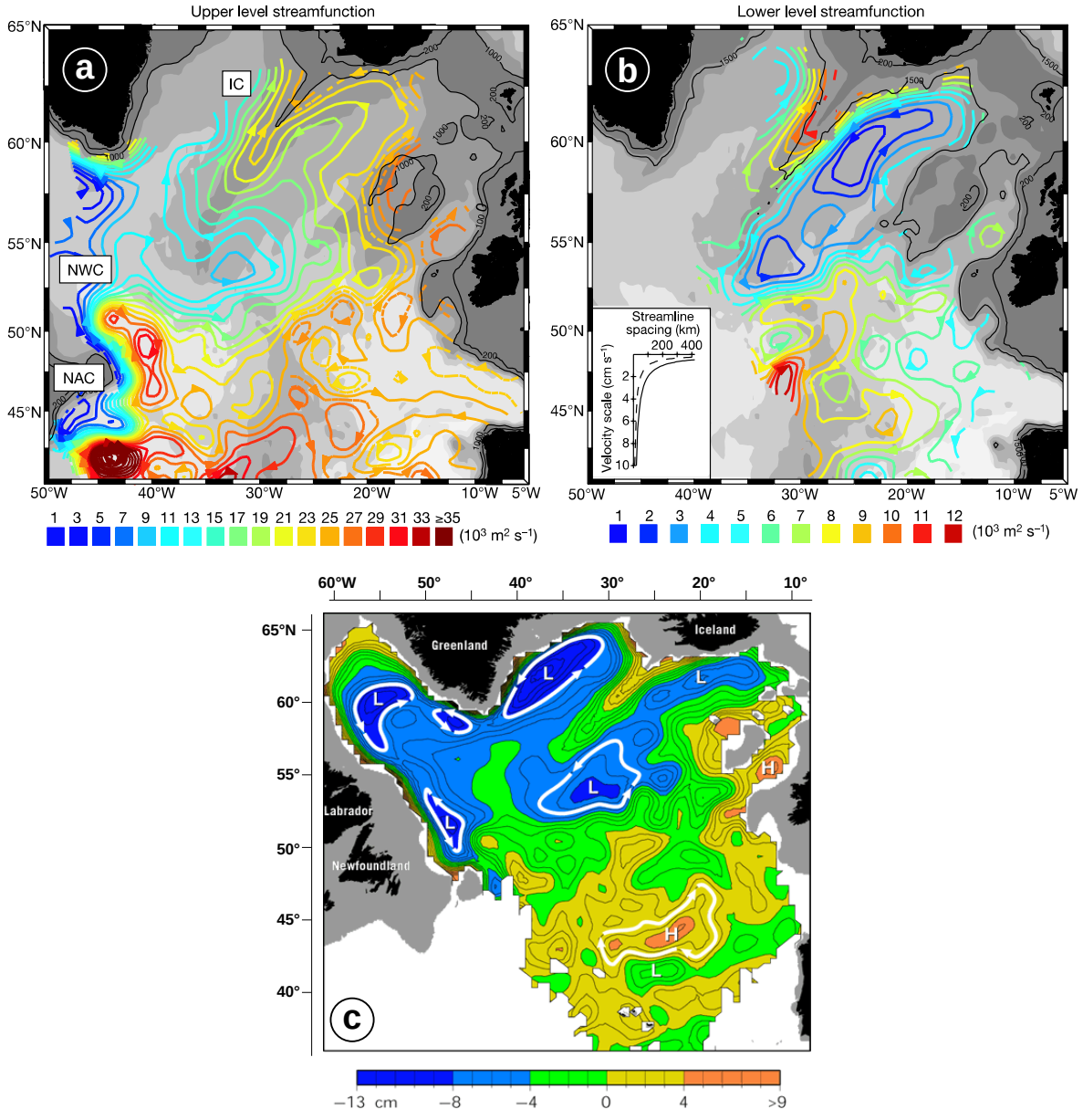

Fig. 3.8.: *a) Mean stream function from subsurface float data on $\sigma_\Theta = 27.5$ kg/m^3 surface, b) the same for LSW level, 1500-1700 m depth. Arrowheads show the direction of flow along the contours. Both figures are adopted from* Bower *et al. (2002). c) Geostrophic pressure (cm of water) at ∼700 m, derived from subsurface floats. Selected low-pressure centres are marked by L. Online-update of Fig. 2b published by* Lavender *et al. (2000), available at http://www.whoi.edu/annualreport02/highlights/floats.html.*

3.4. CFC-11 Inventory variability of ULSW and LSW during 1997-2001

3.4.1. CFC-Inventories

Following R02, the total CFC-11 inventory $\mathbf{CFC_{INV}}$ of a water mass is calculated from the gridded fields of layer thickness and average CFC-11 concentration:

$$\mathbf{CFC_{INV}} = \boldsymbol{\rho} \sum_{ij} (\mathbf{C}_{ij} \cdot \mathbf{A} \cdot \mathbf{D}_{ij}) \tag{3.3}$$

with $\mathbf{C}_{ij}$: CFC-11 concentration (pmol/kg) at a particular location lat(i), lon(j), $\mathbf{D}_{ij}$: layer thickness (m) at location lat(i), lon(j), $\mathbf{A}$: area (m^2) of a grid cell (0.25°lat × 0.5°lon), and $\boldsymbol{\rho}$: density of water (kg/m^3). The inventory $\mathbf{CFC_{INV}}$ is thus given in moles.

3.4.2. Filling data gaps

The data coverage of the SPNA changes considerably throughout the considered years. In the following, three methods have been applied to account for the spatial resolution of the parameter fields and estimate the corresponding inventory of ULSW and classical LSW according to Equation 3.3.

Method 1 (referred to as 'orig'): The data of 1997, 1999, and 2001 have been gridded using the same scaling factors as given in Section 3.2.2. The resulting total inventories of 1999 and 2001 will be severely underestimated, as can be recognised from the horizontal inventory distributions (Figs. 3.9 and 3.10, left column). Large areas of the SPNA are not covered. Since changes between the years are of particular interest, the total CFC-11 inventories of 1999 and 2001 cannot be estimated in the same way as the well-resolved inventory of 1997.

Method 2 (referred to as 'add %'): At first, the inventory of 1997 estimated according to Method 1 ('orig') is artificially reduced. This is done by transferring gaps present in the gridded 'orig'-inventories of 1999 and 2001 to the 'orig'-inventory of 1997. Then the 1997 inventory is re-calculated with the gaps of (a) 1999 and (b) of 2001 included. The result is compared with the full-coverage estimate ('orig') of 1997. A comparison of the original and reduced ULSW inventory distributions is shown in Figure 3.11. Differences give an estimate of what fraction of the inventory was missed in 1999 and 2001 due to data gaps. This fraction (given in %) was added to the 'orig'-inventories of 1999 and 2001. The temporal change during the years is accounted for at those grid points being filled in the 'orig' fields of 1999 and 2001. The most important regions are the Labrador and Irminger Seas which are quite well-covered by observations. In those regions with no data in the 'orig' fields, the inventories of 1999 and 2001 resulting from the 'add %' method are thus adjusted to the 1997 distribution to give at least a lower limit estimate.

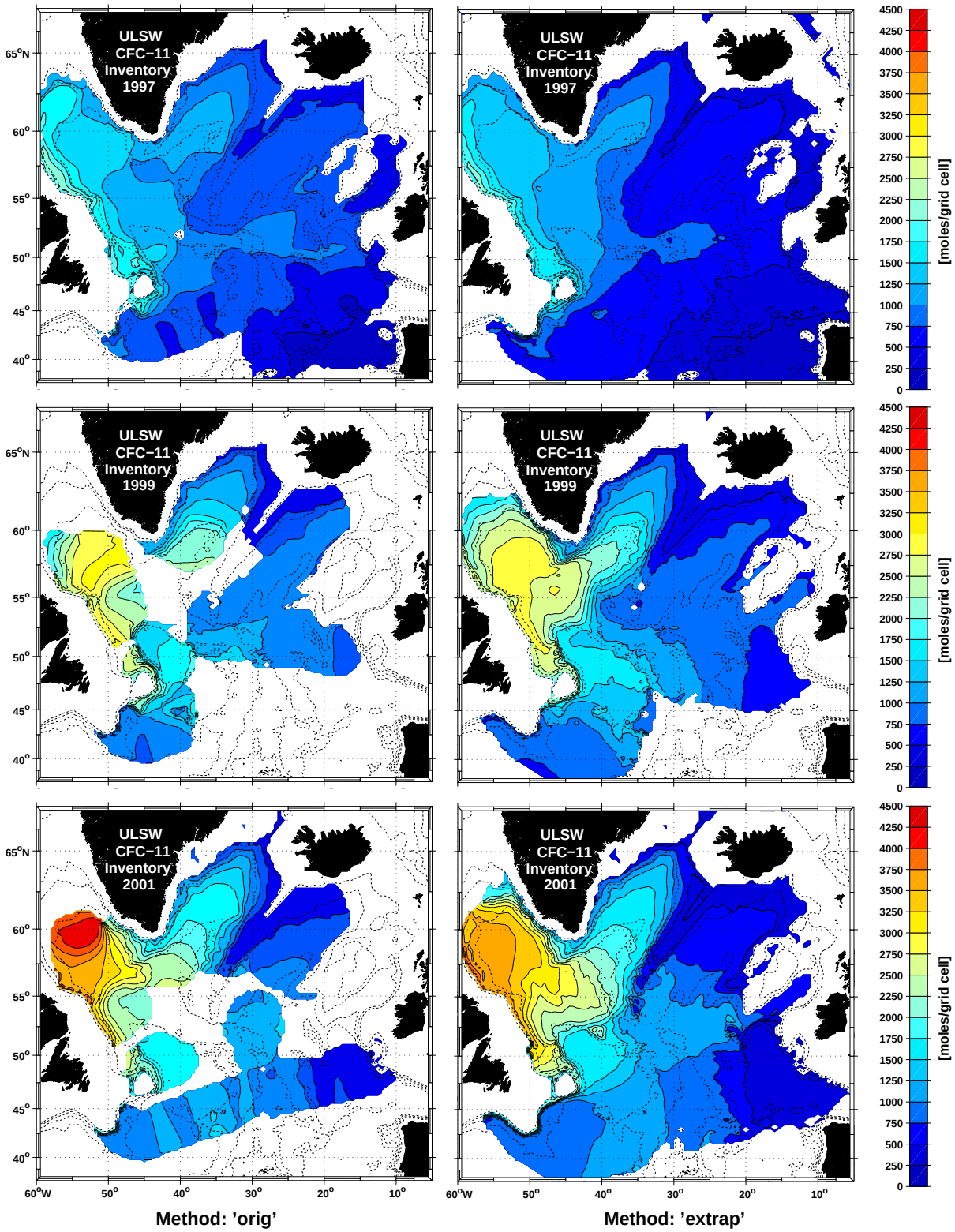

Fig. 3.9.: *Estimated CFC-11 inventory (moles per 0.25°lat × 0.5°lon grid cell) of ULSW, based on the data distribution shown in Figure 3.1. Top: 1997, middle: 1999, bottom: 2001. Left column: results from method 'orig', right column: results from method 'extrap'. Bathymetric contours are given every 1000 m.*

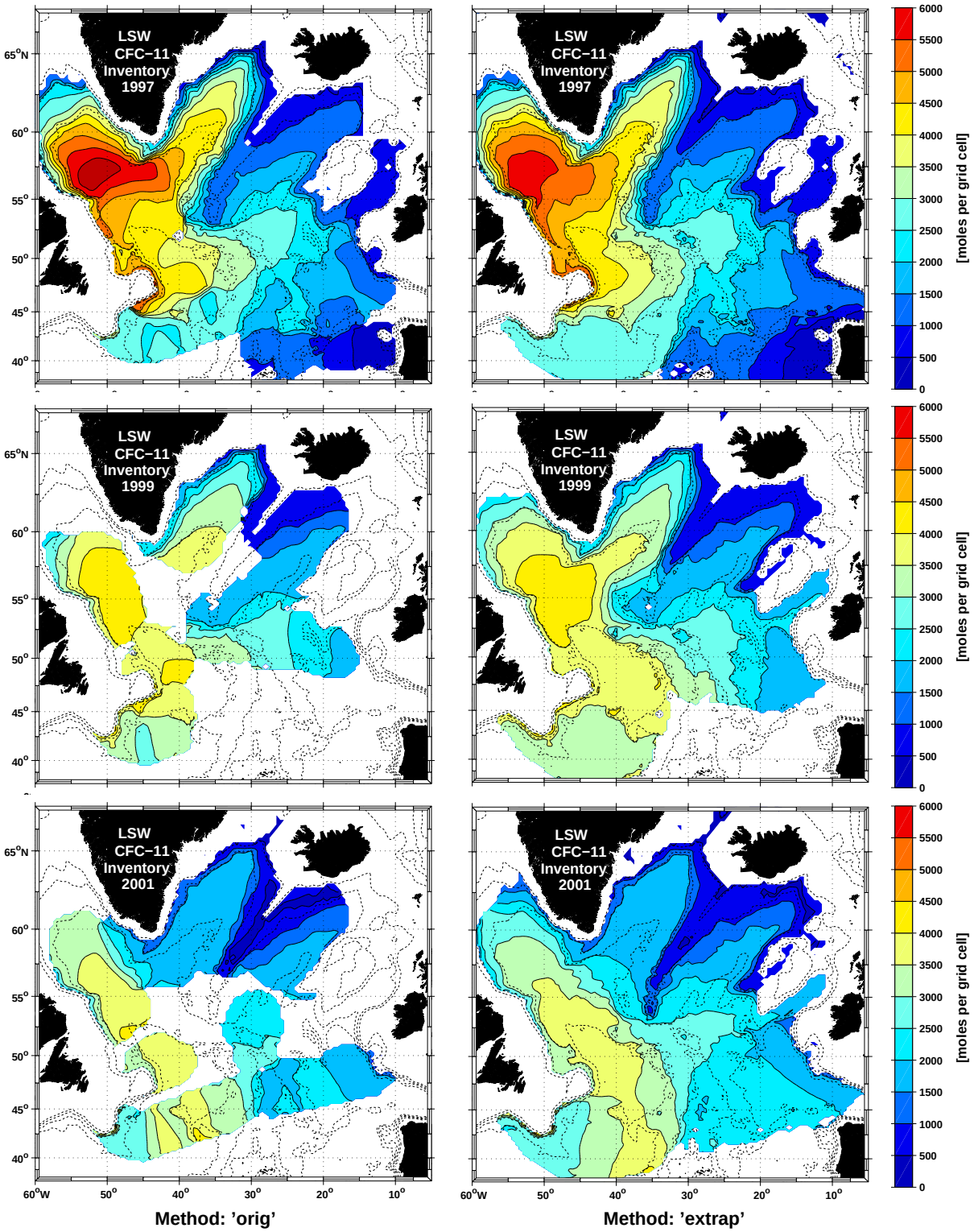

Fig. 3.10.: *Estimated CFC-11 inventory (moles per 0.25°lat × 0.5°lon grid cell) of classical LSW, based on the data distribution shown in Figure 3.1. Top: 1997, middle: 1999, bottom: 2001. Left column: results from method 'orig', right column: results from method 'extrap'. Bathymetric contours are given every 1000 m.*

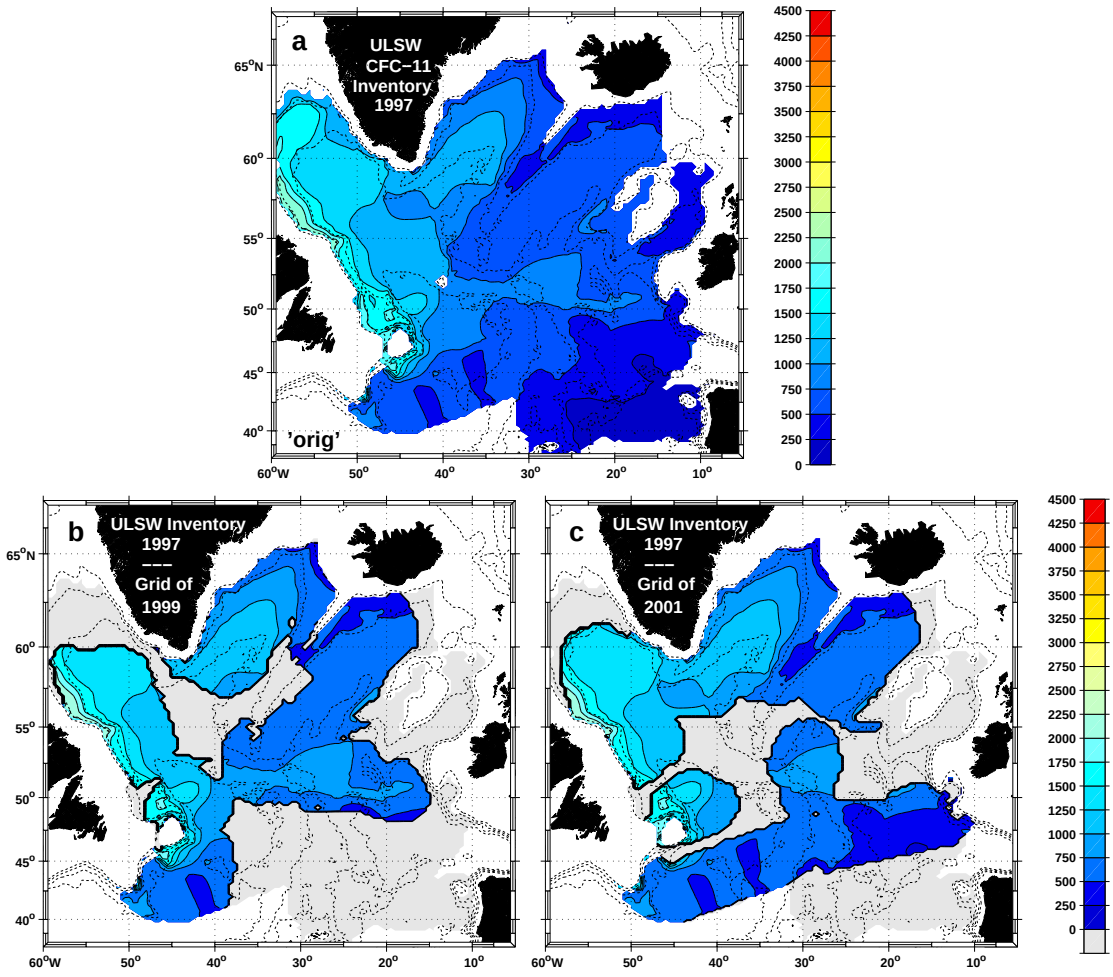

Fig. 3.11.: *(a) ULSW CFC-11 inventory (moles per 0.25°lat × 0.5°lon grid cell) of 1997, calculated according to method 1 ('orig '); (b) and (c) show the same inventory distribution which is reduced to the grid mask of the 1999 and 2001 'orig' inventories. The gray-shading indicates neglected areas with respect to 1997. See "Method 2" for details.*

Method 3 (referred to as 'extrap'): The rather statistical analysis of method 2 is opposed to a more physically-based: The advantage of the applied algorithm to map the data is the preservation of gradients at boundaries. R02 (their Figure 6) presented examples at various grid points, where the influence of the weighting function was either isotropic (basin interior) or followed the topography (near topographic slopes). To include those regions in the fields of 1999 and 2001 that were not covered due to the choice of the R02 scaling, the horizontal scaling parameter $\mathbf{\Lambda}$ given in Equation 3.1 was changed (Tab. 3.2). For comparison, the fields of 1997 were re-calculated. The choice of the scaling parameter results in a larger correlation length scale of $\boldsymbol{\lambda} = 224$ km. A weight of 10 % was considered at a distance of 480 km. Inventory gaps as seen for example in the central North Atlantic region (Figs. 3.9 and 3.10, left column) could be closed (same Figures, but right column). The increased smoothing resulted in an erosion of peak values. On the other hand, higher values were distributed over a larger area. The inventory distribution

	Method 1 R02 ≡ 'orig'	Method 3 'extrap'
$\frac{1}{\Lambda}$ in [1/km^2]	0.5×10^{-4}	0.1×10^{-4}

Tab. 3.2.: *Scaling parameters as applied in methods 1 and 3.*

of ULSW reveals the Labrador Sea as the most important region for the respective formation. The bulk of the inventory is located there. In contrast, the drainage of LSW out of the northwestern part of the SPNA becomes evident, as was expected from the CFC-11 and layer thickness distribution. The interior Newfoundland Basin obviously provides an important pathway for water mass export to the south.

3.4.3. Inventory estimates of ULSW and classical LSW

The total CFC-11 inventory estimates of ULSW and classical LSW, derived from all three methods, are summarised in Table 3.3. They are given for the SPNA between 40°N to 65°N. The CFC-11 inventory of ULSW during 1997 is calculated to 5.6-6.0 million moles, depending on the applied method. Due to the changing extrapolation scales, the SPNA inventory of ULSW in 1997 rose by 7 %. In 1999, the inventory was 8.1–8.4 million moles, and in 2001 ULSW inventory estimates gave in 9.3–9.5 million moles. Thus, within the limits of the methods, the SPNA inventory of ULSW considerably increased from 1997 to 2001.

Respective total CFC-11 inventories for LSW decreased from 18.2-19.5 million moles in 1997 to 15.6-16.7 million moles for the year 2001. The inventory for the classical LSW layer in 1997 has already been evaluated by R02. The authors calculated 16.6 million moles but used a reduced data set compared to this study. As was pointed out in Section 3.2, data from two cruises were not included. R02 estimated the contribution of areas that lacked data in the data set available to them. The extrapolation of the property fields in the northern Labrador Sea gave an inventory increase of 3.6 %. For the regions not covered at the southern rim of the investigation area, they assumed a fixed mean layer thickness of 700 m and a fixed mean CFC-11 concentration of 1 pmol/kg. This added another 3% to the inventory. With these contributions R02 calculated the revised LSW inventory in 1997 to 17.7 million moles. This result is close to the 18.2-19.5 million estimated in this study. The remaining difference is within the error margins. These will be determined later on.

To estimate the regional contributions to the total SPNA CFC-11 inventory, the subpolar North Atlantic has been subdivided into four different basins (cf. Figure 3.2).

	CFC-11 Inventory (10^6 moles)								
	1997			1999			2001		
	1 'orig'	2 'add %'	3 'extrap'	1 'orig'	2 'add %'	3 'extrap'	1 'orig'	2 'add %'	3 'extrap'
ULSW									
total SPNA	5.6	-	6.0	5.3	8.4	8.1	6.6	9.5	9.3
LabSea	1.7	-	1.7	2.0	3.1	2.8	2.8	3.8	3.4
IrmSea	1.0	-	1.0	1.0	1.5	1.5	1.3	1.7	1.8
NFL Basin	1.1	-	1.3	1.2	1.6	1.9	1.2	1.8	1.9
Eastern Basin	1.8	-	2.0	1.1	2.2	1.9	1.3	2.2	2.2
LSW									
total SPNA	18.2	-	19.5	11.1	17.2	17.0	11.1	15.6	16.7
LabSea	5.1	-	5.2	2.9	3.9	3.9	2.7	3.3	3.2
IrmSea	3.5	-	3.5	2.1	3.2	3.1	1.4	1.8	2.2
NFL Basin	4.4	-	5.2	3.5	4.7	5.4	3.5	4.8	5.3
Eastern Basin	5.2	-	5.6	2.6	5.4	4.6	3.5	5.7	6.0

Tab. 3.3.: *Estimated CFC-11 inventories of ULSW and classical LSW. 'orig' represents the inventory without filling the gaps, method 'add %' and method 'extrap' denote estimates derived from either adding missing percentage fractions or changing the extrapolation of data. See section 3.4.2 for details. Estimates are given for 40°N to 65°N*

.

Throughout the observation period, the western SPNA experienced the greater CFC-11 concentrations as well as layer thicknesses than the Eastern Basin. This is reflected in the regional contributions to the total ULSW inventory of 1997. About two-thirds were found in the western North Atlantic (sum of LabSea, IrmSea, and NFL-Basin), while the remaining third was located in the Eastern Basin. A similar regional partition has been estimated by R02 for the LSW in 1997. The greatest part of the ULSW inventory was found in the Labrador Sea throughout the years (Table 3.3). This was already expected, since this region exhibited the greatest changes in layer thickness which in turn is the dominant parameter for the inventory calculation. The ULSW inventory of this region more than doubled from 1.7 million moles in 1997 to 3.4–3.8 million moles during 2001, with the greater changes occurring during the first two years rather than the last. The corresponding increase in layer thickness was stronger during 1997-1999 than during 1999-2001 (Stramma et al., 2004). On the other hand, the corresponding classical LSW inventory of the Labrador Sea considerably reduced from 5.1–5.2 million moles in 1997 to 3.2–3.3 million moles in 2001, reflecting the thinning of this layer in this period. In 2001, about 40 % of the SPNA inventory of ULSW were located in the Labrador Sea. In contrast, about 20 % of the corresponding total LSW inventory was found there, compared to 28 % in 1997.

The Irminger Sea ULSW inventory increased from 1.0 million moles in 1997 by 70–80 % in 2001, depending on the method, while the LSW inventory of the same region reduced from 3.5 million moles in 1997 to 3.2–3.3 million moles in 2001. The change in the Newfoundland Basin was less, but still more than 46 % of the 1997 inventory of ULSW were introduced in the subsequent two years, followed by a minor increase of about 12 % from 1999 to 2001 (method 2, 'add %'). The corresponding LSW inventories are not distinguishable within the limits of the method, which will be shown later in more detail.

The change to greater correlation scales (method 3) led to an inventory increase particularly in the Newfoundland and the Eastern Basins. The inventories of the Eastern Basin are, however, more difficult to interpret. From 1997 to 1999, the local ULSW inventory of the Eastern Basin, calculated according to method 2, rose by 0.4 million moles (+22 %). During these years, the Eastern Basin north of about 50°N experienced an increase in layer thickness of 50–100 m together with an increase in the CFC-11 concentration of up to 0.25 pmol/kg. Both account for the inventory increase. In 1999, there wasn't any sampling along the WOCE-line A2. Even the adjusted extra- and interpolation (method 3) could not cover well the southern part of the West European Basin in 1999 (Figs. 3.9 and 3.10, right column). This might explain the apparent regional inventory decrease from 1997 to 1999 evident, since still an important part is missed. Though this is improved in the gridded fields of 2001 (method 3), the southeastern WEB between 40°N and 43°N was still not covered. The only available CFC-11 samples are from the A2-line. Data to the south of it (as in 1997) do not exist.

The LSW inventories of the Eastern Basin increased from 1997 to 1999 by 0.2 million moles (method 'add %'). This is within the error margins of the methods. Estimates from method 'extrap' indicate an inventory decrease from 1997 to 1999, followed by an increase of 1.4 million moles. Due to the afore mentioned lack in coverage in 1999, the

Region	Inventory of 1997 (10^6 moles)	Regional Contribution (%)
total SPNA	5.6 ± 0.6	100
LabSea	1.7 ± 0.2	30
IrmSea	1.0 ± 0.1	18
NFL-Basin	1.1 ± 0.1	20
Eastern Basin	1.8 ± 0.2	32

Tab. 3.4.: *CFC-11 inventories of ULSW for the year 1997 with error estimates derived from jackknifing. SPNA: Subpolar North Atlantic; LabSea: Labrador Sea; IrmSea: Irminger Sea; NFL-Basin: Newfoundland Basin. Given percentages denote the regional contribution to the corresponding total layer inventory of the SPNA. See text for details.*

regional inventories of either ULSW or LSW in the Eastern Basin in 1999 are assumed to be too small. While the LSW inventory of the Eastern Basin is expected to still increase, the insufficient data distribution of this region does not reflect this clearly enough.

3.4.4. Assessing the uncertainties

A statistical approach to estimate the uncertainty in the horizontal distribution of layer thickness, CFC-11 concentration and the resulting inventory is known as *jackknifing*. This tool relates to resampling a given data set by removing a fixed number of the available data points (Tichelaar and Ruff, 1989). In their analysis of classical LSW during 1997, R02 used the jackknifing approach to randomly remove 50 % of all the data points available in 1997. They calculated the *rms* error of all parameters at each grid point from 100 different sub-samples. The authors further provided maps (Fig. 10 in R02) showing that the *rms* values of the CFC-11 field exceeded 10 % off Newfoundland close to the continental slope. A second region was found on the western side of the MAR between 42°N and 48°N.

With the jackknifing approach applied to gridded fields representing the ULSW layer, the same regions proved to be crucial in the data sets of all three considered years. In 2001, also the region 30°W-20°W in the WEB revealed increased uncertainties. The uncertainty in the total CFC-11 inventory of ULSW in 1997 gives ±0.6 million moles, if the inventory is estimated according to method 1 ('orig') (see Tab. 3.4). The jackknifing approach has been repeated with application to the inventory distribution of 1997, derived

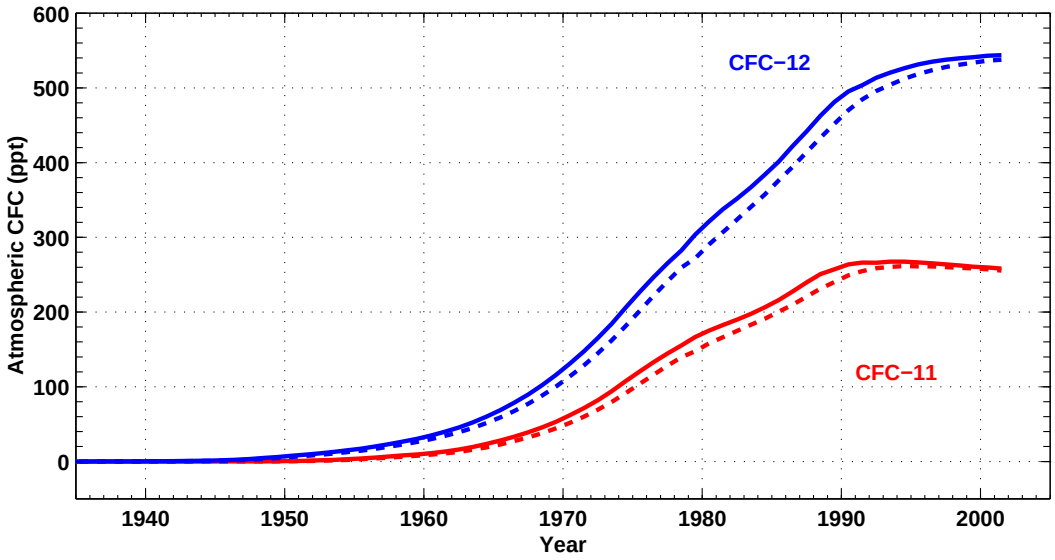

Fig. 3.12.: *Atmospheric history of CFC-11 and CFC-12 given in ppt. Solid lines indicate northern hemispheric estimates while dashed lines denote measurements from the southern hemisphere. Data are according to* Walker *et al. (2000).*

according to method 3 ('extrap'). Here, the resulting *rms* of the total ULSW inventory in the SPNA amounted to ±0.5 million moles. Inventory differences within these limits are thus considered insignificant.

3.5. Formation rates of ULSW and classical LSW

3.5.1. Basic Assumptions

The formation rate is considered as the volume transport of newly formed ULSW/LSW across that particular isopycnal which defines the upper boundary of the respective layer ($\sigma_\Theta = 27.68$ kg/m^3 for ULSW, $\sigma_\Theta = 27.74$ kg/m^3 for LSW). The accumulation of CFC-11 within a water mass increases, starting at the time when CFCs were initially released into the atmosphere to present time. Following Orsi et al. (1999), this equals the current CFC-11 inventory minus a loss of CFC-11 out of the considered water mass and into overlying and/or underlying layers. From the previous findings it is assumed that both ULSW and LSW are formed by winter time convection in the western subpolar North Atlantic. This process is believed to be by far the most important source for CFC-11 in these layers, i.e. lateral mixing with other water masses of the same density is ignored as well as diapycnal mixing.

The atmospheric time history for CFC-11 is well known since its initial release to the atmosphere (Fig. 3.12). With the solubility function of CFC-11 depending on temperature and salinity (Warner and Weiss, 1985) it can be expressed as the CFC-11

concentration which is in equilibrium to the atmosphere to a certain degree. The latter is given by the saturation level. Using Equation 3.3 given in Section 3.4.1, the annual mean formation rate is calculated as follows:

$$\mathbf{R_1} = \frac{\mathbf{CFC_{INV}}(t_n)}{\boldsymbol{\rho}(\int_{t_0}^{t_n} \mathbf{C_{eq}}(t) \times \mathbf{sat})dt} \tag{3.4}$$

with $\mathbf{R_1}$: formation rate (Sv), $\mathbf{CFC_{INV}}$: CFC-11 inventory of ULSW or LSW, $\mathbf{C_{eq}}$(t): CFC-11 concentration (pmol/kg) in water in year t (t_0, ..., t_n) which is in equilibrium with the atmosphere (atmospheric data from S. Walker, see Walker et al., 2000) and **sat** is the degree of saturation of the newly formed water mass.

There aren't any CFC-11 inventory estimates of ULSW for the subpolar North Atlantic prior to 1997 since SF01 excluded that region in their analysis. SF01 calculated an ULSW inventory of 4.2 million moles with ULSW defined in the density range $\sigma_{1.5}$ = 34.35±0.19 - 34.62 kg/m^3. LeBel et al. (2002) evaluated the subtropical/tropical ULSW inventory based on data from 1997 and received 4.2 million moles south of 40°N, but used a broader density-based definition for ULSW (neutral density γ = 27.33 - 27.897 kg/m^3, which roughly corresponds to a density range of σ_Θ = 27.44 - 27.74 kg/m^3; W. M. Smethie, pers. comm.). To get an estimate representative for the subpolar to equatorial Atlantic Ocean, this value is combined with the inventory from the subpolar North Atlantic (5.6–6.0 million moles). By using Equation 3.4, the total ULSW inventory of 9.8–10.2 million moles is then converted into a mean constant formation rate for the period 1930–1997. This is the time when CFCs have been released into the atmosphere (compare Fig. 3.12) and have entered the oceans.

The focus is, however, on changes in the inventories between the years 1997, 1999, and 2001. Equation 3.4 is therefore modified as follows:

$$\mathbf{R_2} = \frac{\mathbf{CFC_{INV}}(t_2) - \mathbf{CFC_{INV}}(t_1)}{\boldsymbol{\rho}(\int_{t_1}^{t_2} \mathbf{C_{eq}}(t) \times \mathbf{sat})dt} \tag{3.5}$$

Equation 3.5 is applied to the time periods 1997–1999 and 1999–2001 and gives corresponding formations rate estimates.

The SPNA as a closed box

The SPNA is considered as a closed basin within 2-year-intervals. This assumption is supported by the following reasoning: From an advective-diffusive model, Straneo et al. (2003) inferred residence times for LSW in the Labrador Basin to be 4-5 years. Stramma et al.(2004) estimated that LSW needs about 1-2 years to flow from its formation region to the Grand Banks at 43°N where it is exported to the south. ULSW formed during the late 1990s was found to spread at a similar spreading rate (about two years from 56°N to 43°N). The estimates from Section 3.3 indicated about 1.5 years for ULSW to reach the CGFZ. Obviously, during two years the SPNA seems large enough to keep

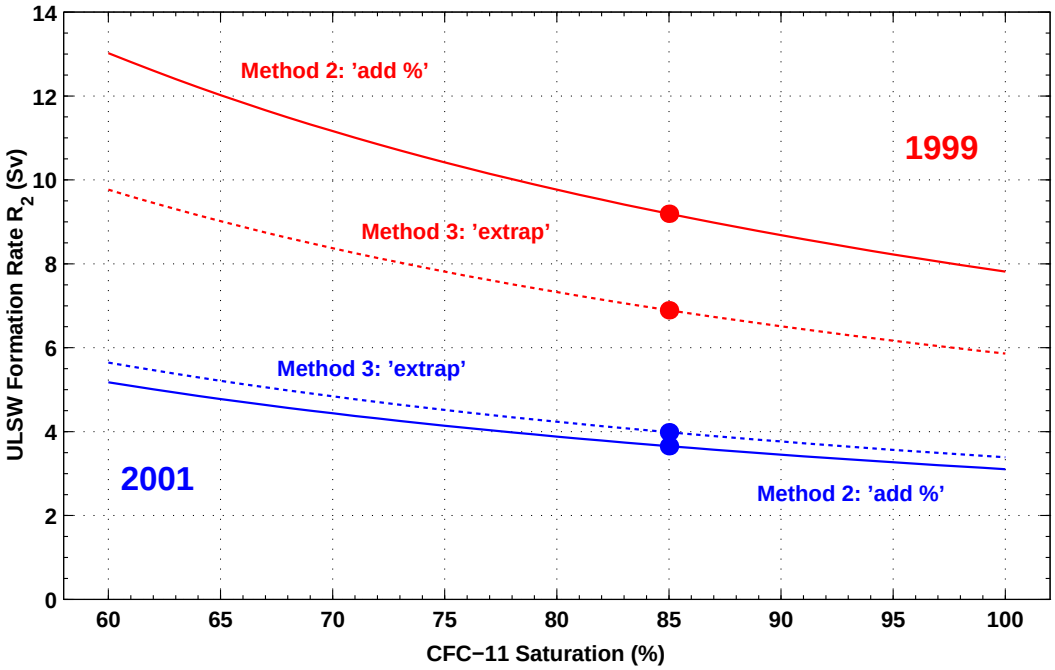

Fig. 3.13.: *Formation rate R_2 (Sv) of ULSW, calculated from corresponding CFC-11 inventories, versus CFC-11 saturation (%). Filled circles indicate the saturation level of ULSW prior to convection, as estimated in this study.*

the bulk of the inventory.

Figures 3.4/3.5 and 3.9/3.10 point to the existence of an export to the south. Though the ULSW layers defined by SF01 and LeBel et al. (2002) for the subtropical to tropical Atlantic are somewhat different, a comparison of these results indicates at least that there is not a remarkable increase in the inventory calculated by LeBel et al. (2002). As a first approximation it is assumed that an export of ULSW out of the subpolar gyre is small within two years.

The total LSW inventories quoted in Table 3.3 point to an export of 1 million moles within two years or 0.5 million moles per year (∼18 million moles to ∼16 million moles, 1997 to 2001). This is about 3 % of the total LSW inventory obtained in 1997. Supposed, this number also holds for ULSW, the respective inventory would be annually decreased by about 0.2 million moles due to southward export. This is much smaller than the assumed uncertainties in the methods.

Saturation

The formation rates calculated according to Equations 3.4 and 3.5 include a dependency on the saturation level of CFC-11. This is illustrated in Figure 3.13 for the ventilation of the ULSW layer. The displayed curves were determined from the differences in the total ULSW inventory between the years 1997 to 1999 and 1999 to 2001 (Eq. 3.5). These are listed in Table 3.5 and will be discussed later on in detail. Generally, low CFC-11

saturation levels lead to higher formation rates and vice versa.

Several investigations from the Labrador Sea show convected water masses exhibiting low CFC-11 saturations. They result from the time scale of convection which is much smaller than the one for air-sea gas-exchange (several days versus a month). Surface waters exposed to the atmospheric input of CFC are transformed to deeper layers much quicker than the time, air-sea gas-exchange needs to bring the atmosphere and surface waters into equilibrium. For the classical LSW, Wallace and Lazier (1988) and Smethie et al. (2000) found saturations in convected water of 60-70 %. Based on CFC data collected in late winter of 1997, the analysis of R02 showed that, prior to convection, water located above LSW was saturated at 85 %. Since the water above the LSW will be transferred to LSW through convection and add its volume and its CFC content to the LSW inventory, R02 adopted this higher value as the more suitable one to calculate the formation rate.
For the ULSW layer of the 1980s/early 1990s, Smethie et al. (2000) estimated ULSW to be saturated at 70 %. Depth-weighted CFC-11 profiles with surface densities of $\sigma_\Theta > 27.68$ kg/m^3 and $\sigma_\Theta <= 27.74$ kg/m^3, sampled during February-March 1997 in the central Labrador Sea, showed mean CFC-11 concentrations of 4.59±0.11 pmol/kg in the upper 700 m. Corresponding mean concentrations from profiles with surface densities smaller $\sigma_\Theta = 27.68$ kg/m^3 were slightly decreased (4.53±0.42 pmol/kg), indicating about 1.5 % being added by air-sea gas-exchange during active convection. Since throughout the considered years the summer isopycnal $\sigma_\Theta = 27.68$ kg/m^3 is located at ∼200 m (compare Figure 2 in Stramma et al., 2004), CFC-11 concentrations of these profiles down to this depth average to 4.9±0.36 pmol/kg which conforms with a saturation of 83.3±4.4 %. This is the volume of water which is assumed to be converted to ULSW by the convection process. A combination of these estimates gives 85 % saturation, which is identical to R02's estimate for LSW. Concerning the observation period, obviously there isn't any difference in the saturations of ULSW and LSW prior to convection. If lower saturations were assumed (e.g., 70 %), the formation rates for the period 1997-1999 would be higher by 1.5-2 Sv, depending on the method to handle data gaps. The formation rate for the subsequent two years would be higher by about 0.8 Sv. (Fig. 3.13)

3.5.2. ULSW and LSW Formation during 1930-1997

Inventory differences and respective formation rates are sumarised in Table 3.5. Available reconstructed histories of the annual mean atmospheric mole fractions of CFCs reach back to 1930 (Fig. 3.12; Walker et al., 2000). At about that time, the release of anthropogenic CFCs into the atmosphere began. Stramma et al. (2004) pointed out that the observed 'new' ULSW of the late 1990s was formed during years, when LSW ventilation had ceased. Since Pickart et al. (1996, 1997) found considerable ULSW formation in the southern Labrador Sea in 1991/92 when simultaneously LSW formation took place in the central Labrador Sea, any years when ULSW formation has ceased cannot be

identified. The following estimate thus represents a mean annual formation rate for the period t_1–t_n = 1930–1997, assuming that the CFC-11 inventory observed in 1997 has been introduced during these years. As was pointed out by SF01 and R02, years prior to the mid 1970s did not contribute much to the CFC-11 inventory, since the atmospheric concentration increased exponentially during this time. About 5.7 % of the CFC-11 inventory were introduced in the ULSW layer between 1930 and 1970. Afterwards, the atmospheric concentrations increased linearly until 1990, making up 57.2 % of the ULSW inventory. The remaining 37.1 % have entered the ULSW layer since then. Assuming a saturation of 85 %, the mean annual formation rate calculated from the combined subpolar and subtropical/tropical inventory in 1997 (9.8–10.2 million moles, Section 3.5.1) yields 2.9–3.1 Sv. It is thus representative for the period 1970-1997.

For the same period, R02 estimated a formation rate of classical LSW. The authors received 4.4-5.6 Sv, using a CFC-11 inventory of 16.6 million moles. These calculations have been repeated in the present study based on the increased inventories due to the larger data set that is now available (compare Section 3.2). The CFC-11 inventories calculations of classical LSW gave 18.2-19.5 million moles (Tab. 3.3) which resulted in LSW formation rates of 5.5-5.9 Sv, representative for the period 1970-1997. The resulting combined ULSW/LSW formation rate is thus 8.4-8.9 Sv (cf. Table 3.5).

3.5.3. Formation rate variability 1997-2001

Depending on the method to handle data gaps, the ULSW formation rate for 1998-1999 is 6.9–9.2 Sv. In the subsequent two years, the formation rate weakened to 3.7–4.0 Sv. The assumed smallest uncertainty of the inventory (±0.6 million moles) leads to a formation rate uncertainty of ±2 Sv. The decrease in ULSW formation is therefore considered significant.

The estimation of the ULSW formation rate has been re-assessed on basis of the corresponding CFC-12 inventories of 1999 and 2001 (4.2 million moles CFC-12 in 1999 and 4.7 million moles in 2001 as a result of method 3 to adjust the coarse data resolution). The corresponding formation rates based on CFC-12 yielded 2.9–3.4 Sv in 1999-2001. Though being smaller than the one derived from CFC-11 inventories, they are still in a similar range.

The LSW inventories in the SPNA decreased indicating that LSW ventilation did not occur during the considered time period. Therefore, the resulting formation rates amount to zero. During 1997-1999, the ULSW formation almost compensated the lack of LSW formation. The corresponding formation rate are of a similar amount as the combined ULSW/LSW formation rates estimated in Section 3.5.2 (cf. Tab. 3.5).

		Inventory Difference (10^6 moles)			Formation Rate (Sv)	
	Years	'add %'	'extrap'	Formation Period	'add %'	'extrap'
ULSW	1997 - 1930	9.8	10.2	1930-1997	2.9	3.1
	1999 - 1997	2.8	2.1	1997-1999	9.2	6.9
	2001 - 1999	1.1	1.2	1999-2001	3.7	4.0
LSW	1997 - 1930	18.2	19.5	1930-1997	5.5	5.9
	1999 - 1997	-1.0	-2.5	1997-1999	0	0
	2001 - 1999	-1.6	-0.3	1999-2001	0	0
ULSW+LSW	1997 - 1930	28.0	29.7	1930-1997	8.4	8.9

Tab. 3.5.: *CFC-11 inventory differences and corresponding formation rates for different periods and methods, assuming 85 % saturation. Positive inventory differences denote an inventory increase from year t_1 to year t_2.*

3.6. Ventilation Regions of ULSW and LSW

The Labrador Sea is an important region for ULSW and LSW ventilation (e.g. Pickart, 1992; Pickart et al., 1996, 1997; Lazier et al., 2002; Stramma et al., 2004). Here, it is verified to a first order whether additional ventilation regions for both water masses might exist. Climatological mixed layer depths (Monterey and Levitus, 1997) have been analysed for the month of March in conjunction with climatological March densities derived from the World Ocean Atlas 1994 (WOA-1994, Levitus, 1994). In general, the northern SPNA is not very well covered by winter-time hydrographic data due to harsh weather conditions. In the Labrador and Irminger Seas, the most recent open-ocean observations for March included in both climatologies are from the early 1980s. The winter climatology thus represents the oceanic conditions almost two decades prior to the observation period previously discussed. The resulting climatological density field at the sea surface (Fig. 3.14a) indicates that the outcropping of the $\sigma_\Theta = 27.68$ kg/m^3 isopycnal during winter only occurs in the Labrador and Irminger Seas. These are the regions with the greatest mixed layer depths (1000 m, the greatest depth analysed in this climatology). A third outcropping region exists to the northeast of Iceland. In contrast, outcropping of the $\sigma_\Theta = 27.74$ kg/m^3-isopycnal, which is the upper boundary of classical LSW, is confined to the Labrador Sea and northeast Icelandic regions. Further deep mixed layer regions (700-900 m) were found over the Rockall Bank and Rockall Trough. However,

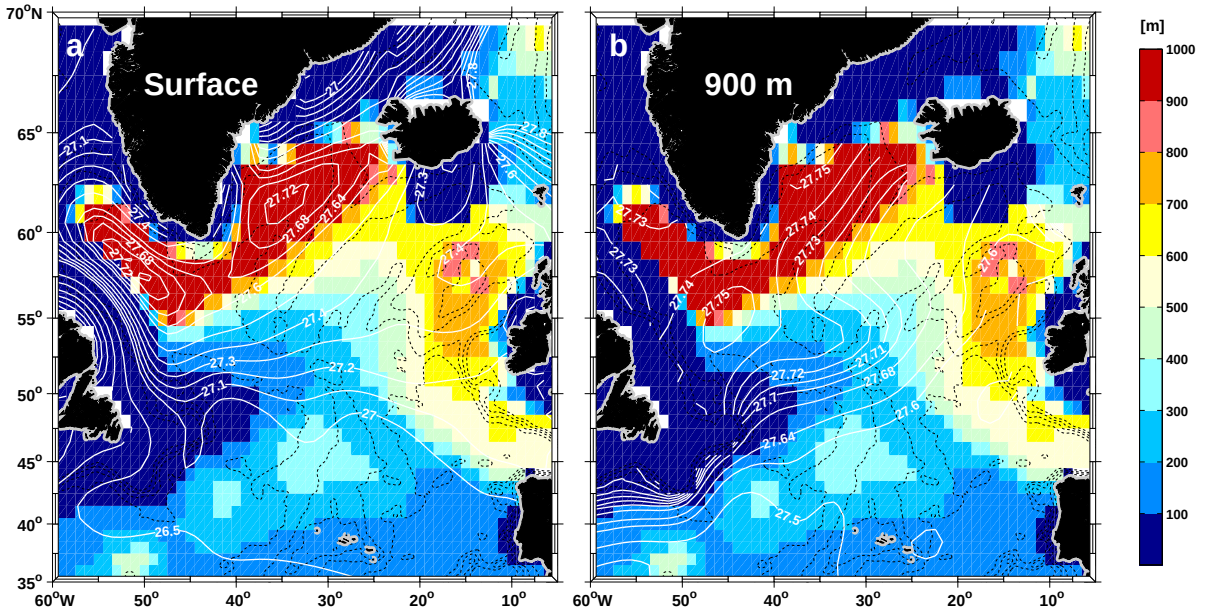

Fig. 3.14.: *Mixed layer depth (m) for climatological March (coloured), derived from the* Monterey *and* Levitus *(1997)-climatology. Superimposed are contours of the climatological* σ_Θ*-field (kg/m*^{3}*) of March. (a) at the sea surface and (b) at 900 m. The density fields are derived from WOA-1994 (*Levitus*, 1994). Thin black lines indicate bathymetric contours given every 1000 m.*

March isopycnals at 900 m (Fig. 3.14b) do not exceed $\sigma_\Theta = 27.64$ kg/m^3 in these regions. Thus, the density classes of ULSW and LSW are supposed to be ventilated entirely in the western subpolar North Atlantic. In the data presented here, there isn't any evidence for ventilation of these water masses in the eastern subpolar Atlantic, that is, to the east of the MAR.

The Labrador Sea

The depth of penetration during convection depends on the stratification of the water column and the strength of the time-integrated winterly surface buoyancy fluxes (Marshall and Schott, 1999). The integrated buoyancy content (**BC**) of a water column can be thought of as a measure for the stratification of the water column. It is given by

$$\mathbf{BC} = \int_{-h}^{0} -\mathbf{g}\frac{(\boldsymbol{\rho} - \boldsymbol{\rho_0})}{\boldsymbol{\rho_0}} dz \tag{3.6}$$

where $\mathbf{g}$ (m/s^2) is the acceleration of gravity, and $\boldsymbol{\rho}$ and $\boldsymbol{\rho_0}$ (both given in kg/m^3) are the actual and reference density. The buoyancy content is derived from hydrographic profiles and hence calculated from the surface down to $-\mathbf{h}$ which is of the depth of the $\sigma_\Theta = 27.68$ kg/m^3-isopycnal. It is proportional to the integral of density anomaly (relative to the background density of the corresponding profile) contained above this depth. High

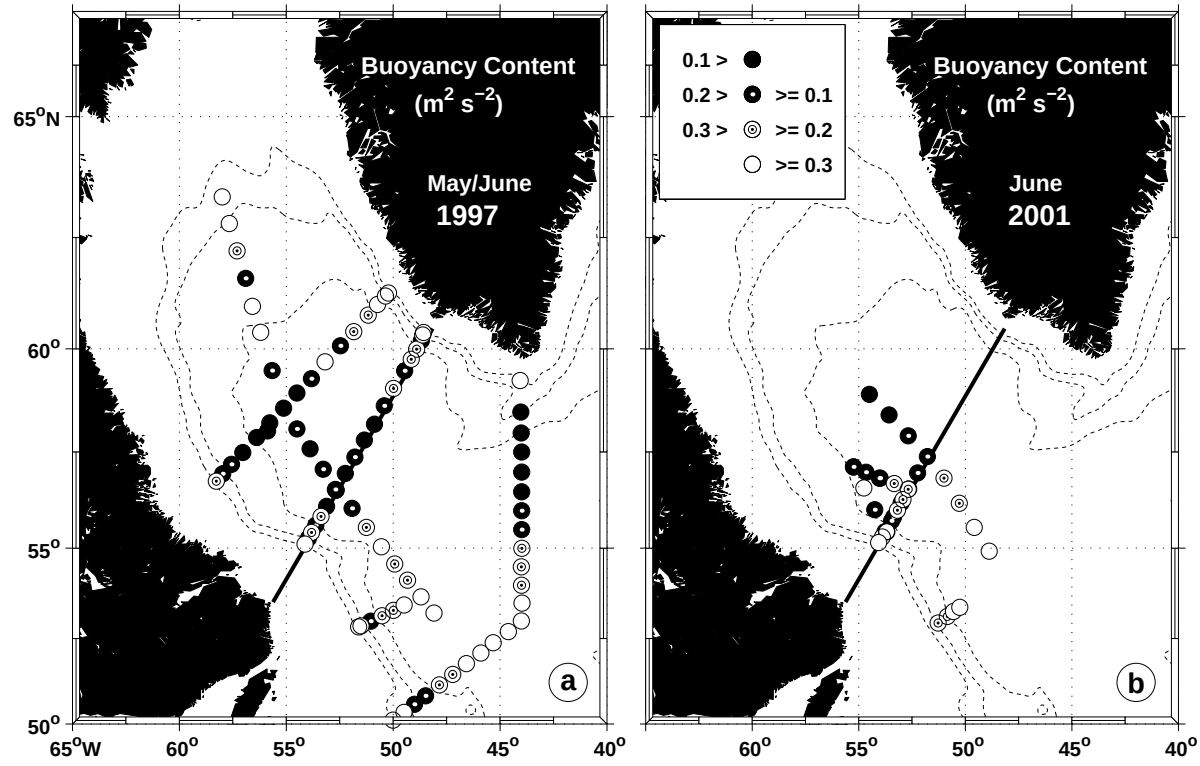

Fig. 3.15.: *Buoyancy content (m^2/s^2) of surface layers [0 m - $z(\sigma_\Theta = 27.68\ kg/m^3)$], derived from CTD profiles: (a) May/June 1997 and (b) June 2001. Solid lines indicate the location of WOCE-line AR7W.*

values of **BC** indicate that a greater rate of buoyancy has to be removed during winter for convection to reach $-\mathbf{h}$.

Lavender et al. (2000, 2002) provide estimates of mixed layer depths that point to convection reaching down to 800 m north of 60°N and >800 m in the western Labrador Sea during the winter of 1996/97. This is to some extent reflected in the buoyancy content displayed in Figure 3.15(a). Analyses of CTD profiles from June 1997 indicate **BC** minima in the central Labrador Sea, its western and northern boundary current region as well as south of Greenland at the exit of the southern Irminger Sea. Hydrographic profiles from June 2001, unfortunately, do not extend as far to the north as during summer 1997. However, hydrographic and CFC-11 data sampled along the axis of the Labrador Sea during summer 2001 (Fig. 4 in Stramma et al., 2004) show the highest CFC-11 concentrations and the thickest ULSW layer in the northern part of this section. The location corresponds to the location of minimum **BC** estimates during 2001 (Fig. 3.15b).

The Irminger Sea

Another region for potential renewal of intermediate water masses probably is the Irminger Sea. The question whether significant deep convection happens in the Irminger Sea is

open to discussion. Historical data of winter 1958 (Dietrich, 1969) and the WOA-1994 climatology pointed to a winter-time outcropping of the $\sigma_\Theta = 27.68$ kg/m^3-isopycnal in the Irminger Sea. Lavender et al. (2002) showed that local mixed layer depths of 600–800 m have been reached in winter 1996/1997 southwest of Greenland (west of about 45°W). From the analyses of potential vorticity distributions and atmospheric conditions, Pickart et al. (2003a) argued that the southwestern Irminger Sea is the most likely location for convection to occur. The succeeding work of Pickart et al. (2003b) suggested the small-scale atmospheric *Greenland tip jet* to be the likely cause for Irminger Sea convection since it has impact on the regional surface fluxes. Bacon et al. (2003) presented results from ship measurements and profiling floats from this region that indicate local formation of convective plumes in the southeast of Greenland during winter 1996/1997. They also noticed an outcropping of the isopycnal $\sigma_\Theta = 27.68$ kg/m^3.

Concerning the observation period 1997-2001 the formation rates previously estimated provide some valuable hints. With 1 Sv corresponding to a volume of $3.2{\cdot}10^{13}$ m^3 formed in one year, the formation rates of ULSW can be used to determine the size of the convection area. The area of the Labrador Sea (for water depths > 500 m) north of 50°N and west of 45°W is about $1{\cdot}10^6$ km^2. However, this large area is certainly not completely affected by winter-time convection. The ULSW formation rates of 6.9–9.2 Sv during 1998-1999 and 3.7–4.0 Sv in 2000-2001 correspond to a convection area of $(1.1–1.5){\cdot}10^6$ km^2 and $(0.6–0.7){\cdot}10^6$ km^2 respectively, if the new water prior to convection occupies the upper 200 m of the water column. During the considered observation period this is the typical depth location of the $\sigma_\Theta = 27.68$ kg/m^3 (Stramma et al., 2004). This water layer lying on top of ULSW that must be transformed to ULSW during winter-time convection. The convection area estimates correspond to approximated circular areas with radii $r_c =$ 590-690 km during 1998-1999 and $r_c =$ 440-470 km in the subsequent two years. At least for the period 1998-1999, the size of the probable formation region was too large to be restricted to the Labrador Sea. Figure 3.16 shows the dependencies of the convection area on the layer thickness of water lying on top of ULSW. The greater estimate of ULSW formation during 1998-1999 (9.2 Sv) indicates that this conclusion holds also, if layer thicknesses of water lying on top of ULSW of up to 300 m are assumed. These results might serve as an indication that the Labrador Sea was not the only location of ULSW formation during these years.

Comprehensive winter data are needed to really give evidence of convection happening in the Irminger Sea. These are to a certain part provided by ARGO. This is a system for operational oceanography and currently under development. ARGO aims at monitoring and forecasting the ocean's behaviour (Argo Science Team, 1998). It is based on in situ measurements from ships, moorings, and drifting autonomous systems such as profiling floats.

Figure 3.17b presents temperature profiles received from one of the very few profiling floats which drifted in the Irminger Sea during late winter of 1998. Data are from the ARGO-project web-site[III]. At least four profiles indicate a homogeneous temperature

[III] ARGO float data centre: http://www.coriolis.eu.org

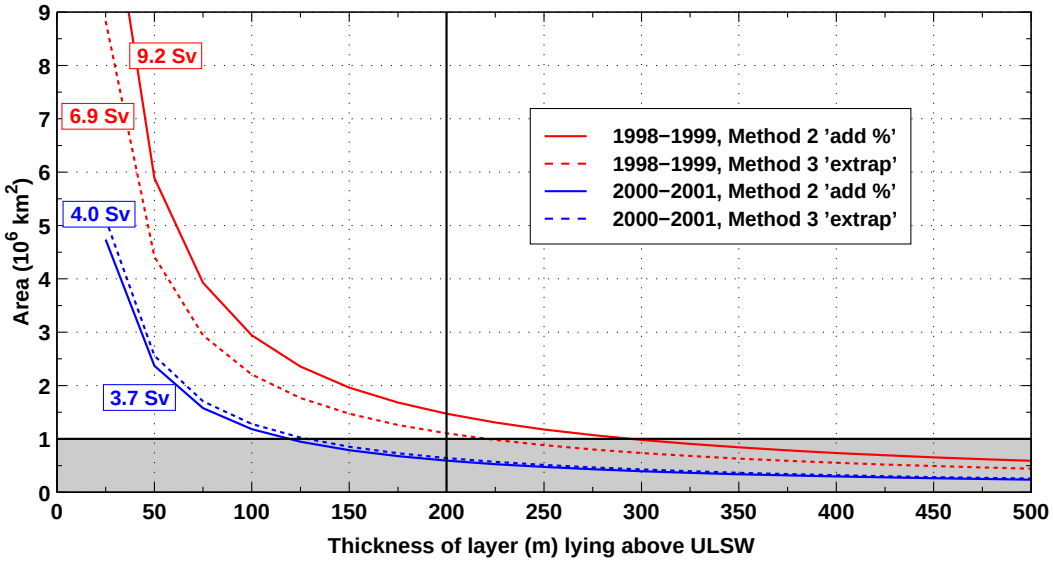

Fig. 3.16.: *Size of convection area (10^6 km^2) derived from ULSW formation rates and assumed layer thickness of water lying on top of ULSW. The grey area marks the size of the Labrador Sea for the region west of 45° W, north of 50° N, and a water depth greater than 500 m.*

distribution reaching down to 300-400 dbar. Since the float was not equipped with a conductivity sensor, salinity data are not available. Knowledge about this parameter is, however, important to estimate the stratification present at that time.

In the subsequent summer CTD profiles were taken within the framework of VEINS close to the winter-time positions of the ARGO float (Fig. 3.17a). The σ_Θ= 27.68 kg/m^3 isopycnal (the upper limit of ULSW) of the corresponding density field was located at 300 dbar at the off-shore end of this section, in contrast to 850 dbar on the Greenland side (Fig. 3.17d). The off-shore end of this section was associated with the lowest salinities within the ULSW as well as the LSW layer. The layer thickness of the denser LSW was more than doubled in size compared to the DWBC region (∼1250 m versus 600 m), while ULSW was thicker by 100 m (350 m versus 250 m in the on-shore region).

Salinities similar to the ones found in the ULSW (S < 34.88) were also present in the top 300 m of the water column. If these features have been caused by local convective events during this particular winter, corresponding convection depths of about 400 m appear to be deep enough to reach into the ULSW layer. The horizontal gradients of CFC-11 and the layer thickness previously presented (Figs. 3.4 and 3.5) suggest, however, that the ULSW formation in the Labrador Sea is of greater importance for the accumulation of CFC-11 in the southwestern Irminger Sea than local convection.

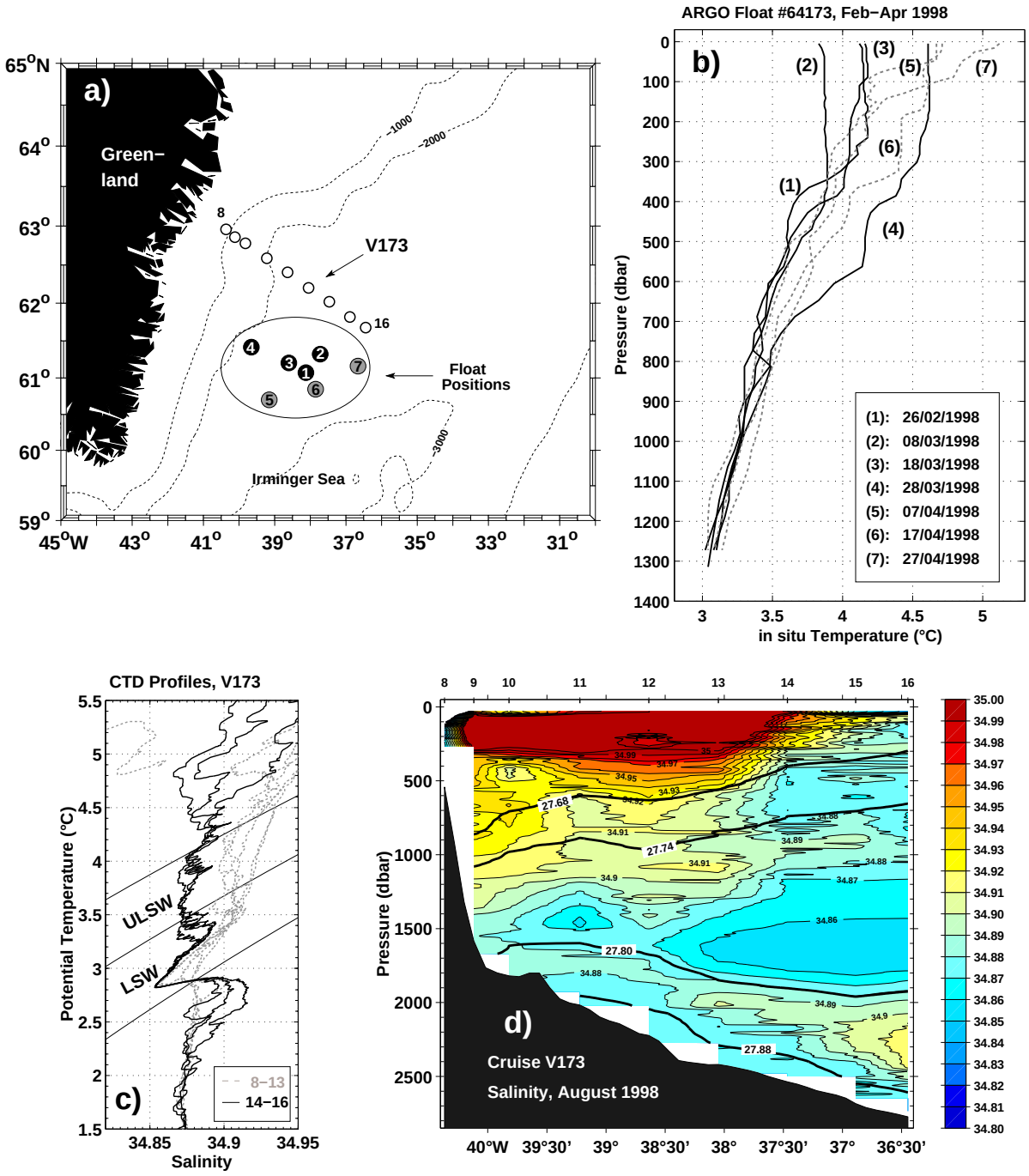

Fig. 3.17.: *(a) Location of temperature profiles from ARGO float No. 64173 taken during winter 1998 in the Irminger Sea (dots within ellipse). The location of CTD profiles from the subsequent summer of 1998 is indicated by white dots. Dashed lines mark the bathymetry given every 1000 m. (b) Corresponding temperature profiles derived from ARGO float data. (c) Θ/S diagram derived from CTD profiles of cruise V173, R/V Valdivia, August 1998. (d) Salinity section of cruise V173. Data are courtesy of IFM Hamburg.*

3.7. Summary and Conclusions

Formation rates of ULSW and the denser classical LSW have been inferred from CFC-11 inventories, calculated for the years 1997, 1999, and 2001. Different methods have been used to account for the occurrence of data gaps in the parameter fields of the years 1999 and 2001. Within the error margins both methods gave very similar estimates of the inventories and corresponding formation rates of ULSW and classical LSW. The application of method 3 ('extrap') resulted in greater correlations scales to map the data and hence a broader extrapolation. Using method 2 ('add %'), those regions that lacked data in the inventory distributions of 1999 and 2001 were adjusted to the well-resolved inventory of 1997. This method may be increasingly problematic for future data to come. Data from the year 1997 were collected shortly after the high-convective activity in the Labrador Sea had ended. As was presented by Stramma et al. (2004) and will be discussed in more detail in Chapter 4, the bulk of ULSW was formed after 1997. It is expected that future CFC inventories of ULSW will continue to increase in the southern and eastern parts of the SPNA. Filling occurring data gaps by a broader inter-/extrapolation of the data will likely be more appropriate in future than continuing to adjust these fields to the 1997 distribution. In any a case, a good data coverage of key regions in the SPNA is highly desirable. While the magnitude of the total ULSW inventories was increasingly dominated by profiles from the Labrador and Irminger Seas, this was different for the denser classical LSW due to its gradual flushing out of the formation region (Tab. 3.3, Figs. 3.9 and 3.10).

In the period 1997-2001, ULSW showed a considerable increase in formation which was stronger in 1997-1999 compared to the subsequent years. In contrast, any significant LSW formation could not be detected. It cannot be ruled out that occasional deep convection events have happened during the winters of 1998-2001. Thus, the isopycnal $\sigma_\Theta = 27.74$ kg/m^3 (upper boundary of LSW) may have out cropped locally. For example, Mertens (2000) noticed from mooring data that convection down to depths of 800-900 m had happened to the northwest of WOCE-line AR7W in March 1999. A mooring deployed at AR7W revealed mixing only down to depths of 500 m. Within the limits of methods and available hydrographic/tracer data, there is, however, no net effect of these local events on the CFC inventories.

There are indications that the convection area needed in 1998/99 to form the observed amount of ULSW exceeded the available area in the Labrador Sea. Winter data (February-March 1998) from a profiling float that traveled in the Irminger Sea have been presented. Corresponding temperature profiles suggest that local ULSW formation has happened there. The horizontal gradients in the layer thickness and CFC-11 fields, however, point to the Labrador Sea as the far more important source for ULSW formation.

Whether the considerable decrease of the combined ULSW/LSW formation rate has an impact on the deep water export into the subtropical Atlantic is an intriguing question. Schott et al. (2004) presented DWBC transport time series derived from moorings that were deployed at ∼43°N. The times series comprise the years 1993-1995 and 1999-2001

and cover water masses with densities greater than $\sigma_\Theta = 27.74$ kg/m^3. Though during both periods considerable short-term variability was evident, the mean southward transports amounted to 11.2 Sv and 11.3 Sv, respectively, which the authors found to be incidental. Transport time series from the second deployment (1999-2001) showed nevertheless a slightly decreasing trend of 1.7 Sv/yr. Whether this is already an imprint of the cessation of LSW formation can only be clarified, if further and longer time series from moorings as well as tracer measurements become available.

4. Long-Term Variability of ULSW and LSW Properties

In the previous chapter, it was shown that the CFC-11 inventory, layer thickness and formation rate of ULSW have increased since the late 1990s. At that time, ULSW had started to displace and even replace the thick layer of LSW formed during the active deep convection period of the early 1990s. The question arises to what extent ULSW is subject to variability on decadal scales. The objective of the present chapter is to derive property time series with respect to ULSW and to compare these with times series related to LSW.

4.1. Introduction

Throughout the last decades a lot of effort has been made to identify the processes involved in LSW production (e.g. Lazier, 1973; Clarke and Gascard, 1983; Marshall and Schott, 1999) and the associated spreading pathways (e.g. Talley and McCartney, 1982; Sy et al., 1997; Rhein et al., 2002). Available time series indicate that LSW properties (e.g. potential temperature, salinity, layer thickness) are subject to considerable change over the past decades (e.g. Talley and McCartney, 1982; Lazier, 1980 & 1988; Sy et al., 1997; Curry et al., 1998, Lazier et al., 2002; Rhein et al., 2002; Stramma et al., 2004).

The maintenance of OWS *Bravo*, operated from 1945 to 1974 in the Labrador Sea, is of great value in this context, since it was accompanied by an extensive oceanographic sampling program lasting from 1964 to 1974. The availability of well-resolved and deep-reaching high-quality profiles in the LSW source region is, however, limited, especially during the mid 1970s to mid 1980s. In the pre-WOCE era, the majority of existing profiles in the central Labrador Sea did not exceed 1500 m. Since LSW occasionally occupies a large vertical depth range (about 500-2000 m), the temporal resolution of respective long-term time series is restricted by the availability of deep profiles.

Two CTD sections from the central Labrador Sea, sampled during 1990 and 2001 (Lazier and Gershey, 1991; Schott et al., 2002), are used to illustrate some of the existing classifications of LSW (Fig. 4.1). The section of 1990 was the first of multiple repeats conducted in the central Labrador Sea within the framework of WOCE. The time of

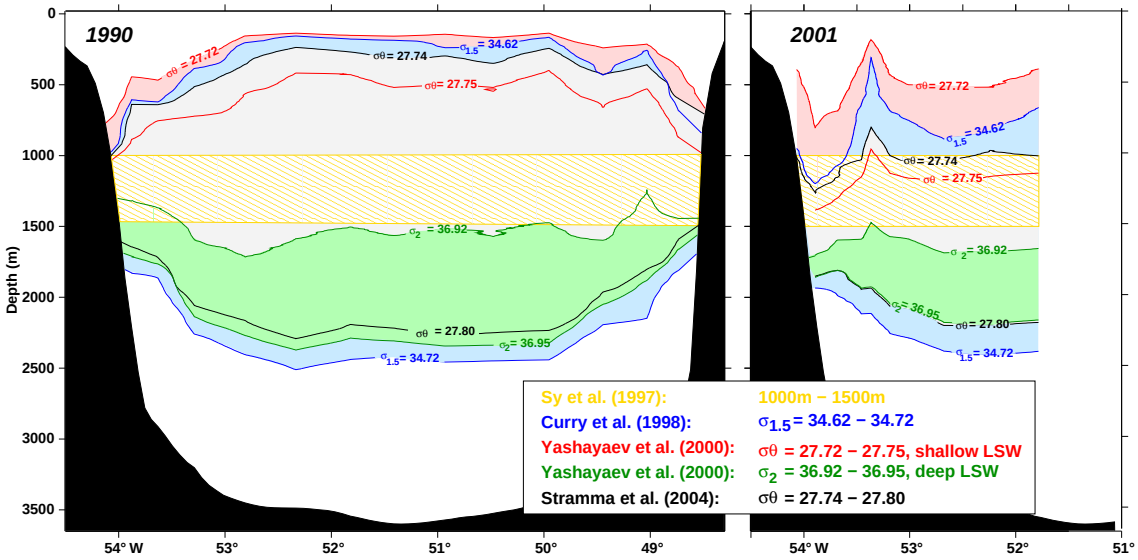

Fig. 4.1.: *Sketch of density and depth ranges used in different studies to define the LSW layer in its formation region. Isopycnals are derived from CTD-data, sampled along WOCE-line AR7W during July 1990 (left) and June 2001 (right). Data of 1990 are from WHPO, the 2001 data from SFB 460. The section location is indicated in Fig. 3.2.*

measurements coincided with a time of increasing LSW formation due to the intensifying deep convection. The occupation of 2001, however, overlapped with the restratification period that had started around 1996 (Lazier et al., 2002) and led to the cessation of classical LSW renewal by the end of the 1990s.

The respective LSW definitions differ in the choice of the reference level used to calculate the potential density and represent different depth ranges. In this notation, the $\sigma_{1.5}$ = 34.62-34.72 kg/m^3 criterion chosen by Curry et al. (1998) resulted in the broadest LSW layer in 1990 which occupied the water column over more than 2000 m. It includes some of the layers defined by other authors (see Fig. 4.1 for details). Yashayaev et al. (2000) introduced a 'deep LSW' and a 'shallow LSW'. The 'deep LSW' corresponds to the cold and dense water mass being formed as a result of the severe winters in the early 1990s. It is defined in the density range σ_2 = 36.92-36.95 kg/m^3 and coincides with local minima of the potential vorticity and salinity (Azetsu-Scott et al., 2003). In the subsequent years, shallower convection down to < 1500 m led to the formation of the lighter variant ('shallow LSW'). This layer (σ_Θ = 27.72-27.75 kg/m^3) comprises to a certain part what is labeled ULSW in the present study (σ_Θ = 27.68-27.74 kg/m^3).

A comparison of both years displayed in Figure 4.1 reveals that the depth of the upper boundary of classical LSW varies much more than the lower boundary. This is regardless of the density based definition. During 1990, the depth range 1000-1500 m as chosen by Sy et al. (1997) characterised the centre of LSW. In 2001, the restratification of the Labrador Sea resulted in the formation of lighter water masses that occupied the upper water column. Properties averaged over the 1000-1500 m depth range are thus much more representative for what was then the upper part of classical LSW. With the exception of

'shallow LSW', all density-defined layer thicknesses have decreased from 1990 to 2001.

The LSW layer is thus subject to considerable changes. A layer definition based on fixed isotherms (Wright and Worthington, 1970; McCartney, 1992) or isopycnals (e.g. Pickart et al., 1996, 1997; Curry et al., 1998; Stramma et al., 2004) may be more appropriate in one year and less in another year. But also the depth level of the core of a water mass is likely to change with time. A fixed depth range chosen as a water mass definition (e.g., Sy et al., 1997) is also not equally representative for all years considered on a longer time scale.

Results presented in Chapter 3 provided evidence on substantial changes in the ventilation of ULSW and classical LSW during the late 1990s/early 2000s. The present chapter is devoted to analysing ULSW formation and associated variability on longer time scales. This is discussed in conjunction with variability in the formation of the denser classical LSW.

4.2. The WOCE and post-WOCE period, 1990-2001

During 1990-2001, a hydrographic section was conducted which crossed the central Labrador Sea in northeastern direction (cf. Fig. 3.2). This section was repeated annually in the framework of WOCE and SFB 460. It is referred to as the AR7W-line. Particular cruises carried out along AR7W are listed in Table 4.1. Joint Canadian/American efforts concentrated on covering the entire deep Labrador Basin. German measurements focused on the western side of this region. The majority of the cruises was carried out during the summer months.

Corresponding data have been used to calculate mean properties of ULSW and classical LSW along the AR7W-line. These comprise layer thickness, mean salinity, and mean potential temperature. Mean values were inter-/extrapolated on a regular grid and illustrated as Hovmöller diagrams with longitude as a fixed parameter plotted versus varying time (Fig. 4.2).

During the first half of the 1990s, LSW occupied the largest fraction of the water column (Fig. 4.2b). Layer thicknesses of more than 2000 m indicate a thick and homogeneous reservoir of LSW which had been ventilated at that time (e.g., Lilly et al., 1999; Lazier et al., 2002). The corresponding ULSW layer was rather thin (thickness $<$ 200 m). Towards the end of the 1990s, when deep convection gradually ceased, a remarkable increase in ULSW layer thickness appeared. It coincided with a decrease of LSW thickness. According to Lazier et al. (2002), this marked the phase, when the Labrador Sea restratified. The shallow convection, initiated by milder and warmer winters, was limited to about 1000 m, and LSW was correspondingly isolated from ventilation. Instead, the production of the lighter ULSW commenced.

The salinity distribution of both water masses reveals a more saline LSW layer (Fig. 4.2c/d). In the interior basin LSW salinities ranged from S $>$ 34.835 to S = 34.865,

Cruise	Date	PI	Institution
D90012	02 Jul-09 Jul 1990	J. Lazier	BIO
H92014	28 May-11 Jun 1992	J. Lazier	BIO
H93019	17 Jun-23 Jun 1993	J. Lazier	BIO
H94008	25 May-09 Jun 1994	J. Lazier	BIO
H95011	09 Jun-02 Jul 1995	J. Lazier	BIO
H96006	12 May-25 May 1996	J. Lazier	BIO
V161	21 Jul-17 Aug 1996	F. Schott	IfMK
H96026	16 Oct-16 Nov 1996	A. Clarke	BIO
K147/5	08 Feb-13 Mar 1997	R. Pickart	WHOI
M39/4	07 Jul-09 Aug 1997	F. Schott	IfMK
H97009	09 May-11 Jun 1997	A. Clarke	BIO
H98023	22 Jun-08 Jul 1998	E. P. Jones	BIO
V172	04 Jul-12 Aug 1998	U. Send	IfMK
H99003	27 Jun-14 Jul 1999	A. Clarke	BIO
M45/3	12 Jul-08 Aug 1999	F. Schott	IfMK
H20009	20 May-08 Jun 2000	G. Harrison	BIO
M50/2	02 Jun-18 Jun 2001	F. Schott	IfMK

Tab. 4.1.: *Summary of hydrographic and tracer data, sampled along WOCE-line AR7W. Data sources are WHPO, BIO, and SFB 460. PI: Principal Investigator; BIO: Bedford Institute of Oceanography, Dartmouth, Canada; IfMK: Institut für Meereskunde Kiel, Germany; WHOI: Woods Hole Oceanographic Institution, Woods Hole, USA.*

whereas ULSW salinities were well below S = 34.85 throughout the decade. In 1993-1995, ULSW located in this region exhibited localised low salinity anomalies, centered around 52°W30' and 51°W. These were also present in the mean salinity distribution of the deeper LSW layer (1994 and 1995). Salinity minima in both layers coincided with the lowest temperatures observed throughout the observation period. The ULSW salinity gradually increased from 1995 until the trend was interrupted in 1999. This year also showed a temporal maximum in ULSW temperature.

Further low salinity events were found in the ULSW in the Canadian DWBC region (∼54°W-53°W) during 1992 and 1995. The fresh anomalies coincided with local and/or temporal temperature minima. The low salinity event found in the DWBC in 1992 is attributed to the passage of the *Great Salinity Anomaly* (GSA), formed in the northwestern Labrador Sea during 1989/90 (Belkin, 2004). Deser et al. (2002) noticed above-normal

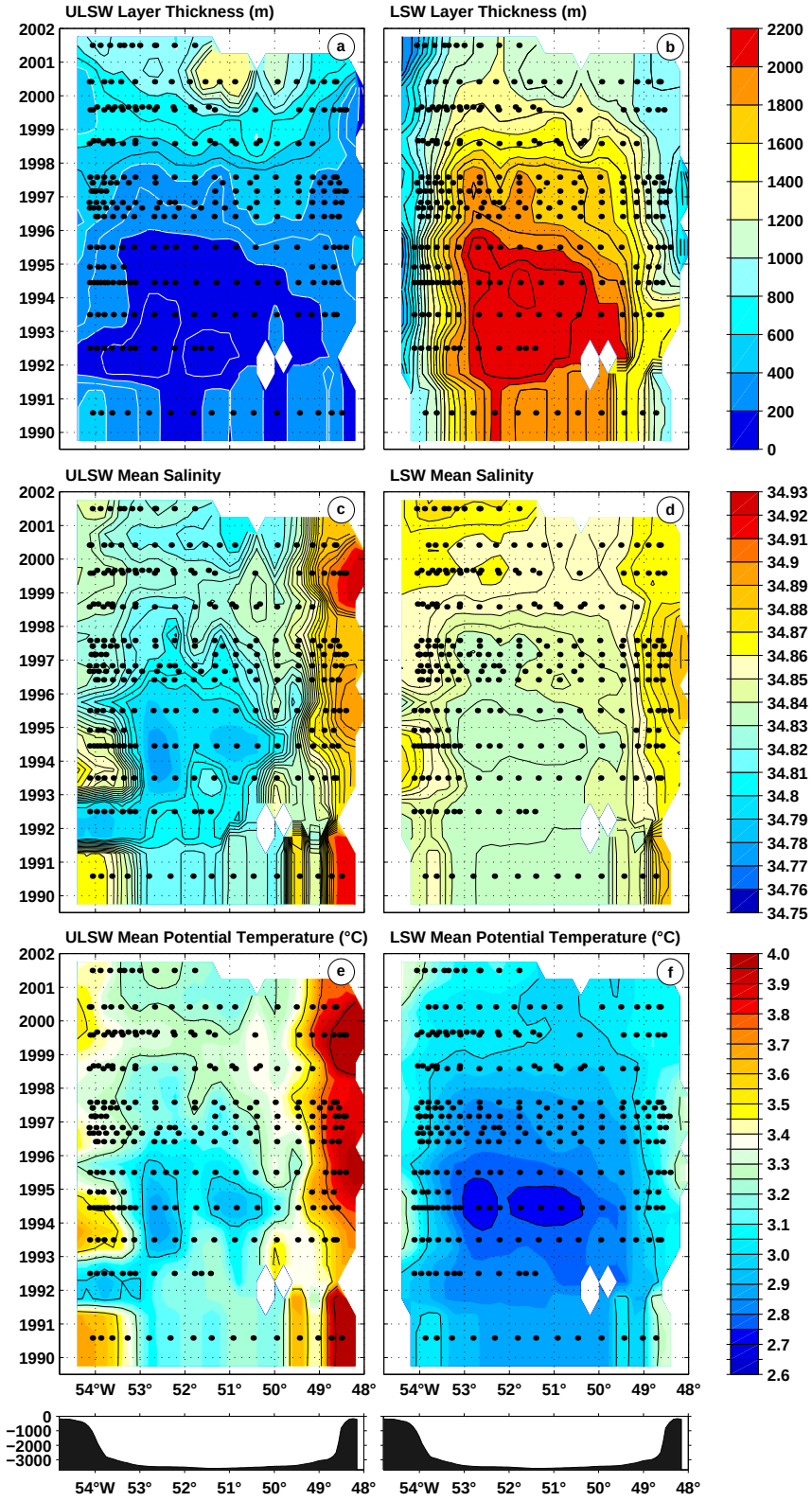

Fig. 4.2.: *Hovmöller diagrams of (a/b) layer thickness (m), (c/d) mean salinity, and (e/f) mean potential temperature (°C) for ULSW (left column) and LSW (right column), displayed along WOCE line AR7W. Labeled years mark the beginning of each year. Black dots indicate the position of available CTD stations. Solid lines denote contour intervals of 100 m (a/b), 0.005 psu (c/d), and 0.25°C (e/f).*

sea ice concentrations that locally occurred there in 1990-93. Within two years these anomalies propagated along the rim of the basin towards Newfoundland. Anomalous low sea surface temperatures are associated with these anomalies.

Localised intrusions of warm and saline Irminger Sea Water (ISW) into both water masses are prominent along the boundaries of the Labrador Basin. These are more obvious in the ULSW, since ISW occupies a shallow depth range (about 100-500 m). Warmer water with higher salinities is observed on the Greenland side of the basin. Cuny et al. (2002) reported on a cooling and freshening of ISW as it is advected around the rim of the basin. Section data presented by Stramma et al. (2004) indicated that the lower boundary limiting ULSW ($\sigma_\Theta = 27.74$ kg/m^3) had shifted to greater depths at the end of the decade. The fresh, CFC-rich ULSW and the salinity minimum of the LSW were separated by an intermediate salinity maximum at about $\sigma_\Theta = 27.76$ kg/m^3. The salinity maximum was present since 1997 and presumably results from the lateral admixture of the saline ISW into the LSW layer (Lazier et al., 2002).

The ULSW shows much more variability in the boundary current regions of the Labrador Sea, which is in contrast to the deeper LSW. Close to the Greenland Sea side (50°W) several events with warm and saline intrusions were present in the ULSW layer (years 1993, 1995, 1999, and 2000). These are supposed to be imported from the West Greenland Current (WGC). As was noted in Section 2.2.1, the WGC region is known for large eddy activity. Eddies are carried into the interior Labrador Sea and thought to contribute to the restratification of the water column after deep convection (e.g., Lilly et al., 1999; Eden and Böning, 2002; Katsman et al., 2004).

On the Labrador side, the layer thickness of ULSW continuously increased throughout the years. On the Greenland side, however, this increase appeared to be delayed in time. In contrast, LSW exhibited greater layer thicknesses for a longer period on the western side of the Labrador Sea. After 1995 the Greenland side did not show any LSW thicker than 1800 m. Float analyses by Lavender et al. (2000) revealed the presence of several anti-cyclonic circulation cells located close to the boundary currents of the Labrador Sea. Based on these results and further model studies, Straneo et al. (2003) discussed the existence of a new advective pathway present in the interior Labrador Sea. This so-called 'internal' branch is supposed to be responsible for the recirculation of water masses from the interior basin to the Greenland coast. Though this particular branch has not been directly observed so far, Straneo and co-authors stress the importance of recirculation cells for the redistribution and storage of water masses. The residence time for LSW in the interior Labrador basin is thus much longer (4-5 years, Straneo et al., 2003) compared to the boundary current region (e.g., LSW takes about 1.5 years from 56°N to about 43°N, Stramma et al., 2004).

A greater amount of lighter and more saline water was found on top of classical LSW by the end of the decade. Mertens (2000) analysed the development of the stratification in the central Labrador Sea based on mooring data. These cover the periods 08/1994-05/1995 and 08/1996-07/1999. Convection depths locally observed in the central Labrador Sea reduced from 1800 m (1995) to 1300 m in 1997 and to ∼500 m in 1999. As was noted

before, deeper convection has, however, happened to the northwest of the AR7W-line in late winter of 1999. The thickness increase of ULSW or thickness decrease of the denser LSW is the result of a substantial vertical displacement of the isopycnal $\sigma_\Theta = 27.74$ kg/m^3 which separates both water masses. The high ULSW formation rates observed at the end of the 1990s (Tab. 3.5) are thus the result of a remarkable switch from deep to rather shallow convection. By the end of the decade the large reservoir of classical LSW was halvened. The CFC-11 inventory distributions shown in Figure 3.10 already pointed to LSW being gradually flushed out of the Labrador Sea in the considered 4-year period (1997-2001). Deeper and thicker parts of the water column were consequently occupied by the lighter ULSW. In 2001, the resulting ULSW layer thickness locally exceeded that of LSW.

Figure 4.3 presents Hovmöller diagrams that illustrate the vertical shift of the isopycnals $\sigma_\Theta = 27.68$ kg/m^3 and $\sigma_\Theta = 27.74$ kg/m^3. From 1990 to 1996/97, summer data indicate that the upper boundary of ULSW was located very closely to the sea surface. In the subsequent years it shifted to depths of 100-200 m, occasionally exceeding 200 m. The upper boundary of classical LSW ($\sigma_\Theta = 27.74$ kg/m^3) was considerably displaced throughout the decade. From near-surface locations in 1992-94 it deepened to depths greater 1000 m after 1999. Only a narrow region close to the western boundary exhibited a shallower depth of $\sigma_\Theta = 27.74$ kg/m^3 (z $<$ 1000 m) in 2000-2001.

The integrated heat content per unit area which is stored in the water layers lying on top of ULSW and classical LSW is shown in Figures 4.3c/d. It is defined as:

$$\mathbf{HC} = \int_{-z(\sigma_\Theta)}^{0} \mathbf{c_p}\boldsymbol{\rho}(\mathbf{T} - \mathbf{T_{ref}})dz \tag{4.1}$$

with **HC**: integrated heat content (J m^{-2}), $\mathbf{c_p}$: specific heat (J K^{-1} kg^{-1}), $\boldsymbol{\rho}$: density of water (kg m^{-3}), **T**: temperature (°C), $\mathbf{T_{ref}}$: reference temperature of 2.8°C. The reference temperature $\mathbf{T_{ref}} = 2.8$°C was chosen to represent classical LSW prior to 1996, though at peak times of deep convection LSW was even colder on average (compare Sy et al., 1997).

Over large parts of the Labrador Basin the summer data of 1990-1995 showed uniform heat content in the water layer located above ULSW (Fig. 4.3c). Values were below 0.5 GJ/m^2 (relative to 2.8°C). On the western side of the basin these continued to summer 1997. This is expected since the layer located above ULSW was very thin at that time. The following two years indicated an increased heat content (HC $<$ 1.5 GJ/m^2) which was again reduced by the end of the period.

The layer located above classical LSW (including ULSW, Fig. 4.3d) carried the lowest heat content (relative to 2.8°C) from 1992-97. This was again due to the shallow location of the bounding isopycnal, which was close to the surface at that time. In the subsequent years the heat content increased to values greater than HC = 2.5 GJ/m^2 in 1999. This is indicative of a considerable warming of the upper 1000 m of the water column. To cool down the upper water layer to the LSW reference temperature, a resulting constant heat

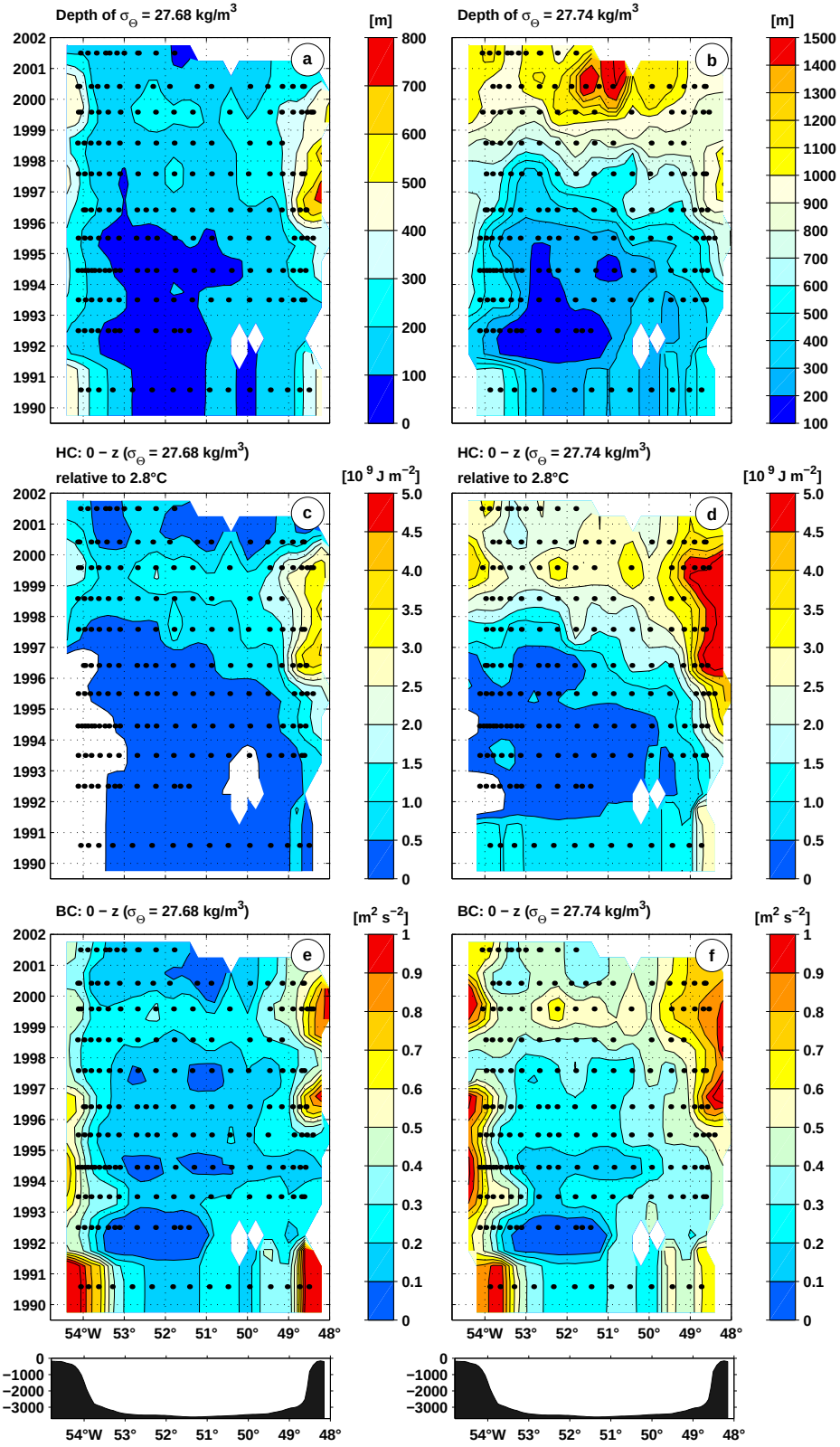

Fig. 4.3.: *Hovmöller diagrams of (a/b) depth of isopycnals (σ_Θ = 27.68/27.74kg/m^3), (c) heat content (10^{10} J/m^2) in layer above σ_Θ = 27.68 kg/m^3, (d) same as (c) but for layer above σ_Θ = 27.74 kg/m^3, (e) buoyancy content in layer above σ_Θ = 27.68 kg/m^3, (f) same as (e) but for layer above σ_Θ = 27.74 kg/m^3, displayed along WOCE line AR7W. Labeled years mark the beginning of each year. Heat content is calculated relative to 2.8°C.*

loss of at least ∼110 W/m^2 would be required for a period of nine month (summer to late winter). After 1999, the heat content in the western part of the Labrador Sea reduced again.

Brandt et al. (2004) calculated interannual time series of the EKE in the WGC region (period 1993-2001). These were derived from sea level anomalies recorded by the altimeters of the TOPEX/Poseidon and ERS-2 satellites. The authors found strong interannual variability in the EKE with pronounced maxima occurring during 1993 as well as 1997-1999. During 1997-2000 the propagation of WGC EKE into the central Labrador Sea was enhanced. The heat content in the surface layer displayed in Figure 4.3c reveals a strong east-west gradient that started to emerge around 1996. This coincided with a considerable downward shift of the isopycnal $\sigma_\Theta = 27.68$ kg/m^3 on the eastern side of the basin and is indicative of import of warm water from the east. Lilly et al. (2003) observed that Irminger-type eddies carrying warm and saline water were very common in the Labrador Sea after mid-1997.

Figures 4.3e/f illustrate the buoyancy content (BC) stored above both isopycnals. Calculation was done according to Equation 3.6 (see Section 3.5.3). The integrated summer buoyancy content stored on top of $\sigma_\Theta = 27.68$ kg/m^3 reveals an extended period of very low values (BC < 0.2 m^2/s^2, 1990-1997). Local minima in 1992, 1994, and 1997 were below 0.1 m^2/s^2. Similar to the temporal evolution of the heat content, the low buoyancy phase was interrupted in 1998-99 by higher values which decreased again by the end of the observation period. The water layer on top of classical LSW showed the most prominent BC minimum in 1993. After 1994 values gradually increased until 1999, followed by a decrease again. In the layer locate above $\sigma_\Theta = 27.74$ kg/m^3 water with minimum buoyancy was restricted to the regions west of 50°W30'. Notable exceptions were found in 1990 and 1994.

In general, buoyancy and heat content reveal similar tendencies in their respective temporal evolution. This is expected since changes of the buoyancy in the Labrador Sea are dominated by changes in the heat content (Mertens, 2000; Lazier et al., 2002). There is, however, a seasonally varying shallow surface layer of approximately 100-150 m thickness whose density stratification is controled by salinity. According to Lazier et al. (2002) about 50 % of the buoyancy variance in this layer can be explained by salinity changes. Lazier et al. (2002) used the AR7W data to calculate mean summer profiles. They divided the water column into different pressure ranges rather than isopycnal layers and integrated the heat content between the pressure levels 0, 150, 1000, and 2000 dbar, referenced to the year 1994. With the exception of the 1000-2000 dbar range, all remaining layers revealed a maximum of integrated heat anomaly in 1999 which is identical to the findings in the present study. The authors did not find any persistent trend in the salinity of the upper 150 m despite the fact that it participated in the warming trend.

4.3. Surface forcing

Changes in the upper ocean are now compared to changes in the atmospheric forcing which acts on the sea surface. The NCEP/NCAR reanalysis project (KALNAY et al., 1996) provides gridded time series of various atmospheric parameters, including heat, freshwater, and momentum fluxes. They are currently available[I] for a period of more than 55 years (start in 01/1948; KISTLER et al., 2001).

The reanalysis time series are generated by assimilating all available quality-controlled atmospheric and surface data into a frozen global data assimilation system which is unchanged over the reanalysis period. Climatic jumps which are associated with changes in the operation of the data assimilation system are thus avoided. Changes in the observing systems, however, still affect the reanalysis (KISTLER et al., 2001).

For the present purpose, winter mean anomalies of wind stress, heat and buoyancy flux have been constructed for three selected grid points in the Labrador Sea. The first is located in the northern Labrador Sea, the second is close to the position of the former OWS *Bravo*. The third grid point is located to the northwest of Orphan Knoll close to the western DWBC region of the Labrador Sea. Winter is defined as the period December to March. Anomalies are constructed by removing the longterm winter mean value from the respective time series. A comparison of time series derived at these positions shall give hints concerning surface related processes that are involved in the changing activity of deep convection and thus variability in water mass formation.

Surface parameters

The wind stress is a measure for the exchange of momentum at the air-sea interface. The classical bulk formulation is:

$$\overrightarrow{\boldsymbol{\tau}} = \boldsymbol{\rho_{air}} \mathbf{C_D} |\overrightarrow{\mathbf{U_{10}}}| \overrightarrow{\mathbf{U_{10}}} \tag{4.2}$$

with $\boldsymbol{\tau}$: wind stress (N/m^2), $\mathbf{C_D}$: turbulent drag coefficient (dimensionless), $\mathbf{U_{10}}$: the wind vector (m/s) at anemometric height (often 10 m), and $\boldsymbol{\rho_{air}}$: air density (kg/m^3).

The net heat flux is the budget of the radiative fluxes (solar or short-wave radiation and long-wave or infrared radiation) as well as the turbulent fluxes (latent and sensible heat). By convention, negative values indicate a flux of heat from the ocean into the atmosphere.

$$\mathbf{Q_{tot}} = \mathbf{Q_{sw}} + \mathbf{Q_{lw}} + \mathbf{Q_{lat}} + \mathbf{Q_{sens}} \tag{4.3}$$

The term "buoyancy flux" has been introduced for reasons of convenience. It comprises fluxes of moisture and heat rather than a real flux of buoyancy (SATHIYAMOORTHY and MOORE, 2002). It is given as:

[I] Climate Diagnostics Center (CDC): http://www.cdc.noaa.gov

$$\mathbf{B} = \mathbf{g}\left[\boldsymbol{\alpha}\frac{\mathbf{Q_{tot}}}{\boldsymbol{\rho_0}\mathbf{c_p}} - \boldsymbol{\beta}\mathbf{S_0}(\mathbf{E}-\mathbf{P})\right] \tag{4.4}$$

with: $\mathbf{B}$: buoyancy flux ($m^2\ s^{-3}$), $\mathbf{g}$: gravitational acceleration ($m\ s^{-2}$), $\boldsymbol{\alpha}$: thermal expansion coefficient (K^{-1}), $\mathbf{Q_{tot}}$: total surface heat flux ($W\ m^{-2}$), $\mathbf{c_p}$: specific heat capacity of sea water ($J\ kg^{-1}\ K^{-1}$), $\boldsymbol{\rho_0}$: surface reference density ($kg\ m^{-3}$), $\boldsymbol{\beta}$: haline contraction coefficient (psu^{-1}), $\mathbf{S_0}$: surface reference salinity (psu), $\mathbf{E}$: evaporation ($m\ s^{-1}$), $\mathbf{P}$: precipitation ($m\ s^{-1}$).

Values for $\boldsymbol{\alpha}$ and $\boldsymbol{\beta}$ are dependent on typical winter surface temperatures and salinities. These were calculated from the winter mean climatology provided by Levitus and Boyer (1994): $\boldsymbol{\alpha} = 0.9\times10^{-4}\ K^{-1}$, $\boldsymbol{\beta} = 7.8\times10^{-4}\ psu^{-1}$.

The evaporation is derived from the following equation:

$$\mathbf{E} = \frac{\mathbf{Q_{lat}}}{\boldsymbol{\rho_0}\mathbf{L}} \tag{4.5}$$

with $\mathbf{L}$: latent heat of evaporation ($J\ kg^{-1}$).

From a comparison with wintertime shipboard meteorological observations (Feb.-Mar. 1997, central Labrador Sea) Renfrew et al. (2002) found a systematic over-estimation of the latent and sensible heat flux provided by NCEP/NCAR. Especially in situations with high winds and large air-sea temperature differences the reanalysis data failed to sufficiently match the direct meteorological observations. The authors suggested a recalculation of the surface heat fluxes using a revised bulk algorithm. On the other hand, Lazier et al. (2002) found reasonable correlation between direct flux measurements and NCEP/NCAR reanalysis fluxes. Atmospheric conditions in the Labrador Sea are highly variable and cover a wide range of air temperatures, wind speeds, etc. As long as there aren't any further comparisons from other seasons and/or other years, it remains unclear to what degree the suggested new bulk algorithms would improve the NCEP/NCAR time series during other times than late winter of 1997. In this context, the original reanalysis time series have been considered in the present study. As was stated by Lazier et al. (2002), the overall quantitative results may be uncertain, but trends are not likely to be significantly affected.

Sathiyamoorthy and Moore (2002) added a caution when mapping monthly mean values. At OWS Bravo they found significant high-frequency variability in the buoyancy flux that was attributed to the passage of synoptic weather systems. Averaging to monthly mean values masked a large portion of this signal. They further emphasised the importance of including a heat flux resulting from precipitation in the calculation of the buoyancy flux. Neglecting it would result in an over-estimation of the buoyancy flux. As the authors themselves mention, precipitation is, however, most difficult to measure or estimate and affected by large uncertainties[II]. For this reason, it was not included in the present calculations. Even Sathiyamoorthy and Moore (2002) could not use directly

[II] Béranger et al. (2000) summarise different methods to measure or derive precipitation estimates.

measured precipitation data but had to rely on recorded weather codes. Here, the aim is to reveal general trends rather than quantitative estimates. For this purpose, winter mean values are still considered appropriate.

Figure 4.4 presents time series of the winter mean wind stress anomaly calculated for the winters 1948/49-2002/03 at selected grid points. Subtracted mean values are (a) 0.16 N/m^2, (b) 0.13 N/m^2, and (c) 0.15 N/m^2. All selected grid points reveal an extended period of anomalous high wind stress that started in winter 1987/88 and ended in 1995/96. Only the northern Labrador Sea exhibited winters that exceeded the wind stress anomalies of the early 1990s (years 1971/72-1972/73). Here, the overall variability is strongest. At the two southern locations the early 1990s marked an absolute post-war maximum (see also Dickson et al., 1996).

The restratification period of the late 1990s was accompanied by moderately increased wind stress compared to the mean. In the central and southern Labrador Sea, the winter mean wind stress anomaly was slightly higher compared to the northern part. The winters of 1995/96 and 2000/01 exhibited anomalous low wind stress compared to the mean. Such periods were much more common in the Labrador Sea prior to 1982.

The temporal evolution of the wind stress is closely related to the temporal evolution of the North Atlantic Oscillation (NAO) index. The NAO is the most important mode of atmospheric variability over the North Atlantic Ocean (see review by Greatbatch, 2000). Classically, the respective index is defined as the difference between normalised sea level pressure (SLP) records representative for two centres of action, the Icelandic Low and the Azores High. It is thus a measure of the westerly wind blowing across the SPNA in the latitude belt 40°N-60°N (e.g. Van Loon and Rogers, 1978; Wallace and Gutzler, 1981; Hurrell, 1995). Several indices exist throughout literature. They differ in the choice of the southern station and thus in the length of the record (e.g., Rogers, 1984; Hurrell, 1995; Jones et al., 1997). The NAO-index shown in Figure 4.4 is derived from Jones et al. (1997). The authors extended existing times series back to 1823 by adding SLP data recorded at Gibraltar and southwest Iceland. The index was normalised by dividing monthly SLP anomalies at each station by the longterm standard deviation of the mean pressure. Since the southern centre of action (the Azores High) shifts towards west during the summer season, the index provided by Jones et al. (1997) is a good proxy only during winter and early spring (e.g., Hurrell and Loon, 1997).

As is obvious from Figure 4.4, wind stress anomalies derived from selected grid points in the Labrador Sea are well correlated to the NAO-index (corresponding coefficients are given in Fig. 4.4). The anomalous high wind stress period of the late 1980s/early 1990s coincided with a high NAO-index period. When the index is high, geostrophic balance implies that westerly winds are stronger than normal. The opposite holds for the low-index periods (e.g., Greatbatch, 2000). During the early 1970s the high-NAO-index phase lagged the prevailing anomalous high wind stress by about a year. During the late 1960s/early 1970s the occurrence of a GSA had led to a shutdown of deep convection in the Labrador Sea. The winter 1971/72 marked the onset of deep convection again (Lazier, 1980; Dickson et al., 1988; Belkin et al., 1998). Dickson et al. (1996) already suggested a correlation between variability in the intensity of deep convection

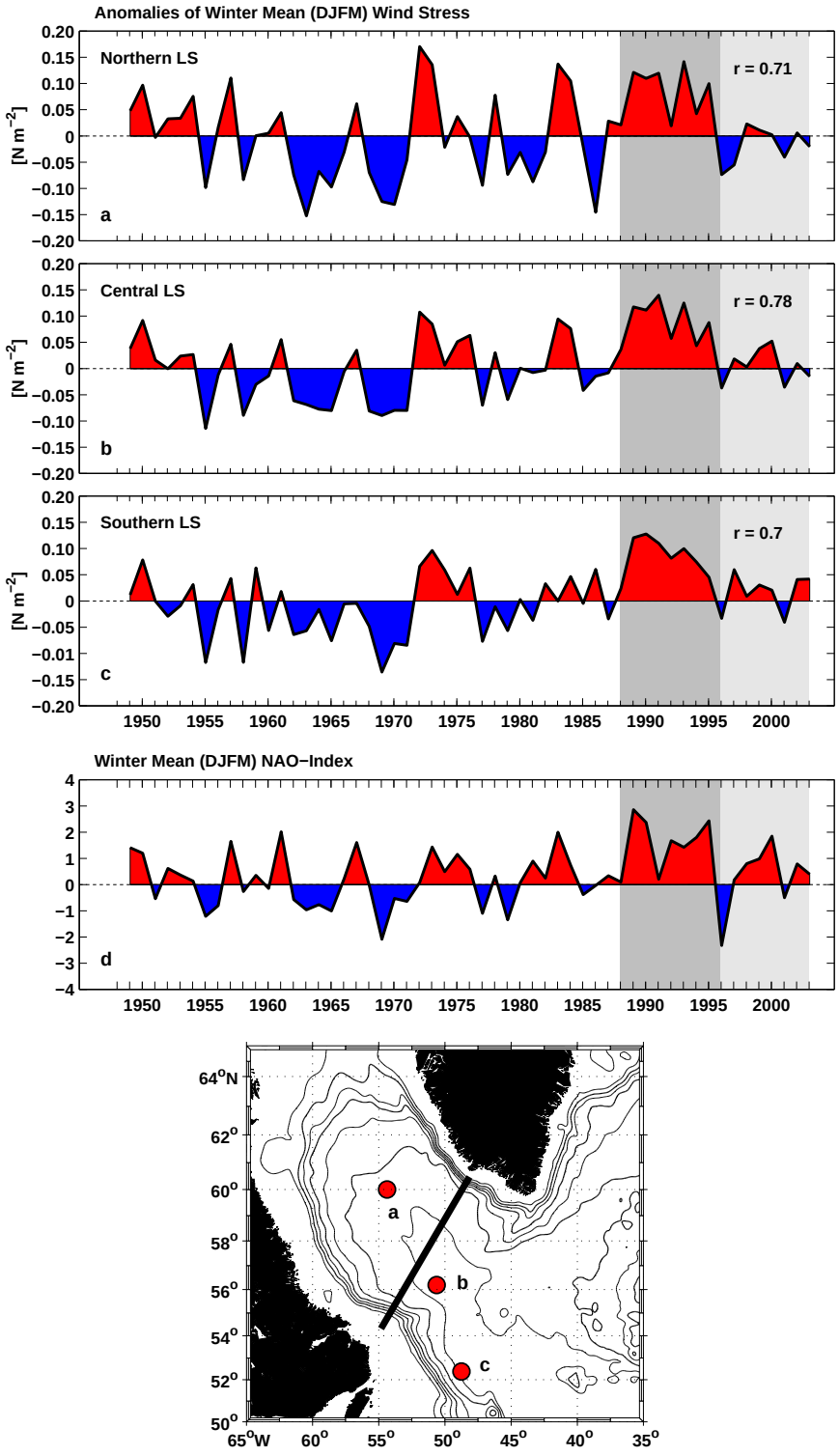

Fig. 4.4.: *(a-c) Time series of winter time (December-March) wind stress anomalies (N/m^2) in selected regions of the Labrador Sea. Time series were derived from NCEP/NCAR reanalyses for the period 1948-2003. Given correlation coefficients* **r** *indicate correlation of respective time series to NAO-index. (d) Time series of the NAO-index (December-March;* Jones *et al., 1997). Indicated years refer to the January of the respective winter. Dark shading indicates the deep convection period of the early 1990s, light shading the subsequent phase of restratification. Bottom row: locations of selected grid points.*

and variability in the NAO.

Figure 4.5 presents anomalies of winter mean heat and buoyancy loss for the same regions. Again, the overall variability is strongest in the northern Labrador Sea. The occurrence of heat loss and buoyancy loss maxima coincide with the phase of anomalous high wind stress (e.g., 1987/88-1995/96). The northern and central Labrador Sea indicated increased surface forcing also during winter 1982/83 to 1983/84. Similar fluxes in the southern Labrador Sea fell below the respective mean value.

The change from intense deep to shallow convection throughout the 1990s was accompanied by a remarkable shift in the atmospheric conditions. The winter of 1995/96 showed a considerable switch to a negative NAO-index. This minimum is unprecedented throughout the entire period covered by the NAO time series (1823-2003). This change also affected the buoyancy and heat loss which became anomalously low. In the subsequent winter, atmospheric conditions recovered again. However, anomalies of heat and buoyancy loss remained smaller and persisted for a shorter period in the central Labrador Sea.

The time series from the selected grid points (Figs. 4.4 and 4.5) indicated only little spatial variability in the surface forcing. The northern Labrador Sea exhibits generally higher values, but the temporal evolution of the trends is very similar at each considered location. To better reveal regional differences, Figure 4.6 illustrates the spatial distribution of the winter mean buoyancy loss for the period 1989/90-2002/03. For example, the large shift in the atmospheric regime happening in 1995/96 was not only restricted to the Labrador Sea but affected large parts of the subpolar gyre to the north of about 50°N. The large-scale surface conditions prior to and after this winter differed very much. The SPNA tended to a greater extent to anomalous low values of buoyancy loss after 1996/97. High values as available during 1992/93 in the Labrador Sea were de facto absent during the second half of the 1990s.

Eden and Willebrand (2001) forced a numerical ocean model with anomalous fluxes associated with the NAO. They succeeded in showing that interdecadal changes in the North Atlantic circulation leave an imprint on the sea surface temperature (SST). They further provided evidence that interdecadal oceanic changes lag behind the NAO by several years. Curry et al. (1998) found a time lag of 2-4 years between the NAO-index and the evolution of the LSW layer thickness. The switch in the atmospheric forcing after 1995/96 together with the increased intrusions of high EKE from the WGC into the central Labrador Sea (Lilly et al., 2003; Brandt et al., 2004) has probably enhanced the restratification of the upper water column. Corresponding water mass ventilation was thus restricted to the upper 1000 m of the water column, enabling only the formation of the lighter ULSW.

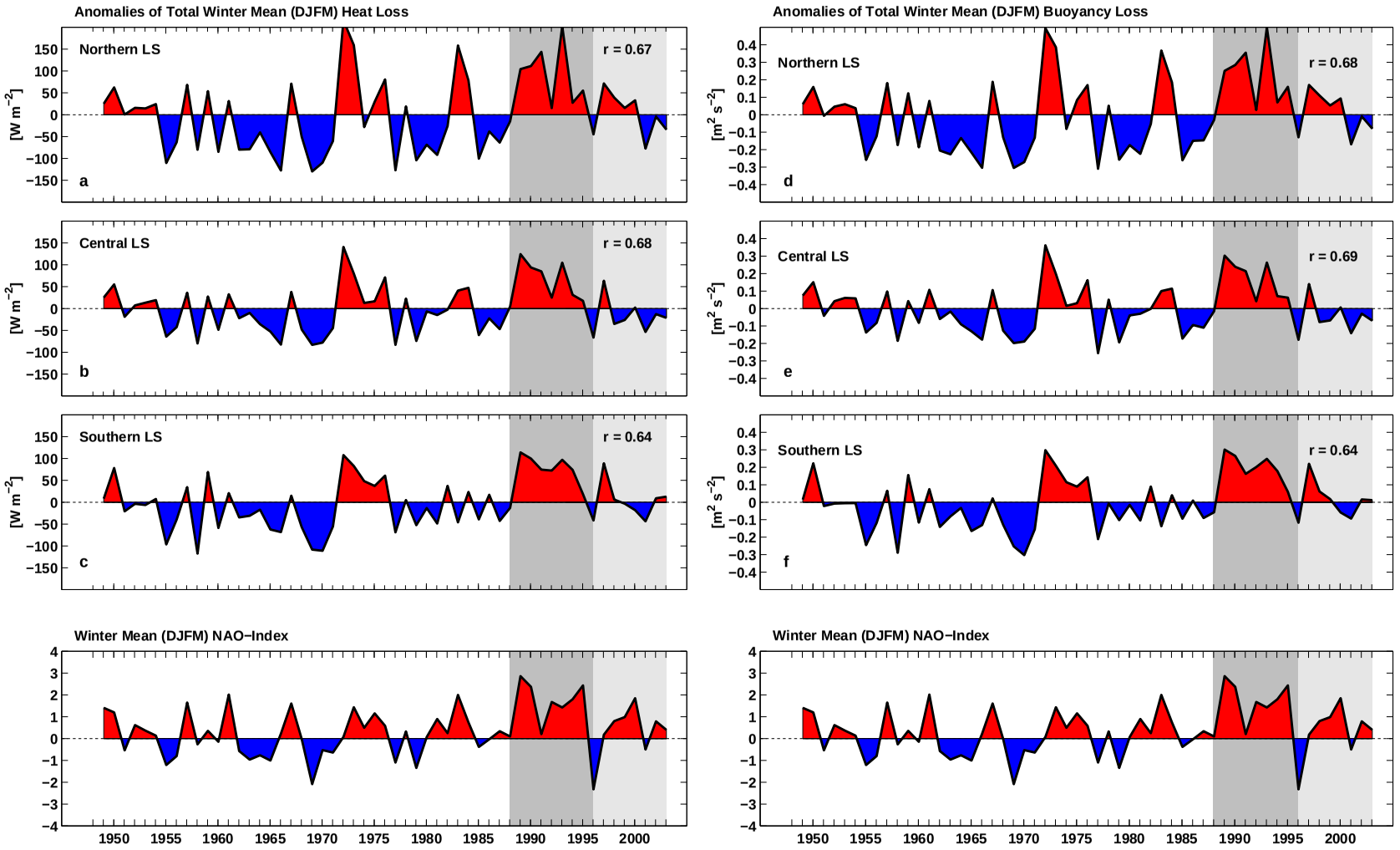

Fig. 4.5.: *Left column (a-c): Time series of total winter time (December-March) heat loss anomalies (W/m^2) in selected regions of the Labrador Sea (see Fig. 4.4). Right column (d-f): total winter time buoyancy flux anomalies (m^2/s^2). Time series were derived from NCEP/NCAR reanalyses for the period 1948-2003. Given correlation coefficients* **r** *indicate the correlation of the respective time series to the NAO-index. Bottom row: Time series of the NAO-index (December-March;* JONES *et al., 1997). Dark shading indicates the deep convection period of the early 1990s, light shading the subsequent phase of restratification.*

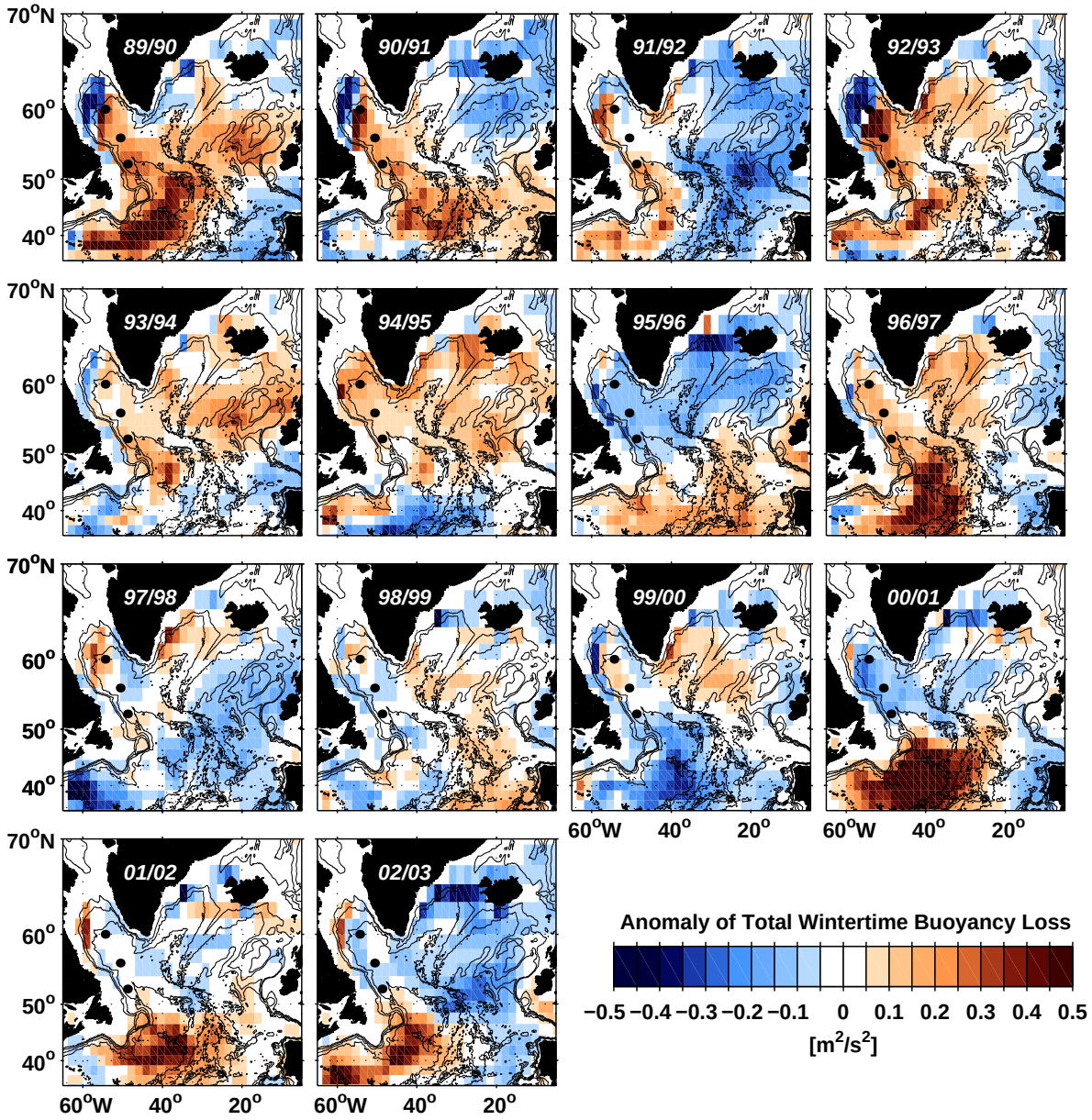

Fig. 4.6.: *Spatial distribution of total winter time (DJFM) buoyancy loss (m^2/s^2). Estimates were derived from NCEP/NCAR reanalysis data and displayed for the winters 1989/90-2002/03. Black dots mark the locations of the selected grid points.*

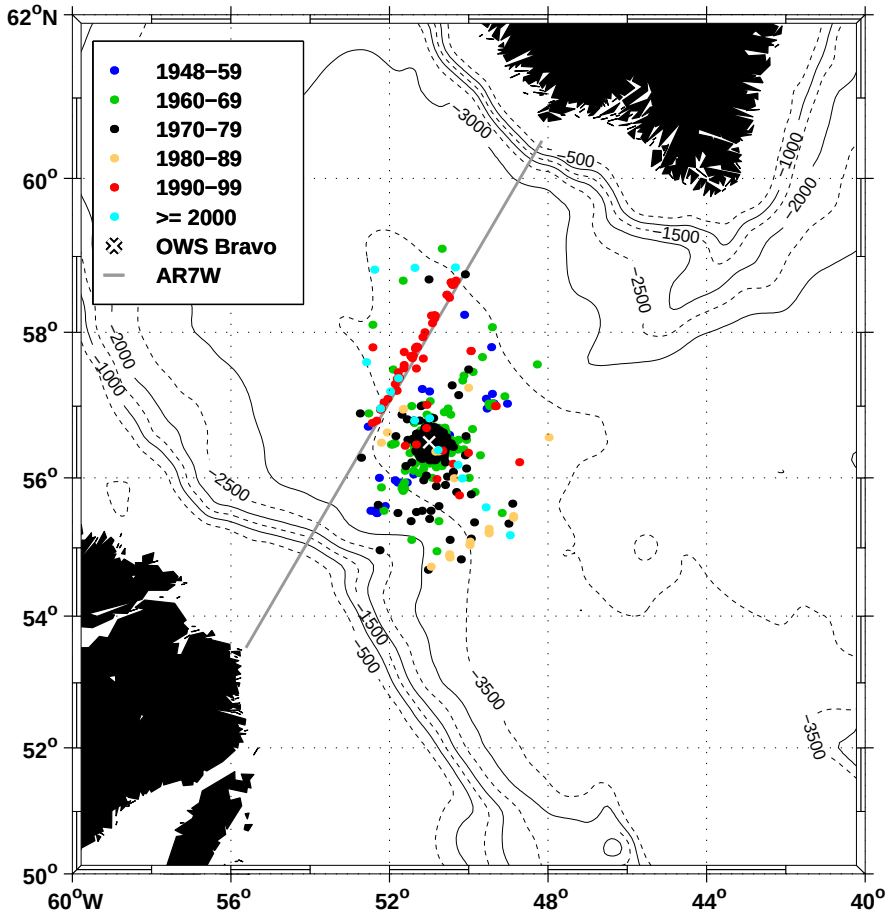

Fig. 4.7.: *Location of hydrographic summer profiles used to reconstruct time series of ULSW and classical LSW properties.*

4.4. Decadal variability of ULSW and LSW ventilation

Based on the OWS Bravo data from the period 1964-1974, Lazier (1980) was the first to present time series showing changes in the composition of LSW. Beside annual variations, he also found variability on interannual time scales. The variability is assumed to be on the one hand caused by changes in the formation rate and on the other hand caused by changes in the properties of those waters from which LSW is later on formed. Talley and McCartney (1982) extended these analyses for the period 1948-1974. They analysed changes of potential vorticity and salinity on selected isopycnals that were isolated from the surface during certain periods. Read and Gould (1992), Sy et al. (1997), and Curry et al. (1998) provided additional time series concerning changes in the LSW layer and potential temperature. Dickson et al. (1996) reported on changes in the LSW density. Common to all of these studies is the fact that all authors noticed particular years when the formation of LSW increased and other years when it decreased. In this context, decadal changes are now analysed with respect to the formation of ULSW.

4.4.1. Data

Hydrographic profiles from different data sets have been put together to investigate variability on decadal time scales. The data sets comprise HydroBase (Curry, 1996), profiles provided by the National Oceanographic Data Center (NODC, 1991), historical data from BIO at Dartmouth, Canada, the WOCE Hydrographic Programme (WHP), as well as data from SFB 460. Only profiles from the open Labrador Sea have been considered. These are located in the assumed formation region of LSW which is close to the position of the former OWS Bravo (51°W, 56°30'N) and WOCE-line AR7W (Fig. 4.7). Data cover the period 1948-2003.

Only profiles with the deepest sampling level located at depths greater than 2500 m were taken into account. This is to ensure that the deeper LSW layer is vertically covered completely. All particular bottle profiles were interpolated on a regular pressure grid (grid spacing 20 dbar) to increase the vertical resolution. The corresponding CTD data were sub-sampled at 20 dbar to ensure monotonicity of the density with depth. Water masses are assumed to rather mix along isopycnals than along isobars. Therefore, in a second step, all profiles were interpolated on σ_Θ-surfaces (grid spacing 0.001 kg/m^3). Profiles from particular cruises and/or specific periods were averaged along these isopycnal surfaces to generate mean profiles. From these, layer properties were estimated by taking the mean value in a given density range.

Deep and bottom water masses are not affected by seasonality. The ULSW layer, however, is located close to surface waters. By means of monthly OWS *Bravo* data (period 1964-1974), Lazier (1980) addressed occurring seasonality in the salinity and potential temperature of the upper 1500 m of the water column. He noted that annual variations in salinity decreased rapidly below 200 m. Over the upper 1500 m, the annual cycle in salinity averaged out to ∼0.01-0.013 ‰. Concerning the precision of salinity sampled at that time (∼ ±0.03 ‰, Lazier, 1980), this seasonal signal was lost in the noise. Concerning temperature, Lazier (1980) found that the seasonal signal averaged over the upper 1500 m amounted to 0.25°C. This is an order of magnitude higher than precision of temperature measurements of that time (∼0.02°C).

Despite the OWS *Bravo* sampling program, data available in the central Labrador Sea were generally sampled irregularly in time. The majority of profiles, however, is from early to late summer (May to September). For time series that cover several decades it is not possible to remove the seasonal cycle, since the data set is not extensive enough to resolve it. In the following analyses, only profiles from the months June to August are taken into account. Profiles from earlier or later months were only considered for those years, when summer profiles were not available and otherwise greater time gaps would arise. The greatest temporal data gaps appear in the period 1975-1985.

The chosen profiles were verified by reconstructing the decadal time series of LSW layer thickness, presented by Curry et al. (1998). They used an LSW definition based on $\sigma_{1.5}$-isopycnals. Both curves are displayed in Figure 4.8. The general shape of the curve and the particular magnitudes could be successfully recovered. Particular differences between both time series appear at the beginning of the 1980s. These result from

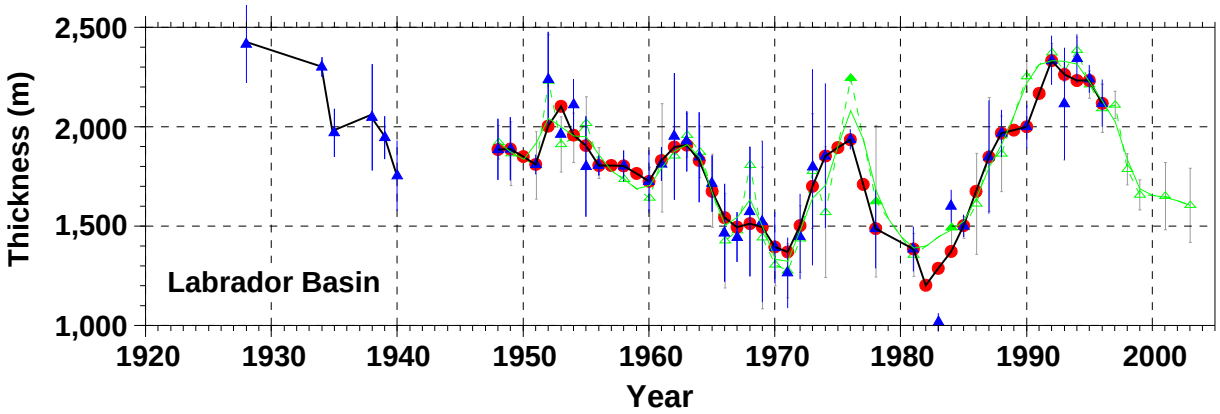

Fig. 4.8.: *Reconstruction of LSW layer thickness calculated by* Curry *et al. (1998). LSW is defined as the density range* $\sigma_{1.5} = 34.62 - 34.72\ kg/m^3$. *Blue triangles indicate the annual mean values from* Curry *and co-authors with blue vertical bars as the corresponding standard deviation. The red circles and the black curve depict 3-year smoothed values. Green markers, grey error bars and the corresponding green curve (3-year filter) illustrate LSW layer thickness estimates as re-calculated in the present study.*

a missing estimate for 1983 in the considered data of the present study.

4.4.2. Variability of Hydrographic Properties

Figures 4.9a/b present time series of mean salinity and mean temperature of ULSW and classical LSW for the period 1948-2003. Corresponding curves published by Sy et al. (1997) are added. These refer to the depth range 1000-1500 m and have been extended for the years 1997 to 2003.

The property time series of ULSW and LSW are positively correlated. For both, salinity and temperature, the highest correlation was found if the respective time series of LSW was lagged by one year. The correlation coefficients are $r_S = 0.80$ (salinity) and $r_T = 0.74$ (temperature). The ULSW time series reveal several periods with increased salinity that corresponds to warm temperatures (1970-71, 1984-85, 1998, 2003). In agreement with Sy et al. (1997) the salinity value of 1985 is questionable due to the location of the profile close to the high-salinity Irminger Water that is carried along the western boundary. Also profiles recovered for the year 1976 were of limited quality.

The general trends in both water masses are similar, but ULSW exhibits greater amplitudes. The ULSW is generally fresher and warmer due to its closer exposure to the surface. The time series presented by Sy et al. (1997) indicate several periods when the chosen depths range reveals mean properties similar to the classical LSW layer mean. Especially the temperature curve follows closely the trends in the classical LSW layer. From 1972 to 1997 the mean temperature in the considered LSW density range was warmer. During these years the time series defined between depth levels obviously better represents

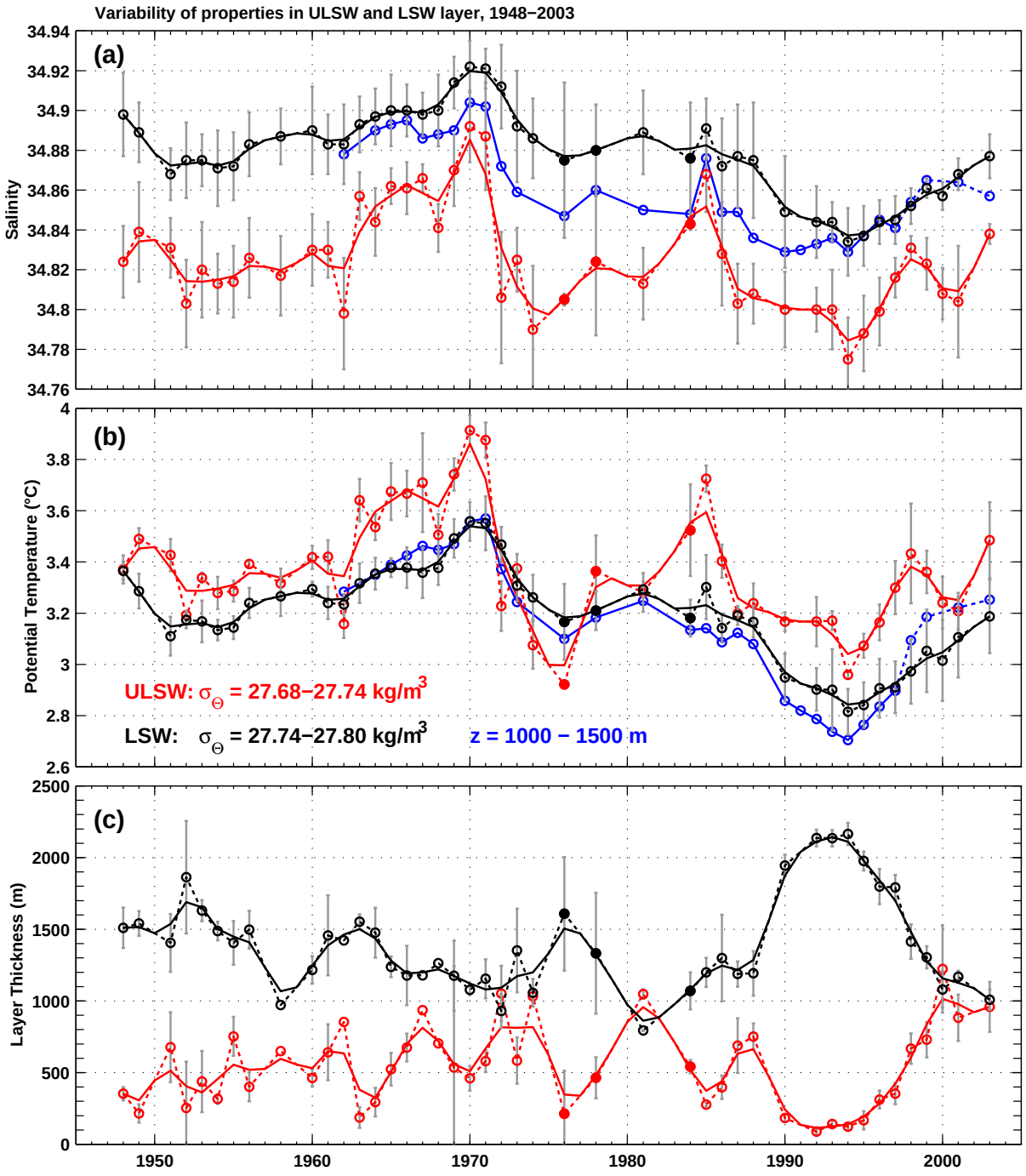

Fig. 4.9.: *Time series of (a) salinity, (b) potential temperature (°C), and (c) layer thickness (m), caluclated for ULSW (red curves) and classical LSW (black curves) during 1948-2003. Circles indicate the individual mean estimate with grey bars as the corresponding standard deviation. Dotted lines mark annual values received by linear interpolation. A 3-year filter is applied to smooth the time series (solid lines). Blue lines indicate time series of mean salinity and mean potential temperature in the depth range 1000-1500 m, as given by* Sy *et al. (1997), but extended for the years 1997-2003. Filled circles mark non-summer data.*

the LSW core layer with minimum temperatures. The general trends revealed in the LSW temperature is consistent with results from Sy et al. (1997) and Curry et al. (1998). The same holds for LSW salinity.

Corresponding time series of layer thicknesses for the period 1948-2003 are displayed in Figure 4.9c. Throughout the decades ULSW appears as a water layer that can be distinguished from the classical LSW. Layer thicknesses of both water masses reveal significant undulations. The time series are anti-correlated (correlation coefficient: r_{LT} = -0.85 at zero lag).

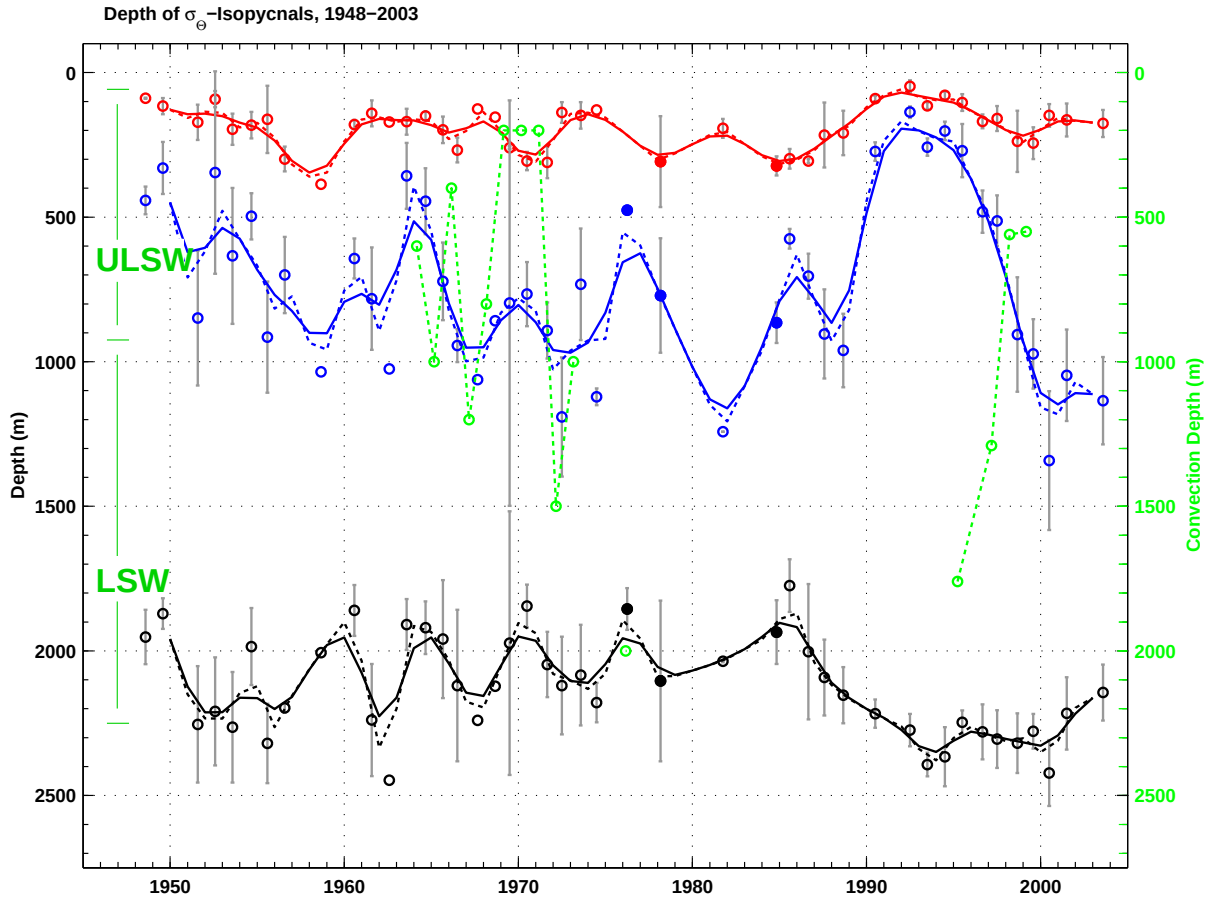

Fig. 4.10.: *Time series of depths (m) of particular isopycnals (σ_Θ = [27.68, 27.74, 27.80] kg/m^3) during 1948-2003. Open circles indicate individual mean estimates based on summer data, with grey bars as the corresponding standard deviation. Filled circles denote estimates based on non-summer data. Dotted lines mark annual values received by linear interpolation, while solid lines represent a 3-year filter. Included (green line/circles) are estimates of convection depths (m) in the Labrador Sea, based on wintertime hydrographic or mooring data (*Lazier, *1980;* Clarke *and* Gascard, *1983;* Mertens, *2000).*

During the early 1990s, climatic conditions have been most favourable for deep convection and thus formation of a huge volume of dense classical LSW (Lazier et al., 2002). During these years, nevertheless a thin layer of ULSW existed. This arises from the fact that the investigated hydrographic profiles represent summer-time conditions rather than

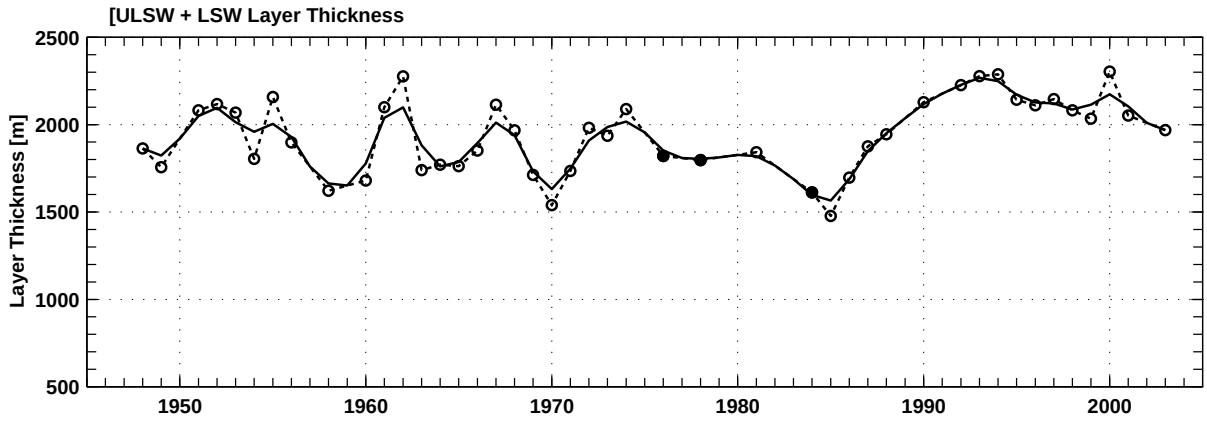

Fig. 4.11.: *Sum of ULSW and LSW layer thickness (m) during 1948-2003. Open circles indicate individual mean estimates based on summer data.*

conditions prevailing during late winter, the time of water mass formation. The deep convection of the early and mid 1970s and early 1990s eroded the existing ULSW layer, while in the subsequent post-convection phases the onset of restratification increased the ULSW layer thickness. The huge reservoir of classical LSW formed during the early 1990s was unprecedented in the investigated years. The ULSW time series revealed a few periods, when layer thickness was similar to the magnitudes observed at the end of the 1990s (>∼1000 m in 1972, 1974, 1981, 2000). Admittingly, the data coverage during the early 1980s is poor and the estimates of 1981 depend on only two profiles.

Figure 4.10 illustrates the depths of those isopycnals that vertically limit ULSW and LSW. The depth of the boundary that separates ULSW and LSW (σ_Θ = 27.74 kg/m^3) is much more variable in time than the remaining isopycnals (σ_Θ = [27.68, 27.80] kg/m^3). This is evident throughout the decades. The vertical shift of σ_Θ = 27.74 kg/m^3 occasionally is up to 1000 m (e.g. from 1993 to 2003). The largest shift in the depth of σ_Θ = 27.68 kg/m^3 is in the order of a few hundred meters. σ_Θ = 27.80 kg/m^3 is vertically displaced by about 500 m (1984 to 1994). While the upward shift of the isopycnal σ_Θ = 27.74 kg/m^3 indicates phases of increasing deep convection, its downward displacement implies a restratification of the water column. A comparison of the vertical displacement of isopycnals with observed convection depths (Fig. 4.10) reveals a quite good agreement. The deep convection observed by Clarke and Gascard (1983) during 1976 is, however, not well represented in the layer thickness time series. As was mentioned, data quality of the respective profiles was poor which might explain the lack of signal.

If ULSW and classical LSW are treated as one huge reservoir of convectively transformed water the decadal variability in both time series does not cancel out completely (Fig. 4.11). The 1990s still show up as a most remarkable period. The peak that emerges in 2000 is dominated by the layer thickness of ULSW which was uniquely large in that year.

The total layer thickness anomaly (thicknesses of ULSW and LSW are summed

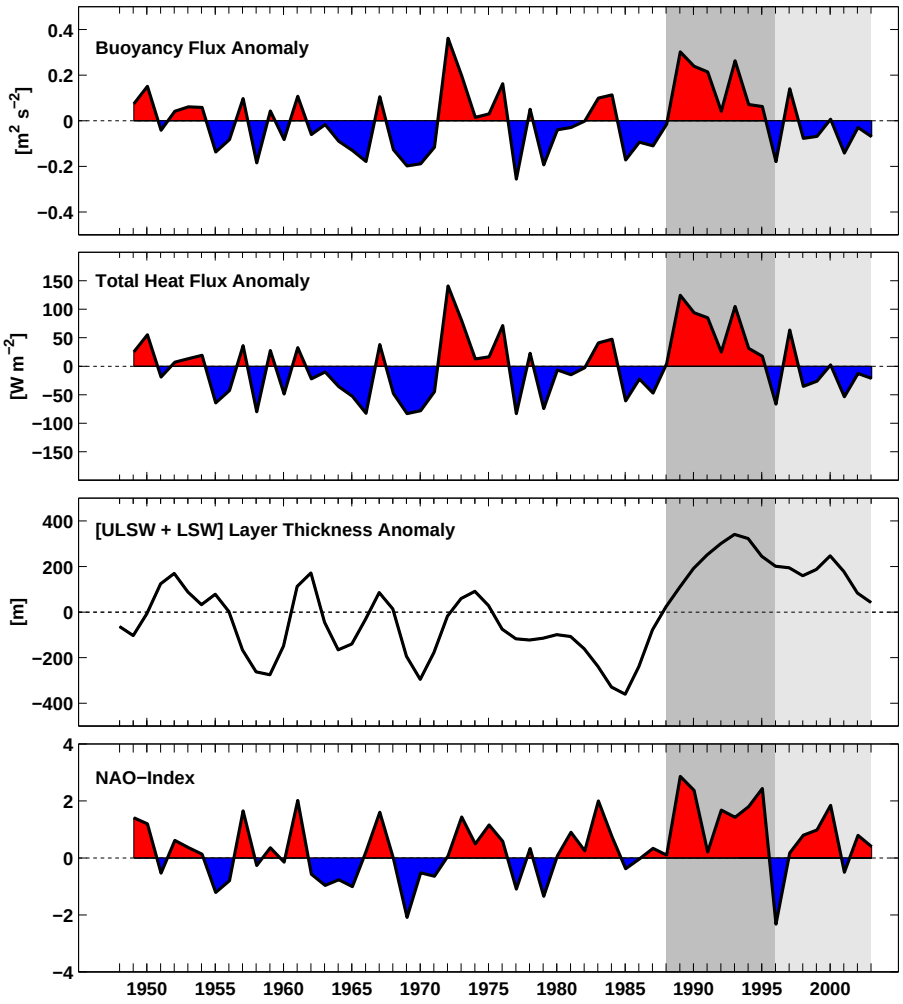

Fig. 4.12.: *Comparison of winter mean surface forcing (DJFM) in the central Labrador Sea with layer thickness anomaly ([ULSW+LSW]-mean) and winter mean NAO-index (DJFM) according to* Jones *et al. (1997).*

and the longterm mean is subtracted) reveals similar trends compared to the winter time surface forcing (Fig. 4.12). The best but weak correlation between the layer thickness evolution and the heat flux/buoyancy flux anomaly was found at a lag of one year ($r_{buoyancy} = 0.37$, $r_{heat} = 0.36$, surface forcing leads). Straneo et al. (2003) estimated large residence times for LSW in the Labrador Sea (4-5 years). Lazier et al. (2002) identified a 'memory effect' according to which the water column of the Labrador Sea reacts on longer time scales than one winter to the surface conditions. A strong surface forcing during winter does not necessarily result in deep convection since the extent of stratification is important in this context. From mooring data of the central Labrador Sea Mertens (2000) did not find a direct link between the NAO-index and the convection activity on interannual time scales (considered period: 1994/95 to 1999).

4.5. Summary and Conclusion

The variability in depth of the isopycnals limiting ULSW and LSW directly affects the variability of layer thickness of both water masses. Following Curry et al. (1998), thickness of the LSW layer and winter-time convection are directly related. While weak convection produces a relatively thin LSW layer, strong (meaning deep-reaching) convection results in a thick layer. For the formation of ULSW, another relation must be applied: if winter-time conditions do not favour convection activity that is strong and deep-reaching enough to ventilate the classical LSW, a lighter water mass, ULSW, is formed (Stramma et al., 2004). Occurring variability in layer thickness of both water masses can therefore be addressed as a proxy for variability in their formation.

The results presented in Chapter 3 indicated the increased formation of ULSW in the central Labrador Sea at the end of the 1990s. This is confirmed by the decadal time series of ULSW and classical LSW layer thicknesses. On decadal time scales the evolution of both properties indicated several switches from ULSW formation to LSW formation in this region and vice versa. Based on data from the early 1990s Pickart et al. (1996, 1997) observed ULSW formation in the DWBC region of the Labrador Sea. This was closely related to the formation of eddies within the DWBC which carried newly formed ULSW to the south. The results of the present study suggest two different mechanisms for ULSW formation:

- Formation in the Labrador Current/DWBC as suggested by Pickart et al. (1996, 1997). This can coincide with intense deep convection in the central Labrador Sea as was found by the authors.
- Formation in the central Labrador Sea in the absence of intense deep convection. As a result of weak forcing and/or strong stratification convection is rather limited to the upper 1000 m. Locally formed ULSW is the lighter substitute of the denser classical LSW.

Labrador Sea mooring data from March 1999 (mooring deployed at 56°N33.6'/52°W39.5'W) revealed water mass properties in the mixed layer that resembled the ULSW properties observed by Pickart et al. (1996) in the DWBC region (Mertens, 2000). The results of the present chapter suggest that, throughout the decades, the formation of ULSW in the Labrador Sea appears to be a common feature. This may account for the permanent ULSW signal present in the subtropical to tropical North Atlantic (Weiss et al., 1985; Fine and Molinari, 1988; Smethie, 1993; Rhein et al., 1998).

5. Export pathways out of the subpolar gyre

Previous analyses in conjunction with already existing studies pointed to the existence of additional routes that might export deep water out of the SPNA. These indications are now studied in more detail by investigating repeated hydrographic and tracer sections that followed the course of WOCE-line A2/AR19 at about 43°N. In the following, this line is referred to as A2. The observation period spans the years 1993 to 2001. The presence of export pathways away from the DWBC region is assumed to be linked to dynamics of the North Atlantic Current (NAC). Gradients of sea surface temperatures (SST) are analysed which serve as an indicator for the NAC pathway. Finally, decadal scale time series of ULSW and classical LSW are reconstructed for the DWBC region. These are compared with corresponding estimates of the central Labrador Sea.

5.1. Introduction

To what extent do hydrographic anomalies, generated in the SPNA and imprinted on the deep water circulation, propagate southward to the subtropical/tropical Atlantic Ocean, and what are the likely export pathways ? A key region to investigate the southward export of anomalies is the southern limit of the subpolar gyre (Fig. 5.1). As was introduced in Chapter 2, the western part of the Newfoundland Basin is a highly dynamical region. Here, the southbound DWBC encounters the strong and swift northbound NAC. The DWBC is closely nestled to the continental shelf and leaves the subpolar gyre, thus supplying young deep water to the subtropical North Atlantic.

Figure 5.2 illustrates the distribution of hydrographic properties along the western part of WOCE-line A2. This section was occupied during May 2001. The shallow and deep parts of the southbound DWBC carry the cold, fresh, and CFC-11-rich flow close to the continental slope. The deep salinity maximum is related to an inflow of GFZW that has low CFC-11 concentrations. Farther offshore, it is more obvious than in the DWBC region, because it is less diluted by the fresher layers located above and below. Layer thicknesses of ULSW and LSW are broadest in the DWBC. Here, both water masses show the highest CFC-11 concentrations and lowest salinities along the entire section.

Adjacent to the DWBC, the presence of the NAC is clearly visible through its warm and saline waters which correspond to minimum CFC-11 and silicate concentrations. Schott et al. (2004) investigated current measurements from combined shipboard and lowered ADCP data that were taken along the onshore part of this section. The velocity

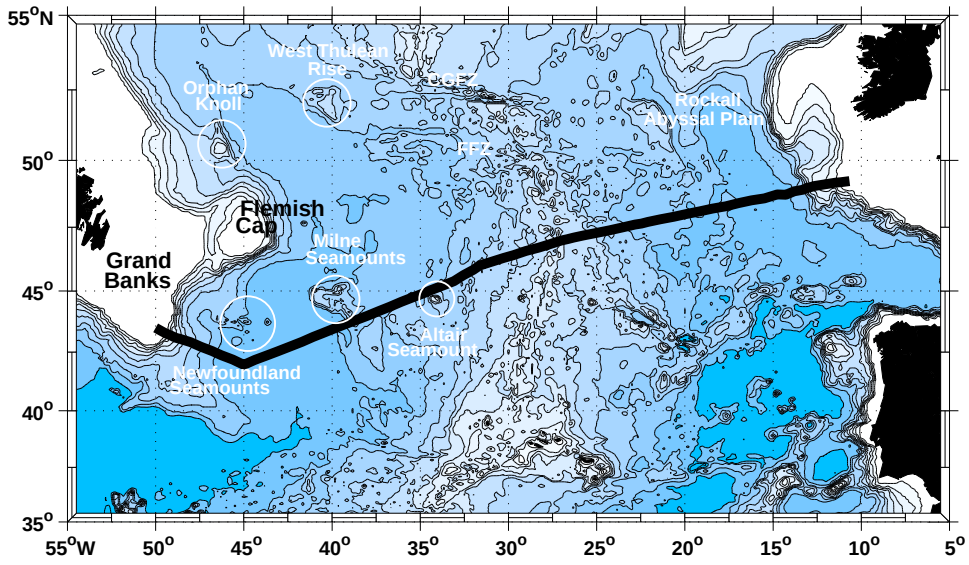

Fig. 5.1.: *Location of repeated WOCE-line A2/AR19. CGFZ: Charlie Gibbs Fracture Zone, FFZ: Faraday Fracture Zone. Bathymetric contours are given every 500 m.*

field revealed that the NAC occupied a large part of the region west of 45°W. It showed up by two surface-intensified branches that were centered at 48°W30' and 46°W45', respectively (Schott et al., 2004, their Fig. 14b). The onshore core, however, was not confined to the surface. It had a deep reaching component featuring velocities of several cm s^{-1} close to the bottom. Southbound DSOW encounters an inflow of northward modified AABW directly at the bottom. The latter carries elevated silicate concentrations (compare Section 2.2).

Stramma et al. (2004) analysed repeated sections that followed the course of WOCE-line A2 in the period 1994-2001. While A2 runs from the Grand Banks to the European Shelf, the authors focused on the western Newfoundland Basin (Grand Banks to 44°W). For this region they reported on considerable interannual variability in the properties of various deep water components carried in and adjacent to the DWBC. Tracing the spreading of anomalies within the boundary current revealed that LSW needs 1-2 years to flow from the central Labrador Sea (∼56°N) to the Grand Banks (∼43°N). Spreading times of about 2 years for the same distance were derived for DSOW.

As was mentioned by Rhein et al. (2002) and indicated in the analyses of Section 3.3, also the offshore part of the basin exhibits oustanding anomalies that are suggestive of additional export routes. The A2-section of 2001 features several locations (Fig. 5.2: e.g. ∼43°W, 39°W-35°W) where ULSW and classical LSW carry increased CFC-11 concentrations. These correspond to low salinities and to some extent to increased layer thicknesses. The low salinity in the ULSW is occasionally masked by the NAC. Koltermann et al. (1999) already provided indications for the existence of LSW pathways along the western and eastern flanks of the Mid-Atlantic Ridge (MAR). Furthermore, a pronounced salinity maximum, indicating the presence of GFZW, is located on the western

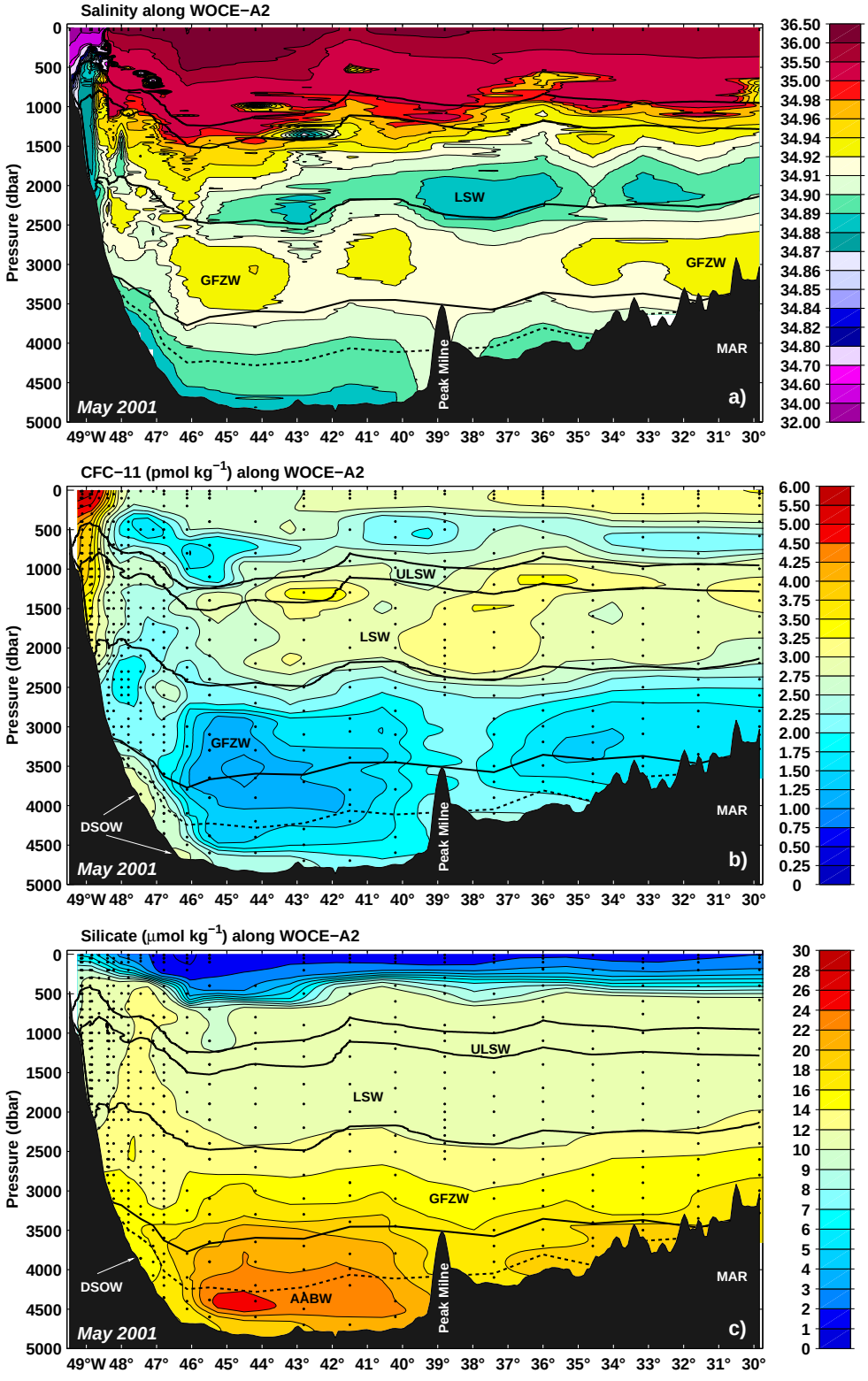

Fig. 5.2.: *Distributions of (a) salinity, (b) CFC-11 (pmol/kg), and (c) silicate (µmol/kg) along the western part of WOCE-line A2, May 2001. Bold solid lines indicate the isopycnals* σ_Θ *= [27.68, 27.74, 27.80, 27.88] kg/m*^{3}*, the dashed line is* σ_4 *= 45.885 kg/m*^{3}*. The section location is shown in Fig. 3.2.*

Cruise	Date	PI	Inst.	CFC	Si
G226	06 Jul-25 Jul 1993	A. Sy	BSH	—	X
M30/2	15 Oct-09 Nov 1994	K.-P. Koltermann	BSH	X	X
Hu95003	19 Apr-17 May 1995	R. A. Clarke	BIO	—	X
G276	04 May-09 Jun 1996	K.-P. Koltermann	BSH	—	X
M39/3	13 Jun-30 Jul 1997	K.-P. Koltermann	BSH	X	X
G316	02 May-20 May 1998	K.-P. Koltermann	BSH	—	—
M45/3	12 Jul-08 Aug 1999	F. Schott	IfMK	X	X
G350	06 May-05 Jun 2000	K.-P. Koltermann	BSH	—	X
M50/1	08 May-31 May 2001	J. Fischer	IfMK	X	X
M50/4	19 Jul-12 Aug 2001	W. Zenk	IfMK	X	X

Tab. 5.1.: *Summary of hydrographic and tracer data, sampled along WOCE-line A2. Data sources are WHPO and SFB 460. PI: Principal Investigator; Inst.: Institution; CFC/Si: chlorofluorocarbon and/or silicate data available; BIO: Bedford Institute of Oceanography, Canada; BSH: Bundesamt für Seeschifffahrt und Hydrographie, Hamburg, Germany; IfMK: Institut für Meereskunde Kiel, Germany.*

flank of the MAR. A CFC-11 profile (∼ 37°W30', Fig. 5.2) located to the east of Peak Milne features elevated concentrations at the bottom that might point to the presence of traces of DSOW.

Variability in the deep water components of the DWBC region was already discussed by Stramma et al. (2004) for the years 1994-2001. The present chapter highlights water mass variability in the offshore regions of this section. Hydrographic data cover the years 1993-2001. The focus is on investigating the existence and possible causes of deep water export pathways that are additional to the DWBC.

5.1.1. Hydrographic and tracer measurements along WOCE-section A2

As part of WOCE and SFB 460, several repeat sections have been accomplished along the A2-line (Tab. 5.1). Starting in 1993, the Newfoundland Basin was covered annually in the western part. Locations to the east of 42°W lack data from the years 1995 and 1999. The western slope region between 48°W25' and 45°W was not covered in 1994 due to bad weather conditions.

CFC measurements have been carried out in 1994, in 1997 and every odd year afterwards. CTD and tracer data from the years 1997, 1999, and 2001 were already introduced in Chapter 3. Information on data accuracies are given in Section 3.2 and in Stramma

et al. (2004). As for the CFC, nutrients including silicate were determined from water samples and measured during all but one cruises (1998). Corresponding concentrations were derived photometrically after converting the analytes into coloured substances (Grasshoff et al., 1999). The analysis was carried out using an Auto-Analyser continuous flow technique. Silicate accuracies for the cruises M30/2, M39/3, and M45/3 to M50/4 are ± 0.5 μmol/l (H. Johannsen, IfMK, pers. comm.). Accuracies for the remaining silicate data are assumed to be similar. The data set covers the years 1993-2001.

5.2. Temporal variability along WOCE-section A2

For both, ULSW and classical LSW, Figure 5.3 presents Hovmöller diagrams (longitude versus time) of layer thickness (a/b), mean salinity (c/d), and mean CFC-11 concentration (e-h). Average CFC-11 values were derived by depth-weighting as described in Section 3.2.2. In the considered period CFC measurements were carried out only during four of nine years (Tab. 5.1). Thus, continuously contouring the mean concentration for the particular layers requires a broader extrapolation. The depth-weighted average CFC-11 concentration at particular locations is added to the inter-/extrapolated contours of the same parameter.

At first glance, the distribution of layer thickness is not very helpful with respect to identifying offshore export routes for ULSW and LSW. The layer thickness of LSW (Fig. 5.3b) reveals a band-like structure, rather than distinct features that suggest the arrival of particular LSW signals. The layer thickness is interrupted by thicker and thinner patches in the order of about 100 m. It further points to a dominant spreading in the western basins of the SPNA. West of 30°W thicknesses generally exceeded 900 m, with maximum values located in the DWBC (> 1200 m, 1994-1998). This is the only region that indicates the arrival of new LSW, formed during the first half of the 1990s.

The layer thickness in the eastern basin gradually decreases towards the eastern margin. A minimum was found in 1994 close to the European Shelf (< 500 m). At the end of the observation period it had increased to at least 700 m. The salinity field (Fig. 5.3d) indicates that this region is occupied by high-saline water which is thought to be related to outflow from the Mediterranean Sea.

Contrary to LSW, layer thicknesses of ULSW do not reveal a pronounced separation between eastern and western basin flow. Lateral changes are small along the sections. In general, ULSW thickness is only one third of the LSW thickness. The lowest thicknesses are again located at the eastern margin. Maxima are found in the DWBC throughout the period. Additional thick anomalies emerged in the eastern basin in 1993 and 1994.

As expected, both water masses are thickest and carry the lowest salinities and highest tracer concentrations in the DWBC region close to the Canadian continental shelf. However, throughout the years, several low salinity anomalies emerged offshore in both layers that were associated to elevated CFC-11. These anomalies are obviously locked at particular locations. The most striking regions are centered around 43°W, 38°W-35°W, and

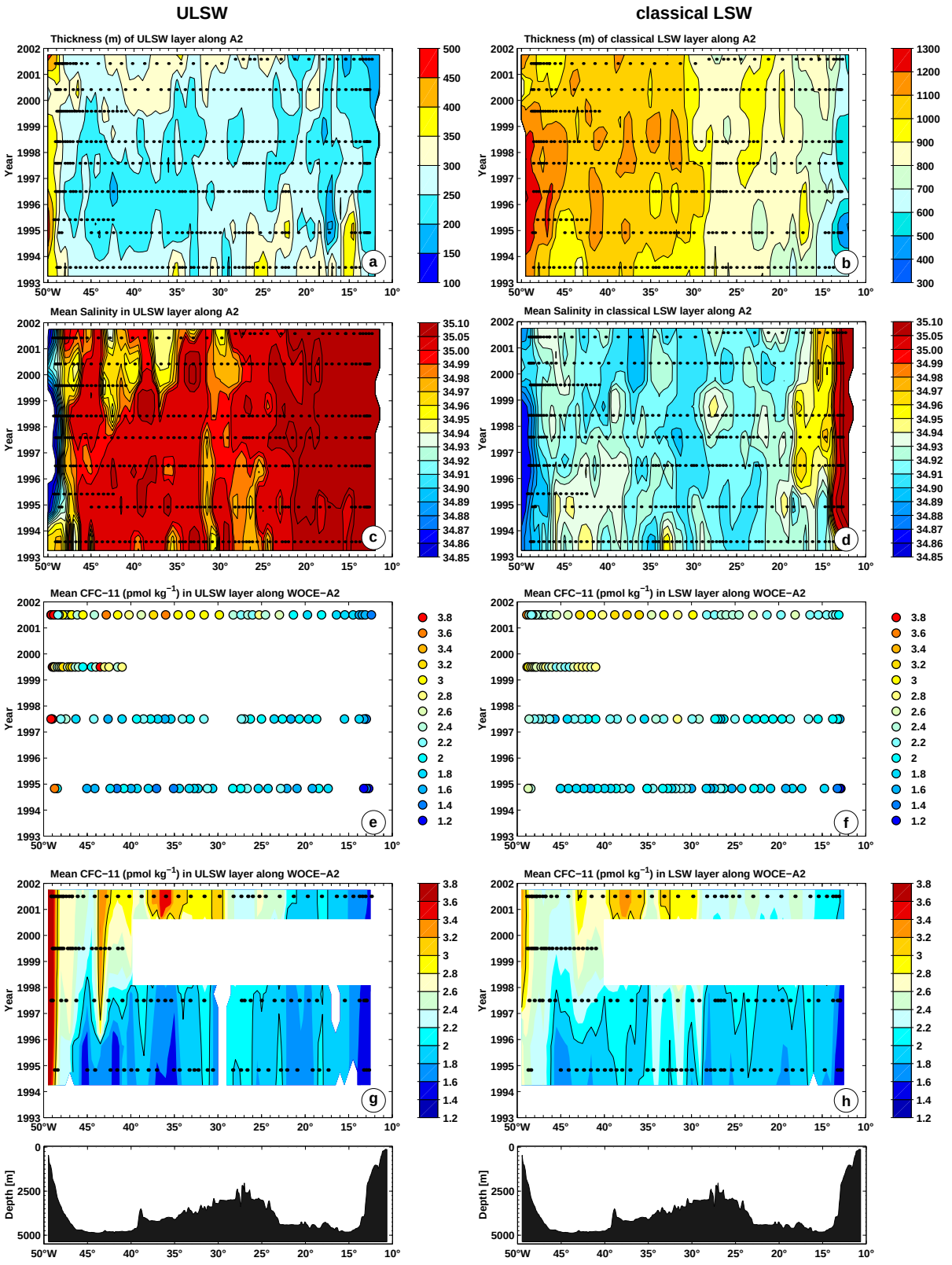

Fig. 5.3.: *Left column: ULSW, right column: classical LSW. (a/b): layer thickness (m), (c/d): mean salinity, (e/f): depth-weighted mean CFC-11 concentrations (pmol/kg), (g/h) inter-/extrapolated mean CFC-11 (pmol/kg), bottom row: topography along WOCE-line A2.*

on the western and eastern flanks of the MAR (about 33°W-30°W and ∼26°W-23°W).

43°W

Beginning in 1998, salinities with S∼34.96 and lower were found in the ULSW, centered around 43°W. These anomalies were much more saline compared to the salinity in the DWBC region (S < 34.85 in 1998), but they were embedded in a high-salinity environment (S > 35). In the same year, low salinities (S < 34.91) appeared at this location also in the deeper LSW. The low salinity trace was present in both water masses throughout 1998 to 2001. In summer 2000, however, the local minimum in the ULSW was shifted to the east (41°W-39°W30').

With the available tracer data the arrival of signals cannot be resolved. In 1999 and 2001 salinity anomalies were accompanied by elevated CFC-11 concentrations in both layers. ULSW and the denser LSW carried intrusion-like small-scale lenses with CFC-11 greater 3.6 pmol/kg and 3.2 pmol/kg, respectively. The local CFC-11 maximum that appears in 1997 in the ULSW contour plot is not supported by the original mean CFC-11 concentrations (compare Fig. 5.3e). It rather results from the broader extrapolation of data.

38°W-35°W

Additional salinity anomalies located at 37°W-36°W were present in both layers in 2000-2001. During these years the ULSW layer thickness had increased and salinity fell below S = 34.95. Classical LSW exhibited the lowest salinities (S < 34.90) in the offshore region, but did not reveal significant changes in the layer thickness. CFC-11 concentrations in both layers were of the same order as at 43°W.

Prior to 2000, ULSW did not show salinities at this location that were similar in magnitude. In 1994 CFC-11 was rather inconspicuous between 37°W to 35°W. 1.8 pmol/kg were found at 38°W. Three years later, CFC-11 maximum increased to 2.2 pmol/kg at 38°W30'.

From 1994 to 1998 LSW carried a quite uniform envelope of salinities smaller than S = 34.92. CFC-11 concentrations between 38°W to 35°W were 2.1 pmol/kg. A considerable increase was noted in 2001 when CFC-11 rose to 3.1-3.2 pmol/kg.

Mid-Atlantic Ridge

There are two further tracks of water showing lower salinities. One is found on the western flank of the MAR, while the other is located to the east of the ridge system. At 31°W ULSW salinities were below S = 34.96 in 1993. From 1994 to 1997 this water mass featured a narrow band with S < 34.98. After an interruption lower salinities re-appeared in 2000 (S < 34.96 in 2001). The denser classical LSW featured salinities of S < 34.91 at this location, which continued throughout the observation period. A local minimum (S < 34.90) was observed in 1997. Both layers carried elevated CFC-11 concentrations that were observed during all four cruises. From 1994 to 2001 CFC-11 in the LSW increased from 2.3 pmol/kg to 3.1 pmol/kg. The profile exhibiting the latter value was located

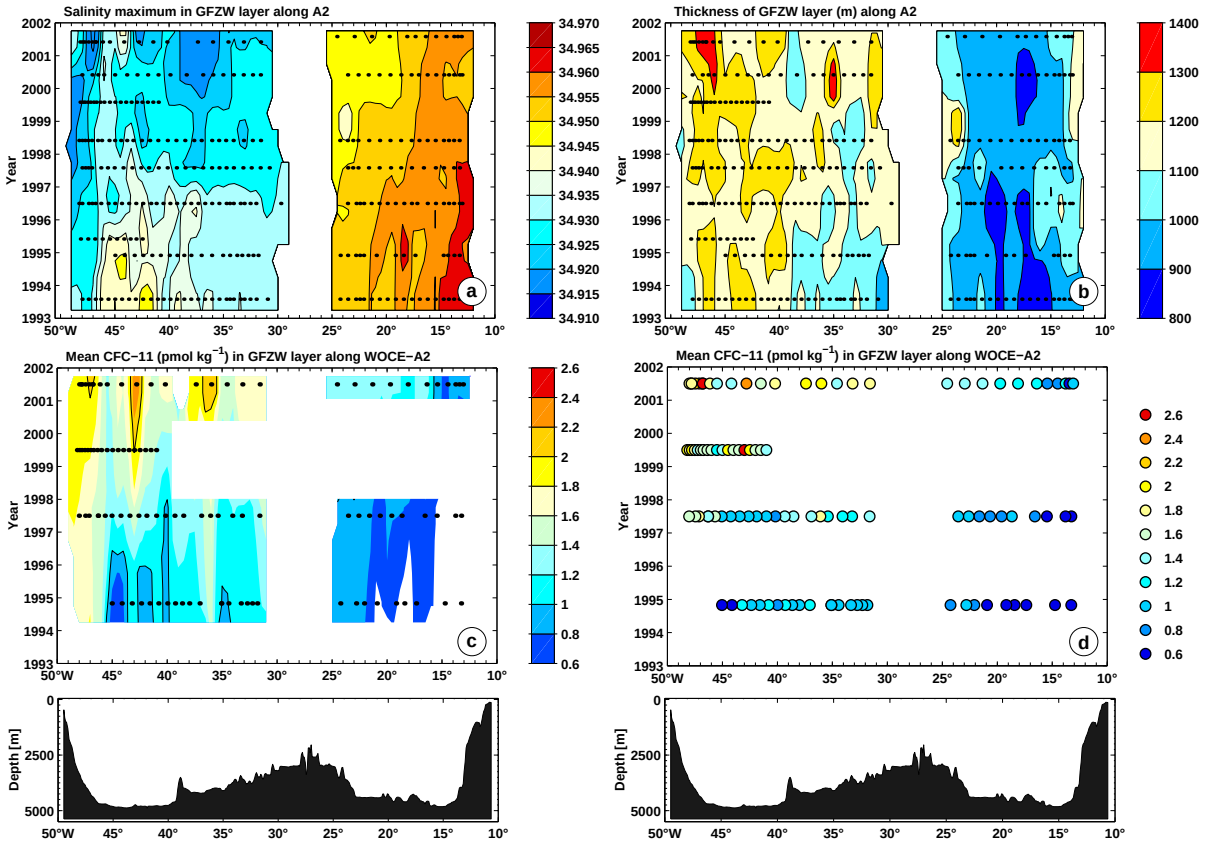

Fig. 5.4.: *(a) Maximum of salinity in GFZW layer, (b) layer thickness (m) of GFZW, (c/d) depth-weighted mean CFC-11 concentration (pmol/kg). Note that colours in (c) and (d) are different: (d) indicates concentration ranges.*

shortly west of 33°W. A similar increase was obvious in the lighter ULSW. Prior to 2001, CFC-11 in the classical LSW exhibited the greater mean values.

The low salinity track located to the east of the MAR is not as pronounced as its western counterpart. From 1993 to 1996, traces of reduced salinity were prominent in the ULSW, centered at about 27°W-26°W. Distinct minima were restricted to regions west of 24°W . This is different from the LSW layer. On the eastern flank of the MAR (26°W-23°W) LSW featured a broad envelope of S $<$ 34.92 that changed in width throughout the years. But it was not until 2000 that salinities of similar magnitude (S $<$ 34.91) as during the beginning of the observation period showed up at this location.

A local CFC-11 maximum (2.2 pmol/kg) was found in the ULSW in 1994 (∼23°W). A similar peak was lower and only weakly pronounced in the deeper layer. In 1999, however, mean CFC-11 in the LSW exceeded that of the lighter ULSW by 0.1-0.2 pmol/kg at 25°W-22°W30'. Two years later this reversed again at this location. East of 23°W mean CFC-11 of ULSW was reduced compared to LSW (0.2-0.4 pmol/kg).

The lower deep water components

Offshore anomalies pointing to the presence of deep water components are not restricted to the ULSW and LSW layers. Also signals in the deeper GFZW and DSOW layers support the previous findings. Figure 5.4 displays corresponding property distributions for GFZW that is located between the isopycnals σ_Θ = [27.80, 27.88] kg/m^3. Thickness and mean CFC-11 are compared to the distribution of the salinity maximum which particularly characterises this water mass. Only those CTD profiles were considered that exhibited maximum densities greater σ_Θ =27.88 kg/m^3. Thus, they vertically cover the water mass completely. The salinity maximum was then searched in the narrow density range σ_Θ =[27.83, 27.877] kg/m^3. This range was chosen to reduce a possible impact from deep-reaching high-salinity intrusions of the upper layers (compare Fig. 5.2, ∼46°W). After identifying the depth of the salinity maximum at each station, a respective mean value for the vertical range z(S_{max}) ± 20 dbar was calculated (Fig. 5.4a).

The salinity distribution reveals very different conditions in the western and eastern basins. As was introduced in Section 2.3.3, water masses of Nordic origin (ISOW) entrain warm and saline SPMW from the surroundings while overflowing the Iceland-Scotland Ridge (e.g. Van Aken, 2000a). The high saline water close to the European continental slope indicates the presence of Deep Mediterranean Water (DMW; Harvey and Arhan, 1988; Paillet et al., 1998). Harvey and Arhan (1988) proposed that this water is not directly related to the Mediterranean outflow but rather gains its high salinity via vertical mixing with the overlying MW.

Having entered the western basin through the deep fracture zones of the MAR, GFZW encounters the fresher LSW lying on top, the fresher DSOW located below, and mixes along its spreading pathways (Swift, 1984). Thus, the salinity of GFZW located in the western basin is diluted compared to the eastern basins.

Throughout the observation period GFZW in the western boundary current was subject to a gradual freshening. Similar events occurred at ∼43°W and ∼37°W. A decrease in salinity after 1996 was stronger pronounced in the latter region. The corresponding layer thickness is rather patchy and does not reveal any clear signals. Dickson et al. (2002) reported on a substantial freshening trend which was observed during 1965-2000 in the lower deep water components of the northern and eastern SPNA. Salinity time series from the eastern flank of the Reykjanes Ridge (∼57°N/30°W) indicated a trend reversal that started in 1996 in the eastern basin (Dickson et al., 2002). Similar time series from the Labrador Sea, however, exhibited still a salinity decrease in 2001. The freshening observed at the A2-line points to an arrival of this signal at the southern exit of the subpolar gyre. Corresponding salinities along A2 are much more closer to GFZW salinities of the Labrador Sea than the eastern Reykjanes Ridge (Dickson et al., 2002). Lazier et al. (2002) noticed that LSW had penetrated into the saline deeper layers during the active deep convection period of the early 1990s. A comparison of Labrador Sea profiles revealed a substantial decrease in salinity (-0.065 psu in the depth range 2000-2600 m) that occurred from 1990 to 1993. A deep penetration would not only alter the salinity but also increase the CFC content of the GFZW. Annually repeated sections from the early

1990s reveal a gradual CFC-12 increase in the GFZW layer (AZETSU-SCOTT et al., 2003). Thus, the high salinities of GFZW are associated to low CFC concentrations and vice versa. Data presented in Figure 5.4 indicate a collocation of low salinities with increased CFC-11 concentrations in the offshore regions of the Newfoundland Basin.

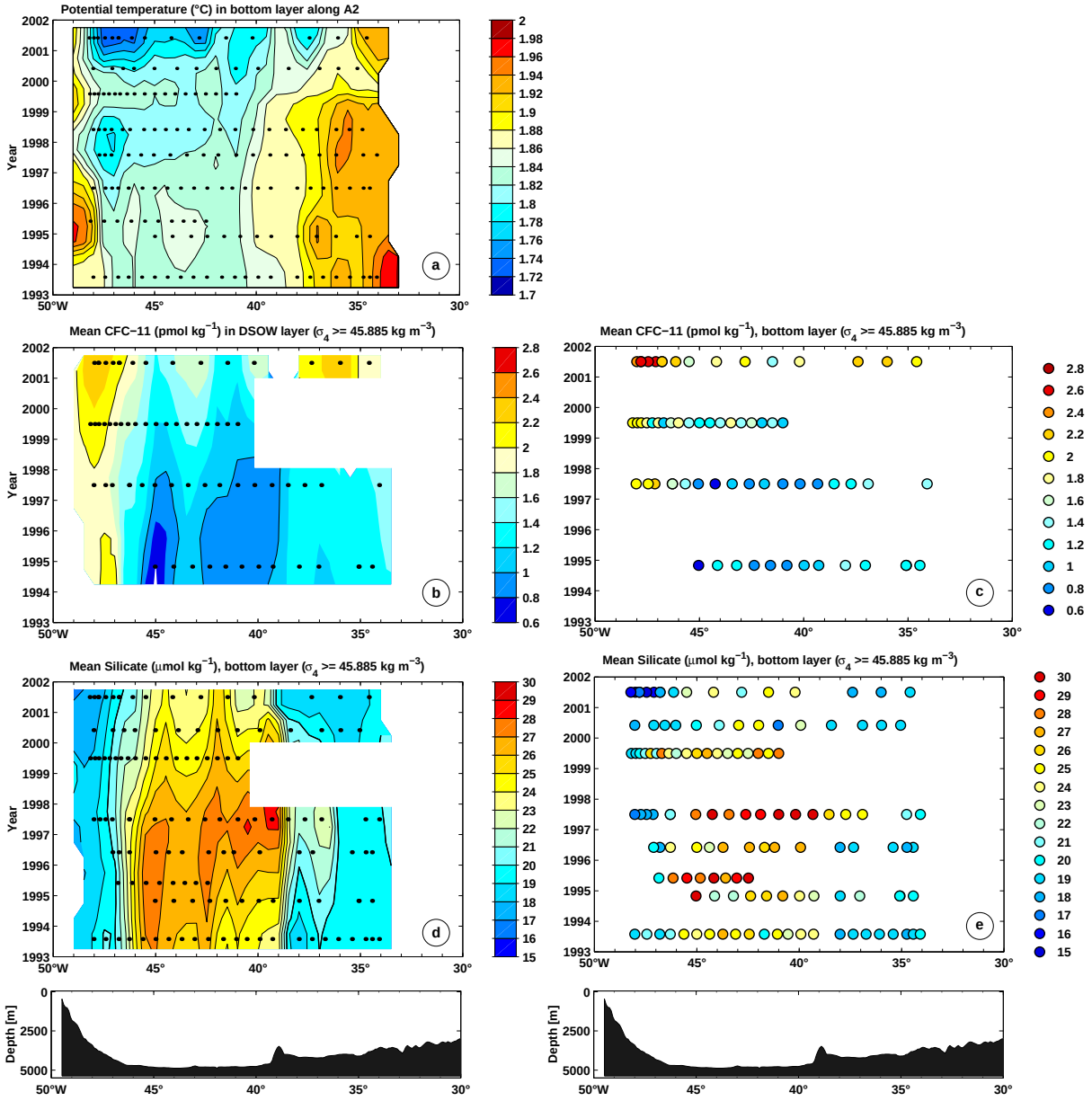

Fig. 5.5.: *(a) Mean potential temperature (°C) for a layer covering the lowest 20 m of the CTD records. See text for details. (b/c) mean CFC-11 (pmol/kg) and (d/e) silicate (µmol/kg) in the bottom layer, calculated for σ_4 >= 45.885 kg/m^3. Only the western part (50° W-30° W) of WOCE-line A2 is shown. Note that colours in left and right columns are different: left column indicates concentration ranges.*

Figure 5.5 presents observations from the bottom layer. Potential temperature and the depth-weighted mean CFC-11 concentrations are opposed to the respective mean silicate content. Only the western part of WOCE-A2 is shown, since a significant spreading of DSOW is limited to the western basin. While high CFC concentrations indicate the presence of DSOW, increased silicate in company with low CFC contents point to remnants of modified AABW. Both, DSOW and modified AABW, are bottom-intensified water masses. Usually, the isopycnal $\sigma_\Theta = 27.88$ kg/m^3 is considered as the upper limit of DSOW. Away from the continental shelf the density field considerably flattens (compare Fig. 5.2). For this reason, densities greater than $\sigma_4 = 45.885$ kg/m^3 are taken into account to better represent the bottom layer. This particular isopycnal is located closer to the sea bottom than the isopycnal $\sigma_\Theta = 27.88$ kg/m^3. Nevertheless, it still comprises the core of DSOW and the major signal of modified AABW. In the interior Newfoundland Basin, however, the upper part of this water mass is neglected (Fig. 5.2). Displayed temperatures represent mean values for the lowest 20 m of the CTD casts. The CTD/water-sampling system was usually lowered down to 10-20 m above sea bottom.

From 1993 to 1998 bottom-near temperatures were lowest in a broad band located between 48°W-47°W to 40°W ($\Theta < 1.86$°C). The western limit is characterised as the DWBC-NAC transition zone (Stramma et al., 2004). Here, the years 1997 and 1998 exhibited a local temperature minimum ($\Theta < 1.8$°C). The range of low temperatures is shifted further to the west and east. A subsequent minimum was even more pronounced in 2001 ($\Theta < 1.74$°C). From 1993 to 1998 warmer water with temperatures greater 1.88°C occupied regions east of 38°W. The bottom layer to the east of Peak Milne exhibited the lowest temperatures in 2001 ($\Theta < 1.8$°C).

Mean silicate and CFC-11 contents of the bottom layer indicate that traces of modified AABW occupied the major part of the deep Newfoundland Basin (Fig. 5.5). The strongest signal was again limited to the region 46°W30'-39°W where the highest silicate contents coincided with the lowest CFC-11 concentrations. Throughout the period CFC-11 gradually increased. The Milne Peak and the adjacent foot hills of the MAR limited the eastward extension of the low-CFC-11/high-silicate signal. An exception was found in 1997, when elevated silicate contents were observed at 37°W. The region east of Peak Milne generally reveals higher CFC and lower silicate contents compared to the deep Newfoundland Basin. Recent analysis of section data along 48°N (Walter et al., 2004, manuscript submitted to Geophys. Res. Letters) indicated increased vertical mixing in abyssal regions close to rough topography. This process might explain the tendency towards warmer temperatures coinciding with elevated CFC-11 concentrations east of Peak Milne. The mid-depths, however, revealed only moderate diffusivities. In 2001, increased CFC-11 signals appeared east of 38°W and coincided with one of the lowest silicate contents observed during this period. This signal is attributed to horizontal advection, since corresponding anomalies were also obvious in all other deep water components (compare Figs. 5.3 and 5.4).

The bottom layer properties in 2001 were very distinct from previous years. Occasionally, maximum values of silicate are not confined to the sea bottom but lifted upwards. This was the case in May 2001 (cf. Fig. 5.2). Such a situation was also observed by

Clarke et al. (1980, their Fig. 10d) on an early section from 1972. The section location was similar to the western part of A2 but extended further to the southeast. Clarke and co-authors noted high oxygen bottom values on the section's offshore end. However, they attributed these to poorer quality in the measurements. In 2001, DSOW occupied very deep parts of the continental slope. One distinct core was located at about 3600-4000 dbar, while a second core was found at about 4700 dbar. The deepest CFC-11 samples in the center of these cores (profiles located at 47°W27' and 46°W8') revealed similar elevated tracer concentrations (2.90 pmol/kg and 2.91 pmol/kg). These were associated to equally high oxygen concentrations (6.63 ml/l for both samples). At locations below the silicate maximum oxygen increased towards the bottom. Either a stronger DSOW had diluted and displaced modified AABW to a greater extent or a weaker inflow of modified AABW enabled DSOW to expand. The LADCP-section from the 2001 cruise revealed that the current field below 4000 m exhibited northeastward velocities of several cm/s in the region ∼47°W to 45°W30' (Schott et al., 2004, Fig. 14d). Though the velocity profiles represent only snapshots, it seems that the apparent deeper DSOW core of 2001 was a feature that probably recirculated northwards.

In summary, there is evidence in all deep water components that points to a significant spreading offshore. Several regions turned out to be of particular importance for spreading in the western basin and along the flanks of the MAR.

5.3. Spreading time scales

Koltermann et al. (1999) determined the spreading time of LSW, from its source region to 48°N on the eastern flank of the MAR. The authors analysed three occupations of the approximate A2-section (1957, 1982, 1993) and calculated the temperature and salinity differences between the particular years. They assumed that both, the transformation of LSW properties along the path and the spreading time, do not significantly change during the considered period. They also differentiated between an LSW warming phase that was referred to the years 1957-1982 (spanning 25 years) and a cooling phase that corresponded to the period 1982-1993 (spanning 11 years). T/S differences observed at 48°N were related to decadal time series of LSW properties (Curry et al., 1998). For the warming as well as the cooling phase Koltermann and co-authors constructed two different source functions. From each particular data point of the original LSW time series of the Labrador Sea the corresponding value 25 years or 11 years before was subtracted. The obtained time series of temperature and salinity differences were analysed with respect to that particular year, when both, ΔT and ΔS, matched the differences observed at 48°N. The resulting time span was thus considered as a spreading time. According to these investigations, LSW needed 7.5 years (warming phase) and 4.5 years (cooling phase), respectively, to reach 48°N to the east of the MAR.

One can argue about whether three repeats of the A2-line during three different decades are sufficient to account for a proper estimation of LSW spreading times. A

further objection refers to the assumption that the transformation of LSW properties does not change along the spreading pathway. Sy et al. (1997) already noted the enhanced mixing of LSW with surrounding water masses, while flowing towards areas in the Newfoundland Basin and east of the MAR. Stramma et al. (2004) compared distributions of potential vorticity at different locations of the western SPNA. Minima of potential vorticity in the ULSW and LSW were much weaker in the Grand Banks regions compared to the Labrador Sea which supports the findings by Sy and co-authors. Nevertheless, spreading times derived by Koltermann et al. (1999) are not too far away from estimates by Sy et al. (1997). Based on repeated sections from the early WOCE period, these authors found 1 year for LSW to enter the Newfoundland Basin, 2-3.5 years to reach the Iceland Basin and 4-5.5 years to get to the Rockall Abyssal Plain. In a recent note, Yashayaev et al. (2004) presented time scales that almost doubled those reported by Sy et al.: 5 years to the Iceland Basin and 7 years to the Rockall abyssal plain.

The identified offshore LSW anomalies are now used to deduce first order spreading times for the western part of the A2-line. From time series reconstructed for the central Labrador Sea it turned out that LSW ventilation peaked during late winter 1993/94 (e.g. Sy et al., 1997; Curry et al., 1998; Fig. 4.9, this study). LSW showed the lowest temperatures and salinities accompanied by the greatest layer thickness. Suppose, this signal needed 1-2 years to reach the Grand Banks regions, as several studies have suggested. Then it should have arrived there at some time in 1995. However, LSW is subject to mixing on its way towards south, thus the salinity gradually increases (Stramma et al., 2004). Furthermore, the meandering warm and saline NAC possibly masks signals pointing to LSW in the interior Newfoundland Basin. With regard to these facts, only a very pronounced anomaly is thought to be able to 'survive' in the offshore regions of the Grand Banks. The core of the DWBC is generally much swifter than the surroundings (e.g. Lazier and Wright, 1993; Fischer and Schott, 2002). Adjacent to it, the flow recirculates in opposite direction (Lavender et al., 2000; Schott et al., 2004). If an LSW signal does not take the fast track via the DWBC, it will probably need a longer time to recur in the interior Newfoundland Basin.

Figure 5.6 shows once more the salinity distribution of LSW in the longitude vs. time space. The appearance of low salinity anomalies, lagged in time and shifted in space (white dashed line), suggests that they refer to the same signal. To a first order, this is assumed to be correct. The low salinity signal superimposed during late winter 1993/94 seems then to have emerged about 2.5 years later in the Newfoundland Basin at ∼45°W. It would further have taken about 3-4 years to reach 43°W-40°W and 5-6 years to get to 37°W-36°W. The latter estimate is crude due to the lack of data east of 42°W in 1999. The LSW signal might have arrived at this location already in that year.

Further to the east, the lowest salinity emerged at about 32°W in 1997. Relating its arrival to a possible generation in late 1993/94 would imply a spreading time scale of more than 3 years. This is much shorter than estimated for the interior western basin. Admittingly, little evidence exists to definitely relate the arrival of this anomaly to a particular formation year. But in 1994 and 1997 local mean CFC-11 values were higher compared to the deep Newfoundland Basin located to the west. This would support a

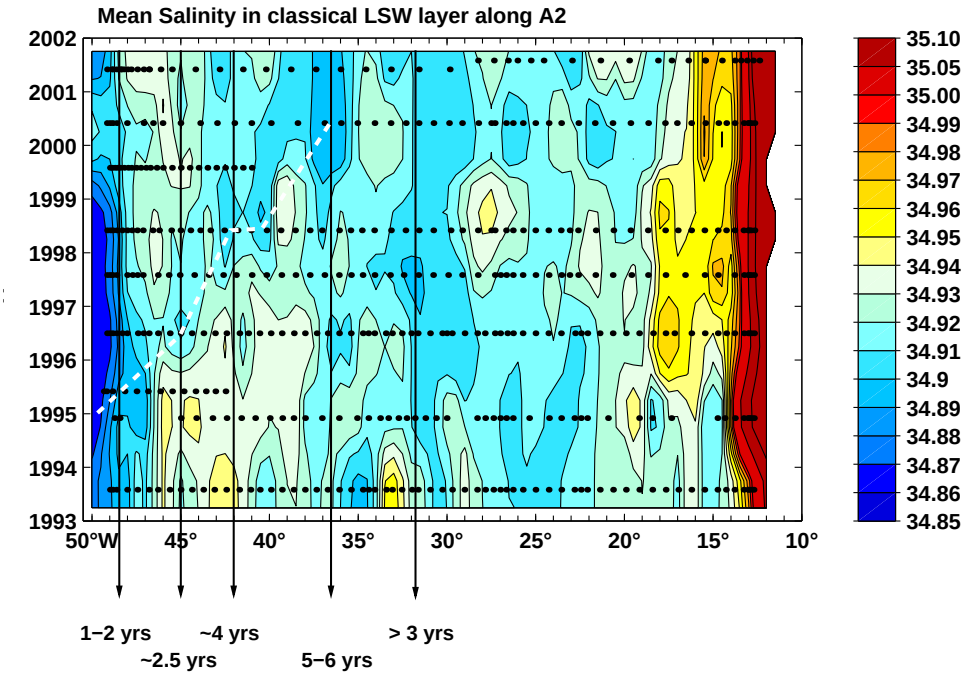

Fig. 5.6.: *Mean salinity of LSW. Same as Figure 5.3b but with indicated spreading time scales for particular locations (black arrows). See text for details.*

faster spreading along the western part of the MAR.

Figure 5.7 presents a comparison of LSW salinity and temperature, averaged over a certain longitudinal range along A2, with corresponding LSW time series derived for the central Labrador Sea. The estimates from the Newfoundland Basin were shifted back in time to match the observed extrema in the Labrador Sea. Though the eastern part of the Newfoundland Basin lacks data in 1994 and 1999, the estimated spreading times can be reasonably well linked to the Labrador Sea time series. Both, salinity and temperature reveal the same variability pattern.

The interannual time series of the ULSW layer thickness (Fig. 4.9) indicated that a noticeable increase in layer thickness started after 1994. Azetsu-Scott et al. (2003) observed the lowest salinity in summer 1995 in what they termed 'shallow LSW'. The density range of this water mass overlaps with the ULSW of the present study, but it neglects the upper part (compare Sect. 3). If this is the signal that emerged at the earliest in 1997 at ~43°W, a resulting spreading time for ULSW would be about 2.5 years. This is equal to LSW and should be expected. The low salinity signal at ~43°W was, however, only weakly pronounced in 1997 (Fig. 5.8). Assuming that ULSW had arrived there in the subsequent year would raise the spreading time to more than 3 years.

These time scales are based on the presumption that the anomaly originated somewhere in the central Labrador Sea. Investigations by Pickart (1992) and Pickart et al. (1996, 1997), however, revealed that ULSW is occasionally formed in the boundary current region of the western Labrador Sea. This would reduce the distance ULSW has to travel from its source region to 43°W. Concerning recent ULSW ventilation (Sect. 3)

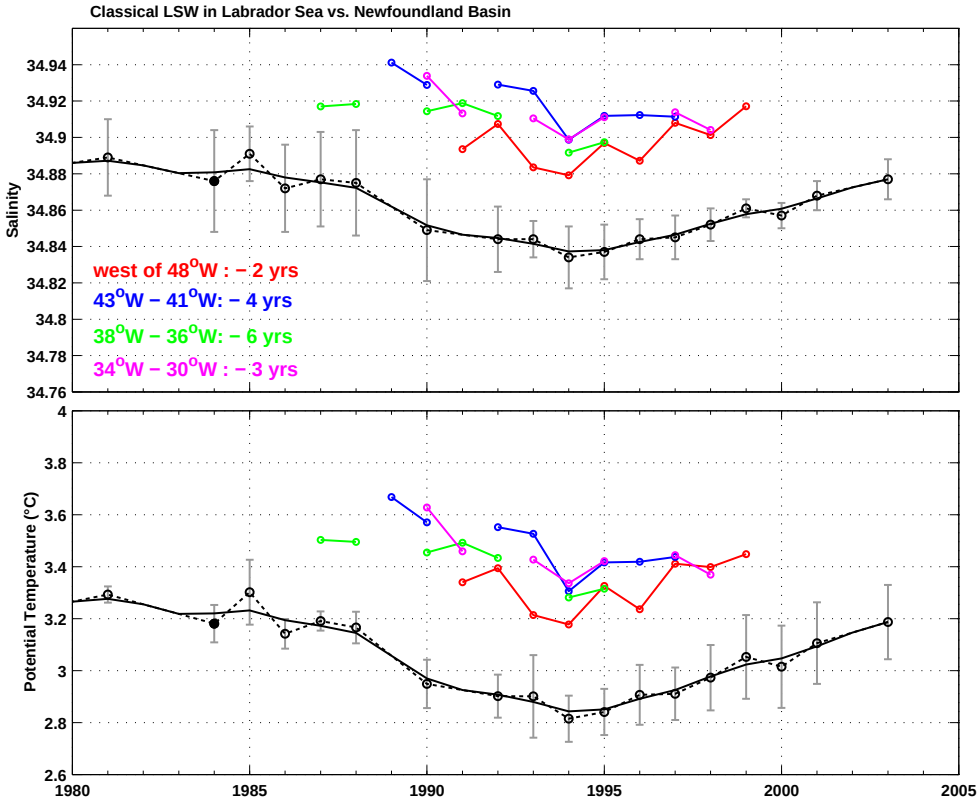

Fig. 5.7.: *Comparison of LSW time series (black lines), reconstructed for the central Labrador Sea in Chapter 4, with corresponding LSW signals observed in the interior Newfoundland Basin. Top: salinity, bottom: temperature (°C). Estimates from the Newfoundland Basin were shifted back in time, see legend.*

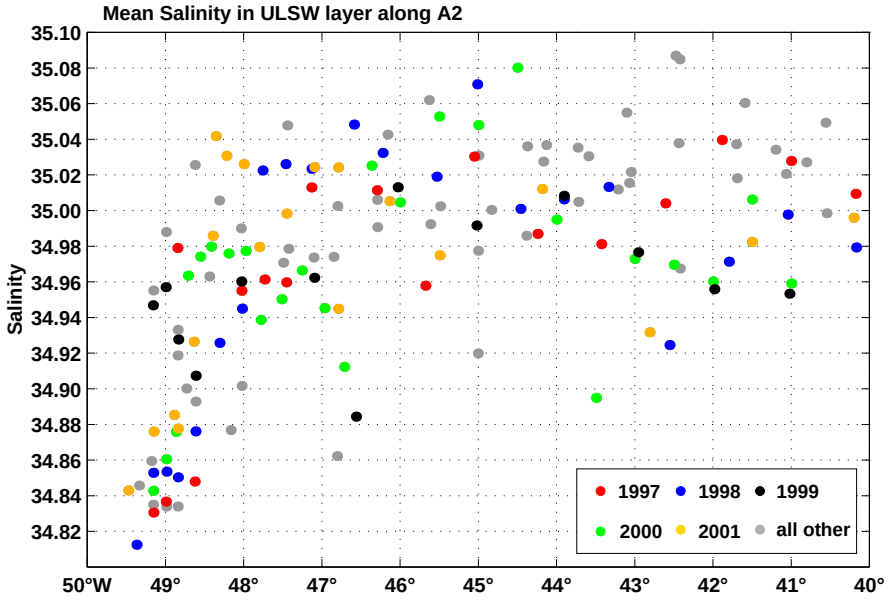

Fig. 5.8.: *Mean salinity of ULSW for the region 50° W-40° W. See text for details.*

there was not made any particular difference between ventilation in the boundary region or the interior Labrador Sea. However, the CFC-11 inventory distributions revealed that the latter region was far more important for explaining the high formation rates at the end of the 1990s. This does certainly not hold for earlier years since the deep convection years favoured the local formation of the denser classical LSW. Anomalies in the ULSW layer arrived already in 1993 and 1994 at 30°W. They carried lower salinities and elevated CFC-11 concentrations compared to the surroundings. These are likely remnants of ULSW formation happening at an earlier time and possibly but not necessarily related to convection in the boundary current. For example, the time series of ULSW layer thickness (Fig. 4.9) revealed increased values in the Labrador Sea prior to 1990.

The GFZW anomaly that emerged at about 37°W is not helpful yet to estimate a spreading time. In 2001 this feature was still part of an on-going trend. Stramma et al. (2004) reported on a trend reversion in the Labrador Sea from 2000 to 2001. Further data are needed that reveal a trend interruption at 43°N. This could then possibly be correlated to remote changes.

5.4. Causes for deep-water anomalies located offshore

From the presented data it turned out that traces of NADW are injected somehow into the interior Newfoundland Basin. But what is the underlying mechanism ? The working hypothesis for the subsequent analyses is as follows: the offshore spreading of the different components of NADW is related to dynamics of the NAC and affected by submarine topographic features. This assumption is based on the observations that the pathway of the NAC has impact on the spreading of deeper water masses. For example, both, ULSW and classical LSW spread along the NAC path into the eastern basin of the SPNA (e.g., Talley and McCartney, 1982; Rhein et al., 2002; this study, Section 3). Occasionally, the NAC is locked above the CGFZ (Belkin and Levitus, 1996). Schott et al. (1999) noticed during such a blocking event that the water column had an eastward flow with a strong barotropic component. Deep water masses of the eastern basin were prevented from entering the western SPNA. Instead, the invasion of western deep water into the eastern basins was triggered. Based on moorings deployed in the channels of the CGFZ Saunders (1994) noticed the occurrence of time-dependent deep current reversals. He suggested that this might be caused by the meandering NAC. Relations between upper and deep flow have also been observed in the Southern Ocean. Here, Whitworth III et al. (1991) reported on variability in the DWBC that was associated to meandering of the Antarctic Circumpolar Current.

The western part of the A2-line is located in the vicinity of isolated seamounts (Fig. 5.1). Especially the Milne and Altair Seamounts are thought to be of particular importance for water mass signals observed at A2. They provide noticeable features with local water depths shallower than 3000 m. The A2-line does not run in a purely zonal direction but follows a northeast course from 45°W to 32°W with the two features located on both sides. Any regional deep flow is assumed to be influenced due to their presence.

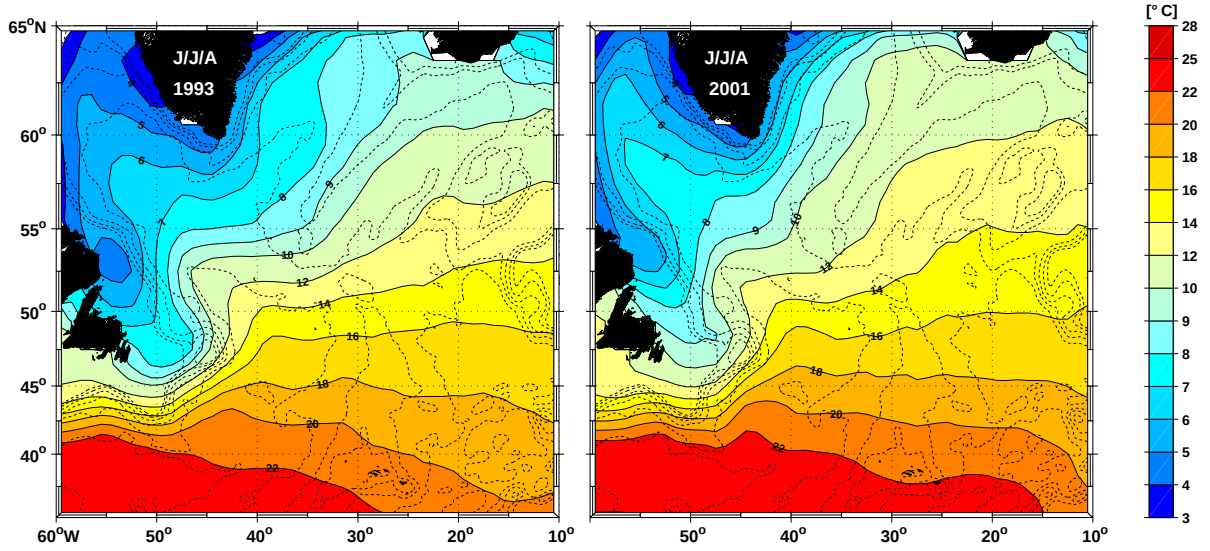

Fig. 5.9.: *Mean sea surface temperature (SST in °C) for summer (J/J/A) 1993 (left) and summer 2001 (right). SST is derived from "Reynolds', Stokes' and Smith's Version 2 Optimum Interpolation SST" (*Reynolds *et al., 2002). The SST data set is available at http://dss.ucar.edu/datasets/ds277.0/data/oiv2.*

To sufficiently answer the question previously posed, a highly-resolved 3-dimensional data set is needed that covers the observation period and allows for tracing and quantifying the deep water flow. Despite all field work that has been and still is carried out, such a data set is, however, not available. Since the NAC imports large amounts of heat into the SPNA and is very intense at the sea surface, sea surface temperatures (SST) are investigated. Especially the horizontal gradient of SST should reveal indications for the NAC pathway.

5.4.1. SST Data Set

SSTs are derived from the "Reynolds', Stokes' and Smith's Version 2 Optimum Interpolation SST" data set, termed RSS data set hereafter (Reynolds et al., 2002). RSS combines in situ temperatures measured from ships and buoys with retrievals from Advanced Very High Resolution Radiometers (AVHRR) mounted on different satellites. SST fields are provided monthly and weekly on a 1°×1° grid. The different data sources were merged using an objective analysis method that, in general, works similar to the algorithm introduced in Section 3.2.2. Reynolds and co-authors computed data increments, i.e. differences between an initial background field and the data. These were Gaussian-weighted according to the distance between data and grid points and the variance and co-variance of the initial field and the data increments. In comparison to an earlier version of the optimum interpolation SSTs, RSS relies on an improved algorithm to convert climatological sea ice to SST. Sea ice is used to deduce the SST in the marginal ice zone,

a region that is typically sparsely covered by satellites or ship observations. Furthermore, the data set is corrected for satellite biases. These may result from cloud contamination, instrument errors, and large amounts of atmospheric aerosols.

Mean SST fields derived for summer 1993 and summer 2001 are shown in Figure 5.9. General features include a temperature front that is narrow south of the Grand Banks and widens to the east of the Canadian continental shelf. Krauss et al. (1987) identified the 12°C isotherm as the separation between the NAC and the Labrador Current. East of Flemish Cap isotherms fan out broadly, which is indicative of the course of the NAC. South of 50°N isotherms run almost zonally, while in the northern part of the SPNA they are shifted to the northeast. The Irminger and Labrador Seas are dominated by an inflow of cold water that is imported via the East and West Greenland Currents and exported to the south by the Labrador Current. Differences between the displayed summers exhibit overall warmer temperatures during 2001. The temperature difference exceeds 2°C over the Reykjanes Ridge and 1°C in large areas of the Newfoundland Basin and in the northern Labrador Sea.

5.4.2. Horizontal SST Gradients

The monthly SST fields were used to derive the horizontal SST gradient which is considered as an indicator for the location of the NAC path (Fig. 5.10). The chosen months and years correspond to the time of the particular occupation of the A2-line. For the sake of clarity, values falling below 0.4°C/1° are blanked. The particular snapshots reveal substantial differences in the distribution and magnitude of the SST gradient. As was pointed out in Section 2.2.1, this is expected since the considered region features intense eddy activity (Rossby, 1996; Fratantoni, 2001; Reverdin et al., 2003). One should be careful when interpreting these distributions since they do not reveal a real circulation scheme. Nevertheless, some features are very striking. The entry of the Gulf Stream into the SPNA and its continuation as the NAC are clearly exhibited by SST gradients exceeding 2°C/1°. The NAC carries warm and saline water into an environment that is generally colder and fresher. As a result, opposite gradients are maintained on both sides of the inflowing water masses. Gradients to the northwest indicate the presence of the Labrador Current (Krauss et al., 1987). The Northwest Corner (NWC) is identified by the curvature around an anti-cyclonic eddy feature located to the north of Flemish Cap. It limits the offshore expansion of the southbound Labrador Current. Käse and Krauss (1996) suggested that two different states are likely. (1) The NAC follows the 4000 m isobath, loops into the NWC and head eastwards towards the CGFZ. (2) The loop converts into an anti-cyclonic eddy. As a result, the NAC turns northeastward north of the Flemish Cap without passing into the NWC. Carr and Rossby (2001) analysed the NAC pathway by means of surface drifters and isopycnic floats. They observed that drifters as well as floats were able to enter the NWC or to bypass it. The probability to choose one way or the other was equal.

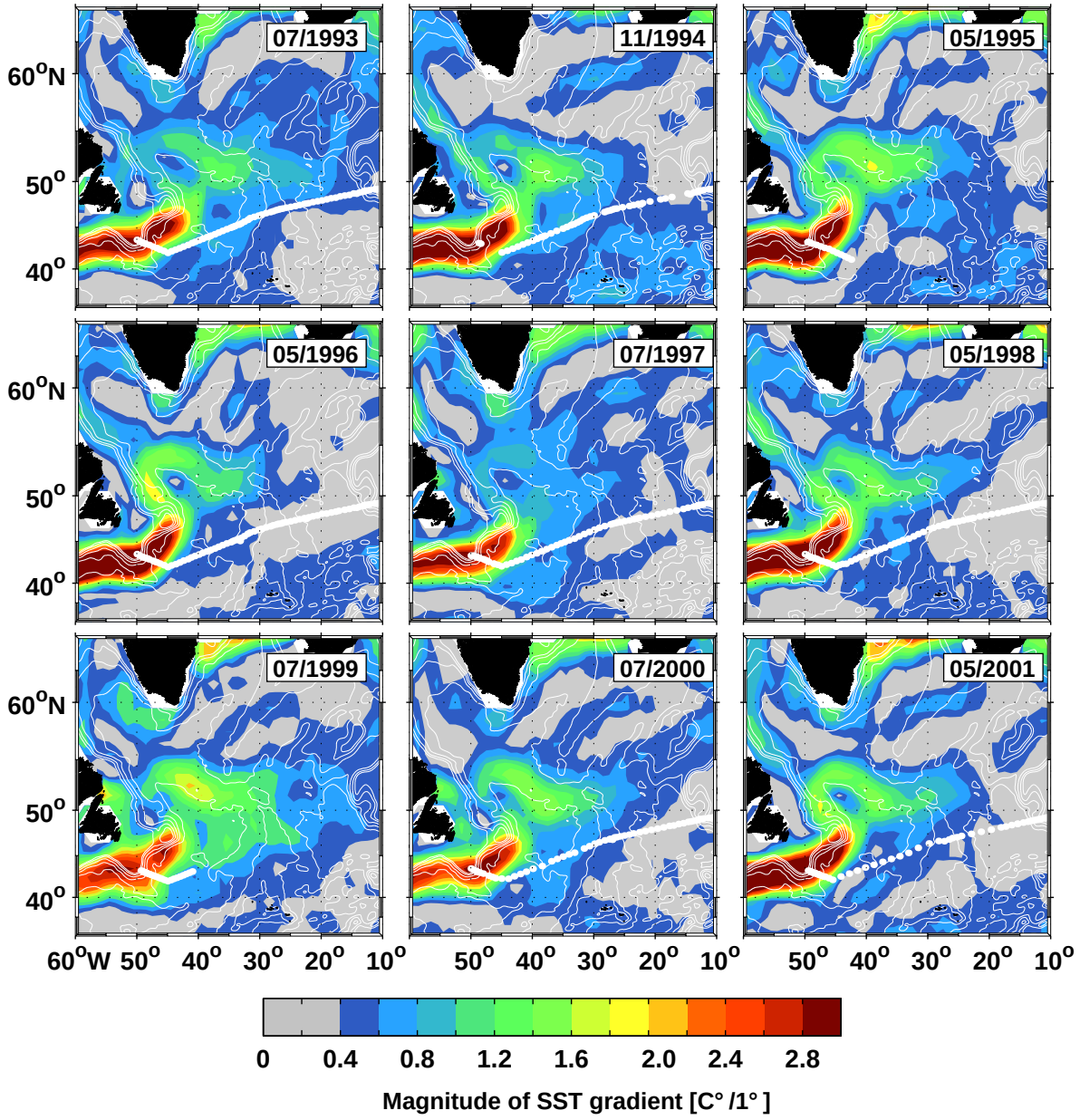

Fig. 5.10.: *Magnitude of SST gradient for particular months and years. The gradient is derived from monthly SST fields, available on a 1°×1° grid (*Reynolds *et al., 2002). Thin white lines show bathymetric contours (every 1000 m and 500 m isobath). White dots indicate the particular occupation of the A2-line.*

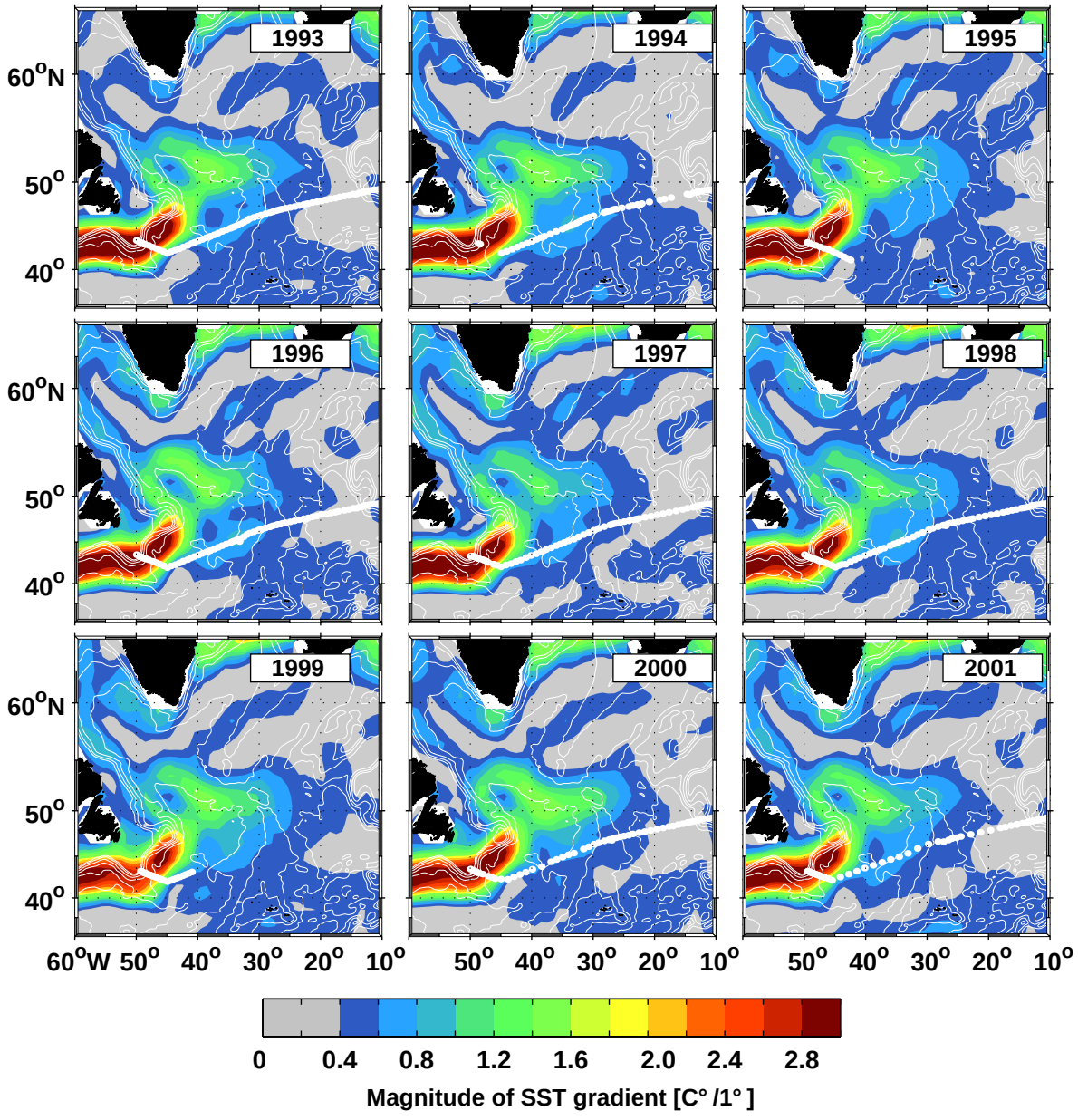

Fig. 5.11.: *Same as Figure 5.10, but shown as annual mean values.*

Following the course of NWC, values of high SST gradient extend more or less zonally towards the fracture zones within the Mid-Atlantic Ridge. This is in generally good agreement with maps of stream functions derived from floats (Bower et al., 2002, Fig. 3.8; Pérez-Brunius et al., 2004). Apart from the boundary currents in the Irminger and Labrador Seas the highest temperature gradients are located to the west of the Mid-Atlantic Ridge.

Carr and Rossby (2001) noticed the appearance of a cyclonic eddy located to the east of Flemish Cap, centered at ∼46°N, 42°W. Some of the SST-gradient snapshots reveal a similar feature in the vicinity of this location. The distributions show similarity to a circulation sketch presented by Käse and Krauss (1996). They suggested the existence of three major high pressure cells which are associated to anti-cyclonic flow. These approximately correspond to the location of the recirculation-like features in the SST gradient distributions. According to Käse and Krauss (1996) flow around these cells is considered as the main gateway for water located on the warmer side of the NAC. Caniaux et al. (2001) calculated the surface current field for winter 1997. They combined sea surface height derived from TOPEX/Poseidon and ERS-2 satellite missions with the dynamic topography provided by Kearns and Rossby (1998). The authors proposed the existence of a recirculation area centered at 40°W and located between 45°N to 49°N. The velocity field indicated an anti-cyclonic flow in the northern part of this area and cyclonic circulation in the southern part.

The Mann eddy, supposed to be centered at 42°N, 44°W, is not very prominent in the SST gradient fields. Carr and Rossby (2001) compared the surface velocity field with corresponding distributions on certain isopycnal surfaces (σ_T = 27.2 kg/m^3 and σ_T =27.5 kg/m^3). They noted that the Mann eddy is more pronounced at depth which might explain the lack of signal in the gradient distributions. At several occasions patches or branches of high SST gradient are present at WOCE-A2 along 40°W-35°W. Among the snapshots the most obvious feature appeared in July 1999. However, the occupation of A2-line ended at 42°W at that time.

Figure 5.11 displays the same fields, now shown as annual mean values. The results confirm the previous findings. On average, three major cells (including the Mann eddy) show up: (1) to the north of Flemish Cap (center of the NWC), (2) to the southeast of Flemish Cap, and (3) the Mann eddy. The latter has a stronger signature in the mean fields compared to the temporal snapshots. Almost all years exhibited an increased SST gradient at about 40°W-35°W. The origin of this feature cannot be explained alone from SST. Using near-surface buoys Krauss (1986) verified of a flow branch that was supposed to detach from the main NAC path at about 43°N to 45°N. Evidence was weak so he considered it as part of broad eastward drift. However, Caniaux et al. (2001) identified such a branch in the current fields they had compiled for winter 1997. At this time it meandered across the location of the A2-line in reversing directions. Käse and Krauss (1996) noted that the off-slope region of the Newfoundland Basin is occupied by quite persistent but non-permanent eddies. These form and decay and thus block or support a branching of the flow. Small-scale features in the interior Newfoundland Basin cannot be detected due to the limited resolution of the SST data set.

The eastern flank of the MAR features much lower values of SST gradient. There are no particular regions that indicate a southward recirculation. The zonal continuation of the NWC that extends into the eastern basin is variable in time and location and not very pronounced to the east of the fracture zones of the MAR.

Several authors have presented stream functions for the Newfoundland Basin that were derived from analyses of isopycnal floats. Bower et al. (2002) and Pérez-Brunius et al. (2004) used essentially the same data that covered the years 1993-1995 and 1997-1999. RAFOS-type floats were ballasted to drift on the isopycnal σ_Θ =27.5 kg/m^3 and acoustically tracked. Bower and co-authors determined the absolute velocity field on this surface, whereas Perez-Brunius et al. calculated the transport of the upper 1000 m. They derived 3-dimensional mean fields of temperature and density from a historical hydrographic data set (Curry, 1996). The resulting baroclinic velocity fields were converted into absolute fields using the velocity directly measured by the floats. Resulting flow fields for the baroclinic and absolute transport differed considerably. The baroclinic field revealed a weak and broad flow heading eastward. It detached from the NAC around Flemish Cap. The absolute transports fields, however, indicated a well-defined narrow band (the 'NAC-pipe') that meandered northward. Any branching was not evident until reaching the NWC. Pérez-Brunius et al. (2004a) calculated the temperature transport that is associated with this NAC pipe. It decreased from almost $0.5{\cdot}10^{15}$W at the southeastern tip of the Grand Banks to $0.3{\cdot}10^{15}$W at Flemish Cap. Most of the heat is supposed to be lost along the pathway. However, the authors stress the importance of lateral exchange by the eddy field. Dutkiewicz et al. (2001) noted a significant mean movement of subpolar water across the entire frontal zone into the subtropical region.

A salinity section heading from Flemish Cap to CGFZ during summer 1997 revealed very fresh intrusions that were carried across the front into the centre of the NWC (Fig. 5.12, 42°W). These intrusions were located below the high salinity cap of the NAC at depths of 450 m, 800 m and 1100-1400 m and thus affected the ULSW and LSW layers. The respective salinities were comparable to the salinity carried in the DWBC. Note that the horizontal extent of these features is exaggerated in Figure 5.12 due to greater station distances off Flemish Cap. To the north of Flemish Cap, Fischer and Schott (2002) noticed that profiling floats were caught in eddies for several months. The authors stressed the influence of an isolated seamount (Orphan Knoll) on the flow fields and suggested that the flow in the LSW branches into different routes. Also Lavender et al. (2000) reported on cross-isobath flow in their respective float data. These observations support the importance of interaction between the DWBC and the NAC around Flemish Cap.

While a lot of studies dealt with the near-surface circulation of the Newfoundland Basin on larger scales, direct observational evidence from the deeper circulation is poor. Mooring arrays as analysed and presented by Schott et al. (2004) were focused on the DWBC region close to the Grand Banks. Data were received from two mooring campaigns of the years 1993-1995 and 1997-1999. Measurement started and ended during the respective summers. The easternmost extension of the mooring line was about 44°W30'. A top-to-bottom mean velocity field was compiled from the two mooring arrays and extrap-

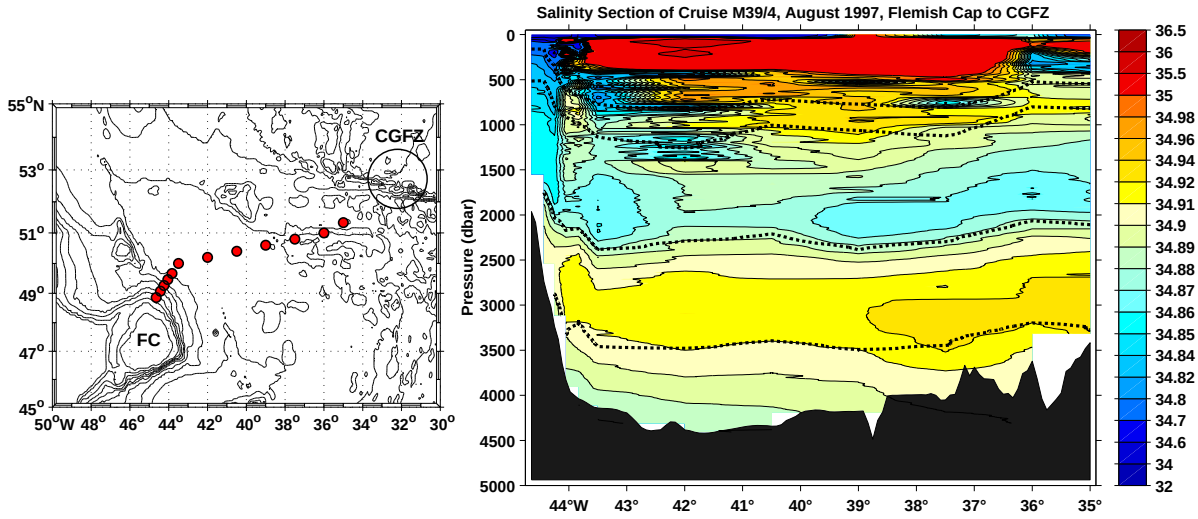

Fig. 5.12.: *Salinity section from August 1997 (cruise M39/4, Tab. 3.1). Dashed lines denote the isopycnals* σ_Θ *= [27.68, 27.74, 27.80, 27.88] kg/m*^{3}*.*

olated from 800 m to the surface using mean geostrophic shears. These were derived from seven hydrographic repeats. The mean velocity structure did not reveal any southward signals off the DWBC. However, time series of the particular current meter measurements indicated a current reversal on the easternmost mooring. Instrument records at 800 m and at the bottom showed a considerable southward flow exhibiting velocities of several cm/s. It started around November 1994 and generally lasted on to March 1995 despite occasional interruptions.

5.4.3. Evidence from numerical ocean models

Getzlaff (2003) analysed the deep water export pathways by means of a numerical ocean model that covered the Atlantic Ocean from 18°S to 70°N. The model is part of the FLAME[I] model hierarchy. It is computed in z-coordinates and run at high-resolution ($\frac{1}{12}^\circ \times \frac{1}{12}^\circ cos(\phi)$, thus eddy-resolving). A climatological surface forcing was implemented with wind stress and surface heat fluxes having been derived from three years of ECMWF data following Barnier et al. (1995). Surface fields for salinity were generated by combining the spatially higher-resolved climatology of Boyer and Levitus (1997) with the temporally better resolved climatology of Levitus and Boyer (1994). Temperature fields were received from flux terms from the ECMWF-climatology and a flux correction, which was determined from the Levitus and Boyer (1994) climatology. Closed boundary conditions were implemented at 70°N and the Strait of Gibraltar, while the southern boundary was left open. The modeled circulations agreed well with available observations, e.g. from Fischer et al. (2004) who depicted strength and structure of the

[I]Family of linked Atlantic model experiments

DWBC and the adjacent recirculation at 53°N. Fields of annual mean model velocities, averaged over 1800-5500 m, revealed a continuous southward flow on the western flank of the MAR. The region adjacent to the Grand Banks was occupied by a striking amount of meso-scale eddies. Cold core rings were detached from the boundary current at about 40°N to 45°N and converted into quasi-stationary eddies can last on for weeks.

Getzlaff (2003) investigated the model behaviour with respect to the deployment of different kinds of synthetic floats. Mean export pathways were verified by deploying 6500 Lagrangian floats in the DWBC region at 53°N (deployment depth below 700 m) and integrating the corresponding trajectories. Lagrangian floats follow the 3-dimensional velocity field. The trajectories of this model experiment are displayed in Figure 5.13a. About 35% of these floats left the SPNA in southward direction and about 15% finally reached the DWBC region at 32°W with an associated transport of 4.4 Sv. The trajectories reveal a distinct and continuous boundary current that follows the course of the Grand Banks in southwestward direction. Several recirculation cells exist on its offshore side. A noticeable flow along the western flank of the MAR becomes evident. It is fed by waters that recirculate to the east of Flemish Cap. While following the course of the MAR, the model floats pass the Altair Seamount in a westward loop. At 37°N they leave the MAR and turn westward into the North American Basin.

5.4.4. Discussion

Getzlaff (2003) did not particularly analyse the surface currents but restricted himself to the deep flow. There is, however, a general similarity between the large-scale spreading of the model floats (Fig. 5.13) and the large-scale distribution of the SST gradient (Fig. 5.11). Both suggest a broad large-scale anti-cyclonic loop from the DWBC to the MAR. Lazier (1994) analysed a mooring array that crossed the NWC in northwestern direction during 1982-83. The moorings on the north side of the NAC revealed a rather barotropic velocity structure throughout the water column.

The model floats then continued to the south along the topography which may thus explain the observed emergence of deep water anomalies in the vicinity of the MAR along the A2-line. However, based on transport analyses Getzlaff found minor importance of the MAR route for the export of subpolar water compared to the DWBC.

The region around Flemish Cap revealed several pathways for model floats to be detached from the DWBC and transported offshore. The cyclonic eddy located to the southeast of Flemish Cap is in accordance with the near-surface observations (Carr and Rossby, 2001). The downstream flow along the course of the Grand Banks is complicated by several recirculations. The trajectories are deflected by the Newfoundland and Milne Seamounts. The observed anomalies in the western Newfoundland Basin might thus represent deep water swept across the A2-line as part of these recirculations. This would be in agreement with the increased spreading times compared to the DWBC (2.5-4 years vs. 1-2 years in the DWBC, cf. Fig. 5.6).

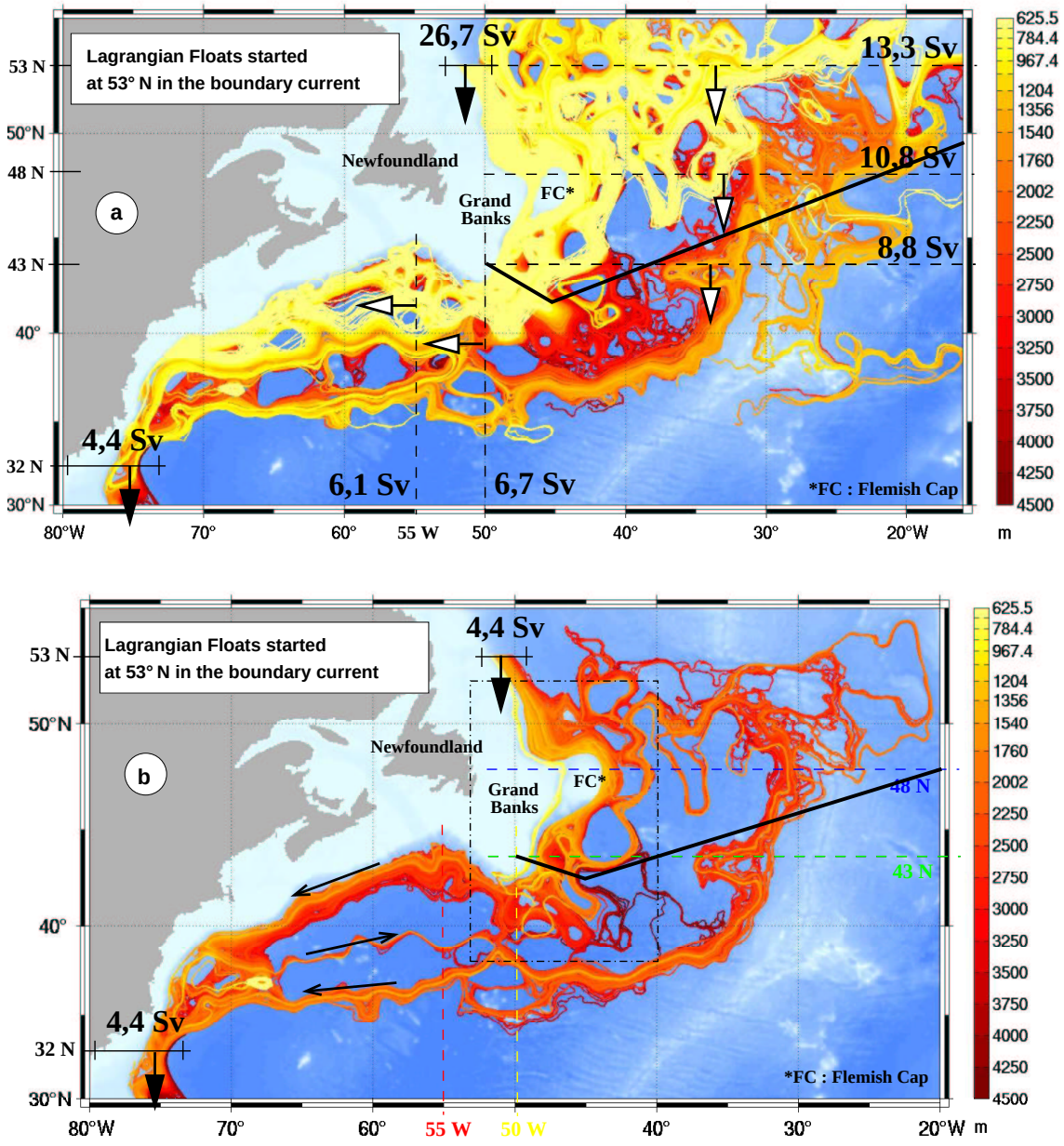

Fig. 5.13.: *Trajectories of synthetic floats in a high-resolution ocean model, adopted from* Getzlaff *(2003). Colours indicate the depth of floats. (a) All deployed floats with associated transport across particular sections. (b) Only those floats are displayed that ended in the DWBC at 32° N. The deployment region is 53° N, deployment depths were below 700 m. Black line indicate the approximate location of the A2-line.*

The model also revealed float trajectories that crossed the A2-line to the west of 40°W. The observed water mass signals at this location might similarly be explained by recirculating flow detached from the boundary current.

The estimated LSW spreading time of 5-6 years at about 37°W is difficult to interpret. The model does not reveal a significant mid-basin flow. From about 45°W to 30°W the A2-line follows a northeast course (cf. Fig. 5.1). Any signal that is transported along the MAR is expected to emerge earlier in the eastern part of the Newfoundland Basin than further to the west. Assuming that LSW needs about three years to propagate from about 33°W to 37°W appears unreasonably high. The large spreading times might thus be the result of a complicated local flow field with no preferred spreading direction but occasional intrusions from the western side.

Fischer and Schott (2002) and Schott et al. (2004) analysed trajectories of floats released at 1500 dbar in the southern Labrador Sea. Due to their profiling nature none of the floats was able to leave the subpolar gyre via the DWBC route since they did not remain within this flow all the time. Two profiling floats deployed in 2001 managed, however, to follow the MAR in southward direction (Schott et al., 2004). As was mentioned earlier this movement is not truly Lagrangian but at least gives support to the offshore spreading of LSW.

5.5. Decadal variability in the DWBC

The analyses of historical data from the Labrador Sea revealed significant variability in the formation and composition of ULSW and classical LSW (Talley and McCartney, 1982; Lazier, 1988; Sy et al., 1997; Curry et al., 1998; Dickson et al., 2002; Chapt. 4). Investigations by Stramma et al. (2004) and results from the present chapter pointed to a spreading of water mass anomalies within the DWBC into the Newfoundland Basin. This is the region where deep water leaves the subpolar gyre. Curry et al. (1998) could link temperature changes observed at Bermuda to decadal variability in the LSW layer thickness in the source region. The estimated signal spreading time yielded about six years. Molinari et al. (1998) analysed LSW time series of salinity, temperature and CFC at 26.5°N. They were able to relate occurring changes to anomalies having been imprinted on the LSW ten years before in the Labrador Sea. Another study by Stramma and Rhein (2001) evidenced the arrival of corresponding salinity and temperature anomalies in the equatorial Atlantic (44°W) 13 to 17 years after formation. Steinfeldt and Rhein (2004) speculated on the arrival of LSW at 2°S about 25 years after generation.

Knowledge is needed to what extent water mass variability on interannual and longer time scales is related to variability of the THC. The strength of the THC does change when its components are subject to variability in flow strength and/or volume. The DWBC transport time series presented by Schott et al. (2004) for the Grand Banks regions revealed significant changes in the strength of the deep water flow. This was calculated for densities greater $\sigma_\Theta = 27.74$ kg/m^3. However, the authors attributed vari-

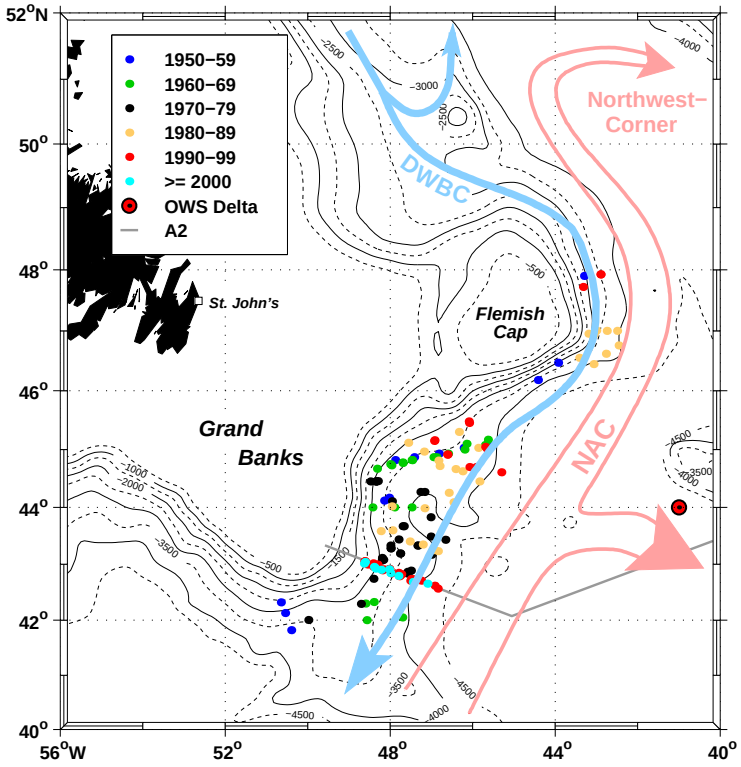

Fig. 5.14.: *Location of selected hydrographic profiles in the boundary current region, close to the southwestern exit of the subpolar gyre. These profiles are taken to reconstruct time series of layer thickness for ULSW and classical LSW. The underlying flow scheme is adopted from* Schott *et al. (2004).*

ability in the deep water transport to local dynamics (variability in the NAC) rather than to remote processes (variability in the deep water sources). The respective DWBC transport time series were calculated in fixed sub-areas rather than between isopycnal surfaces. The upper flow was separated from the deep flow by the mean location of the $\sigma_\Theta = 27.74$ kg/m^3 isopycnal. The eastward extension of these subareas was fixed by the mean location of the zero isotach. The effect of e.g. LSW layer thickness changes throughout the mooring period was thus not addressed. The design of the mooring array did otherwise not allow to resolve the evolution of the density field, neither in time, nor in space.

Similar to the central Labrador Sea, decadal time series of ULSW/LSW layer thickness have been derived for the DWBC region off the Grand Banks. The locations of bottle/CTD profiles together with the major circulation pathways according to Schott et al. (2004) are given in Fig. 5.14. Data sources are the same as for the Labrador Sea time series. Several profiles located upstream and downstream of the A2-line were included to improve the temporal resolution of the time series. All selected stations had to meet two criteria: first, to have deepest sampling levels of at least 2400 dbar and second, to lie onshore of the 4000 m-isobath. Some few stations chosen to improve statistics and/or time series resolution, however, are located at water depths of 4000-4500 m. ULSW

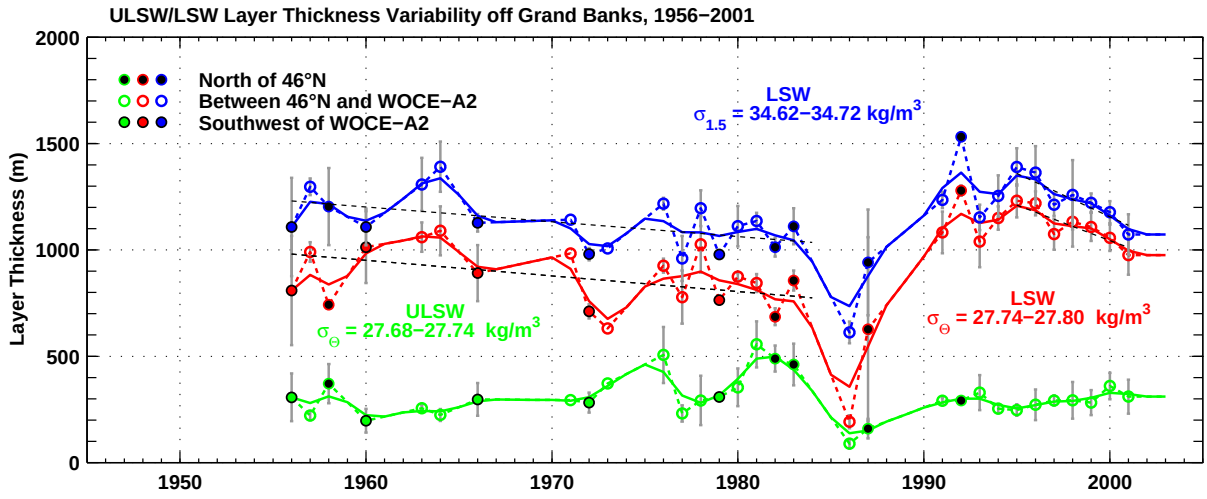

Fig. 5.15.: *Layer thickness evolution of ULSW (green) and LSW (red/blue) off the Grand Banks. The position of the considered hydrographic stations is shown in Fig. 5.14. Solid lines indicate 3-year-smoothed values, while circles and grey bars represent the particular mean estimates with the associated standard deviation. Red and blue lines illustrate the LSW evolution, based on two different density-based water mass definitions. Black dashed lines indicate a trend that is calculated for selected periods.*

and LSW follow the continental slope at shallower depths (cf. Fig. 5.2). The chosen depth-criterion is to reassure that both layers are fully resolved which is complicated due the inclination of the continental slope. The second condition is applied to reduce the influence of the NAC as much as possible. Stramma et al. (2004) noted that in 1994 to 2001 the strongest gradients of LSW salinity and layer thickness emerged at 48°W-47°W. This corresponds to water depths of about 3500 m to 4400 m.

Unlike in the central Labrador Sea, the resolution of a resulting time series has not been restricted by considering only those hydrographic profiles that were sampled during summer months. Mixed layer estimates from a seasonal climatology (Monterey and Levitus, 1997) (cf. Fig. 3.14) revealed that the deepest mixed layer depths develop in the Labrador and Irminger Sea (> 900 m) during late winter. Off the Grand Banks, shallow mixed layer depths of only 100-200 m are prominent during March. The density field at 900 m (Fig. 3.14b) indicated that water masses like ULSW and LSW are not ventilated in this region. Following Curry and McCartney (2001), seasonal heating is likely to be confined to the surface layers, i.e. the upper 200 dbar. Schott et al. (2004) investigated seasonal effects by means of the two mooring arrays. All current meters were equipped with temperature sensors, the uppermost instruments being located at depths of 330-500 m. The authors concluded that seasonal variability can be neglected at depths below 500 m. The seasonal displacement of isotherms did not show any considerable effect below this depth. The seasonal signal of current variability was also found small and only explained less than 10 % of the variance.

Schott et al. (2004) noted that the vertical displacement of the isopycnals, esti-

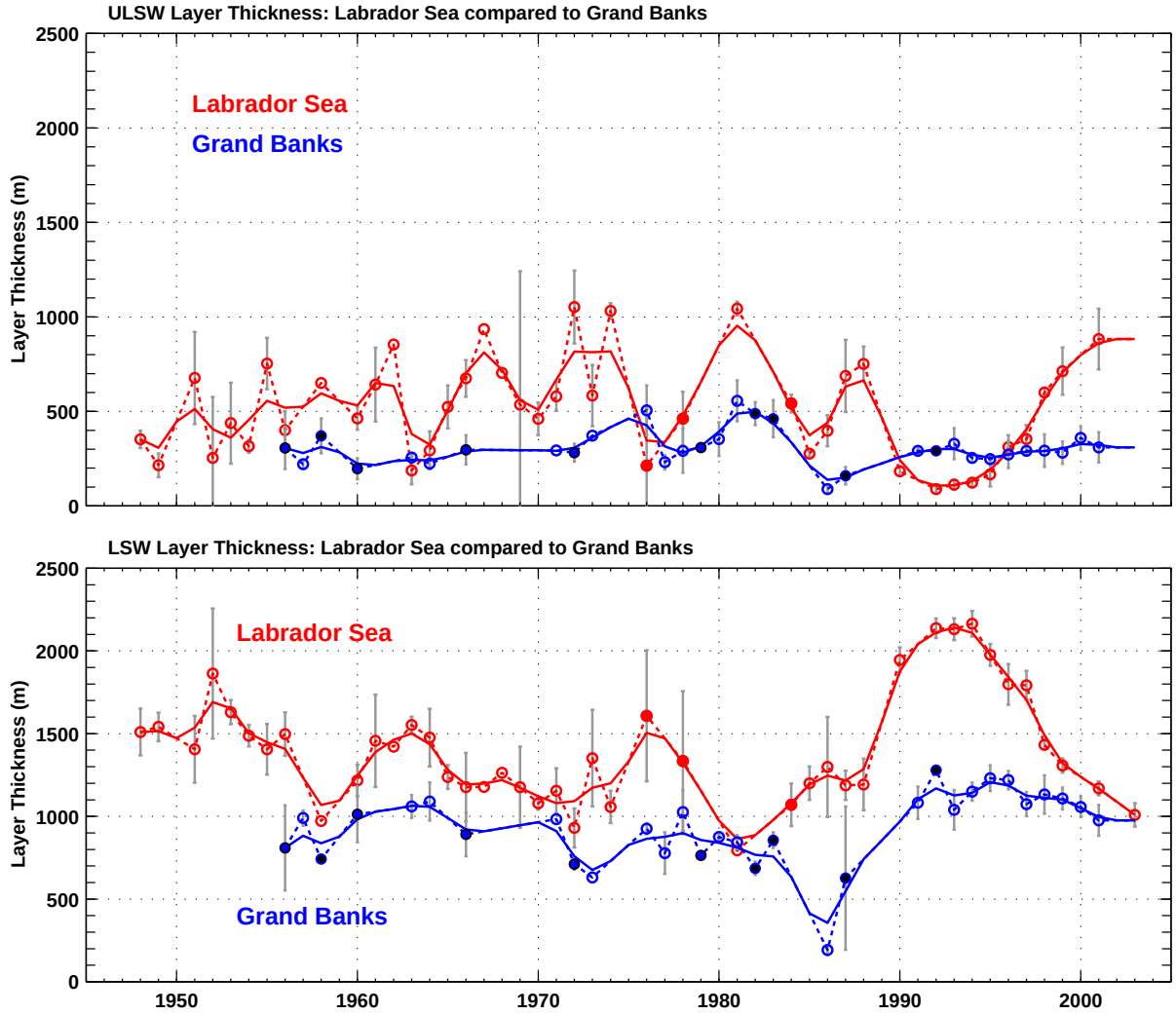

Fig. 5.16.: *Comparison of layer thickness evolution in the central Labrador Sea (red) and off the Grand Banks (blue). Top: ULSW, bottom: LSW. Time series are the same as shown in Figure 4.9 and Figure 5.15.*

mated from seven different hydrographic sections along A2, is of the order ±100 m. This is obvious in Figures 5.3 and 5.4. During May 2001, for example, the upper limit of ULSW was shallowest at about 420 dbar (Fig. 5.2).

The procedure to reconstruct mean values was presented in Section 4. Figure 5.15 illustrates the resulting time series of ULSW and LSW layer thickness, generated from profiles in the western Newfoundland Basin. A time series is included using the LSW definition of Curry et al. (1998). The curves for both water masses exhibit significant variability on decadal time scales. It is stronger pronounced in the classical LSW. The two respective LSW curves show an offset but equal tendencies. From the mid 1950s to the early 1980s LSW featured a trend towards lower thickness. During this period the thickness decreased by 200 m. A similar trend was not observed in the overlying ULSW. From 1956 to 1972 it was rather unchanged with mean thicknesses of 300 m. From the

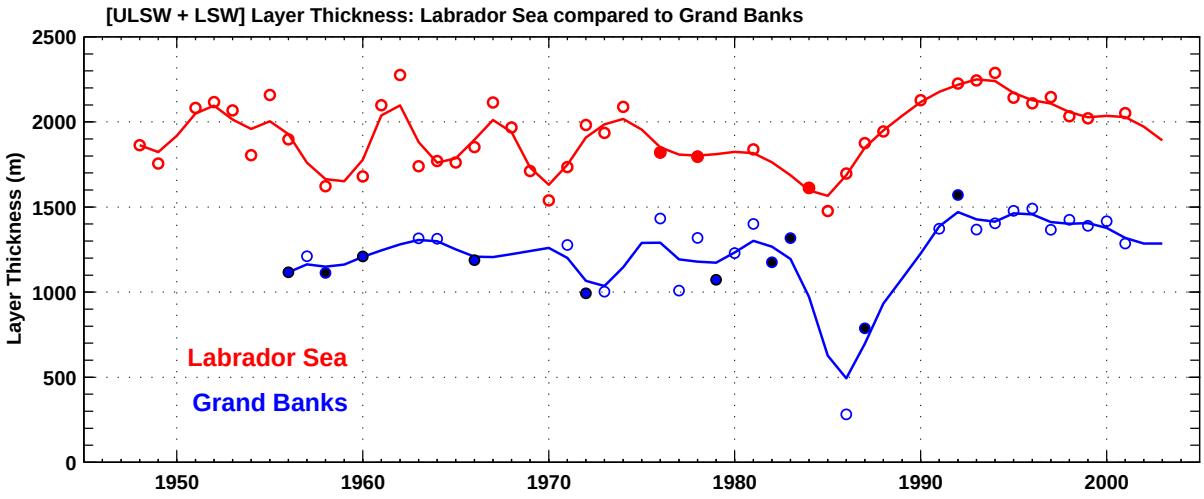

Fig. 5.17.: *Comparison of layer thickness sum (ULSW + LSW). Red: central Labrador Sea, blue: off the Grand Banks. Markers denote individual estimates while solid lines represent 3-year-smoothed values.*

mid 1970s to the mid 1980s the ULSW record revealed the greatest changes observed throughout the complete period. Several thickness estimates were derived from remote profiles. Nevertheless, they are in line with observations at A2. In 1986 both water masses were subject to a significant drop to extremely low thicknesses. Remote profiles from the following year revealed a thicker LSW again, while ULSW remained extraordinary thin.

The records display data gaps for the late 1980s. The early 1990s revealed a very thick LSW. This reflects the intensified formation in the source region at that time. ULSW featured values that are generally comparable to the 1950s to 1960s. From 1995 to 2000 there is a slight increasing trend. The latter year marks a maximum which is, however, lower compared to maxima of 1976 and 1981-83.

Figure 5.16 compares the Grand Banks with respective curves from the central Labrador Sea. Both water masses exhibit variability in the southern area that strikingly resembles changes having occurred some time before in the source region. This is evident despite the coarser resolution of the Grand Banks time series. The reconstructed LSW curve is significantly correlated to the one generated from central Labrador Sea profiles. The correlation is best assuming a time lag of two years for the Newfoundland Basin (correlation coefficient: $r = 0.72$). A correlation of the respective ULSW time series is greatest with a lag of one year but worse compared to LSW (correlation coefficient: $r = 0.51$).

Figure 5.17 presents the sum of the ULSW and the LSW layer thickness, calculated for both regions. These curves feature the best correlation with a lag of 2-3 years for the Newfoundland Basin (correlation coefficient: $r = 0.73$-0.77). This is despite the irregular spacing of profiles contributing to the Newfoundland Basin estimates. The variability in the formation of both water masses can therefore definitely be tracked southward into the Newfoundland Basin.

5.6. Summary and Conclusion

There is evidence in all deep water components that point to a significant spreading offshore. Regions around 43°W, 37°W-36°W, and 30°W turned out to be of particular importance for spreading in the western basin of the SPNA. Areas at 26°W-23°W are meaningful for spreading of ULSW and LSW along the flank of the MAR.

The bottom topography in the Newfoundland Basin exhibits seamounts like Peak Milne and the Newfoundland Seamounts. These limit and deflect the spreading of deep water anomalies. LSW spreading times are in the order of 1-2 to 5-6 years for the Newfoundland Basin. The faster times correspond to flow in the fast track, the DWBC. The greater times refer to spreading in the interior basin and the western flank of the MAR. With respect to the export of deep water the DWBC is the far more important gateway to the south.

The dynamics in the pathway of the NAC was assumed to affect the deep water flow. Gradients of the SST revealed general features that are in agreement with results from a high-resolution ocean model (Getzlaff, 2003). Deep water is supposed to leave the DWBC region via recirculation cells and eddy exchange with the NAC.

Time series reconstruction indicated considerable variability in the layer thicknesses of ULSW and LSW. These could be correlated to changes in the source region, i.e. the central Labrador Sea. Analyses of moored current meters revealed that the local dynamics of the DWBC-NAC system provide the dominant source of observed variability in the deep water transports (Schott et al., 2004). The decadal time series suggest that remotely caused variability in the upper deep water is still observable at the Grand Banks.

6. Summary and Outlook

The present study focused on large-scale spreading and formation of Upper Labrador Sea Water (ULSW) and classical Labrador Sea Water (LSW). Both water masses are convectively formed in the Labrador Sea during winter (Lazier, 1973; Clarke and Gascard, 1983; Pickart et al., 1996, 1997; The Lab Sea Group, 1998). The major formation region of ULSW was supposed to be the Labrador Current/Deep Western Boundary Current region of the Labrador Sea (Pickart et al., 1996, 1997), whereas several studies revealed the highly-variable nature of LSW formation in the western part of the central Labrador Sea (e.g., Lazier, Talley and McCartney, 1982; Sy et al., 1997; Curry et al., 1998).

Azetsu-Scott et al. (2003) and Stramma et al. (2004) reported on a recent switch to ventilation of a lighter variant of LSW in the central Labrador Sea. This was termed ULSW by Stramma et al. (2004). The estimation of corresponding formation rates of this water mass was one of the aims of the present study. For this reason, hydrographic and chlorofluorocarbon (CFC) data have been used to highlight the formation of ULSW on interannual to decadal time scales. This was compared to variability in the formation of the denser classical LSW.

Several studies inferred water mass formation rates solely based on sea surface fluxes (e.g., Speer and Tziperman, 1992; Speer et al., 1995; Marsh, 2000). Smethie and Fine (2001) and Rhein et al. (2002), however, derived water mass formation rates of ULSW and classical LSW based on tracer inventories. This method benefits from the well-known atmospheric history of CFCs and the fact that CFCs enter the deep ocean in only a few regions of the world. Smethie and Fine (2001) analysed the formation of ULSW and LSW using tracer data from the late 1980s/early 1990s. They traced ULSW spreading into the subtropical/tropical North Atlantic and gave mean annual formation rates of 2.2 Sv. The source region was however excluded in their analyses. Rhein et al. (2002) investigated the spreading of the denser classical LSW in the subpolar North Atlantic during 1997 and inferred mean annual LSW formation rates representative for the period 1970-1997 (4.4-5.6 Sv).

The inventory method has been used in the present study to reveal changes in the ULSW and LSW formation after 1997. For this purpose, a large-scale hydrographic/tracer data set covering the years 1997, 1999, and 2001 has been analysed (Chapter 3). The major findings are summarised as follows:

At the end of the 1990s the large-scale distributions of water mass properties showed a spreading of ULSW that is similar to the denser classical LSW. Different to what was found for ULSW formed in the early 1990s, the recently ventilated ULSW was not confined to the Deep Western Boundary Current (DWBC) region. It rather spread throughout

the subpolar North Atlantic on shallower but similar pathways as LSW and also reached the eastern basins of the subpolar North Atlantic. This is consistent with results by Lavender et al. (2000) who showed that floats at 700 m originating from the Labrador Sea escaped into the eastern North Atlantic.

Due to the coarser data resolution in 1999 and 2001 compared to 1997, different methods have been applied to estimate the inventories of both water masses in the SPNA. They gave similar results of the CFC-11 inventory within 5-11 %. From 1997 to 2001, CFC-11 inventories of ULSW revealed a striking increase (6.0 $\pm$ 0.6 to 9.3 $\pm$ 0.6 million moles). The dominant change was a considerable thickening of the ULSW layer especially in the Labrador Sea, accompanied by a spreading of high CFC-11 concentrations from the northern and central Labrador Sea into the Newfoundland Basin and the Irminger Sea. The greater change occurred from 1997 to 1999 rather than from 1999 to 2001. Corresponding LSW inventories reduced over the same period and indicated a flushing of the large LSW reservoir out of the central Labrador Sea.

For the years 1997-1999 ULSW formation rates derived from the CFC-11 inventories yielded 6.9-9.2 Sv. At least in winters 1998-1999 ULSW could not be formed solely in the Labrador Sea. The most likely region for additional formation of ULSW appeared to be the Irminger Sea. Nevertheless, the northern and central Labrador Sea remained the most important sites for ULSW formation. The subsequent two years (2000-2001) indicated a decrease of ULSW formation to 3.7-4.0 Sv. Significant LSW production over the four-year period was not observed. The mean combined formation rate of ULSW and LSW prior to 1997 was 8.4–8.9 Sv. In 1998-99, the high ULSW formation rate almost compensated the lack of LSW formation. In 2000-2001, however, the combined ULSW/LSW formation rate decreased to 3.7–4.0 Sv.

The analyses of Chapter 4 revealed significant changes of ULSW and LSW in the central Labrador Sea. The reconstruction of time series for both ULSW and classical LSW indicates that ULSW formation in the central Labrador Sea is a common process throughout the decades. The temporal evolution of ULSW and LSW layer thicknesses is out of phase and significantly correlated (r = -0.85). There is a weak correlation to the sea surface forcing, but variability at the surface cannot fully explain the observed variability in the ULSW and LSW properties. As was noted by Lazier et al. (2002) the Labrador Sea reacts on longer time scales than one winter to surface related process. Considerable warm and saline intrusion from the West Greenland Current into the central Labrador Sea influence the stratification of the water column and together with the surface forcing are important for setting the strength of deep convection.

Two different mechanisms have been suggested for ULSW ventilation: (1) Formation in the Labrador Current/DWBC as suggested by Pickart et al. (1996, 1997). This can coincide with times of intense deep convection in the central Labrador Sea as was found by the authors. (2) Formation in the central Labrador Sea in the absence of intense deep convection. As a result of weak forcing and/or strong stratification convection is rather limited to the upper 1000 m. Locally formed ULSW is the lighter substitute of the denser classical LSW and spreads on similar pathways.

The spreading of deep water components has been further investigated in the interior

Newfoundland Basin (Chapter 5). The analyses benefitted from many annually repeated sections carried out within the *World Ocean Circulation Experiment* along the A2-line at about 43°N. The purpose was to reveal water mass spreading pathways that are additional to propagation in the DWBC.

There is evidence in all deep water components that points to a significant offshore spreading. Pathways are constrained by submarine features like the Milne Seamount which is located in the centre of the Newfoundland Basin. An estimation of LSW spreading times pointed to a fast propagation of water mass signals from the Labrador Sea to 43°N within the DWBC (1-2 years). This was already noticed by Sy et al. (1997) and Stramma et al. (2004) but confirmed based on decadal time series. A slower LSW spreading (4-6 years) was found along different pathways within the interior Newfoundland Basin. Spreading of LSW along the western flank of the Mid-Atlantic Ridge takes about 3 years to reach the A2-line.

Gradients of sea surface temperatures served as an indicator for the pathway of the North Atlantic Current. Variability in this pathway and in the dynamics was assumed to be responsible for offshore deep water spreading. Large-scale surface patterns are in general agreement with model results presented by Getzlaff (2003). He analysed the Lagrangian spreading of synthetic floats implemented in a high-resolution numerical ocean model and successfully detected a weak but significant deep water propagation along the western flank of the Mid-Atlantic Ridge.

Also for the DWBC region in the Newfoundland Basin decadal time series of ULSW and LSW layer thickness have been reconstructed. They reveal substantial variability that can be correlated to water mass changes happening in the Labrador Sea.

At present, it is not clear whether the considerable decrease of the combined ULSW/LSW formation, rate found in 2000-2001, has an impact on the deep water export into the subtropical Atlantic. Deep water transport time series derived from a mooring array at 43°N (1997-1999) indicated a slight decreasing trend of 1.7 Sv/yr (Schott et al., 2004). The CFC-inventory method has proven to be a valuable tool for detecting variability in the ventilation of ULSW and classical LSW of the recent years. Longer time series from moorings as well as tracer measurements are needed to reveal, if this is already an imprint of the cessation of LSW and as such an indication for a weakening thermohaline circulation.

A. Appendix

A.1. Abbreviations & Acronyms

AABW	Antarctic Bottom Water	**LDW**	Lower Deep Water
ACSYS	Arctic Climate System Study	**LSW**	Labrador Sea Water
ADCP	Acoustic Doppler Current Profiler	**MAR**	Mid-Atlantic Ridge
AIMS	Analysis, Interpretation, Modelling and Synthesis	**MOC**	meridional overturning circulation
AIW	Arctic Intermediate Water	**MW**	Mediterranean Water
ARGO	broad-scale global array of temperature/salinity profiling floats	**NAC**	North Atlantic Current
ASOF	Arctic - Subarctic Ocean Fluxes	**NADW**	North Atlantic Deep Water
AVHRR	Advanced Very High Resolution Radiometer	**NANSEN**	North Atlantic and Norwegian Sea Exchange
BIO	Bedford Institute of Oceanography, Dartmouth, Canada	**NAO**	North Atlantic Oscillation
CLIVAR	Climate Variability and Predictability	**NEAW**	North East Atlantic Water
CFC	chlorofluorocarbon	**NODC**	National Oceanographic Data Centre
CGFZ	Charlie-Gibbs Fracture Zone	**NSDW**	Norwegian Sea Deep Water
CME	Community Modelling Effort	**NWC**	Northwest Corner
CTD	Conductivity Temperature Depth	**OWS**	Ocean Weather Station
DMW	Deep Mediterranean Water	**PI**	Principal Investigator
DSOW	Denmark Strait Overflow Water	**RRS**	SST data set after Reynolds et al. (2002)
DWBC	Deep Western Boundary Current	**SENR**	Southeast Newfoundland Rise
EGC	East Greenland Current	**SFB**	Sonderforschungsbereich
EKE	eddy kinetic energy	**SIO**	Scripps Institution of Oceanography
ESOP	European Subpolar Ocean Programme	**SOC**	Southampton Oceanography Centre
ETOPO5	Earth Topography Five Minute Bathymetry data set	**SPF**	Subpolar Front
GEOSECS	Geochemical Oceans Sections Study	**SPMW**	Subpolar Mode Water
GFZW	Gibbs Fracture Zone Water	**SST**	Sea Surface Temperature
GSA	Great Salinity Anomaly	**SPNA**	Subpolar North Atlantic
IfMH	Institut für Meereskunde, Hamburg	**Sv**	Sverdrup (1 Sv = 10^6 m^3/sec)
IfMK	Institut für Meereskunde, Kiel	**THC**	thermohaline circulation
ISOW	Iceland Scotland Overflow Water	**TTO**	Transient Tracers in the Ocean
ISW	Irminger Sea Water	**uAIW**	upper Arctic Intermediate Water
IUP	Institut für Umweltphysik, Bremen	**UGot**	University of Gothenburg
LADCP	lowered Acoustic Doppler Current Profiler	**ULSW**	Upper Labrador Sea Water
lAIW	lower Arctic Intermediate Water	**VEINS**	Variability of Exchanges in the Northern Seas
LC	Labrador Current	**WGC**	West Greenland Current
LDEO	Lamont-Doherty Earth Observatory	**WHPO**	WOCE Hydrographic Program Office
		WOCE	World Ocean Circulation Experiment

A.2. Background Information on Chlorofluorocarbons

During the late 1800s and early 1900s, toxic gases like ammonia (NH_3) and methyl chloride (CH_3Cl_2) were widely used as coolants in the early refrigerators. Recurring accidental leakages, however, led to an increased search for less toxic substitutes. In 1928, chlorofluorocarbons (CFCs) were successfully synthesised for the first time (Elkins 1999) and became the preferred refrigerant since then. Up to now several components exist. The ones used in the present study comprise CFC-11 (CCl_3F) and CFC-12 (CCl_2F_2). Both are anthropogenic, non-toxic, non-flammable compounds and chemically inert (concerning the ocean and the lower atmosphere). After World War II, they were used among others to manufacture blowing agents for foams, aerosol sprays, packing materials and as propellants, solvents, and refrigerants. Since then, the production of CFCs has significantly increased, leading to an enhanced release to the atmosphere (Fig. A.1). The production and release of CFCs have mainly occured in the northern hemisphere, but the chemical stability of CFCs and rapid mixing rates of the lower atmosphere have resulted in a quite uniform distribution of CFCs over the troposphere.

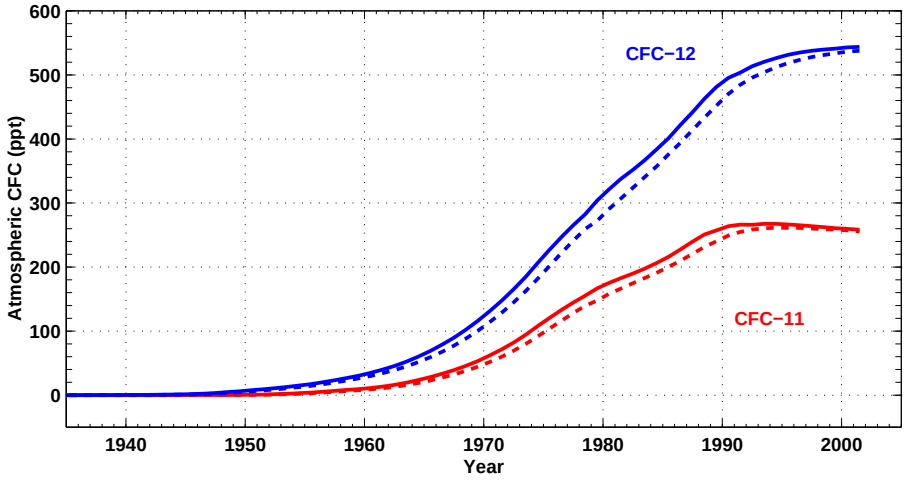

Fig. A.1.: *Atmospheric history of CFC-11 and CFC-12 given in ppt. Solid lines indicate northern hemisphere estimates while dashed lines denote measurements from the southern hemisphere. Data according to* Walker *et al. (2000).*

Investigations of the early 1970s have indicated that CFCs are an important source of inorganic chlorine in the stratosphere that actively decomposes ozone through catalytic reactions. As a consequence, the stratosphere is more permeable for harmful UV-B radiation (Molina and Rowland, 1974). The occurrence of the Antarctic ozone hole is one of the most prominent and inglorious aftereffects (Farman et al., 1985). Since the early 1990s, the atmospheric accumulation of CFC-11 has decreased, while CFC-12 still

increases at a reduced rate. This is a direct response to the *Montreal Protocol*, a global environmental treaty signed by 27 nations in 1987. It aims at reducing substances that deplete the stratospheric ozone layer.

Since their release to the atmosphere, CFCs have continuously entered the ocean via air-sea gas exchange mechanisms. If surface waters are in contact to the atmosphere long enough, they build up an equilibrium concentration which is dependent on the solubility (a function of temperature and salinity) of the corresponding atmospheric CFC component (Warner and Weiss, 1985). Biological interactions are negligible. After they have dissolved at the sea surface, CFCs are transferred to deeper layers by subduction and convection processes. The horizontal distribution is driven by mixing and interior ocean currents. The relatively well-known solubility and atmospheric histories of CFCs make them an ideal tracer for the ocean circulation on interannual to interdecadal timescales. Furthermore, several ocean circulation model studies exist that use CFCs as water mass tracers to investigate oceanic ventilation processes and validate model results in comparison to observations (for a review, see England and Maier-Reimer, 2001).

Technical Aspects

CFCs are analysed by means of gas-chromatography. In Germany, sea-going measurement equipment exists since 1987 at the *Institut für Umweltphysik* (IUP), University of Bremen and since 1989 at the *Leibniz-Institut für Meereswissenschaften IFM-GEOMAR* in Kiel (the former *Institut für Meereskunde Kiel*, IFM Kiel). Both measurement systems are set up following Bullister and Weiss (1988). The 'Bremen system' has undergone some changes and improvements concerning the unattended automation of sample analysis and the analysis of additional trace gases (Bulsiewicz et al., 1998).

To estimate the CFC concentration of seawater, water samples are collected by means of precleaned 10 litre Niskin bottles. These are attached to a CTD/rosette system. Afterwards, water is taken in amounts of about 20 ml using different sampling containers (glass syringes in case of 'Kiel system' and glass ampoules in case of 'Bremen system'). Both are flushed several times to avoid air bubbles within the water samples which would otherwise falsify the results. A carrier gas (nitrogen cleaned by molsieves) transfers samples to a purge and trap gas-chromatographic unit. Magnesiumperchlorate inserted into this unit acts as drying agent. The separation of the dissolved gases is performed using either a packed column filled with *Porasil C* ('Kiel system') or a capillary column ('Bremen system'). The use of the latter allows the analysis of two additional components (CFC-113 and CCl_4). The subsequent detection is done with an Electron Capture Detector (ECD). ECD-signals are calibrated and converted into CFC concentration by means of a known gas standard. The temporal drift of the ECD is corrected through the application of calibration curves that are derived for different gas volumes. These curves are taken before and after each station. Temporal changes between two calibrations are assumed to be linear in time.

The calculated CFC concentrations can be falsified by occurring contamination of water samples. CFCs are lipophilic, thus the contact of water samples with grease and oil has to be avoided. Some years ago, several air conditioning systems installed on research vessels were run using CFC-12 as a refrigerant. Leakages in these systems resulted in a severe contamination of the air present in the laboratory (e.g. PLÄHN, 1999). To detect such possible contaminations, additional air samples are taken in the laboratory and at several outside positions on the vessel. These are compared to existing atmospheric measurements. The precision of the measurements is checked by analysing about 10 % of the samples twice. Table A.2 summarises information on the quality of CFC measurements carried out during the German cruises to the subpolar North Atlantic.

Cruise	Precision of CFC-11 [%]	Precision of CFC-12 [%]	Standard	Peculiarities
M30/2	0.8	0.7	BREMEN 1992	—
M30/3	1.1	1.2	ALM-83959	—
V161	0.6	0.9	ALM-0383034	CFC-12 questionable for profiles different from profiles 30-37
M39/2	0.7	0.8	ALM-0383034	disturbance of CFC-12 peak at several stations
M39/3	0.47	0.39		—
M39/4	0.7	1.2	ALM-0383034	CFC-12 questionable due to an unknown substance with similar retention times
M39/5	0.8	0.8	ALM-0383034	CFC-12 questionable at stations 470-483 due to an unknown substance with similar retention times
V172	0.6	0.8	ALM-0383034	CFC-12 questionable at profiles 14-21 due to an unknown substance with similar retention times
M45/2	0.9	0.9	ALM-066676	—
M45/3	0.7	0.7	ALM-066676	—
M45/4	0.53	0.45	ALM-066676	—
M50/1	0.6	0.8	CC-76511	anomalous high CFC-11/CFC-12 ratio: CFC-11 reduced by 1 %
M50/2	0.52	0.54	CC-76511	anomalous high CFC-11/CFC-12 ratio: CFC-11 reduced by 5 %
M50/3	0.40	0.28	CC-76511	
M50/4	0.40	0.31	CC-76511	

Tab. A.2.: *Precision of German CFC measurements carried out during supolar North Atlantic cruises (1994-2001). Samples were analysed by either using the CFC system built at IUP Bremen or the CFC system built at IfM-GEOMAR Kiel. Corresponding PI's are listed in Tab. 3.1.*

Bibliography

Argo Science Team (1998). On the design and implementation of Argo. An initial plan for a global array of profiling floats. Technical Report, ICPO Report No. 21, GODAE Report No. 5, Bureau of Meteorology, Melbourne, Australia, 32 pp.

Arhan, Michel (1990). The North Atlantic Current and Subarctic Intermediate Water. *J. Mar. Res.*, 48(1):109–144.

Azetsu-Scott, Kumiko, E. Peter Jones, Igor Yashayaev, and Robert M. Gershey (2003). Time series study of CFC concentrations in the Labrador Sea during deep and shallow convection regimes (1991-2000). *J. Geophys. Res.*, 108(C11):3354, doi:10.1029/2002JC001317.

Bacon, Sheldon (1997). Circulation and fluxes in the North Atlantic between Greenland and Ireland. *J. Phys. Oceanogr.*, 27(7):1421–1435.

Bacon, Sheldon (1998). Decadal variability in the outflow from the Nordic Seas to the deep Atlantic Ocean. *Nature*, 394:871–874.

Bacon, Sheldon, W. John Gould, and Yanli Jia (2003). Open-ocean convection in the Irminger Sea. *Geophys. Res. Letters*, 30(5):1246, doi:10.1029/2002GL016271.

Barnier, Bernard, Laure Siefridt, and Patrick Marchesiello (1995). Thermal forcing for a global ocean circulation model using a three–year climatology of ECMWF analyses. *J. Mar. Systems*, 6:363–380.

Beismann, Jens-Olaf and Bernard Barnier (2004). Variability of the meridional overturning circulation of the North Atlantic: Sensitivity to overflows of dense water masses. *Ocean Dynamics*, 54(1):92–106.

Belkin, Igor M. (2004). Propagation of the "Great Salinity Anomaly" of the 1990s around the northern North Atlantic. *Geophys. Res. Letters*, 31:L08306,doi:10.1029/2003GL019334.

Belkin, Igor M. and Sydney Levitus (1996). Temporal variability of the Subarctic Front near the Charlie Gibbs Fracture Zone. *J. Geophys. Res.*, 101(C12):28,317–28,324.

Belkin, Igor M., Sydney Levitus, John Antonov, and Svend-Aage Malmberg (1998). "Great Salinity Anomalies" in the North Atlantic. *Prog. Oceanogr.*, 41(1):1–68.

Béranger, Karine, Karelle Viau, Bernard Barnier, Elodie Garnier, Jean Marc Molines, Laure Siefridt, and Guillaume Barnier (2000). An atlas of climatic estimates of air-sea fluxes. Technical Report, Equipe MEOM - Modélisation des Ecoulements Océaniques de Moyenne et Grande Échelle, LEGI, B.P. 53 F-38041 Grenoble Cedex.

Böning, Claus W., Frank O. Bryan, William R. Holland, and Ralf Döscher (1996). Deep-water formation and meridional overturning in a high-resolution model of the North Atlantic. *J. Phys. Oceanogr.*, 26(7):1142–1164.

Böning, Claus W., Monika Rhein, Joachim Dengg, and Catrin Dorow (2003). Modeling CFC inventories and formation rates of Labrador Sea Water. *Geophys. Res. Letters*, 30(2):10.1029/2002GL014855.

Bower, Amy S., Bernard Le Cann, Thomas Rossby, Walter Zenk, John Gould, Kevin Speer, Phil Richardson, Mark D. Prater, and Huai-Min Zhang (2002). Directly measured mid-depth circulation in the northeastern North Atlantic Ocean. *Nature*, 419:603–607.

Boyer, Tim P. and Sydney Levitus (1997). Objective analyses of temperature and salinity for the world ocean on a $1/4^o$ grid. Technical Report, NOAA Atlas NESDIS 11, U. S. Gov. Printing Office, Washington, D. C.

Brandt, Peter, Friedrich A. Schott, Andreas Funk, and Carlos Sena Martins (2004). Seasonal to interannual variability of the eddy field in the Labrador Sea from satellite altimetry. *J. Geophys. Res.*, 109(C2):C02028, doi:10.1029/2002JC001551.

Broecker, Wallace S. (1991). The Great Ocean Conveyor. *Oceanography*, 4(2):79–89.

Bryden, Harry L., Dean H. Roemmich, and John A. Church (1991). Ocean heat transport across 24°N in the Pacific. *Deep-Sea Res.*, Part A, 38:297–324.

Bullister, John L. (1989). Chlorofluorocarbons as time-dependent tracers in the ocean. *Oceanography*, 2:12–17.

Bullister, John L. and Ray F. Weiss (1988). Determination of CCl_3F and CCl_2F_2 in seawater and air. *Deep-Sea Res.*, 35:839–853.

Bulsiewicz, Klaus, Henning Rose, Olaf Klatt, Alfred Putzka, and Wolfgang Roether (1998). A capillary-column chromatographic system for efficient chlorofluorocarbon measurements in ocean waters. *J. Geophys. Res.*, 103(C8):15,959–15,970.

Caniaux, Guy, Louis Prieur, Herve Giordani, Fabrice Hernandez, and Laurence Eymard (2001). Observation of the circulation in the newfoundland basin in winter 1997. *J. Phys. Oceanogr.*, 31(3):689–710.

Carr, Mary-Elena and H. Thomas Rossby (2001). Pathways of the North Atlantic Current from surface drifters and subsurface floats. *J. Geophys. Res.*, 106(C3):4405–4419.

Cheng, Wei and Peter B. Rhines (2004). Response of the overturning circulation to high-latitude fresh-water perturbations in the North Atlantic. *Climate Dynamics*, 22(4):359–372.

Clarke, R. Allyn (1984). Transport through the Cape Farewell–Flemish Cap section. *Rapp. P.-v. Reun. Cons. int. Explor. Mer.*, 185:120–130.

Clarke, R. Allyn and Jean-Claude Gascard (1983). The formation of Labrador Sea Water. Part I: Large–scale processes. *J. Phys. Oceanogr.*, 13(10):1764–1778.

Clarke, R. Allyn, Ross M. Hendry, and Igor Yashayaev (1998). A western boundary current meter array in the North Atlantic near 42°N. *International WOCE Newsletter*, 33:33–34.

Clarke, R. Allyn, Harry W. Hill, Robert F. Reiniger, and Bruce A. Warren (1980). Current system south and east of the Grand Banks of Newfoundland. *J. Phys. Oceanogr.*, 10(2):25–65.

Cunnold, Derek M., Paul J. Fraser, Ray F. Weiss, Ronald G. Prinn, Peter G. Simmonds, Ben R. Miller, Fred N. Alyea, and A. J. Crawford (1994). Global trends and annual releases of CCl_3F and CCl_2F_2 estimated from ALE/GAGE and other measurements from July 1987 to June 1991. *J. Geophys. Res.*, 99(D1):1107–1126.

Cuny, Jerome, Peter B. Rhines, Pearn P. Niiler, and Sheldon Bacon (2002). Labrador Sea boundary currents and the fate of the Irminger Sea Water. *J. Phys. Oceanogr.*, 32:627–547.

Curry, Ruth G. (1996). A database of hydrographic stations and tools for climatological analysis. Technical Report WHOI–96–01, Woods Hole Oceanographic Institution. 50 pp.

Curry, Ruth G., Bob Dickson, and Igor Yashayaev (2003). A change in the freshwater balance of the Atlantic Ocean over the past four decades. *Nature*, 426:826–829.

Curry, Ruth G. and Michael S. McCartney (2001). Ocean gyre circulation changes associated with the North Atlantic Oscillation. *J. Phys. Oceanogr.*, 31(12):3374–3400.

Curry, Ruth G., Michael S. McCartney, and Terrence M. Joyce (1998). Oceanic transport of subpolar climate signals to mid-depth subtropical waters. *Nature*, 391:575–577.

Davis, Russ E. (1998). Preliminary results from directly measuring mid-depth circulation in the tropical and South Pacific. *J. Geophys. Res.*, 103(C11):24619–24639.

Delworth, Thomas, Syukuru Manabe, and Ronald J. Stouffer (1993). Interdecadal variations of the thermohaline circulation in a coupled ocean–atmosphere model. *J. Climate*, 6(11):1993–2011.

Deser, Clara, Marika Holland, and Gilles Reverdin (2002). Decadal variations in Labrador Sea ice cover and North Atlantic sea surface temperatures. *J. Geophys. Res.*, 107(C5):doi:10.1029/200JC000683.

Dickson, Bob (1999). All change in the Arctic. *Nature*, 397:389–391.

Dickson, Bob, Igor Yashayaev, Jens Meincke, Bill Turrell, Stephen Dye, and Jürgen Holfort (2002). Rapid freshening of the deep North Atlantic over the past four decades. *Nature*, 416:832–837.

Dickson, Robert R. and Juan Brown (1994). The production of North Atlantic Deep Water: Sources, rates and pathways. *J. Geophys. Res.*, 99(C6):12,319–12,341.

Dickson, Robert R., Ed M. Gmitrowicz, and Andrew J. Watson (1990). Deep-water renewal in the northern North Atlantic. *Nature*, 344:848–850.

Dickson, Robert R., John Lazier, Jens Meincke, Peter Rhines, and James Swift (1996). Long-term coordinated changes in the convective activity of the North Atlantic. *Prog. Oceanogr.*, 38:241–295.

Dickson, Robert R., Jens Meincke, Svend-Aage Malmberg, and Arthur J. Lee (1988). The Great Salinity Anomaly in the northern North Atlantic 1968-1982. *Prog. Oceanogr.*, 20(2):103–151.

Dietrich, Günther (1969). *Atlas of the Hydrography of the Northern North Atlantic Ocean.* Conseil International pour l'Exploration de la Mer, Service Hydrographique, Charlottenlund Slot, Denmark.

Dietrich, Günther, Kurt Kalle, Wolfgang Krauss, and Gerold Siedler (1975). *Allgemeine Meereskunde – Eine Einführung in die Ozeanographie.* Gebr. Bornträger, Berlin, Stuttgart, third edition.

Dobroliubov, Sergey, Bob Tereschenkov, and Alexey Sokov (1996). Mass and heat fluxes at 36°N in the Atlantic: Comparison of 1993, 1981 and 1959 hydrographic surveys. *International WOCE Newsletter*, 22:34–37.

Doney, Scott C. and John L. Bullister (1992). A chloroflourocarbon section in the eastern North Atlantic. *Prog. Oceanogr.*, 39:1857–1883.

Döscher, Ralf and René Redler (1997). The relative importance of northern overflow and subpolar deep convection for the North Atlantic thermohaline circulation. *J. Phys. Oceanogr.*, 27(9):1894–1902.

Dutkiewicz, Stephanie, Lewis Rothstein, and Thomas Rossby (2001). Pathways of cross-frontal exchange in the North Atlantic Current. *J. Geophys. Res.*, 106(C11):26917–26928.

Eden, Carsten and Claus Böning (2002). Sources of eddy kinetic energy in the Labrador Sea. *J. Phys. Oceanogr.*, 32(12):3346–3363.

Eden, Carsten and Jürgen Willebrand (2001). Mechanism of interannual to decadal variability of the North Atlantic circulation. *J. Climate*, 14(10):2266–2280.

Elkins, James W. (1999). Chlorofluorocarbons (CFCs). In: *The Chapman & Hall Encyclopedia of Environmental Science*. Alexander, David E. and Rhodes W. Fairbridge, Eds., p. 78–80. Kluwer Academic, Boston, MA.

Emery, William J. and Jens Meincke (1986). Global water masses: Summary and review. *Oceanol. Acta*, 9(4):383–391.

Emile-Geay, Julien, Mark A. Cane, Naomi Naik, Richard Seager, Amy C. Clement, and Alexander van Geen (2003). Warren revisited: Atmospheric freshwater fluxes and "Why is no deep water formed in the North Pacific". *J. Geophys. Res.*, 108(C6):3178, doi:10.1029/2001JC001058.

England, Matthew H. and Ernst Maier-Reimer (2001). Using chemical tracers to assess ocean models. *Rev. Geophys.*, 39(1):29–70.

Farman, Joseph C., Brian G. Gardiner, and Jonathan D. Shanklin (1985). Large losses of total ozone in Antarctica reveal seasonal ClO_x/NO_x interaction. *Nature*, 315:207–210.

Fine, Rana A. (1995). Tracers, time scales, and the thermohaline circulation: The lower limb in the North Atlantic Ocean. *Rev. Geophys.*, 33, Part 2, Suppl. S:1353–1365.

Fine, Rana A. and Robert L. Molinari (1988). A continous deep western boundary current between Abaco (26.5°N) and Barbados (13°N). *Deep-Sea Res.*, 35(9):1441–1450.

Fischer, Jürgen and Friedrich A. Schott (2002). Labrador Sea Water tracked by profiling floats — From the boundary current into the open North Atlantic. *J. Phys. Oceanogr.*, 32(2):573–584.

Fischer, Jürgen, Friedrich A. Schott, and Marcus Dengler (2004). Boundary circulation at the exit of the Labrador Sea. *J. Phys. Oceanogr.*, 34(7):1548–1570.

Fleischmann, Uli, Hauke Hildebrandt, Alfred Putzka, and Reinhold Bayer (2001). Transport of newly ventilated deep water from the Iceland Basin to the Westeuropean Basin. *Deep-Sea Res. I*, 48(8):1793–1819.

Fratantoni, David M. (2001). North Atlantic surface circulation during the 1990's observed with satellite-tracked drifters. *J. Geophys. Res.*, 106(C10):22067–22093.

Ganachaud, Alexandre and Carl Wunsch (2000). Improved estimates of global ocean circulation, heat transport and mixing from hydrographic data. *Nature*, 408:453–457.

Ganachaud, Alexandre and Carl Wunsch (2003). Large-scale ocean heat and freshwater transports during the World Ocean Circulation Experiment and mixing from hydrographic data. *J. Climate*, 16(4):696–705.

Getzlaff, Klaus (2003). Exportpfade von Tiefenwasser aus der Labradorsee: Synthetische Floats in einem hochauflösenden numerischen Modell. Diplomarbeit, Institut für Meereskunde, Universität Kiel.

Girton, James B., Thomas B. Sanford, and Rolf H. Käse (2001). Synoptic sections of the Denmark Strait Overflow. *Geophys. Res. Letters*, 28(8):1619–1622.

Gordon, Arnold L. (1986). Interocean exchange of thermohaline water. *J. Geophys. Res.*, 91(C4):5037–5046.

Grasshoff, Klaus, Manfred Erhardt, and Klaus Kremling (1999). *Methods of Seawater Analysis*. Wiley-VCH, Weinheim, 3th edition.

Gray, Suzanne L. and Thomas W. N. Haine (2001). Constraining a North Atlantic Ocean General Circulation Model with Chlorofluorocarbon Observations. *J. Phys. Oceanogr.*, 31:1157–1181.

Greatbatch, Richard J. (2000). The North Atlantic Oscillation. *Stochastic Environmental Research And Risk Assessment*, 14:213–242.

Gruber, Nicolas (1998). Anthropogenic CO_2 in the Atlantic Ocean. *Global Biogeochem. Cycles*, 12(1):165–191.

Haine, Thomas W. N., Kelvin J. Richards, and Yanli Jia (2003). Chlorofluorocarbon constraints on North Atlantic Ventilation. *J. Phys. Oceanogr.*, 33(8):1798–1814.

Häkkinen, Sirpa (2002). Freshening of the Labrador Sea surface waters in the 1990s: Another great salinity anomaly ? *Geophys. Res. Letters*, 29(24):2232, doi:10.1029/2002GL015243.

Hall, Mindy M. and Harry L. Bryden (1982). Direct estimates and mechanisms of ocean heat transport. *Deep-Sea Res.*, 29(3A):229–359.

Hanawa, Kimio and Lynne D. Talley (2001). Mode Waters. In: *Ocean Circulation and Climate*. Siedler, G., J. Church, and J. Gould, Eds., Band 77 *International Geophysics Series*, p. 373–386. Academic Press.

Hansen, Bogi and Svein Østerhus (2000). North Atlantic-Nordic Seas exchanges. *Prog. Oceanogr.*, 45(1):109–208.

Hansen, Bogi, William R. Turrell, and Svein Østerhus (2001). Decreasing overflow from the Nordic Seas into the Atlantic Ocean through the Faroe Bank channel since 1950. *Nature*, 411:927–930.

Harvey, John and Michel Arhan (1988). The water masses of the central North Atlantic in 1983–84. *J. Phys. Oceanogr.*, 18(12):1855–1875.

Harvey, John G. (1980). Deep and bottom water in the Charlie-Gibbs Fracture Zone. *J. Mar. Res.*, 38(1):173–182.

Harvey, John G. and A. Theodorou (1986). The circulation of Norwegian Sea overflow water in the eastern North Atlantic. *Oceanol. Acta*, 9(4):393–402.

Holfort, Jürgen and Gerold Siedler (2001). The meridional oceanic transports of heat and nutrients in the South Atlantic. *J. Phys. Oceanogr.*, 31(1):5–29.

Hurrell, James W. (1995). Decadal trends in the North Atlantic Oscillation: Regional temperatures and precipitation. *Science*, 269:676–679.

Hurrell, James W. and Harry Van Loon (1997). Dedadal variations in climate associated with the North Atlantic Oscillation. *Climate Change*, 36:301–326.

Iorga, Michaela Ciobotaru and M. Susan Lozier (1999). Signatures of the Mediterranean outflow from a North Atlantic climatology: 1. Salinity and density fields. *J. Geophys. Res.*, 104(C11):25985–26009.

Jenkins, William J. and Peter B. Rhines (1980). Tritium in the deep North Atlantic Oceans. *Nature*, 286:877–880.

Jones, Phil D., Trausti Jónsson, and Dennis Wheeler (1997). Extension to the North Atlantic Oscillation using early instrumental pressure observations from Gibraltar and South-West Iceland. *Int. Journ. of Climatol.*, 17(13):1433–1450.

Josey, Simon A., Elisabeth C. Kent, and Peter K. Taylor (2004). New insights into the ocean heat budget closure problem from analysis of the SOC air-sea flux climatology. *J. Climate*, 12(9):2856–2880.

Kalnay, Eugenia, Masao Kanamitsu, Robert Kistler, William Collins, D. Deaven, L. Gandin, M. Iredell, Suranjana Saha, Glenn White, John Woollen, Y. Zhu., Muthuvel Chelliah, Wesley Ebiszusaki, W. Higgins, J. Janowiak, K. Mo, C. Ropelewski, J. Wang, A. Leetmaa, R. Reynolds, Roy Jenne, and J. Joseph (1996). The NCEP/NCAR 40-Year Renanalysis Project. *Bull. Amer. Meteor. Soc.*, 77(3):437–471.

Käse, Rolf H. and Wolfgang Krauss (1996). The Gulf Stream, the North Atlantic Current and the origin of the Azores Current. In: *The Warmwatersphere of the North Atlantic Ocean.* Krauss, Wolfgang, Eds., p. 446. Gebr. Bornträger, Berlin–Stuttgart.

Katsman, Caroline, Michael A. Spall, and Robert S. Pickart (2004). Boundary current eddies and their role in the restratification of the Labrador Sea. *J. Phys. Oceanogr.*, 34(9):1967–1983.

Kearns, Edward J. and H. Thomas Rossby (1998). Historical position of the North Atlantic Current. *J. Geophys. Res.*, 103(C8):15,509–15,524.

Kieke, Dagmar and Monika Rhein (2004). Variability of the overflow water transport in the western subpolar North Atlantic, 1950-1997. *J. Phys. Oceanogr.*, in revision.

Kistler, Robert, Eugenia Kalnay, William Collins, Suranjana Saha, Glenn White, John Woollen, Muthuvel Chelliah, Wesley Ebisuzaki, Masao Kanamitsu, Vernon Kousky, Huug van den Dool, Roy Jenne, and Michael Fiorino (2001). The NCEP/NCAR 50-year renanalysis: Monthly means CD-ROM and documentation. *Bull. Amer. Meteor. Soc.*, 82(2):247–267.

Klein, Birgit, Robert L. Molinari, Thomas J. Müller, and Gerold Siedler (1995). A transatlantic section at 14.5N: Meridional volume and heat fluxes. *J. Mar. Res.*, 53(6):929–957.

Koltermann, Klaus Peter, Alex V. Sokov, Vladimir P. Tereschenkov, Sergey A. Dobroliubov, Katja Lorbacher, and Alexander Sy (1999). Decadal changes in the thermohaline circulation of the North Atlantic. *Deep-Sea Res. II*, 46(1–2):109–138.

Krahmann, Gerd et al. (2003). The Labrador Sea Deep Convection Experiment data collection. *Geochem., Geophys., Geosys. (G^3)*, 4(10):1091, doi:10.1029/2003GC000536.

Krauss, Wolfgang (1986). The North Atlantic Current. *J. Geophys. Res.*, 91(C4):5061–5074.

Krauss, Wolfgang (1995). Currents and mixing in the Irminger Sea and in the Iceland Basin. *J. Geophys. Res.*, 100(C6):10,851–10,871.

Krauss, Wolfgang (1996). Comments on the development of our knowledge of the general circulation of the North Atlantic Ocean. In: *The Warmwatersphere of the North Atlantic Ocean.* Krauss, Wolfgang, Eds., p. 1–31. Gebr. Bornträger, Stuttgart.

Krauss, Wolfgang, Eberhard Fahrbach, Ain Aitsam, Jüri Elken, and Peter Koske (1987). The North Atlantic Current and its associated eddy field southeast of Flemish Cap. *Deep-Sea Res.*, 34(7):1163–1185.

Lavender, Kara L., Russ E. Davis, and W. Brechner Owens (2000). Mid-depth recirculation observed in the interior Labrador and Irminger seas by direct velocity measurements. *Nature*, 407:66–69.

Lavender, Kara L., Russ E. Davis, and W. Brechner Owens (2002). Observations of open-ocean deep convection in the Labrador Sea from subsurface floats. *J. Phys. Oceanogr.*, 32(2):511–526.

Lavín, Alicia M., Harry L. Bryden, and Gregorio Parilla (2003). Mechanisms of heat, freshwater, oxygen and nutrient transports and budgets at 24.5°N in the subtropical North Atlantic. *Deep-Sea Res. I*, 50(9):1099–1128.

Lazier, John R. N. (1973). The renewal of Labrador Sea Water. *Deep-Sea Res.*, 20:341–353.

Lazier, John R. N. (1980). Oceanographic conditions at Ocean Weather Ship Bravo, 1964–1974. *Atmos.-Ocean*, 18(3):227–238.

Lazier, John R. N. (1988). Temperature and salinity changes in the deep Labrador Sea, 1962–1986. *Deep-Sea Res.*, 35(8):1247–1253.

Lazier, John R. N. (1994). Observations in the Northwest Corner of the North Atlantic Current. *J. Phys. Oceanogr.*, 24(7):1449–1463.

Lazier, John R. N. and Robert M. Gershey (1991). AR7W: Labrador Sea Line - July 1990. *International WOCE Newsletter*, 11:5–7.

Lazier, John R. N., Ross Hendry, Allyn Clarke, Igor Yashayaev, and Peter B. Rhines (2002). Convection and restratification in the Labrador Sea, 1990-2000. *Deep-Sea Res. I*, 49(10):1819–1835.

Lazier, John R. N. and Daniel G. Wright (1993). Annual velocitiy variations in the Labrador Current. *J. Phys. Oceanogr.*, 23(4):659–678.

LeBel, Deborah A., Wlliam M. Smethie, Chantal Andrié, John L. Bullister, E. Peter Jones, Dong-Ha Min, Monika Rhein, Wolfgang Roether, Denise Smythe-Wright, and Ray F. Weiss (2002). CFC-11 inventory distributions in the water masses of the North Atlantic during the WOCE period. Poster presentation, WOCE-2002 Conference, San Antonio, USA.

Levitus, Sydney (1982). Climatological atlas of the world ocean. Professional paper no. 13, NOAA, Rockville, MD.

Levitus, Sydney (1994). World Ocean Atlas 1994 CD-ROM Sets. Information report, NOAA, Washington D. C.

Levitus, Sydney and Tim P. Boyer (1994). World Ocean Atlas 1994. Volume 1: Salinity. Technical Report, NOAA, U. S. Gov. Print. Off., Washington D. C, USA.

Lilly, Jonathan M., Peter B. Rhines, Friedrich Schott, Kara Lavender, John Lazier, Uwe Send, and Eric D'Asaro (2003). Observations of the Labrador Sea eddy field. *Prog. Oceanogr.*, 59(1):75–176.

Lilly, Jonathan M., Peter B. Rhines, Martin Visbeck, Russ Davis, John R. N. Lazier, Friedrich Schott, and David Farmer (1999). Observing deep convection in the Labrador Sea during winter 1994/95. *J. Phys. Oceanogr.*, 29(8):2065–2098.

Loder, John W., Brian Petrie, and Glen Garkiewicz (1998). The coastal ocean off northeastern North America: A large-scale view. In: *The Sea.* Brink, Kenneth H. and Allan R. Robinson, Eds., Band 11, chapter 5, p. 105–133. John Wiley & Sons.

Macdonald, Alison M. (1998). The global ocean circulation: A hydrographic estimate and regional analysis. *Prog. Oceanogr.*, 41(3):281–382.

Macrander, Andreas and Rolf H. Käse (2004). Recent changes in Denmark Strait overflow transports. Poster presentation, Bjerknes-Centenary-2004 Conference, Bergen, Norway.

Manabe, Syukuro and Ronald J. Stouffer (1995). Simulation of abrupt climatic change induced by freshwater input to the North Atlantic Ocean. *Nature*, 378:165–167.

Mann, M. R. (1967). The termination of the Gulf Stream and the beginning of the North Atlantic Current. *Deep-Sea Res.*, 14:337–359.

Marsh, Robert (2000). Recent variability of the North Atlantic thermohaline circulation inferred from surface heat and freshwater fluxes. *J. Climate*, 13(9):3239–3260.

Marshall, John and Friedrich Schott (1999). Open-ocean convection: Observations, theory, and models. *Rev. Geophys.*, 37(1):1–64.

Mauritzen, Cecilie (1996). Production of dense overflow waters feeding the North Atlantic across the Greenland-Scotland Ridge. Part 1: Evidence for a revised circulation scheme. *Deep-Sea Res.*, 43(6):769–806.

Mauritzen, Cecilie (1996). Production of dense overflow waters feeding the North Atlantic across the Greenland-Scotland Ridge. Part 2: An inverse model. *Deep-Sea Res.*, 43(6):807–835.

McCartney, Michael S. (1992). Recirculating components to the deep boundary current of the northern North Atlantic. *Prog. Oceanogr.*, 29(4):283–383.

McCartney, Michael S. (1993). Crossing of the equator by the Deep Western Boundary Current in the western Atlantic Ocean. *J. Phys. Oceanogr.*, 23:1953–1974.

McCartney, Michael S. and R. Allyn Curry (1993). Transequatorial flow of Antarctic Bottom Water in the western Atlantic Ocean: Abyssal geostrophy at the equator. *J. Phys. Oceanogr.*, 23(6):1264–1276.

McCartney, Michael S. and Lynne D. Talley (1982). The Subpolar Mode Water of the North Atlantic Ocean. *J. Phys. Oceanogr.*, 12(11):1169–1188.

McCartney, Michael S. and Lynne D. Talley (1984). Warm-to-cold water conversion in the Northern North Atlantic Ocean. *J. Phys. Oceanogr.*, 14(5):922–935.

Meinen, Christopher S. (2001). Structure of the North Atlantic Current in stream-coordinates and the circulation in the Newfoundland basin. *Deep-Sea Res. I*, 48(7):1553–1580.

Meinen, Christopher S., D. Randolph Watts, and R. Allyn Clarke (2000). Absolutely referenced geostrophic velocity and transport on a section across the North Atlantic Current. *Deep-Sea Res.*, 47(2):309–322.

Mertens, Christian (2000). *Open-Ocean Convection in the Labrador and Greenland Seas: Plume Scales and Interannual Variability.* Dissertation, Institut für Meereskunde an der Christian-Albrechts-Universität Kiel, Kiel.

Molina, Mario J. and F. Sherwood Rowland (1974). Stratospheric sink for chlorofluoromethanes: Chlorine atom catalysed destruction of ozone. *Nature*, 249:810–814.

Molinari, Robert L., Rana A. Fine, W. Douglas Wilson, Ruth G. Curry, Jeff Abell, and Michael S. McCartney (1998). The arrival of recently formed Labrador Sea Water in the Deep Western Boundary Current at 26°N. *Geophys. Res. Letters*, 25(13):2249–2252.

Monterey, Grigori and Sydney Levitus (1997). Seasonal variability of mixed layer depth for the World Ocean. NOAA Atlas NESDIS 14. Technical Report, U.S. Gov. Printing Office, Washington D.C, USA.

Munk, Walter (2000). Achievements in Physical Oceanography. In: *50 Years of Ocean Discovery: National Science Foundation 1950-2000.* National Research Council (U.S.). Ocean Studies Board, Eds., p. 44–50. National Academies Press.

Munk, Walter H. (1966). Abyssal recipes. *Deep-Sea Res.*, 13:707–730.

National Oceanographic Data Center (1991). Global ocean temperature and salinity profiles, Vol. 1. CD-ROM, Washington DC.

Orsi, Alejandro H., Gregory C. Johnson, and John L. Bullister (1999). Circulation, mixing and production of Antarctic Bottom Water. *Prog. Oceanogr.*, 43(1):55–110.

Paillet, Jerôme, Michel Arhan, and Michael S. McCartney (1998). Spreading of Labrador Sea Water in the eastern North Atlantic. *J. Geophys. Res.*, 103:10223–10239.

Pérez-Brunius, Paula, H. Thomas Rossby, and D. Randolph Watts (2004). Absolute transports of mass and temperature for the North Atlantic Current–Subpolar Front System. *J. Phys. Oceanogr.*, 34(8):1870–1883.

Pickard, Geroge L. and William J. Emery (1989). *Descriptive physical oceanography - An introduction.* Pergamon Press, 5th edition.

Pickart, Robert S. (1992). Water mass components of the North Atlantic deep western boundary current. *Deep-Sea Res.*, 39(9):1553–1572.

Pickart, Robert S. and William M. Smethie (1998). Temporal evolution of the deep western boundary current where it enters the sub-tropical domain. *Deep-Sea Res. I*, 45(7):1053–1083.

Pickart, Robert S., William M. Smethie, John R. N. Lazier, E. Peter Jones, and William J. Jenkins (1996). Eddies of newly formed upper Labrador Sea Water. *J. Geophys. Res.*, 101(C9):20,711–20,726.

Pickart, Robert S., Michael A. Spall, and John R. N. Lazier (1997). Mid-depth ventilation in the western boundary current system of the sub-polar gyre. *Deep-Sea Res.*, 44(6):1025–1054.

Pickart, Robert S., Michael A. Spall, Mads Hvid Ribergaard, G. W. Kent Moore, and Ralph F. Milliff (2003b). Deep convection in the Irminger Sea forced by the Greenland tip jet. *Nature*, 424:152–156.

Pickart, Robert S., Fiametta Straneo, and G. W. Kent Moore (2003a). Is Labrador Sea Water formed in the Irminger Basin? *Deep-Sea Res. I*, 50(1):23–52.

Plähn, Olaf (1999). *Ventilation und Zirkulation in der Arabischen See: Ergebnisse aus Beobachtungen und Modellanalysen.* Dissertation, Institut für Meereskunde an der Christian-Albrechts-Universität Kiel.

Pollard, Raymond T., Michael J. Griffiths, Stuart A. Cunningham, Jane F. Read, Fiz F. Pérez, and Aida F. Rios (1996). Vivaldi 1991 - A study of the formation, circulation and ventialtion of the Eastern North Atlantic Central Water. *Prog. Oceanogr.*, 37(2):167–192.

Pond, Stephen and George L. Pickard (1983). *Introductory Dynamical Oceanography.* Pergamon Press, second edition.

Prater, Mark D. (2002). Eddies in the Labrador Sea as observed by profiling RAFOS floats and remote sensing. *J. Phys. Oceanogr.*, 32(2):411–427.

Rahmstorf, Stefan (2002). Ocean circulation and climate during the past 120,000 years. *Nature*, 419:207–214.

Rahmstorf, Stefan and Andrey Ganopolski (1999). Long-term global warming scenarios computed with an efficient coupled climate model. *Climate Change*, 43(2):353–367.

Read, Jane F. and W. John Gould (1992). Cooling and freshening of the subpolar North Atlantic Ocean since the 1960s. *Nature*, 360:55–57.

Redler, René and Claus W. Böning (1997). Effects of the overflows on the circulation in the subpolar North Atlantic: A regional model study. *J. Geophys. Res.*, 102(C8):18,529–18,552.

Renfrew, Ian A., G. W. Kent Moore, Peter S. Guest, and Karl Bumke (2002). A comparison of surface layer and surface turbulent flux observations over the Labrador Sea with ECMWF analyses and NCEP reanalyses. *J. Phys. Oceanogr.*, 32(2):383–400.

Reverdin, Gilles, Pearn P. Niiler, and Hedinn Valdimarsson (2003). North Atlantic Ocean surface currents. *J. Geophys. Res.*, 108(C1):3002, doi:10.1029/2001JC001020.

Reynolds, Richard W., Nick A Rayner, Thomas M. Smith, Diane C. Stokes, and Wanqiu Wang (2002). An improved in situ and satellite SST analysis for climate. *J. Climate*, 15(13):1609–1625.

Rhein, Monika (1994). The Deep Western Boundary Current: tracers and velocities. *Deep-Sea Res.*, 41(2):263–281.

Rhein, Monika, Jürgen Fischer, William M. Smethie, Denise Smythe-Wright, Ray F. Weiss, Christian Mertens, Dong-Ha Min, Uli Fleischmann, and Alfred Putzka (2002). Labrador Sea Water: pathways, CFC-inventory and formation rates. *J. Phys. Oceanogr.*, 32(2):648–665.

Rhein, Monika, Lothar Stramma, and Gerd Krahmann (1998). The spreading of Antarctic Bottom Water in the tropical Atlantic. *Deep-Sea Res.*, 45:507–527.

Rintoul, Stephen R. and Carl Wunsch (1991). Mass, heat, oxygen and nutrient fluxes and budget in the North Atlantic Ocean. *Deep-Sea Res.*, 38 (Suppl.):355–377.

Roberts, Malcolm J. and Richard A. Wood (1997). Topographic sensitivity studies with a Bryan–Cox type ocean model. *J. Phys. Oceanogr.*, 27(5):823–836.

Roemmich, Dean H., John Gilson, Bruce Cornuelle, and Robert Weller (2001). Mean and time-varying meridional transport of heat at the tropical/subtropical boundary of the North Pacific. *J. Geophys. Res.*, 106(C5):8957–8970.

Rogers, Jeffrey C. (1984). The association between the North Atlantic Oscillation and the Southern Oscillation in the northern hemisphere. *Mon. Wea. Rev.*, 112:1999–2015.

Ross, Charles K. (1984). Temperature – salinity characteristics of the "overflow" water in Denmark Strait during "OVERFLOW '73". *Rapp. P.-v. Reun. Cons. int. Explor. Mer.*, 185:111–119.

Rossby, Thomas (1996). The North Atlantic Current and surrounding waters: At the crossroads. *Rev. Geophys.*, 34(4):463–481.

Sathiyamoorthy, Sudharshan and G. W. Kent Moore (2002). Buoyancy flux at Ocean Weather Sation Bravo. *J. Phys. Oceanogr.*, 32(2):458–474.

Saunders, Peter M. (1994). The flux of overflow water through the Charlie Gibbs Fracture Zone. *J. Geophys. Res.*, 99(C6):12,343–12,355.

Saunders, Peter M. (2001). The Dense Northern Overflows. In: *Ocean Circulation and Climate*. Siedler, G., J. Church, and J. Gould, Eds., Band 77 *International Geophysics Series*, p. 401–417. Academic Press.

Saunders, Peter M. and Brian M. King (1995). Oceanic fluxes on the WOCE A11 Section. *J. Phys. Oceanogr.*, 25:1942–1958.

Schiller, Andreas, Uwe Mikolajewicz, and Reinhard Voss (1997). The stability of the North Atlantic thermohaline circulation in a coupled ocean-atmosphere general circulation model. *Climate Dynamics*, 13:325–347.

Schmitz, William J. (1996). On the World Ocean Circulation: Volume 1. Technical Report WHOI-96-03, Woods Hole Oceanographic Institution.

Schott, Friedrich, Jürgen Fischer, Jürgen Holfort, and Walter Zenk (2002). North Atlantic 2001, Cruise No. 50, 7 May - 12 August 2001. METEOR-Berichte 02-2, Universität Hamburg.

Schott, Friedrich, Klaus-Peter Koltermann, Lothar Stramma, Alexander Sy, Rainer Zahn, and Walter Zenk (1999). North Atlantic 1997, Cruise No. 39, 18 April - 14 September 1997. METEOR-Berichte 99-1, Universität Hamburg.

Schott, Friedrich, Lothar Stramma, and Jürgen Fischer (1999). Interaction of the North Atlantic Current with the deep Charlie Gibbs Fracture Zone throughflow. *Geophys. Res. Letters*, 26(3):369–372.

Schott, Friedrich A., Rainer Zantopp, Lothar Stramma, Marcus Dengler, Jürgen Fischer, and Mathieu Wibaux (2004). Circulation and deep-water export at the western exit of the subpolar North Atlantic. *J. Phys. Oceanogr.*, 34(4):817–843.

Sena Martins, Carlos, Meike Hamann, and Armando F. G. Fiúza (2002). Surface circulation in the eastern North atlantic, from drifters and altimetry. *J. Geophys. Res.*, 107(C12):3217, doi:10.1029/2000JC000345.

Sloyan, Bernadette M. and Stephen R. Rintoul (2001). Circulation, renewal, and modification of Antarctic Mode and Intermediate Water. *J. Phys. Oceanogr.*, 31(4):1005–1030.

Sloyan, Bernadette M. and Stephen R. Rintoul (2001). The Southern Ocean limb of the global deep overturning circulation. *J. Phys. Oceanogr.*, 31(1):143–173.

Smethie, William M. (1993). Tracing the thermohaline circulation in the western North Atlantic using chlorofluorocarbons. *Prog. Oceanogr.*, 31(1):51–99.

Smethie, William M. and Rana A. Fine (2001). Rates of North Atlantic Deep Water formation calculated from chlorofluorocarbon inventories. *Deep-Sea Res. I*, 48(1):189–215.

Smethie, William M., Rana A. Fine, Alfred Putzka, and E. Peter Jones (2000). Tracing the flow of North Atlantic Deep Water using chlorofluorocarbons. *J. Geophys. Res.*, 105(C6):14297–14323.

Smethie, William M. and James H. Swift (1989). The Tritium-Krypton-85 Age of Denmark Strait Overflow Water and Gibbs Fracture Zone Water Just South of Denmark Strait. *J. Geophys. Res.*, 94(C6):8265–8275.

Speer, Kevin G., Jürgen Holfort, Thierry Reynaud, and Gerold Siedler (1996). South Atlantic heat transport at 11°S. In: *The South Atlantic: Present and Past Circulation.* Wefer, G., W. H. Berger, G. Siedler, and D. J. Webb, Eds., p. 105–120. Springer–Verlag, Berlin.

Speer, Kevin G. and Michael S. McCartney (1992). Bottom Water Circulation in the Western North Atlantic. *J. Phys. Oceanogr.*, 22:83–92.

Speer, Kevin G., Gerold Siedler, and Lynne Talley (1995). The Namib Col Current. *Deep-Sea Res. I*, 42(11/12):1933–1950.

Speer, Kevin G. and Eli Tziperman (1992). Rates of water mass formation in the North Atlantic Ocean. *J. Phys. Oceanogr.*, 22:93–104.

Steinfeldt, Reiner and Monika Rhein (2004). Spreading velocities and dilution of North Atlantic Deep Water in the tropical Atlantic based on CFC time series. *J. Geophys. Res.*, C03046:doi:10.1029/2003JC002050.

Stommel, Henry and A. B. Arons (1960a). On the abyssal circulation of the world ocean. –I. Stationary planetary flow patterns on a sphere. *Deep-Sea Res.*, 6:140–154.

Stommel, Henry and A. B. Arons (1960b). On the abyssal circulation of the world ocean. –II. An idealized model of the circulation pattern and amplitude in oceanic basins. *Deep-Sea Res.*, 6:217–233.

Stramma, Lothar, Dagmar Kieke, Monika Rhein, Igor Yashayaev, Friedrich Schott, and Klaus-Peter Koltermann (2004). Deep Water changes at the western boundary of the subpolar North Atlantic during 1996 to 2001. *Deep-Sea Res. I*, 51(8):1033–1056.

Stramma, Lothar and Monika Rhein (2001). Variability in the Deep Western Boundary Current in the equatorial Atlantic at 44°w. *Geophys. Res. Letters*, 28(8):1623–1626.

Straneo, Fiammetta, Robert S. Pickart, and Kara Lavender (2003). Spreading of Labrador Sea Water: An advective-diffusive study based on Lagrangian data. *Deep-Sea Res. I*, 50(6):701–719.

Strass, Volker H., Eberhard Fahrbach, Ursula Schauer, and Lutz Sellmann (1993). Formation of Denmark Strait Overflow Water by Mixing in the East Greenland Current. *J. Geophys. Res.*, 98(C4):6907–6919.

Sverdrup, Harald U., Martin W. Johnson, and Richard H. Fleming (1942). *The Oceans*. Prentice-Hall, Inc., 1087 pgs.

Swift, James H. (1984). The circulation of the Denmark Strait and Iceland- Scotland Overflow Waters in the North Atlantic. *Deep-Sea Res.*, 31:1339–1355.

Sy, Alexander, Monika Rhein, John R. N. Lazier, Klaus Peter Koltermann, Jens Meincke, Alfred Putzka, and Manfred Bersch (1997). Surprisingly rapid spreading of newly formed intermediate waters across the North Atlantic Ocean. *Nature*, 386:675–679.

Sy, Alexander, Ursula Schauer, and Jens Meincke (1992). The North Atlantic Current and its associated hydrographic structure above and eastwards of the Mid-Atlantic Ridge. *Deep-Sea Res.*, 39(5):825–853.

Talley, Lynne D. (1999). Mode waters in the subpolar North Atlantic in historical data and during the WOCE period. *International WOCE Newsletter*, 37:3–7.

Talley, Lynne D. and Michael S. McCartney (1982). Distribution and circulation of Labrador Sea Water. *J. Phys. Oceanogr.*, 12(11):1189–1204.

The Lab Sea Group (1998). The Labrador Sea Deep Convection Experiment. *Bull. Amer. Meteor. Soc.*, 79(10):2033–2058.

Tichelaar, Bart W. and Larry J. Ruff (1989). How good are our best models? Jackknifing, bootstrapping, and earthquake depth. *Eos Trans. AGU*, 70(20):593, 605–606.

Tomczak, Matthias and J. Stuart Godfrey (1994). *Regional Oceanography: An Introduction*. Pergamon Press, New York, pgs. 422.

Tsimplis, Micahl N., Harry L. Bryden, and Sheldon Bacon (1998). The circulation of the subtropical South Pacific derived from hydrographic data. *J. Geophys. Res.*, 103(C10):21,443–21,468.

Van Aken, Hendrik M. (2000a). The hydrography of the mid-latitude northeast Atlantic Ocean I: The deep water masses. *Deep-Sea Res. I*, 47(5):757–788.

Van Aken, Hendrik M. (2000b). The hydrography of the mid-latitude northeast Atlantic Ocean II: The intermediate water masses. *Deep-Sea Res. I*, 47(5):789–824.

Van Aken, Hendrik M. and C. J. De Boer (1995). On the synoptic hydrography of intermediate and deep water masses in the Iceland Basin. *Deep-Sea Res.*, 42(2):165–189.

Van Loon, Harry and Jeffrey C. Rogers (1978). The seesaw in winter temperatures between Greenland and Northern Europe: Part I: General description. *Mon. Wea. Rev.*, 106:296–310.

Vellinga, Michael and Richard A. Wood (2002). Global climatic impacts of a collapse of the Atlantic thermohaline circulation. *Climate Change*, 54(3):251–267.

Walin, Gosta (1982). On the relation between sea-surface heat flow and thermal circulation in the ocean. *Tellus*, 34:187–195.

Walker, Stephen J., Ray F. Weiss, and Peter K. Salameh (2000). Reconstructed histories of the annual atmospheric mole fractions for the halocarbons CFC-11, CFC-12, CFC-113 and carbon tetrachloride. *J. Geophys. Res.*, 105(C6):14285–14296.

Wallace, Douglas W. R. and John R. N. Lazier (1988). Anthropogenic chlorofluoromethanes in newly formed Labrador Sea Water. *Nature*, 332:61–63.

Wallace, John M. and David S. Gutzler (1981). Teleconnections in the geopotential height field during the Northern Hemisphere winter. *Mon. Wea. Rev.*, 109:784–812.

Warner, Mark J. and Ray F. Weiss (1985). Solubilities of chlorofluorocarbons 11 and 12 in water and seawater. *Deep-Sea Res.*, 32(12):1485–1497.

Warren, Bruce A. (1983). Why is no deep water formed in the North Pacific? *J. Mar. Res.*, 41:327–347.

Weaver, Andrew J., Cecilia M. Bitz, Augustus F. Fanning, and Marika M. Holland (1999). Thermohaline circulation: High-latitude phenomena and the difference between the Pacific and Atlantic. *Ann. Rev. Earth Planet. Sci.*, 27:231–285.

Weiss, Ray F., John L. Bullister, Richard H. Gammon, and Mark J. Warner (1985). Atmospheric chlorofluoromethanes in the deep equatorial Atlantic. *Nature*, 314:608–610.

Weisse, Ralf, Uwe Mikolajewicz, and Ernst Maier-Reimer (1994). Decadal variability of the North Atlantic in an ocean general circulation model. *J. Geophys. Res.*, 99(C6):12411–12421.

White, Margaret A. and Karen J. Heywood (1995). Seasonal and interannual changes in the North Atlantic subpolar gyre from Geosat and TOPEX/POSEIDON altimetry. *J. Geophys. Res.*, 100(C12):24,931–24,941.

Whitworth III, Thomas, Worth D. Nowlin Jr., R. Dale Pillsbury, Mike I. Moore, and Ray F. Weiss (1991). Observations of the Antarctic Circumpolar Current and Deep Boundary Current in the southwest Atlantic. *J. Geophys. Res.*, 96(C8):15105–15118.

Wijffels, Susan E., John M. Toole, Harry L. Bryden, Rana A. Fine, and William M. Jenkins (1996). The water masses and circulation at 10°N in the Pacific. *Deep-Sea Res. I*, 43(4):501–544.

Willebrand, Jürgen, Bernard Barnier, Claus Böning, Christian Dieterich, Peter Killworth, Christian Le Provost, Yanli Jia, Jean-Marc Molines, and Adrian L. New (2001). Circulation characteristics in three eddy-permitting models of the North Atlantic. *Prog. Oceanogr.*, 48(2–3):123–161.

Wood, Richard A., Ann B. Keel, John F. B. Mitchell, and Jonathan M. Gregory (1999). Changing spatial structure of the thermohaline circulation in response to atmospheric CO_2 forcing in a climate model. *Nature*, 399:572–575.

Worthington, L. Valentine (1970). The Norwegian Sea as a mediterranean basin. *Deep-Sea Res.*, 17:77–84.

Worthington, L. Valentine (1976). *On the North Atlantic circulation.* The John Hopkins University Press, 170 pgs.

Wright, W. R. and L. Valentine Worthington (1970). North Atlantic Ocean atlas of potential temperature and salinity in the Deep Water, including temperature, salinity and oxygen profiles from the Erika Dan cruise of 1962. Technical Report, Woods Hole Oceanographic Institution Atlas Series.

Wu, Peili, Richard Wood, and Peter Stott (2004). Does the recent freshening trend in the North Atlantic indicate a weakening thermohaline circulation? *Geophys. Res. Letters*, 31(L02301):doi:10.1029/2003GL018584.

Wunsch, Carl (2002). What is the thermohaline circulation? *Science*, 298:1180–1181.

Wunsch, Carl, Dunxin Hu, and Barbara Grant (1983). Mass, heat, salt and nutrient fluxes in the south Pacific Ocean. *J. Phys. Oceanogr.*, 13(5):725–753.

Wyrtki, Klaus (1961). The thermohaline circulation in relation to the general circulation in the oceans. *Deep-Sea Res.*, 8:39–64.

Yashayaev, Igor, Manfred Bersch, Hendrik van Aken, and R. Allyn Clarke (2004). A new study of the production, spreading and fate of Labrador Sea Water in the subpolar North Atlantic. *ASOF Newsletter*, 2(March):20–23.

Yashayaev, Igor, R. Allyn Clarke, and John R. N. Lazier (2000). Recent decline of the Labrador Sea Water. *Int. Counc. for the Explor. of the Sea (ICES)*, 2000/L:18 pp.

Acknowledgements

After so many pages dealing with water mass formation in the North Atlantic, for me, personally, this is the most important page. This thesis was started at the former *Department of Regional Oceanography* in the former *Institut für Meereskunde* Kiel (now IFM-GEOMAR, Kiel). It was finished at the Institute of Enviromental Physics of the University of Bremen in what is today the *Department of Oceanography*. So, there is a lot of variability, too...

My warmest thanks goes to Monika Rhein who supervised this thesis. She encouraged me throughout all stages of this work and let me find my way. Thanks for advice and sharing experiences.

I further thank Claus Böning from IFM-GEOMAR for providing the co-evaluation of this thesis.

This thesis would have been impossible without the help of so many people involved in observational field work. Tina Schütt (Kiel) and Klaus Bulsiewicz (Bremen) were responsible for the German CFC measurements, assisted by many students, known and unknown to me. Many of the data have been received from the WOCE Hydrographic Programme Office. I thank all the PIs responsible for CTD and/or CFC measurements for sharing data, especially Friedrich Schott (formerly at IFM-GEOMAR), John Lazier, Igor Yashayaev and Allyn Clarke from BIO, Dartmouth, Canada, and Peter Koltermann from BSH, Hamburg. I would further like to thank William M. Smethie and Deborah LeBel from LDEO, Palisades, USA, for working together on a paper concerning ULSW formation and for sharing their data with me.

Joachim Dengg, Walter Zenk, and especially Lothar Stramma from IFM-GEOMAR kept up the connection from Bremen to Kiel. Thanks for exchanging scientific and fun stuff.

The members of the former *'Tracer-Ozeanographie'* gave me a very warm welcome when I moved from Kiel to Bremen, the members of today's *Ozeanographie* provided a very comfortable working environment. Thanks to all of you and especially to Reiner Steinfeldt, Maren Walter, and Christian Mertens. In the meantime, Birgit Klein has moved to the *Bundesamt für Seeschifffahrt und Hydrographie* in Hamburg. I am happy for the colleagues in Hamburg that they have the chance to meet Birgit's fast brain, critical thoughts and sense of humour. Thanks for *"Gehirnwartung"*.

My friends living near-by or far away, occasionally reminded me of the importance of having picknicks, walking through 'Bürgerpark' or along the river Weser, enjoying Portuguese-style kitchen: Olaf Plähn, Michael Schodlok, Mario Müller, Thomas Badewien, Marianne Boere and Petra Gudat, Meike and Carlos Sena Martins, Olaf Klatt.

Furthermore, Kerstin Kirchner, Olaf Plähn, Michael Schodlok, and Birgit Klein assisted me in proof-reading.

Björk (singer-songwriter from Iceland) ones said *"home is where the laptop is ..."*. Though things may have occasionally appeared so, it's definitely not my guiding theme. I would therefore like to thank my family, including Walter, Erika, Rolf, and Bettina Kieke and Martina Sacher, for providing love, help, and happiness, sending cookies and good thoughts, talking to answering machines, and spending a lot of time on the 'Autobahn'.

The *Deutsche Forschungsgemeinschaft* provided financial support in the framework of *Sonderforschungsbereich 460* 'Dynamik thermohaliner Zirkulationsschwankungen'.